

Characterising CD8$^+$ T cell Transcriptomic and Clonal Consequences of Immune Checkpoint Blockade for the Treatment of Cancer

Robert A. Watson

Magdalen College

Fairfax Lab, Department of Oncology

MRC Weatherall Institute of Molecular Medicine

University of Oxford

A thesis presented for the degree of

Doctor of Philosophy

Hilary Term 2023

Copyright © 2023 by Robert A. Watson

All Rights Reserved

Acknowledgements

I would like to express enormous gratitude to my supervisor Prof. Ben Fairfax for his unwavering guidance, support and intellectual repartee which have all made this work possible. The opportunity to work directly on an academic passion - the T cell response to immune checkpoint blockade - for a number of years has been a real privilege and I am extremely grateful for him making this a reality. I would also like to thank Prof. Mark Middleton, my co-supervisor, for his ongoing support of my progress and career, and for facilitating many elements of this research. I am grateful to a number of colleagues and mentors including Dr. Hussein Al-Mossawi who taught me blood separation and flow cytometry at the start of my time in the Lab, as well as Prof. David Church who has consistently given me good advice throughout my career. I have been helped enormously by the fantastic staff at the MRC WIMM, especially the facilities staff in flow cytometry and single cell sequencing, as well as the extremely helpful staff at OGC. I wholeheartedly thank all my colleagues in the Fairfax Lab - past and present - whom I've had the honour of working alongside. They have certainly brightened many of the darker days and I have been left in awe of their talent and capabilities. I would like to mention the staff of OUH, particularly the DTU nurses, who have facilitated the collection of the blood, and the patients and their relatives who have very generously donated samples for research. It is a sad fact of cancer research that a number of those individuals have since departed, but I hope this work honours their desire that some knowledge can be gained from their illness. My research has been supported by the NIHR, Cancer Research UK and primarily by the Wellcome Trust; I am extremely grateful for all the funding and support provided. Last, but by no means least, I would like to thank my entire extended family and in particular my wife, Maria, and children, Maia and Alfred, who have supported me throughout the DPhil, especially putting up with me working on and writing this piece over many months - I dedicate this thesis to them.

Declaration

I, Robert A. Watson, declare that the work presented in this thesis is my own, except where explicitly stated and acknowledged (see below). I confirm that no part of this thesis has been submitted for another degree within this University or externally.

A number of elements of the work presented were performed in collaboration with colleagues in the Fairfax Lab, Weatherall Institute of Molecular Medicine, University of Oxford (WIMM). Multiple individuals (myself included) have been responsible for collecting and processing donated blood samples, constructing libraries for sequencing and pre-processing the data. In particular, major contributors to blood collection include Sara Danielli, Chelsea Taylor, Rosalin Cooper, Alba Verge de los Aires, Elise Mahé, Flavia Matos Santo, Surya Koturan, Orion Tong, Piyush Kumar Sharma and Christina Ye. Bulk RNA sequencing was primarily performed by Alba Verge de los Aires, Chelsea Taylor, Orion Tong and Elise Mahé. Bioinformatic support was provided by Isar Nassiri. Genotyping of all clinical samples was performed by Orion Tong and Christina Ye with work on assigning HLA type undertaken by Elsita Jungkurth, with substantial input from James Gilchrist and contributions from myself. Clinical follow-up data and metadata collection was performed by myself with significant contributions from Christina Ye, Benjamin Fairfax, Robert Morgan and Martin Little. Patient recruitment was performed by myself with significant contributions from Miranda Payne, Nick Coupe, Ben Fairfax, Martin Little and Mark Middleton.

Chapter-specific acknowledgements, detailing contributions to the work presented, are included at the start of each results chapter (chapters 3, 4, 5 and 6). For all results presented, I was a principal contributor to the wet laboratory research and sole author of analysis, with all results figures presented generated entirely by me.

Reading this thesis

This thesis, when in PDF format, is highly interactive with multiple hyperlinks. It is designed so that the reader can rapidly jump between relevant sections - all section, figure, table and page references will link to the associated object allowing for quick navigation. All acronyms and abbreviations are defined in the glossary and will also hyperlink, as will citations which are coloured in grey. When a link is clicked, if using Adobe Acrobat reader, to return to the previous point in the text use cmd+← (Mac OS) or Alt+← (Windows) or navigate to 'View' menu, 'page navigation', 'previous view'. If using Preview (Mac OS) use cmd+[. Web hyperlinks are coloured in teal and will link to the relevant website. There are extensive page references for ease of navigation of this thesis in its printed form. All sections (chapters, sections and subsections) are bookmarked and will appear in Adobe Acrobat reader's 'bookmark' pane ('View' menu, 'show/hide' option, 'Navigation panes' option, select 'Bookmarks') or Preview's 'table of contents' ('View' menu, select 'Table of contents'). On Mac OS, Preview lends itself to easier scrolling than Adobe. All images are vectorised and so can be zoomed and enlarged without losing resolution.

Word count

```
Words in text: 49994
Number of headers: 203
Number of floats/tables/figures: 121
```

Compilation date: Tuesday 15th August, 2023

Abstract

Background: Immune checkpoint blockade (ICB) is arguably the greatest advance in medical oncology this century. Nonetheless, responses are highly variable. Mechanistic insights into this heterogeneity promises to improve patient stratification and identification of therapeutic targets.

Methods: Single-cell RNA sequencing and T cell receptor (TCR) sequencing was performed on peripheral $CD8^+$ T cells taken at multiple time points before, during and after treatment with ICB from patients with metastatic melanoma and renal cell carcinoma (n=30 scRNAseq, n=139 TCRseq), coupled with bulk RNAseq, genotyping and clinical follow-up data across a larger cohort (n=214 patients). Analysis was via custom-written R scripts.

Results: The clonal size of $CD8^+$ T cells is key to their response to ICB, with large clones differentially regulating more genes relevant to anti-tumour immunity. Through analysis of peripheral repertoires, highly public TCRs that strongly associate with clinical outcomes in patients with melanoma can be identified. These TCRs are found intra-tumourally, associate with HLA type, and their importance validates in two external datasets. $CD8^+$ T cell clones which persist long-term post cessation of ICB have a cytotoxic 'long-lived effector cell', rather than conventional memory, phenotype – an entirely novel finding in the context of human cancer. Finally, carriers of a single nucleotide polymorphism at rs16906115 have increased odds of toxicity following ICB, with differential $CD8^+$ T cell repertoire features. Risk-allele carriers are also less likely to experience decreases in lymphocyte count following ICB. A stable lymphocyte count post-treatment is a strong predictor of overall survival across multiple tumour types, regardless of genotype, a finding which replicates across multiple cohorts.

Conclusions: This work has high translational potential. Descriptions of key TCR in the anti-cancer response could inform vaccine or cellular therapeutic approaches. Further understanding lymphocyte stability may guide biomarker or drug development and the novel description of cytotoxic persistent clones in cancer is fundamentally relevant to human immunology.

Executive summary

Background and aims

ICB - consisting of antibodies to CTLA-4 and PD-1/PD-L1 - to treat cancer is arguably the greatest advance in medical oncology this century, having transformed outcomes across a wide range of tumours - most notably metastatic melanoma (MM). Nonetheless, responses to these treatments are highly variable, both in terms of long-term clinical outcome and occurrence of highly toxic side effects (so-called immune-related adverse events (irAEs)). Whilst some patients are able to achieve a complete response to treatment (CR), others derive minimal or no benefit. irAEs associate with improved outcomes, but these events are neither necessary nor sufficient for oncological response. Mechanistic insight into this heterogeneity promises to improve patient stratification and yield identification of further therapeutic targets.

This DPhil has three core objectives. By examining $CD8^+$ T cell gene expression and repertoire changes in the peripheral blood over time, I aim to:

1. Improve understanding of the molecular mechanisms of ICB
2. Describe $CD8^+$ T cell clonal and receptor features of a successful response to ICB
3. Identify clinically applicable biomarkers for response and adverse events

Methods

In order to investigate these questions, I primarily focus on single-cell RNA sequencing (scRNAseq) of both transcriptomes and gene expression of peripheral $CD8^+$ T cells. I have performed several scRNAseq experiments, coupling my findings in these datasets with gene expression changes across a much larger bulk RNA sequencing (bulk RNAseq) cohort to bring statistical

power and allow for survival analyses. I also utilise T cell receptor sequencing (TCRseq) - whereby T cell receptor (TCR) genes are selectively amplified and sequenced in depth - to understand $CD8^+$ T cell repertoire changes across a large cohort (n=364 samples) as well as end-organ sites of irAEs. This data is complemented by carefully-annotated clinical follow-up data, bulk RNAseq across a large cohort of patients with MM (n>200), whole-cohort genotyping and flow cytometry (performed by others) across a subset of samples. The analysis of the data generated requires computational approaches and I have applied a range of *R* packages, via multiple custom-written scripts, to process, handle and analyse the data.

Results

I first examine early changes in peripheral $CD8^+$ T cells following ICB at a single-cell level, showing that gene expression changes following ICB diverge as a result of $CD8^+$ T cell clone size, with clones occupying >0.5% of the peripheral repertoire (large clones) modulating markedly more genes with treatment than small clones (those occupying $\leq$0.5%) in both MM and metastatic renal cell carcinoma (mRCC). Further, large clones are more cytotoxic and more likely to persist long term in the peripheral blood, as well as be found in public datasets of tumour-associated TCR. Applying a cytotoxicity score to a large cohort of patients with bulk RNAseq demonstrates that the baseline, *a priori*, cytotoxicity of $CD8^+$ T cells significantly correlates with progression-free survival (PFS) in MM.

I then turn my attention to early and late repertoire changes following ICB, performing bulk TCRseq. Focussing on $CD8^+$ T cell receptor beta chains (TCRβs), I use the *GLIPH2* algorithm to cluster TCR into 'specificity groups' of putative shared antigen specificity. Filtering for groups containing expanded TCR from at least three individuals, I identify those that significantly increase in size, primarily in responders to treatment - calling these Emergent Responder Specificity Groups

(ERSGs) and their member clones Emergent Responder clones. These Emergent Responder clones (ER clones) significantly associate with outcome in the discovery cohort - not just post-treatment, following expansion - but at baseline. ER clones are large, cytotoxic and of memory phenotype, as well as demonstrating human leukocyte antigen (HLA) specificity. Filtering for HLA-restricted ER clones maintains the association with response whilst reducing the list of key clones to just several dozen. Further, ER clones are enriched and expanded within resected tumours pre-treatment and persist long term in the peripheral blood. Finally, these findings validate in two replication cohorts - a peripheral blood dataset from our group and a public tumour-infiltrating lymphocyte (TIL) dataset.

To understand long-term clonal persistence, I subsequently perform scRNAseq of both transcriptomes and TCR receptors across a cohort of 18 patients with MM and two healthy donors (HDs). 10 patients with MM had an ongoing CR following single-agent PD-1 blockade, with blood sampled many years after cessation of ICB. Examining changes in subset abundance over time, I find a long-term increase of a group of cells with a highly cytotoxic, 'killer-like' phenotype. Examining patterns of expression of the genes differentially upregulated by this neighbourhood of cells across multiple samples demonstrates that in those with a CR to treatment, there is a modest but significant increase in expression of this killer phenotype over time, which is not seen in patients with progressive disease (PD) or in HDs. Examining clonal dynamics over the long term demonstrates remarkable clonal stability, with baseline highly-expanded clones remaining stable and of similar size for many years. Surprisingly, clones which initially expand and then remain in the peripheral blood (which I term large expanding persistent clones (LEP clones)) are primarily comprised of cytotoxic effector cells, with a gene expression profile consistent with a recently-described subset called long-lived effector cells (LLECs). They upregulate gene sets shown by others to associate with tumour specificity and cytotoxicity, and this transcriptional change remains elevated above baseline for years post-cessation of ICB.

Finally, I investigate molecular and clonal changes in the context of irAEs, performing TCRseq on peripheral blood and tissue samples taken from three individuals with severe myocarditis and myositis. These cases are unusual in their extreme severity and clustering around the time of introduction of the Covid-19 booster vaccine. They demonstrate high levels of repertoire overlap, significantly in excess of that seen between control samples. Further, when adjusting for number of chains, there is a marked increase in TCR described to recognise the Spike protein of SARS-CoV-2 virus in public datasets. I next examine genetic determinants of irAEs, replicating an observed association between the minor allele at rs16906115, intronic to *IL7*, and the development of irAEs following ICB. I show that carriers of this polymorphism have changes to their $CD8^+$ T cell subsets and clonal repertoires, and those with the minor allele have stable lymphocyte counts from pre-treatment to post-treatment. I subsequently follow up this finding in a larger dataset, describing a "lymphocyte stability index" (LSI) and showing that a stable LSI strongly associates with both improved PFS and overall survival (OS) across multiple tumour types.

Conclusions

A number of the findings of this DPhil have translational potential and raise further, important questions, the investigation of which is likely to yield even greater insight into the tumour-specific T cell response. However, from this work, there are three main conclusions:

1. The baseline immune repertoire is key in determining future outcomes. I provide multiple pieces of evidence to support the conclusion that the *a priori* immune landscape is a crucial factor in determining future responses.

2. Clones that persist long-term following a CR to ICB have a cytotoxic LLEC phenotype. Contrary to the perceived wisdom that chronically-expanded clones have a memory or exhausted phenotype, I show that in the context of a CR to ICB, these clones actually have

a highly cytotoxic, ‘killer-like’ gene expression profile.

3. The peripheral blood provides a fertile ground for investigation of responses to ICB with key response clones identifiable. I am able to draw a number of meaningful conclusions regarding the $CD8^+$ T cell immune response to cancer, notably including the identification of key clones which are putatively mediating tumour rejection.

Whilst there is still progress to make, by using systematic molecular biology techniques and leveraging the power of large cohorts with carefully-annotated follow-up data, it is possible to meaningfully advance towards novel biomarkers and therapeutic approaches - and with that, improved quality and length of life for those with cancer.

Table of Contents

1 Introduction **1**

1.1 Immune checkpoint blockade and the treatment of cancer 1

1.1.1 Mechanism of action of ICB 3

1.1.1.1 CTLA-4 blockade 3

1.1.1.2 PD-1 blockade 5

1.1.2 ICB and the treatment of melanoma 6

1.1.2.1 Stages of melanoma 6

1.1.2.2 ICB for melanoma in the adjuvant setting 8

1.1.2.3 sICB versus cICB in the metastatic setting 8

1.1.3 ICB and the treatment of renal cell carcinoma 9

1.1.4 Immune-related adverse events 9

1.1.4.1 Clinical syndromes and epidemiology 10

1.1.4.2 Molecular mechanisms 11

1.1.4.3 Biomarkers of irAEs 11

1.1.4.4 Management of irAEs 13

1.1.4.5 Unanswered questions 14

1.2 The role of $CD8^+$ T cells in the response to ICB 14

1.2.1 A key molecular target 14

1.2.2 Site of action of ICB 15

1.2.3 Molecular effects of ICB on T cells . . . 18
1.2.3.1 Reinvigoration of T cell exhaustion . . . 19
1.2.3.2 Proliferation of stem-like $CD8^+$ T cells . . . 20
1.2.3.3 Mobilisation of peripheral T cells . . . 22
1.2.3.4 Clonal expansion and persistence of T cells . . . 25
1.2.3.5 Other transcriptomic effects of ICB . . . 25
1.2.4 Overlap between the peripheral and tumour-infiltrating compartments . 26
1.2.5 Long term persistence of $CD8^+$ T cell clones . . . 27
1.2.6 Tertiary lymphoid structures . . . 29
1.3 Biomarkers of response to ICB . . . 30
1.3.1 Tumour genetic factors . . . 31
1.3.2 Germline genetic factors . . . 34
1.3.3 The tumour and immune microenvironment . . . 35
1.3.4 Peripheral blood factors . . . 36
1.3.4.1 Immune cell counts . . . 36
1.3.4.2 Circulating molecules . . . 37
1.3.5 Other factors . . . 39
1.4 The T Cell Receptor (TCR) . . . 39
1.4.1 Thymic development and V(D)J rearrangement . . . 39
1.4.2 The MHC and antigen recognition by TCRs . . . 41
1.4.3 TCR signalling . . . 42
1.5 T cell receptor repertoire analysis . . . 43
1.5.1 Molecular biology approaches for TCRseq . . . 43
1.5.2 Repertoire metrics . . . 46
1.5.3 Repertoire features and ICB . . . 48

1.5.3.1 Tumour-infiltrating T cell repertoires . . . 48
1.5.3.2 Peripheral blood T cell repertoires . . . 50
1.5.4 T cell clustering algorithms . . . 56
1.5.5 Antigen identification . . . 59
1.6 Thesis aims and objectives . . . 62
1.7 Thesis Outline . . . 63
1.8 Scientific output thus far . . . 63

2 Methods **65**

2.1 Clinical sample collection . . . 65
2.1.1 Patient recruitment . . . 65
2.1.2 Post-mortem tissue collection . . . 66
2.1.3 HRA approval for lymphocyte stability index (LSI) data . . . 66
2.1.4 Laboratory blood counts . . . 66
2.1.5 Blood collection . . . 67
2.1.6 RNA extraction . . . 67
2.1.7 Sequencing . . . 67
2.2 Single cell RNA sequencing . . . 68
2.2.1 Sample preparation and sequencing . . . 69
2.2.1.1 Sample preparation and sequencing: the SciImm experiment . 69
2.2.1.2 Sample preparation and sequencing: the LT experiment 69
2.2.2 Pre-processing, QC and cell filtering . . . 70
2.2.2.1 Pre-processing, QC and cell filtering: the SciImm experiment 70
2.2.2.2 Pre-processing, QC and cell filtering: the LT experiment . . . 71
2.2.2.3 Clonal definitions in analysis of scRNAseq data . . . 72

2.2.2.4 Cell numbers per sample . . . 73
2.2.3 Dimensionality reduction and annotation . . . 74
2.2.3.1 Dimensionality reduction and annotation: the SciImm experiment 74
2.2.3.2 Dimensionality reduction and annotation: the LT experiment . 74
2.2.4 Downstream analysis . . . 76
2.2.4.1 Defining stable/expanding clones . . . 76
2.2.4.2 Defining clone phenotype . . . 76
2.2.4.3 Differential abundance analysis . . . 77
2.2.4.4 *AddModuleScore* and *AddModuleScore_Ucell* . . . 78
2.2.4.5 Differentially expressed gene (DEG) analysis . . . 79
2.2.4.6 GOBP analysis . . . 80
2.2.4.7 Identifying annotated TCR from public data . . . 81
2.3 Bulk RNA sequencing and genotyping . . . 81
2.3.1 Bulk RNA library preparation and sequencing . . . 81
2.3.2 TCR mapping . . . 81
2.3.3 Genotyping and HLA typing . . . 82
2.3.4 Downstream analysis . . . 82
2.3.4.1 Applying expression scores to bulk data . . . 82
2.3.4.2 Determining clone size in bulk data . . . 83
2.4 TCR sequencing . . . 83
2.4.1 RNA extraction from tissue . . . 83
2.4.2 Library preparation, sequencing and pre-processing . . . 84
2.4.3 Downstream analysis . . . 85
2.4.3.1 Determining clone size . . . 85
2.4.3.2 *GLIPH2* clustering . . . 85

2.4.3.3 Defining ER clones . . . 85
2.4.3.4 Repertoire metrics . . . 86
2.4.3.5 TCR gene usage . . . 86
2.4.4 External and validation datasets . . . 86
2.4.4.1 Antigen-specific TCR calling . . . 86
2.4.4.2 Tumour-associated TCR . . . 87
2.4.4.3 Peripheral blood validation cohort . . . 87
2.4.4.4 Intra tumoural validation dataset . . . 87
2.5 Flow cytometry . . . 87
2.6 General statistical analysis . . . 88
2.6.1 Survival analysis . . . 89
2.6.2 LSI analysis . . . 89

3 Analysis of peripheral CD8$^+$ T cell subsets before and after ICB 90

3.1 Chapter-specific acknowledgements . . . 90
3.2 Chapter-specific background . . . 90
3.3 Results . . . 92
3.3.1 Single-cell sequencing of eight patients with metastatic melanoma . . . 92
3.3.2 CD8$^+$ T cell subset distribution and gene modulation post-ICB varies as a function of clone size . . . 94
3.3.3 Cytotoxic CD8$^+$ T cell clones persist following ICB treatment . . . 96
3.3.4 Large, cytotoxic CD8$^+$ T cell clones are more likely to be found within melanomas . . . 100
3.3.5 Cytotoxicity score at baseline predicts outcome following ICB . . . 100
3.3.6 Single-cell sequencing of nine patients with mRCC . . . 102

3.3.7 Effect of clone size on subset distribution and gene expression in mRCC 104
3.3.8 Cytotoxicity of persistent CD8+ T cell clones in mRCC 106
3.3.9 Comparison of effector CD8+ T cell gene expression between MM and mRCC 107
3.3.9.1 DEGs pre-treatment between samples from patients with mRCC and MM 108
3.3.9.2 Cytotoxicity scores in MM and mRCC 110
3.4 Discussion 111

4 Clonal analysis of CD8+ T cell repertoires following ICB 114

4.1 Chapter-specific acknowledgements 114
4.2 Chapter-specific background 114
4.3 Results 116
4.3.1 Deep sequencing of the T cell receptor 116
4.3.1.1 Resolution of index hopping and QC 116
4.3.1.2 Post-QC dataset 118
4.3.2 CD8+ T cell repertoire metrics 119
4.3.3 Comparison of CD8+ T cell alpha and beta chain repertoires 123
4.3.4 Comparison of CD8+ T cell with CD4+ T cell repertoires 123
4.3.5 Identification of key response groups of CD8+ T cells 125
4.3.6 ER clone repertoire occupancy corresponds with clinical response and is HLA specific 128
4.3.7 ER clones are large, persistent and of memory phenotype 132
4.3.8 ER clones are enriched and expanded within tumours and are cytotoxic in the peripheral blood 135

4.3.9 ER clones are found within the repertoires of healthy donors 137
4.3.10 Importance of ER clones replicates in validation datasets 139
4.4 Discussion 142

5 Long term effects of ICB on peripheral CD8⁺ T cell subsets 146

5.1 Chapter-specific acknowledgements 146
5.2 Chapter-specific background 146
5.3 Results 148
5.3.1 Single cell sequencing of individuals with a complete response to programmed cell death protein 1 (PD-1) blockade 148
5.3.1.1 Sample cohort 148
5.3.1.2 PBMC annotation reveals classical subsets 151
5.3.1.3 CD8⁺ T cell cohort 155
5.3.2 Changes to subset abundances over time 161
5.3.3 Differential abundance with *Milo* - PBMC subsets 162
5.3.4 Differential abundance with *Milo* - CD8⁺ T cell neighbourhoods 166
5.3.5 A Killer-like expression profile in CD8⁺ T cells persists in those with a CR to ICB 172
5.3.6 Killer score subsection summary 175
5.3.7 Clonal dynamics following a complete response to ICB 176
5.3.7.1 Changes to clonal size over time 176
5.3.7.2 Defining large expanding persistent (LEP) clones 179
5.3.7.3 Changes to clonal phenotype over time 181
5.3.7.4 Comparison with healthy donor samples 183
5.3.8 Clonal dynamics subsection summary 184

5.3.9 Transcriptomic description of large expanding persistent clones 185
5.3.9.1 Differentially expressed genes of large expanding persistent clones 185
5.3.9.2 Expression scores of large expanding persistent clones 185
5.3.9.3 Antigen specificity of large expanding persistent clones 189
5.4 Discussion 191
5.4.1 Conclusions 196

6 CD8⁺ T cell features associated with immune-related adverse events 197
6.1 Chapter-specific acknowledgements 197
6.2 Chapter-specific background 197
6.2.1 Myositis and myocarditis in the context of PD-1 blockade and vaccination for Covid-19 198
6.2.2 The molecular effects of rs16906115 and importance of peripheral lymphocyte stability 199
6.3 Results: T cell receptor analysis of three cases of myositis with myocarditis . . . 200
6.3.1 Clinical case reports 200
6.3.2 Clinical sample collection 201
6.3.3 Analysis of occurrence of irAEs within existing cohort 202
6.3.4 Analysis of T cell repertories reveals a high degree of overlap between samples 203
6.3.5 Evidence of expansion of Spike-specific TCR within skeletal muscle . . 205
6.3.6 Section summary 206
6.4 Results: The effect of B cell *IL7* on peripheral T cell repertoires and lymphocyte counts 207

6.4.1 Replication of association between carriage of risk allele at rs16906115 and irAEs . . . 207
6.4.2 Carriers of the minor allele at rs16906115 have skewed CD8+ T cell subsets and repertoires . . . 208
6.4.3 rs16906115 affects lymphocyte stability post ICB . . . 210
6.4.4 Lymphocyte stability predicts clinical outcome in discovery melanoma cohort . . . 211
6.4.5 Lymphocyte stability predicts clinical outcome in melanoma replication cohort and across multiple tumour types . . . 213
6.4.6 LSI and outcome in a third cohort (Liverpool) . . . 216
6.4.7 LSI may enable improved patient stratification . . . 217
6.4.8 Section summary . . . 218
6.5 Discussion . . . 219
6.5.1 Conclusion . . . 223

7 Discussion **224**

7.1 Summary of key findings . . . 224
7.2 Importance of results in the context of existing literature . . . 227
7.3 Strengths and weaknesses . . . 232
7.4 Future directions . . . 234
7.5 Concluding remarks . . . 236

References **239**

Appendix A Supplementary Tables **271**

Appendix B Treatment of melanoma based on stage **273**

Appendix C Clinical trial data to support the use of ICB in the adjuvant setting 275

Appendix D Myositis and myocarditis - full clinical cases 276

Appendix E Science Immunology Paper 279

Appendix F Nature Medicine Paper (2022) 280

List of Figures

1.1 Kaplan Meier overall survival curve taken from Checkmate 500 1

1.2 Timeline of licenced ICBs by tumour type. 2

1.3 Phenotypic features of tumour-reactive, intratumoural $CD8^+$ T cells 17

1.4 Model for role of peripheral T cells 18

1.5 Graphic of T_{pex} model of immunity 23

1.6 Timeline of ICB biomarker approval by the FDA 31

1.7 TMB of a range of tumours 33

1.8 Peripheral biomarkers of response to ICB 38

1.9 V(D)J recombination 40

1.10 Equations for repertoire metrics 53

1.11 Visualisation of T cell repertoire metrics 54

1.12 Peripheral blood repertoire characteristics and response 55

2.1 Phenotypic make-up of clones 77

2.2 Flow cytometry gating strategy 88

3.1 Single cell sequencing identifies seven distinct $CD8^+$ T cell subsets 93

3.2 Subset identities of clones of different sizes 94

3.3 Number of DEGs post-ICB is a feature of clonal size 95

3.4 GOBP for effector clones dichotomised on size 96

3.5 Comparison between involuting and stable/expanding clones 98

3.6 Clonal changes from day 21 to day 63+ 99
3.7 Large cytotoxic effector clones are found within melanomas 101
3.8 KM curve based on baseline cytotoxicity score 101
3.9 Comparison between subset annotations 103
3.10 UMAP of $CD8^+$ T cells from mRCC samples 104
3.11 Subset identities of clones of different sizes 105
3.12 Larger clones differentially regulate more genes following ICB in mRCC 106
3.13 Changes to clones from d21 to d63 in mRCC samples 107
3.14 DEGs between samples from patients with MM and mRCC at baseline 109
3.15 PCA of pseudobulk approach 110
3.16 Comparison of cytotoxicity scores in MM and mRCC 111

4.1 Quantifying overlap between samples - raw data 117
4.2 Quantifying overlap between samples - post QC 119
4.3 Correlation between Shannon/Gini and CMV antibody titre and age 121
4.4 Correlation between repertoire metrics and clinical outcome 122
4.5 Correlation between repertoire metrics of TCRα and TCRβ chains 123
4.6 Correlation between repertoire metrics of $CD4^+$ T cells and $CD8^+$ T cells . . . 124
4.7 Correlation between large clones of $CD4^+$ T cells and $CD8^+$ T cells 125
4.8 Gene usage by $CD8^+$ T cells and $CD4^+$ T cells 126
4.9 Filtering and identification of ER clones 127
4.10 Proportion of repertoire occupied by ER clones by age and sex 128
4.11 Proportion of repertoire occupied by ER clones by CMV status 128
4.12 Proportion of repertoire occupied by ER clones and outcome in discovery cohort 130
4.13 Heatmap of association between ER specificity groups and HLA 131

4.14 HLA specificity of ER clones . . . 132
4.15 Size of ER clones and outcome . . . 133
4.16 Phenotypes of ER clones . . . 134
4.17 Long term persistence of ER clones in the peripheral blood . . . 135
4.18 Intra-tumoural analysis of ER clones . . . 136
4.19 Cytotoxicity and differential gene expression of ER clones . . . 137
4.20 ER clone presence in healthy donors . . . 138
4.21 TA-TCR repertoire occupancy . . . 139
4.22 Validation of relevance of ER clones in peripheral blood . . . 141
4.23 Validation of relevance of ER clones in tumour-infiltrating compartment . . . 142

5.1 Schematic of timing of samples for melanoma patients and healthy donors . . . 149
5.2 UMAP of PBMCs . . . 151
5.3 Canonical gene expression of PBMC subsets . . . 153
5.4 UMAP of PBMCs coloured by variables . . . 154
5.5 UMAP of $CD8^+$ T cells coloured by experiment . . . 155
5.6 Comparison of QC metrics of SciImm samples from each experiment . . . 156
5.7 UMAP of $CD8^+$ T cells . . . 157
5.8 UMAP of $CD8^+$ T cells coloured by variables . . . 159
5.9 Canonical gene expression of $CD8^+$ T cell subsets . . . 160
5.10 Changes to proportions of cell subsets . . . 162
5.11 Changes to cell subset abundance over time using *edgeR* . . . 163
5.12 Differential abundance of PBMC subsets . . . 163
5.13 Differential abundance of cell type subsets . . . 165

5.14 Differential abundance of CD8$^+$ T cells with neighbourhoods grouped in an agnostic manner 166
5.15 Location of neighbourhood groups on CD8$^+$ T cell UMAP 168
5.16 DEG analysis of neighbourhood groups 9 and 11 171
5.17 Changes to killer score over time in effector T cell (T_{eff}) clones 173
5.18 Changes to killer score over time on an individual basis 174
5.19 Comparison of killer score between those with PD and those with CR 175
5.20 Analysis of killer score in bulk RNAseq 175
5.21 Clonal dynamics over time 177
5.22 Phenotypes of hyper-expanded clones over time 178
5.23 Defining a killer cluster 179
5.24 Phenotypes of hyper-expanded clones over time, including killer-like cluster . . 180
5.25 Proportion of the repertoire occupied by persistent clones 181
5.26 Alluvial plots of long term persistent clones 182
5.27 Cellular make up of post-treatment clones in patients with a CR 183
5.28 Comparison of findings in HD samples 184
5.29 DEG analysis for LEPCs from patients with CR versus HDs 186
5.30 Expression scores for LEP clones over time 187
5.31 Expression scores for LEP clones vs all other clones 188
5.32 Proportions of tumour reactive cells 189
5.33 Gene expression of long-lived effector clone genes by LEP clones 190
5.34 Antigen specificity of LEP clones 190
5.35 Characterisation of clones which carry TCRβ associated with melanoma antigens 191

6.1 Blood markers and histopathology slides for three cases identified. 201

6.2 Repertoire overlap between samples 204
6.3 Repertoire overlap between PM tumour sample and other tissue sites 204
6.4 Morisita-Horn index overlap of repertoires 205
6.5 Epitope reactivity of shared clones 206
6.6 Replication of polymorphism at rs16906115 and odds of developing irAEs . . . 208
6.7 T cell effects of rs16906115 209
6.8 rs16906115 is associated with lymphocyte stability 211
6.9 LSI predicts outcome in melanoma discovery cohort 212
6.10 Survival analysis of LSI in melanoma replication cohort 214
6.11 Survival analysis of LSI in patients with NSCLC and mRCC 216
6.12 Hazard ratios for OS based on LSI 217
6.13 LSI and OS in Liverpool replication data 218
6.14 Comparison of Liverpool and Oxford cohorts 219
6.15 LSI and OS in all data combined 220
6.16 LSI treatment stratification 221

7.1 Model for effects of ICB 231

List of Tables

1.1 AJCC melanoma staging classification 2018 7

2.1 Numbers of non-CD8$^+$ T cells in magnetically sorted populations 72

2.2 Cell numbers per sample for scRNAseq experiments 73

3.1 Summary of patients 92

3.2 scRNAseq mRCC cohort characteristics 102

4.1 TCRseq cohort characteristics 120

4.2 Association of Shannon/Gini with outcome using a linear model 122

4.3 Characteristics of validation cohort 140

5.1 scRNAseq melanoma cohort and healthy donor characteristics 150

5.2 Number of cells in PBMC subsets 152

5.3 Number of cells in CD8$^+$ T cell subsets 158

5.4 Top 25 upregulated genes in neighbourhood groups 9 and 11 170

5.5 Number of large expanding persistent clones (LEP clones) per individual with CR 180

6.1 Myositis/myocarditis sample summary 202

6.2 Summary of cases of myositis or myocarditis 203

6.3 Patient numbers and tumour type, Oxford LSI cohort 213

A.1 List of gene sets for expression scores 271

A.2 Table of Cox PH models used in assessing association between LSI and OS . . 272

Glossary

Symbols

5'RACE rapid amplification of 5' complementary DNA ends

95% CI 95% confidence interval

A

ADCC antibody-dependent cellular cytotoxicity

AJCC American Joint Committee on Cancer

APC antigen-presenting cell

AUC area under the curve

B

BiTE bispecific T cell engager

bp base pair

BRAFi BRAF inhibitor

bulk RNAseq bulk RNA sequencing

C

CAR T cell chimeric antigen receptor T cell

CD4m memory $CD4^+$ T cell

CD4n naive $CD4^+$ T cell

CDR3 complementary determining region 3

cICB combination immune checkpoint blockade; Ipilimumab plus Nivolumab

CITE-seq cellular indexing of transcriptomes and epitopes by sequencing

CK creatine kinase

CMV cytomegalovirus

CNS central nervous system

CR complete response to treatment

CRP C-reactive protein

CT cancer testis

CTC circulating tumour cell

CTCAE common terminology criteria for adverse events

ctDNA circulating tumour DNA

CTLA-4 cytotoxic T-lymphocyte-associated antigen 4

CUREC Central University Research Ethics Committee

CyTOF cytometry time of flight

D

DA differential abundance

DEG differentially expressed gene

DMSO dimethyl sulfoxide

DN T cell double negative T cell

DTT dithiothreitol

E

EBV Epstein-Barr virus

ER clone Emergent Responder clone

ERSGs Emergent Responder Specificity Groups

ESMO European Society for Medical Oncology

F

FcγR Fc gamma receptor

FCS foetal calf serum

FDA Food and Drug Administration

FDR false discovery rate

FFPE formalin-fixed paraffin-embedded

G

gDNA genomic DNA

GEM gel bead in emulsion

GI gastrointestinal

GOBP Gene ontology biological process

GWAS genome-wide association study

H

H&E Haematoxylin and Eosin

HBSS Hank's balanced salt solution

HD healthy donor

HLA human leukocyte antigen

HR hazard ratio

HRA Health Research Authority

I

ICB immune checkpoint blockade

IEDB The Immune Epitope Database

IFNγ interferon gamma

IHC immunohistochemistry

IIM idiopathic inflammatory myositis

IMDC International Metastatic RCC Database Consortium

IQR inter-quartile range

irAE immune-related adverse event

ITAM immunoreceptor tyrosine-based activation motif

ITH intra-tumoural heterogeneity

K

KM Kaplan-Meier curve

kNN *k*-nearest neighbours

L

large clones clones occupying >0.5% of the peripheral repertoire

LCMV lymphocytic choriomeningitis virus

LDH lactate dehydrogenase

LEP clones large expanding persistent clones

LLECs long-lived effector cells

LoH loss of heterozygosity

LSI lymphocyte stability index

M

MAIT cell mucosal associated invariant T cell

MART-1 melanoma antigen recognised by T cells 1

MH Morisita-Horn index

MHC major histocompatability complex

MM metastatic melanoma

mMDSC monocytic myeloid-derived suppressor cell

MMR mismatch repair

mRCC metastatic renal cell carcinoma

mRNA messenger RNA

MS IDREC Medical Sciences Interdivisional Research Ethics Committee

MSI micro-satellite instability

N

NGS Next Generation Sequencing

NICE National Institute for Clinical Excellence

NLR neutrophil:lymphocyte ratio

NSCLC non-small cell lung cancer

O

OR odds ratio

ORB Oxford Radcliffe Biobank

OS overall survival

OUHFT Oxford University Hospitals NHS Foundation Trust

P

PBMC peripheral blood mononuclear cell

PC principal component

PCA principal component analysis

PD progressive disease

PD-1 programmed cell death protein 1

PD-L1 programmed cell death ligand 1

PE paired-end

PFS progression-free survival

PM post-mortem

pMHC peptide-MHC complex

PS ECOG performance status

Q

QC quality control

qRT-PCR real-time quantitative reverse transcription PCR

R

ROC receiver operating characteristic

RT reverse transcription

S

SACT systemic anti-cancer treatment

scRNAseq single-cell RNA sequencing

sICB single-agent immune checkpoint blockade; either nivolumab or pembrolizumab

SNP single nucleotide polymorphism

T

$\mathbf{T_{cm}}$ central memory T cell

$\mathbf{T_{eff}}$ effector T cell

$\mathbf{T_{em}}$ effector memory T cell

$\mathbf{T_{ex}}$ exhausted $CD8^+$ T cells

$\mathbf{T_{pex}}$ progenitor exhausted (stem-like) $CD8^+$ T cells

T_{rm} resident memory T cell

TA-TCR tumour-associated TCR

TCR T cell receptor

TCRα T cell receptor alpha chain

TCRβ T cell receptor beta chain

TCRseq T cell receptor sequencing

TDLN tumour-draining lymph node

TI tumour-infiltrating

TIL tumour-infiltrating lymphocyte

TLS tertiary lymphoid structures

TMB tumour mutational burden

TME tumour microenvironment

TNM the Union for International Cancer Control TNM classification of malignant tumours

U

UMAP uniform manifold approximation and projection

UMI unique molecular identifier

V

VEGF vascular endothelial growth factor

W

WIMM Weatherall Institute of Molecular Medicine, University of Oxford

1 | Introduction

1.1 Immune checkpoint blockade and the treatment of cancer

It is hard to overstate the impact that cancer immunotherapy – in the form of immune checkpoint blockade (ICB) – has had in the last decade. It is perhaps the greatest medical success story of the current millennium and received mainstream recognition with the award of the 2018 Nobel Prize in Physiology or Medicine to James P. Allison and Tasuko Honjo for the discovery of cytotoxic T-lymphocyte-associated antigen 4 (CTLA-4) and programmed cell death protein 1 (PD-1) respectively[1]. It is not just the astounding effect that drugging these targets has had on overall outcomes that is so impressive – 5 year survival for metastatic melanoma has gone from under 5% in 2010 to 52% in 2019[2] (Figure 1.1) – but the fact that some patients go on to have a durable clinical response. Whilst time will tell how 'durable' the response will be – and long follow-up times simply don't currently exist – this is the first time that metastatic cancer has been 'cured' by drug treatment. This is the Holy Grail of medical oncology and challenges the central dogma that once the tumour has metastasized, it can only be slowed, not eradicated.

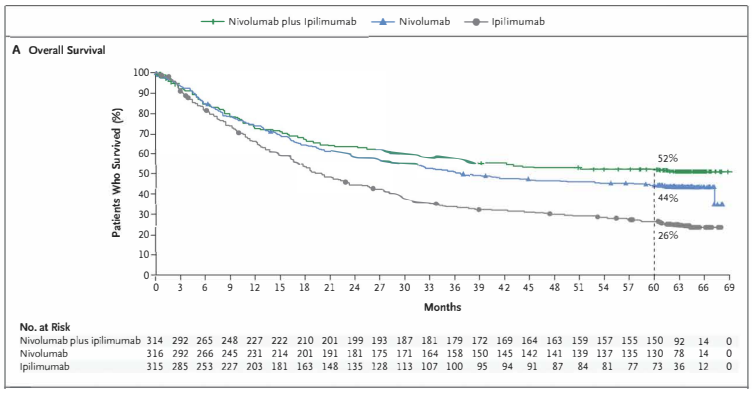


Figure 1.1. Kaplan Meier overall survival curve taken from Checkmate 067, coloured by treatment received, demonstrates long term benefit of ICB. Reproduced with permission from [2], Copyright Massachusetts Medical Society.

Whilst melanoma can be considered a "poster-child" of anti-tumour immunotherapy, at the time

of writing there are eight licensed checkpoint blockers for the treatment of a range of cancers including non-small cell lung cancer (NSCLC), urothelial cancers and head and neck cancers - with timelines for approval detailed in Figure 1.2.

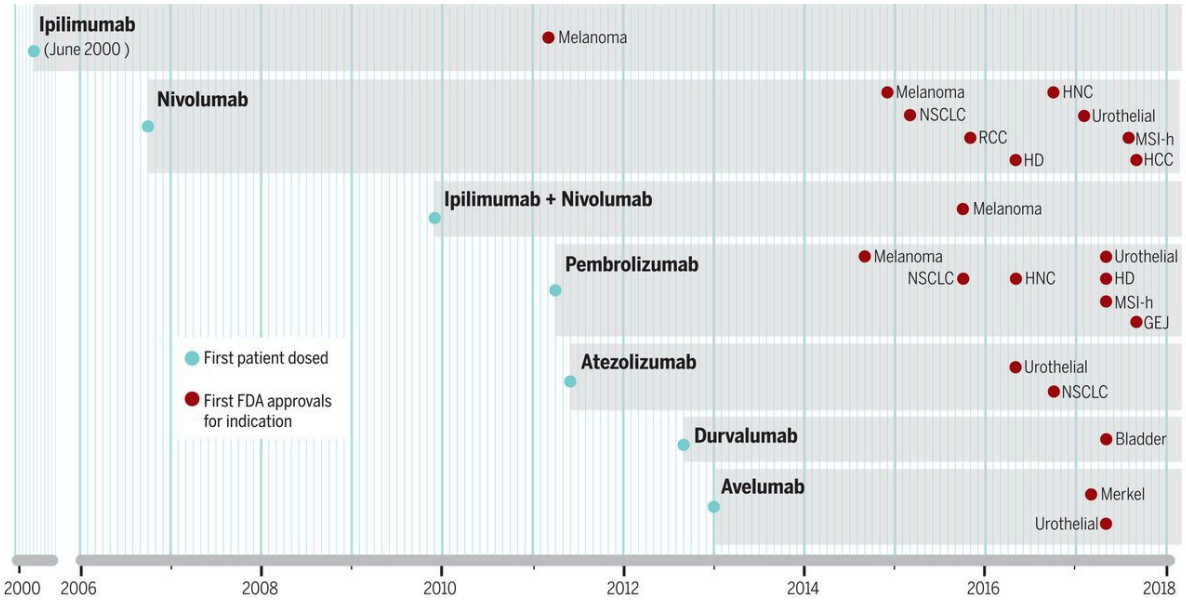


Figure 1.2. Timeline of licenced ICBs by tumour type. HNC - head and neck cancer; RCC - renal cell carcinoma; MSI-h - high microsatellite instability (usually in the context of colorectal cancer); HD - Hodgkin's disease (lymphoma); HCC - hepatocellular carcinoma; GEJ - gastroesophageal junction. Since this figure was published, Relatlimab - a LAG-3 inhibitor - has been licenced for melanoma, as has Cemiplimab for squamous and basal cell caricinoma and NSCLC. From [3]. Reprinted with permission from AAAS.

However, the successes have not come without failures. Even in melanoma, for every patient who is alive at 5 years, there's one who has died. A durable response, that apogean outcome, is only seen in less than four in ten patients[2]. Moreover, ICB has failed to make an impact in those cancers, such as hepatobiliary or primary central nervous system (CNS) tumours, with some of the poorest prognoses and lack of efficacious therapies.

Although, as per the above, there is an increasingly-large armamentarium of immune checkpoint blockers (Figure 1.2), for the purposes of this work and thesis, ICB will be used to refer to the drugs pembrolizumab, ipilimumab and nivolumab; given as a systemic anti-cancer therapy. Pembrolizumab and nivolumab both target the inhibitory PD-1 receptor, whilst ipilimumab

recognises CTLA-4[4]. All three drugs are monoclonal antibodies which block their cognate ligand. They can be given in isolation, however ipilimumab is no longer given first-line as a single-agent and in this thesis, 'sICB' is used to refer to either single-agent pembrolizumab or nivolumab. Ipilimumab is usually given in combination with nivolumab (referred to as 'cICB'). The clinical indications and rationale for treatment is detailed in section 1.1.2, page 6.

1.1.1 Mechanism of action of ICB

1.1.1.1 CTLA-4 blockade

CTLA-4 is an exclusive T cell intracellular protein in the resting state, but following activation of T cells by TCR ligation and co-stimulation of CD28 by CD80/86, traffics to the plasma membrane and serves to outcompete CD28 (a key T cell co-stimulatory receptor). It therefore suppresses T cell responses via multiple mechanisms. Firstly, simply by competing with CD28, it prevents an important co-stimulatory signal[5]. Secondly, inhibitory signalling via CTLA-4 dampens proliferation and activation of the T cell[6]. Thirdly, it can remove CD80/86 from the antigen-presenting cell (APC) via 'trans-endocytosis'[7] thereby hampering the ability of the APC to provide continuing co-stimulation. This process of trans-endocytosis is utilised by T_{regs} to mediate an immunosuppressive effect[8]. As such, CTLA-4 is a potent immunosuppressor and inhibitor of T cell responses, as demonstrated by mouse knock-out experiments which showed widespread fatal lymphocytic infiltration of multiple organs in CTLA-4$^{-/-}$ animals[6,9], as well as severe immune dysregulation identified in humans with CTLA-4 haploinsufficiency[10].

Nonetheless, the exact mechanism by which CTLA-4 blockade inhibits immunosuppression in humans remains incompletely defined and subject to some controversy, in particular the balance between ipilimumab's effect on T_{effs} versus T_{regs}. Early mouse experiments identified an important role for both these target cells, and in particular suggested that T_{regs} were depleted by

ipilimumab via antibody-dependent cellular cytotoxicity (ADCC) - a consequence of the fact that ipilimumab is an IgG1 antibody and hence should engage the Fc gamma receptor (FcγR). For example, Selby *et al.* modified anti-CTLA-4 antibodies to contain a variety of constant regions with a range of affinities to the FcγR. They found that those constant regions with a higher affinity exhibited enhanced anti-tumour activity, whilst those with a mutated IgG1 constant region (which abrogates binding to FcγR) had no immune rejection[11]. Further, upon analysing T cell subsets ($CD8^+$, $CD4^+$ and $FOXP3^+$) by flow cytometry, they described that higher-affinity constant regions led to depletion of T_{regs} at the tumour margin (but not in peripheral blood), along with expansion of T_{effs}. They concluded that anti-CTLA-4 leads to depletion of intra-tumoural T_{regs} with concurrent activation of T_{effs}, the combination of which result in immune-mediated tumour rejection[11]. Similar findings were reported by multiple groups and this mechanism became an accepted paradigm[12,13].

However, subsequent human work contradicted this dogma. Sharma and colleagues used immunohistochemistry (IHC) to quantify infiltrating T cell subsets and identified that across a range of cancers (melanoma, prostate cancer and bladder cancer), both ipilimumab and tremelimumab (another anti-CTLA-4) led to increased infiltration by both $CD8^+$ T cells and $CD4^+$ T cells but no change in the number of T_{regs}. They conclude that depletion of T_{regs} is not a major mechanism of action of these drugs in humans[14]. Whilst some commentators felt that there were a number of caveats to this finding - such as the time interval between treatment and biopsy and the fact that many of the patients received tremelimumab which is not FcγR binding and therefore not expected to confer substantial ADCC[15], this work nonetheless highlights the complexities and inherent uncertainties in clearly elucidating the effects of ICB in humans.

CTLA-4 has previously been described as a 'godfather' of immune checkpoints[4]. This is an appropriate term because whilst CTLA-4 is active on $CD8^+$ T cells, it has a major role on helper

$CD4^+$ T cells in lymph nodes and - regardless of whether or not ipilimumab leads to depletion of T_{regs} - CTLA-4 is crucial in the functioning of these immunosuppressive cells[8,16]. As such, CTLA-4 has a broad, systemic and widespread role. Blockade of CTLA-4 with ipilimumab can therefore be considered generalised immune disinhibition, and this explains the very high rates of irAE seen with this therapy (see section 1.1.4, page 9).

1.1.1.2 PD-1 blockade

PD-1 is a surface protein and member of the CD28 family, expressed on a range of immune cells including T cells, B cells, monocytes and dendritic cells[17]. It recognises its cognate ligand programmed cell death ligand 1 (PD-L1)[18] which is expressed on tissues and is upregulated following antigenic stimulation and T cell activation, particularly by interferon gamma (IFNγ)[19,20]. PD-1 ligation primarily functions to limit the activity of T cells, by a combination of kinase dephosphorylation, mediated by the tyrosine phosphatase SHP-2, and modifying the T cell-APC contact[18,21]. It therefore has a major role in limiting T cell activity within the context of inflammation in tissues[22–24]. As T cells become activated and secrete IFNγ, so do target tissues upregulate PD-L1, serving to suppress the response. Continuous ligation of PD-1 by its ligand can drive T cells towards exhaustion and an anergic epigenetic profile[25]. Further, in a similar manner to CTLA-4, PD-1 is found at high levels on T_{regs} where it facilitates their maintenance and proliferation[26]. The localised and primarily end-organ expression of PD-L1 explains why interference with this pathway with anti-PD-1 drugs results in a lower frequency of irAEs (see section 1.1.4, page 9).

The homeostatic roles of PD-1 are therefore ripe for co-option by tumours[4]. Whilst PD-L1 is normally expressed by macrophages, and is inducible on adaptive immune cells, as well as end-organ tissue cells in response to localised inflammation, tumour PD-L1 expression is a key tenant of tumour immune evasion[27,28]. Whilst some tumours can constitutively express PD-L1 as

a result of oncogenic mutations[29], others can up-regulate PD-L1 in response to immune attack - a concept termed 'adaptive immune resistance'[27]. Counter-intuitively, such tumours often carry a better prognosis, as the PD-L1 expression on the tumour is likely driven by a cytotoxic T cell response and is therefore a sign of immunogenicity[30].

At a basic level, the mechanism of action of anti-PD-1 ICB is primarily to interrupt tissue-based immunosuppression, and abrogate PD-1-PD-L1 signalling in cases where PD-L1 expression has been upregulated by tumours. Thus, it allows for reinvigoration and cytotoxic activity of tumour-infiltrating $CD8^+$ T cells[3]. A more detailed exploration of the effect of PD-1 blockade on $CD8^+$ T cells is below (section 1.2, page 14).

1.1.2 ICB and the treatment of melanoma

1.1.2.1 Stages of melanoma

The most common staging system used in the clinical management of melanoma is the American Joint Committee on Cancer (AJCC) classification, which is built on the TNM system, widely used across multiple cancers. Whilst the AJCC system is somewhat complicated (Table 1.1), it is broadly based on three elements:

- Tumour features - primarily thickness and presence/absence of ulceration
- Lymph node features - whether the tumour has spread to nearby nodes
- Metastatic features - whether the tumour has spread to other organs in the body.

The stage of melanoma is of critical importance as it determines the treatment indicated. A broad summary of the treatment for each stage of disease is given in Appendix B. Simply, for metastatic disease (stage IV) or un-resectable local disease (stage IIIC-D), systemic treatment - e.g. ICB - is indicated. For resected localised disease, ICB can be given adjuvantly (see below, section

AJCC Stage	Melanoma Stage Description
0	The cancer is confined to the epidermis, the outermost skin layer (Tis). It has not spread to nearby lymph nodes (N0) or to distant parts of the body (M0). Also known as melanoma in situ.
I	The tumor is no more than 2mm thick and might or might not be ulcerated (T1 or T2a). The cancer has not spread to nearby lymph nodes (N0) or to distant parts of the body (M0)
II	The tumor is more than 1 mm thick (T2b or T3) and may be thicker than 4 mm (T4). It might or might not be ulcerated. The cancer has not spread to nearby lymph nodes (N0) or to distant parts of the body (M0).
IIIA	The tumor is no more than 2 mm thick and might or might not be ulcerated (T1 or T2a). The cancer has spread to 1 to 3 nearby lymph nodes, but it is so small that it is only seen under the microscope (N1a or N2a). It has not spread to distant parts of the body (M0).
IIIB	There is no sign of the primary tumor (T0) **AND:** The cancer has spread to only one nearby lymph node (N1b) **OR** It has spread to very small areas of nearby skin (satellite tumors) or to skin lymphatic channels around the tumor (without reaching the nearby lymph nodes) (N1c) It has not spread to distant parts of the body (M0).
	OR
	The tumor is no more than 4 mm thick and might or might not be ulcerated (T1, T2, or T3a) **AND:** The cancer has spread to only one nearby lymph node (N1a or N1b) **OR** It has spread to very small areas of nearby skin (satellite tumors) or to skin lymphatic channels around the tumor (without reaching the nearby lymph nodes) (N1c) **OR** It has spread to 2 or 3 nearby lymph nodes (N2a or N2b) It has not spread to distant parts of the body (M0).
IIIC	There is no sign of the primary tumor (T0) **AND:** The cancer has spread to 2 or more nearby lymph nodes, at least one of which could be seen or felt (N2b or N3b) **OR** It has spread to very small areas of nearby skin (satellite tumors) or to skin lymphatic channels around the tumor, and it has reached the nearby lymph nodes (N2c or N3c) **OR** It has spread to nearby lymph nodes that are clumped together (N3b or N3c) It has not spread to distant parts of the body (M0).
	OR
	The tumor is no more than 4 mm thick, and might or might not be ulcerated (T1, T2, or T3a) **AND:** The cancer has spread to very small areas of nearby skin (satellite tumors) or to skin lymphatic channels around the tumor, and it has reached nearby lymph nodes (N2c or N3c) **OR** The cancer has spread to 4 or more nearby lymph nodes (N3a or N3b), or it has spread to nearby lymph nodes that are clumped together (N3b or N3c) It has not spread to distant parts of the body (M0).
	OR
	The tumor is more than 2 mm but no more than 4 mm thick and is ulcerated (T3b) **OR** it is thicker than 4 mm but is not ulcerated (T4a). The cancer has spread to one or more nearby lymph nodes **AND/OR** it has spread to very small areas of nearby skin (satellite tumors) or to skin lymphatic channels around the tumor (N1 or higher). It has not spread to distant parts of the body.
	OR
	The tumor is thicker than 4 mm and is ulcerated (T4b) **AND:** The cancer has spread to 1 to 3 nearby lymph nodes, which are not clumped together (N1a/b or N2a/b) **OR** It has spread to very small areas of nearby skin (satellite tumors) or to skin lymphatic channels around the tumor, and it might (N2c) or might not (N1c) have reached 1 nearby lymph node) It has not spread to distant parts of the body (M0).
IIID	The tumor is thicker than 4 mm and is ulcerated (T4b) **AND:** The cancer has spread to 4 or more nearby lymph nodes (N3a or N3b) **OR** It has spread to nearby lymph nodes that are clumped together (N3b) It has spread to very small areas of nearby skin (satellite tumors) or to skin lymphatic channels around the tumor, **AND** it has spread to at least 2 nearby lymph nodes, or to lymph nodes that are clumped together (N3c) It has not spread to distant parts of the body (M0).
IV	The tumor can be any thickness and might or might not be ulcerated (any T). The cancer might or might not have spread to nearby lymph nodes (any N). It has spread to distant lymph nodes or to organs such as the lungs, liver or brain (M1).

Table 1.1. American Joint Committee on Cancer (AJCC) melanoma staging classification 2018. Adapted from American Cancer Society. N.B. stage II disease is further subdivided into stages IIA, B and C but these are grouped together in this table. The increasing letters represent increasing thickness of the lesion and presence/absence of ulceration.

1.1.2.2).

1.1.2.2 ICB for melanoma in the adjuvant setting

From 2020, ICB (along with BRAF/MEK inhibition) was offered in the adjuvant setting for stage III melanoma. This means it can be given to people after complete resection to reduce the risk of recurrence (or more accurately to kill any cancerous cells that remain following resection). Adjuvant ICB is given in the form of either pembrolizumab or nivolumab for 1 year. This was based on clinical trial data, which is described in Appendix C, page 275. Both pembrolizumab and nivolumab are licensed in this setting and there is no evidence-based rationale to decide between the two treatments, which are usually prescribed based on physician choice.

1.1.2.3 sICB versus cICB in the metastatic setting

As set out in National Institute for Clinical Excellence (NICE) guidance NG14 July 2022 Update, when deciding whether to prescribe single-agent immune checkpoint blockade; either nivolumab or pembrolizumab (sICB) or combination immune checkpoint blockade; Ipilimumab plus Nivolumab (cICB) in the context of MM (i.e. stage IV or unresectable stage III disease) a number of factors need to be taken into account including performance status of the patient, risk of toxicity, presence of CNS disease and tumour biology (such as disease burden, rate of progression). In general, ICB is preferred to BRAF/MEK inhibition as first-line therapy, which would only be possible to prescribe in those cases where the melanoma contains a BRAF mutation. Indeed, this sequence was confirmed as having superior efficacy in the *DREAMseq* study[31] with a 20% better 2 year OS (p=0.010). Nonetheless, it is not possible to give ICB in the case of symptomatic CNS metastases and so in the context of a BRAF mutation being present, BRAF inhibitor (BRAFi) treatment would be the only treatment option. The dose of cICB for MM is 1mg/kg nivolumab and 3mg/kg ipilimumab for up to four cycles, and then 480mg of nivolumab

every four weeks.

By 'default' cICB is preferred over sICB, although there may be a number of reasons due to factors such as those listed above which lead to sICB being chosen. There is no evidence-based reason to choose one of pembrolizumab or nivolumab over the other.

1.1.3 ICB and the treatment of renal cell carcinoma

cICB is licensed for first-line treatment of mRCC[32] following the successful reporting of Check-Mate 214[33] which demonstrated (at 4 years follow up) improved OS (hazard ratio (HR) 0.69, 95% confidence interval (95% CI) 0.59-0.81), PFS and objective response rate when compared to sunitinib (previous standard-of-care treatment). Importantly, the dose of cICB in mRCC is different - 3mg/kg nivolumab and 1mg/kg ipilimumab for up to four cycles and then 480mg nivolumab every four weeks. It continues to be recommended for intermediate and poor-risk disease groups (as per the International Metastatic RCC Database Consortium (IMDC) classification) but there are a number of alternative therapies including combinations of vascular endothelial growth factor (VEGF) tyrosine kinase inhibitors (TKIs) and pembrolizumab plus a TKI. Much like the choice of therapies in MM (section 1.1.2.3), the decision of which treatment to prescribe involves a range of factors including patient fitness, tumour biological features such as rate of progression, probability of toxicities and patient preference. Nonetheless, cICB remains an important treatment for mRCC and I have collected blood from these patients as part of my DPhil.

1.1.4 Immune-related adverse events

Whilst ICB has undoubtedly changed the field of immuno-oncology, opening hearts, minds (and wallets) across academia, industry, clinicians and patients to the potential of this treatment,

perhaps *the* major "Achilles' heel" is the risk of developing immune-related adverse events (irAEs). These toxicities have a very different spectrum when compared to side effects following 'standard' chemotherapy or systemic anti-cancer treatment (SACT). In essence, irAEs are uncontrolled autoimmune disease directed against any tissue.

1.1.4.1 Clinical syndromes and epidemiology

When considering toxicity in the clinical practice of oncology, primarily the common terminology criteria for adverse events (CTCAE) grading criteria are used[34]. This system ranges from 1-5, where 1 is 'mild' and 5 is 'death from adverse event'. Typically, grade 3-4 refers to 'severe' events, with grade 3 requiring pharmacological management and grade 4 usually requiring hospital admission; grades 1-2 are usually managed in the outpatient setting.

irAEs can affect any organ or tissue and have a median onset of 2-16 weeks from initiation of therapy, with the peak onset during the first four weeks of treatment, although they have been described as occurring just days after treatment and after one or more years[35]. The clinical manifestations are that of inflammation - for example, colitis causing abdominal pain and diarrhoea or dermatitis causing a rash. Endocrine organs are frequently involved and this can affect functioning - resulting in a requirement for lifelong hormone replacement therapy. Some work has suggested different patterns of toxicity for individual drugs - with dermatological, gastrointestinal (GI) and renal toxicities seen with ipilimumab; arthritis, pneumonitis and hepatitis more common following pembrolizumab and endocrine toxicity associated with nivolumab[36,37]. Nonetheless, it is clear that sICB is associated with much lower rate of irAEs than cICB - based on the fact that CTLA-4 is such a generalised immunosuppressant. The frequency of grade $\geq$3 irAE is upwards of 55% in those treated with cICB, whereas it is around 10-20% in those treated with sICB[38]. Indeed, up to 95% of individuals receiving cICB develop some form of irAE[38,39].

1.1.4.2 Molecular mechanisms

At a very simplistic level, both CTLA-4 and PD-1 signalling pathways are fundamental methods for peripheral immune tolerance, and so interrupting these processes increases the risk of irAEs. Further to this, however, there is evidence of possible cross-reactivity between tumour and self-antigens. This is particularly notable for vitiligo, which is significantly over-represented in patients with melanoma, suggestive of overlap between the immune response to healthy and cancerous skin[40,41]. Further, in cases of ICB-associated myocarditis, there is overlap between TCRs found in the myocardium and tumour[42], a finding that I am able to replicate and expand on (Chapter 6, page 200). Supportive of both of these mechanisms is the observation - made by both ourselves and others - that individuals who develop irAEs have improved oncological outcome[43–45].

In addition to the role of T cells, it is thought likely that some irAEs are related to B cell autoantibody production. For example, in mouse models of hypophysitis, repeated injections of anti-CTLA-4 antibody resulted in pituitary failure along with the development of circulating pituitary antibodies[46]. This finding was then replicated in humans with circulating pituitary antibodies developing in patients with MM or prostate cancer who had hypophysitis following ipilimumab, with no such antibodies found in those without hypophysitis[46]. Consistent with the role of B cells, we have described a germline single nucleotide polymorphism (SNP) which confers an increased risk of irAEs, primarily via a B cell-related mechanism. This effect is described in Chapter 6 (page 207) and Appendix F.

1.1.4.3 Biomarkers of irAEs

There are a number of candidate biomarkers for risk of irAE both pre- and on-treatment, although notably no biomarker has been approved for use in stratifying risk of irAEs. A number of these overlap with biomarkers for response to ICB (discussed below, section 1.3, page 30). For example,

patients with a lower neutrophil:lymphocyte ratio (NLR), high baseline lymphocyte count or higher baseline eosinophil counts have all been demonstrated to be at increased risk of irAEs[39]. However, these markers likely reflect 'immune fitness', with the association of lymphocytes and irAEs suggestive of an important role for the adaptive immune response. Notably, it has been reported that lower proportion of PD-1-expressing $CD8^+$ T cells and $CD4^+$ T cells, along with increased PD-1 expression post-treatment has been associated with increased risk of irAEs post-ipilimumab, although this result is hard to interpret due to a small sample size and the absence of a comparison to irAE development post PD-1 blockade[47].

Clonal changes to the T cell repertoire have also been reported to associate with irAE development, with two studies reporting that both baseline diversity, and post-treatment expansion of $CD8^+$ T cell clones correlated with irAEs. Subudhi and colleagues reported that clonal expansion following ipilimumab was strongly associated with grade 2+ irAEs in patients with prostate cancer treated with androgen-deprivation therapy[48]. Similarly, Oh *et al.*[49] also found an association with post-ipilimumab clonal expansion and irAE development, but they also found that diversification of the repertoire was important, with approximately 50% of T cell clones being 'novel' (i.e. not present pre-treatment) following ipilimumab in those who developed irAEs. However, these results should be interpreted with caution as the included patients were treated with both ipilimumab and granulocyte-monocyte colony-stimulating factor (GM-CSF) - a potent inducer of lymphoproliferation.

In addition to immune cell factors, a number of circulating cytokines have been described as biomarkers for irAE development. In particular, IL-6 and IL-17 have been implicated as potential biomarkers. Perhaps counterintuitively, lower pre-treatment levels of IL-6 associate with increased risk of irAEs[50]. This could be explained by the fact that whilst IL-6 is pro-inflammatory, it is also thought to polarise towards immunosuppression and aid tumour invasion[50,51]. Conversely, IL-17,

also a pro-inflammatory cytokine implicated in inflammatory bowel disease, is associated with higher risk of irAEs - particularly colitis[52].

A number of studies have tried to correlate germline genetic features with development of irAEs. Whilst Refae and colleagues[53] identified associations with SNPs in genes including UNG, IFNW1, CTLA4, PD-L1 and IFNL4 and toxicity, this was only performed retrospectively in a very small cohort (n=94) and there was no validation cohort. Similarly, Bins *et al.* found a strong association with a SNP at rs2227981 (in PDCD1) and reduced odds of toxicity - however, this failed to validate[54]. Others have attempted to generate polygenic risk scores for irAE development[55]. However, none of these studies could conclusively prove a genetic link to irAEs, and until the publication of the first genome-wide association study (GWAS)[56] looking at associations with irAEs, there was limited evidence that germline genetics impacted the response to ICB. However, in December 2022 Sasha Gusev's group performed a GWAS and identified 3 genome-wide significant associations for all-grade irAEs in the discovery cohort[56]. One of these - at rs16906115, intronic to *IL7* - gave a HR for irAE development of 2.1 ($p=2.6x10^{-11}$) and replicated in two further cohorts. We collaborated with the authors of this study to further describe the molecular mechanisms of this observed association, with some of these results presented in Chapter 6 and the full manuscript found in Appendix F.

1.1.4.4 Management of irAEs

In general, irAEs are managed depending on their grade. Grade 1-2 toxicities might be managed with cessation of therapy and a period of observation, whilst grade 3-4 events require immunosuppression. Usually this is with corticosteroids in the first instance and, should that prove incompletely effective, biologic therapies can be used. Detailed clinical guidelines exist for management of organ-specific toxicity[57]. Whilst it is possible to have a good (including CR) response to ICB, even with toxicity-related immunosuppression, it is increasingly recognised that

such therapies can result in poorer oncological outcomes[58,59]. As such, strategies to identify those most at risk of irAEs, early mitigation methods and an understanding of differences between the anti-self and anti-cancer immune response are of paramount importance.

1.1.4.5 Unanswered questions

Whilst there is a reasonable body of literature on irAEs, there are still large gaps in our understanding. Specifically, the precise immune mechanisms of toxicity are incompletely described, and there is minimal description of how these differ from anti-tumour responses. Whilst toxicity associates with response, there is still a modest proportion of individuals who do not develop any toxicity and have a CR. Similarly, unfortunately some patients develop severe irAEs, and yet do not have any oncological benefit. An understanding of these divergent responses is lacking. Further, the relative importance of innate inflammation versus adaptive immunity is unclear. Finally, no biomarker currently exists on which to stratify risk of irAE development.

1.2 The role of $CD8^+$ T cells in the response to ICB

1.2.1 A key molecular target

Given the high levels of expression of immune checkpoints on $CD8^+$ T cells, they are considered one of, if not the primary cellular target of ICB. $CD8^+$ T cells - also known as cytotoxic T lymphocytes - are able to seek and destroy tumour cells by recognising transformed proteins presented by MHC class I molecules. They are therefore considered the backbone of tumour immunotherapy[60]. On recognition of their cognate antigen, $CD8^+$ T cells mediate target-cell death by inducing pore formation in the target membrane (often via mechanical forces[61]) and the secretion of death-inducing granules containing a variety of cytotoxic enzymes such as perforin, granulysin and granzymes. Additionally, they can express Fas ligand, which binds to Fas receptors

on target cells and induces cellular death[62]. Understanding the exact molecular mechanisms by which ICB affects $CD8^+$ T cells and generates clinical responses has become a key area of interest, and there now exists a vast body of literature exploring this.

1.2.2 Site of action of ICB

Multiple studies, dating back over a decade, have confirmed the important role that tumour-infiltrating lymphocytes (TILs) have to play in the anti-tumour response[63]. A seminal piece of evidence for the role of TILs came from a widely-cited paper by Tumeh *et al*[64]. Here they performed IHC, immunofluorescence and TCRseq on resected melanomas pre- and post-anti-PD-1 therapy in 46 patients. They were able to demonstrate that those individuals with a response to treatment had greater density of $CD8^+$ T cells at the tumour margin than those who progressed, and that, on-treatment, those responders gained $CD8^+$ T cells density at both the invasive margin and tumour centre[64]. Further, in those with a response, there were significantly higher numbers of $CD8^+$, PD-1^+ and PD-$L1^+$ cells at baseline (in both the tumour centre and invasive margin). This paper was also one of the first to demonstrate that clonality of the tumour-infiltrating repertoire is an important correlate of response - discussed below (section 1.5.3, page 48). Taken together, these findings suggested the importance of $CD8^+$ T cells and that a paucity of these cells in and around the tumour micro-environment was associated with poor response to ICB. As a result of this work and others[63,65], a school of thought developed whereby the effects of ICB were thought to predominantly occur with the tumour microenvironment (TME).

However, just because a T cell is tumour *infiltrating* does not mean that it is necessarily tumour *reactive* - some clones may be 'bystanders' and could in fact be detrimental to the immune response[66]. Identifying the subset of tumour-infiltrating (TI) $CD8^+$ T cells that are tumour reactive is an area of great interest, and numerous scRNAseq experiments have attempted to dissect this[67].

In general, phenotypes of $CD8^+$ T cells which appear to be mediating tumour rejection tend to align with an 'exhausted' or 'dysfunctional' programme. One of the earliest studies - by Tirosh *et al.* - described high levels of T cell exhaustion within the TME[68]. This was built on by a number of studies, including that of Li *et al*[69]. Here, scRNAseq from 25 patients with melanoma demonstrated a large pool of intratumoural $CD8^+$ T cells that transition into a dysfunctional state. These cells display the highest level of clonal expansion, and are highly proliferative (as evidenced by cell cycle progression and expression of Ki67). In contrast, they also identified a smaller pool of *cytotoxic* $CD8^+$ T cells which showed limited evidence of proliferation and was not linked to the dysfunctional group by TCR. Paradoxically, it was the *dysfunctional* $CD8^+$ T cells which were more tumour reactive (using an *ex vivo* model of T cell activation).

This notion that the dysfunctional TILs are mediating tumour rejection is supported by more recent work from Catherine Wu's group[70]. Here they used a combination of TCRseq, scRNAseq and cellular indexing of transcriptomes and epitopes by sequencing (CITE-seq) to describe the phenotypes of tumour-specific T cells. They first described that most expanded clones were of an exhausted phenotype. They then classified all T cells into one of two phenotypes - exhausted or non-exhausted memory. Using patient-derived melanoma cell lines, they were then able to show that most tumour-reactive T cells (>80%) were from exhausted phenotypes, whilst a much higher proportion of the non-exhausted memory $CD8^+$ T cells were viral-reactive. By clustering cells based on known tumour-reactive TCR, they were able to classify phenotypic subtypes of tumour-reactive $CD8^+$ T cells, finding that the vast majority were from either exhausted or activated phenotypes. In summary, there are a mixture of tumour-reactive and non-tumour-reactive $CD8^+$ T cells within the TIL pool, with tumour-reactive TILs having an exhausted phenotype.

The key tumour-*reactive* TI $CD8^+$ T cells are therefore those of a dysfunctional/exhausted phenotype. As such, these terms are perhaps unhelpful and confusing as these cells are not inert

but have assumed a novel function and play an important role in anti-tumour immunity. This is summarised by a recent review on the topic, which proposes a model whereby antigen recognition drives cell state changes, with tumour-reactive T cells more prone to differentiate towards a dysfunctional state. Intra-tumoural T cell dysfunctionality therefore serves as an indicator for the presence of a tumour-reactive T cell pool, with less dysfunctional cells helping to self-renew this pool[67]. Phenotypic features of dysfunctional, tumour-reactive, CD8$^+$ T cells are summarised in Figure 1.3

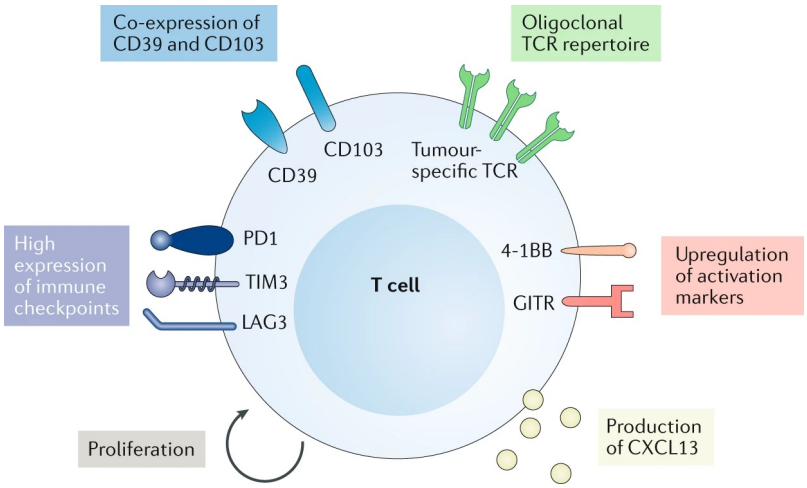


Figure 1.3. Diagram of protein/gene expression markers of dysfunctional tumour-reactive CD8$^+$ T cells - relative to bystander T cells at the tumour site. Taken from [67] and reproduced with licence number 5585241436846.

Despite the importance of the TIL compartment - regardless of the phenotype of key TI CD8$^+$ T cells - a number of findings have shed light on the importance of peripheral and systemic effects of ICB. For example, regression of multiple metastases is observed after ICB, suggestive of a widespread, systemic, effect originating from circulating cells rather than localised tumoural responses which would likely have a greater degree of heterogeneity[71]. This is consistent across other studies, which also observed that a systemic response - defined by sustained proliferation of peripheral immune cells - was necessary for tumour rejection in mouse models[72]. Further, in mouse models and human samples, the importance of the tumour-draining lymph node (TDLN) has been noted with anti-PD-L1 targeted to the TDLN in mice demonstrating tumour control,

and PD-1-PD-L1 interactions in TDLNs in patients with melanoma being associated with early recurrence[73].

A number of studies have now leant support to the theory that reinvigoration and recirculation of *peripheral* T cells is an important component of the response to ICB (further evidence for this is discussed below in section 1.2.3.1, page 19). As such this had led to the development of a model whereby post-ICB, and particularly PD-1 blockade, tumour-extrinsic T cells are reinvigorated, activated and primed peripherally - e.g. in TDLNs - and subsequently traffic to the tumour to mediate their response (Figure 1.4)[74].

In summary, it is likely that ICB has an effect on both TILs and *peripheral* T cells, the latter of which are likely to be as important, if not more so, than the former. Therefore, study of the peripheral blood has the potential to provide deep insights into the anti-tumour T cell response.

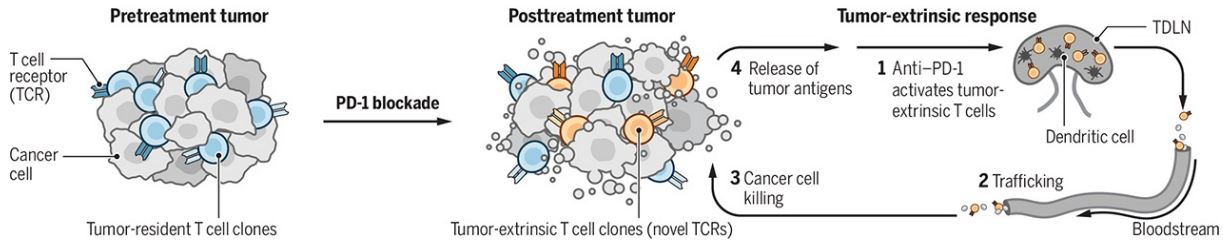


Figure 1.4. Model for recirculation and role of peripheral T cells. Tumour-extrinsic T cells are activated and primed, particularly in the TDLN from where they recirculate and enter the tumour to mediate an anti-cancer response. From [74]. Reprinted with permission from AAAS.

1.2.3 Molecular effects of ICB on T cells

The molecular mechanisms by which ICB exerts an effect on T cells can be considered according to the following domains:

- reinvigoration of T cell exhaustion

- proliferation of stem-like $CD8^+$ T cells
- mobilisation of peripheral T cells
- clonal expansion and persistence of T cells
- other transcriptomic effects of ICB

These effects can impact both TILs and peripheral T cells, and this is considered in the discussion of each of these domains, below.

1.2.3.1 Reinvigoration of T cell exhaustion

An early model for the mechanism of action of ICB - and particularly PD-1 blockade - is via the 'reinvigoration' of exhausted T cells[63,75]. T cell exhaustion can be defined as a dysfunctional state associated with phenotypic changes such as an impairment of effector function, expression of inhibitory receptors and a reduced ability to persist[75,76]. It is a common feature of many chronic infections such as HIV or hepatitis B/C.

A widely-cited paper describing the importance of reinvigoration of exhausted $CD8^+$ T cells (T_{ex}) following PD-1 blockade in melanoma came from John Wherry's group[77]. In this study they profiled (by flow cytometry and cytometry time of flight (CyTOF)) 29 patients with MM, treated with pembrolizumab. Notably, they found that after pembrolizumab, there was an increase in the frequency of $Ki67^+$ $CD8^+$ T cells but these had an exhausted phenotype - compared to $Ki67^+$ cells from healthy donors which had an effector phenotype. Increased Ki67 expression was most prominent in PD-1^+ cells. Further, there were notable increases in proportion of IFNγ-producing PD-1^+CTLA-4^+ and PD-$1^+$$CXCR5^+$ subsets. They also describe a high degree of overlap of responding peripheral clones with those found in TILs. As a result of these findings, the authors conclude that exhausted T cells are a major target of PD-1 blockade. Whilst they were

unable to correlate Ki67 levels with clinical response, they did find that by relating changes to exhausted T cells to overall tumour burden (i.e. high ratio of reinvigoration to tumour burden) significantly correlated with PFS. Nonetheless, these findings have limited clinical applicability and the importance of mitotic cells post-ICB is not unanimously agreed, including in my own work whereby we find that highly mitotic $CD8^+$ T cells are from short-lived and small clones[78].

1.2.3.2 Proliferation of stem-like $CD8^+$ T cells

Whilst 'reinvigoration' is felt to be one possible mechanism of action of ICB, as further understanding has developed, it has become clear that 'exhausted' T cells are a heterogenous group with both terminally exhausted, and progenitor subsets. Indeed, genomic profiling of terminally exhausted T cells suggests epigenetic fixing of their transcriptional state[75]. One of the key transcription factors which defines terminal exhaustion is TOX, which has been shown to result in a fixed transcriptional and epigenetic landscape[79]. TOX expression has been shown within tumour-specific T cells and is a function of chronic TCR stimulation and NFAT activation. Whilst TOX expression mediates an exhausted phenotype and knocking out this gene in mice can abrogate the exhaustion programme, chromatin changes of exhaustion remain and the *tox*-deleted cells are short-lived. As such, the transcription factor TOX is felt to define terminal exhaustion, but it also prevents apoptosis in the context of chronic antigen stimulation[80].

The relative 'permanence' of terminal exhaustion calls into question the ability of T_{ex} to be reinvigorated. Another suggested mechanism for ICB is the proliferation of an exhausted but self-renewing, stem-like, $CD8^+$ T cell subset defined by expression of TCF1. Such a subset has been given various names, but it was recently proposed that 'progenitor exhausted' or T_{pex} was an appropriate term (and which will subsequently be used here)[76].

TCF7 (TCF1 in mice) is a transcription factor, encoded by the gene *TCF7* and first discovered

in 1991[81], which is abundantly expressed in T cells and has a regulatory and self-renewal role. In $CD8^+$ T cells and the context of the TME, TCF1 sustains stem-like T_{ex} TILs (i.e. progenitor exhausted (stem-like) $CD8^+$ T cells (T_{pex})). These $TCF1^+PD\text{-}1^+$ TILs mediate a proliferative response to immunotherapy, leading to the generation of both $TCF1^+PD\text{-}1^+$ self-renewing stem-like TILs and $TCF1^-PD\text{-}1^+$ terminally differentiated cells[82]. It is proposed that the ability of these stem-like, $TCF1^+$ $CD8^+$ T cells (i.e. T_{pex}), to proliferate post-ICB and produce more terminally differentiated cells is a hallmark of a successful immune response following ICB. There are a number of pieces of experimental work to support this model.

Sade-Feldman *et al.* sequenced the transcriptomes of over 16,000 immune cells from 48 resected melanomas from patients treated with ICB. They were able to define two $CD8^+$ T cell states which were associated with either progression or regression of tumours, calling these CD8_G or CD8_B. The 'G' cluster was associated with increased expression of genes linked to memory activation and cell survival - e.g. *IL7R, TCF7, REL, FOXP1, FOSL2, STAT4* - whilst the 'B' cluster was enriched in genes associated with exhaustion - such as *CD38, HAVCR2, ENTPD1, PDCD1, BATF, LAG3, CTLA4*. Cells from the G cluster were enriched in responding lesions, whilst those from the B cluster were found in progression. Crucially, *TCF7* was the top marker associated with response, and they subsequently validated this on an independent cohort - by staining resected tumours for CD8 and TCF7, they were able to show that greater expression of TCF7 correlated with improved outcomes[83]. Simply put, the presence of TCF7 was able to predict response to ICB in MM.

Similarly, Miller *et al.* used a model of chronic viral infection to dissect exhaustion states of $CD8^+$ T cells, finding that there are two distinct states with transcriptional and chromatin structures. The progenitor subset have greater polyfunctionality and ability to persist, whilst the terminally-exhausted subset have greater cytotoxicity and poorer long term survival. These phenotypes

could also be found within tumour models and indeed, in looking at human melanomas, those with a greater proportion of $TCF1^+$ cells had improved PFS[84]. Also using an lymphocytic choriomeningitis virus (LCMV) model, Im *et al.* similarly demonstrated that TCF1 defined a subset of PD-1^+ $CD8^+$ T cells which was almost exclusively responsible for a 'proliferative burst' following PD-1 blockade, resulting in terminally exhausted $CD8^+$ T cells. Notably, this population was found only in lymphoid tissues. There are a multitude of studies of tumours demonstrating the importance of TCF7/TCF1 expression in the response to ICB and supporting the presence of these stem-like T_{pex} in draining lymph nodes[85–88]. Work from type I diabetes mellitus (T1DM) has also demonstrated the role of this transcription factor in autoimmune disease - with $TCF1^{hi}$ T cells found in the peripheral lymph node and $TCF1^{lo}$ cells found in the pancreas[89]. Using transplant models, it is the $TCF1^{hi}$ cells (i.e. T_{pex}) which mediate the auto-immunity and conferred T1DM in mice. The fact that T_{pex} reside in regional lymph nodes and maintain a T_{ex} pool within the TME has been further shown by clonal tracking in resected tissue from patients with NSCLC treated with ICB[90].

In summary, this has led to the proposition of a model of anti-tumour immunity whereby the TCF1/TCF7 high T_{pex} cells self renew in the lymphoid tissues, and proliferate following ICB (Figure 1.5). They subsequently traffic to the tumour, whereby they mediate effector function.

1.2.3.3 Mobilisation of peripheral T cells

Intriguing work from Yost *et al.* published in 2019 provided a parallel mechanism for ICB[91]. Looking at 11 patients with basal cell carcinoma who received PD-1 blockade, they performed scRNAseq and TCRseq on resected tumours. They found that the largest clones had a more exhausted phenotype. Importantly they also found that cells within a clone were more likely to have a similar phenotype than randomly-grouped cells, and that those cells found within a specificity group (as defined by *GLIPH* - see section 1.5.4, page 56) were also more likely to

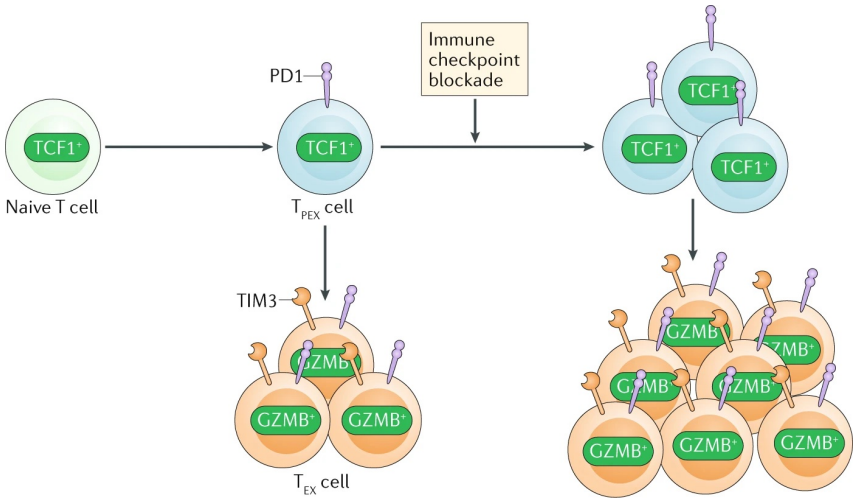


Figure 1.5. Graphic outlining T_{pex} model of immunity - in the case of persistent antigen, TCF1$^+$ T_{pex} cells self-renew and maintain a pool of exhausted effector T cells (T_{ex}). Following ICB, these T_{pex} proliferate and increase the pool of terminal effector cells. Taken from [76] and reproduced with licence number 5585250269386.

share a phenotype than randomly-grouped cells. This suggests that antigen specificity is important in determining cell fate. Further, they then went on to examine changes to TI clones following treatment and found that the clonal repertoire of *exhausted* CD8$^+$ T cells - but not non-exhausted - was largely replaced by novel clones following PD-1 blockade. They were also unable to find much evidence of TILs transitioning from an exhausted to a non-exhausted phenotype post-treatment, supporting the notion that reinvigoration of tumour-infiltrating T cells is a minor mechanism of ICB. They conclude that chronic activation and exhaustion of existing TILs limits their ability to re-invigorate following ICB, and instead, the response is derived from clonal replacement by a distinct repertoire of tumour-specific T cells. They observed a high level of overlap with the peripheral blood, and indeed novel TIL clones *post*-treatment were only detectable in the blood *pre*-treatment, suggesting that the observed 'clonal replacement' might come from peripheral sources.

A subsequent paper by Wu *et al.* in 2020[92] supported this theory. Here the authors sequenced T cells from tumours, normal adjacent tissue and peripheral blood, pre-treatment across four tumour types. They commonly found 'dual-expanded' clones - i.e. those that are expanded in both tumours

and normal adjacent tissue - as well as a high degree of overlap between intra-tumoural clones and the peripheral blood. Notably, those clones that were expanded in both the peripheral blood and within the tumour were predominantly of the T_{eff} phenotype - in contrast to other descriptions of dual blood/tumour expanded clones, where T_{ex} cells were in the majority[70]. Interestingly, T_{eff} clones in the peripheral blood had phenotypic overlap with resident memory T cell (T_{rm}) and effector memory T cell (T_{em}) when found in the tumour - suggesting that peripheral T_{effs} may supply the tumour with cells which subsequently change phenotype. Finally, by integrating their analysis with public datasets, they identified significant correlations between pre-ICB peripheral blood clone size and post-ICB TIL clone size - suggesting that following ICB, intra-tumoural clonal expansion is derived from flux from the peripheral blood.

Recent work (pre-print at time of writing) by Pai, Chow *et al.*[90], using scRNAseq of multiple metastases from three patients with NSCLC treated with ICB (further discussed below, section 1.2.5, page 27), has identified clonally-expanded $CD8^+$ T cells across multiple tumour metastases. Notably, on examination of the proliferation of clone-matched T cells in tumour regions with and without viable cancer cells, there was no transcriptional evidence for increased proliferation of T cells in the context of viable tumours. Further, in viable tumours there was increased expression of chemokines including CXCL9, 10 and 16, with increased expression of the cognate receptors on T cells found within these tumours. This suggests that tumour-induced proliferation of T cells is not necessarily the primary mechanism of clonal expansion, and indeed expanded clones may be migrating into the tumours from peripheral sources.

Together, these findings are supportive of the models discussed above in section 1.2.2 - whereby the importance of peripheral activation and tumour-trafficking of key $CD8^+$ T cells is becoming increasingly realised.

1.2.3.4 Clonal expansion and persistence of T cells

An important effect of ICB is the expansion and maintenance of key T cell clones - observed particularly following CTLA-4 blockade, but also post-PD-1. This is discussed in detail below (section 1.5.3, page 48).

1.2.3.5 Other transcriptomic effects of ICB

Work performed in our lab, to which I contributed, sought to understand transcriptomic effects of ICB on peripheral $CD8^+$ T cells[93]. Here we performed bulk RNAseq on sorted peripheral $CD8^+$ T cells from 69 patients with MM receiving ICB. We identified transcriptomic signatures of ICB response - in particular we noted marked upregulation of both cell division and mitochondrial translation. The pathways modulated by cICB and sICB were similar, although the magnitude of change was markedly greater with cICB. Additionally, we described over 4700 transcripts differentially regulated by outcome following ICB, with pathways upregulated in response to ICB including mitochondrial translation and TCR signalling. In addition to these findings, we also described repertoire features associated with response to ICB - discussed below (section 1.5.3, page 48).

Riaz *et al.* examined the transcriptomic effects of nivolumab on TILs taken from resected melanomas[94]. They identified baseline immune activation - such as upregulation of T cell activation and lymphocyte aggregation pathways - in those patients who went on to have a good clinical response to treatment. Further, treatment with nivolumab resulted in differential regulation of >2500 genes related to pathways including immune regulation, lymphocyte activation, chemotaxis and cytokine signalling. Tumours from patients who responded to treatment had a broader set of upregulated genes than tumours from those who progressed following treatment.

Taken together, these studies demonstrate that ICB has a diverse range of transcriptomic effects

on both peripheral $CD8^+$ T cells and TILs.

1.2.4 Overlap between the peripheral and tumour-infiltrating compartments

As described in many of the studies discussed above, it is now established that there is a high level of overlap between the peripheral blood and TIL compartment, with a large degree of clonal sharing. A number of widely-cited papers have shown this - examples are as summarised below:

- Valpione *et al.*[95] demonstrated that approximately 1/3 of tumour-infiltrating clones are found in the periphery.
- Forde *et al.*[96] examined TCR repertoires in melanomas following neoadjuvant nivolumab treatment and noted a high degree of overlap between tumour and peripheral blood in patients, with a great degree of clonal sharing in those with a major pathological response.
- Huang *et al.*[77] demonstrated that many clones found in the peripheral blood expressing high levels of Ki67 were also found pre-treatment within tumours and these were responding to PD-1 blockade (as defined by HLA-DR and CD38 expression, as well as Ki67).
- Yost *et al.*[91] identified that 41% of TIL TCRβ clonotypes could be detected in peripheral blood, and represented all TIL phenotypes. Further, novel TIL clones *post*-treatment were detectable in the blood *pre*-treatment. These findings led the authors to conclude that novel TIL clones might be recruited from peripheral sources.
- Wu *et al.*[92] found a high degree of overlap between TILs and clones in the peripheral blood across multiple tumour types, with a high degree of correlation between intra-tumoural and peripheral blood clonotypes.
- Joshi *et al.*[97] reported that they were able to identify many expanded intra-tumoural TCR

in the peripheral blood at multiple time points, including at tumour resection.

- Lucca *et al.*[98] performed paired single cell sequencing of matched tumour and peripheral blood samples in 12 individuals with MM. They found that clones which overlapped between tumour and peripheral blood had a higher cytotoxic gene expression profile, whilst those that were found exclusively in the tumour had a more exhausted profile. Further, the cytotoxic signature of intra-tumoural T cells increased following ICB.
- In my own work, I also find a high degree of overlap between the tumour and peripheral blood, particularly for key clones, in data that is presented in Chapter 4 (section 4.3.8, page 135).

In summary, the importance of the peripheral blood T cell repertoires is clear - both in terms of providing a readily accessible 'window' into the tumour and also because these cells are likely key targets for ICB.

1.2.5 Long term persistence of CD8$^+$ T cell clones

Whilst the studies discussed above examine changes to CD8$^+$ T cells in the relative short term post-ICB, long term changes to CD8$^+$ T cells have only been addressed in a handful of studies. In Cha *et al.*'s work from 2014[99], an overall survival benefit was seen in those individuals with MM treated with anti-CTLA-4 where there was maintenance of large, pre-existing clones in the peripheral blood, whilst those in whom there was a decline in size of large clones had worse survival[99]. However, this study only compared pre-treatment bloods with those taken one month post-treatment.

In the paper by Oliveira *et al.*, also discussed above (section 1.2.2), they briefly examine persistence of CD8$^+$ T cells clones in the peripheral blood, finding that both TCRβ and T cell receptor alpha chain (TCRα) chains persist at stable levels long term in the peripheral blood. They

further identified that those with poorer disease outcomes (death from progressive disease) had a higher proportion of their circulating TCR overlapping with the TCR found on exhausted TILs. Nonetheless, they performed bulk TCRseq on the peripheral blood and tied the circulating phenotypes to the TIL phenotypes by way of clonotype matching - they did not *directly* describe the phenotypes of the long term circulating T cells.

A recent piece of work by Pai *et al.*, still in pre-print at time of writing[90], has shed some more light on clonal persistence - albeit in NSCLC. In this work, they performed scRNAseq on 31 tumour regions from three patients who had resection for progressing lung cancer post ICB. All patients had a mixed response, with some progressing and some responding lesions. Of note, there was extremely limited TCR overlap between patients. They collected blood up to 1013 days following commencement of ICB and were therefore able to track clonal persistence over a prolonged period. They found that there was a large degree of persistence of 'ubiquitous' clones (i.e. those found in the peripheral blood, normal adjacent tissue and tumour of the same patient). On the whole, these clones were large. In one of the three patients, there was a loss of persistence of ubiquitous clones, which correlated with disease recurrence. In the other two patients, there was persistence of ubiquitous clones with associated disease control. By further examining the phenotypes of persistent clones, they describe that cytotoxic and exhausted $CD8^+$ T cells - as well as those with a tumour-reactive phenotype (as defined elsewhere[67]) - declined at the time of metastatic resection, suggesting that loss of peripheral persistence coincided with disease progression. However, similar to Oliveira *et al.*, the peripheral blood phenotype of persistent clones was derived based on their *tissue* phenotypes, rather than directly profiling the peripheral cells.

A paper by Han *et al.* examined phenotypes and clonal identity of $CD8^+$ T cells long term in those with a CR to MM across tumours, skin and the peripheral blood[100]. They found a positively-

prognostic phenotype of TI $CD8^+$ T cells associated with IFNγ production and found that clones with this phenotype persisted long term, particularly in skin compartments. They describe that TI and skin clones with matching TCR persist - and are expanded - long term in the peripheral blood (up to 9 years post excision of melanoma). Further, they describe the phenotype of long term peripheral clones as T_{em}[100]. This is a highly-relevant study looking at TCR across multiple tissue compartments - however, whilst the long term clonotype data is from seven patients, they were only able to describe the long term peripheral phenotype in four clones from one individual. Hence, this description should be interpreted with some caution. Further, in a similar manner to other studies, the long term phenotype is defined based on scRNAseq of the same *clone* at prior time points - they did not phenotypically describe long term persistent clones directly at the later time points.

Finally, work in NSCLC also described long term persistence of TCR - particularly ubiquitous TCR (i.e. those found in every metastasis) - in the peripheral blood[97]. Indeed, the proportion of these TCR decreased at the time of surgical resection but remained detectable up to 2 years later. For those patients with recurrence, the patterns of TCR change were variable - with ubiquitous TCR decreasing in some cases and increasing in others.

In summary, whilst there are examples of work describing long term persistent clones in response to ICB the literature on this topic is extremely limited. Specifically, there is very limited understanding of the phenotypes of long term persistent peripheral clones and their role following a complete response to treatment.

1.2.6 Tertiary lymphoid structures

As outlined above, an influx of tumour-extrinsic T cells post-ICB into the tumour has been associated with an improved response. Whilst draining lymph nodes and peripheral blood have

been considered important sources of T cells, it is possible that tertiary lymphoid structures (TLS) also play an important role. Further, whilst the focus of this thesis is $CD8^+$ T cells, the importance of other immune cells - and B cells in particular - should not be ignored. This is particularly relevant for some of my recently-published work, presented in Chapter 6, in which we demonstrate a key role of B cell *IL7* expression in the development of irAEs[101].

TLS are aggregates of lymphoid-like tissue, primarily comprised of B cells, which form in inflamed tissues including cancer, where their presence has been associated with a favourable prognosis[102]. Further, the presence of tumour-associated B cells and TLS has been associated with improved outcomes following ICB for MM[103,104]. Notably, in Cabrita *et al.*'s work, it was noted that B-cell-rich tumours associated with higher levels of $TCF7^+$ T cells - potentially suggestive of these structures, and in particular B cells, providing a locus for patterning T cells in the anti-cancer response[103]. Notably, 'dysfunctional' $CD8^+$ T cells which are felt to be most tumour-reactive (as discussed above in section 1.2.2, page 15) acquire the ability to express and secrete CXCL13 - a B cell chemoattractant which may aid in the formation of TLS.

1.3 Biomarkers of response to ICB

Despite the remarkable successes wrought by the introduction of ICB, the majority of patients (across all tumour types) and up to half of those receiving ICB for MM do not derive any benefit from this treatment. As such, predictive biomarkers are urgently required[105] but on the whole only exist in the experimental setting. Only three biomarkers (across five assays) have been approved by the Food and Drug Administration (FDA) for clinical use - these are assays for PD-L1, tumour mutational burden (TMB) and micro-satellite instability (MSI) (Figure 1.6). The evidence for these is discussed below, alongside other promising experimental approaches.

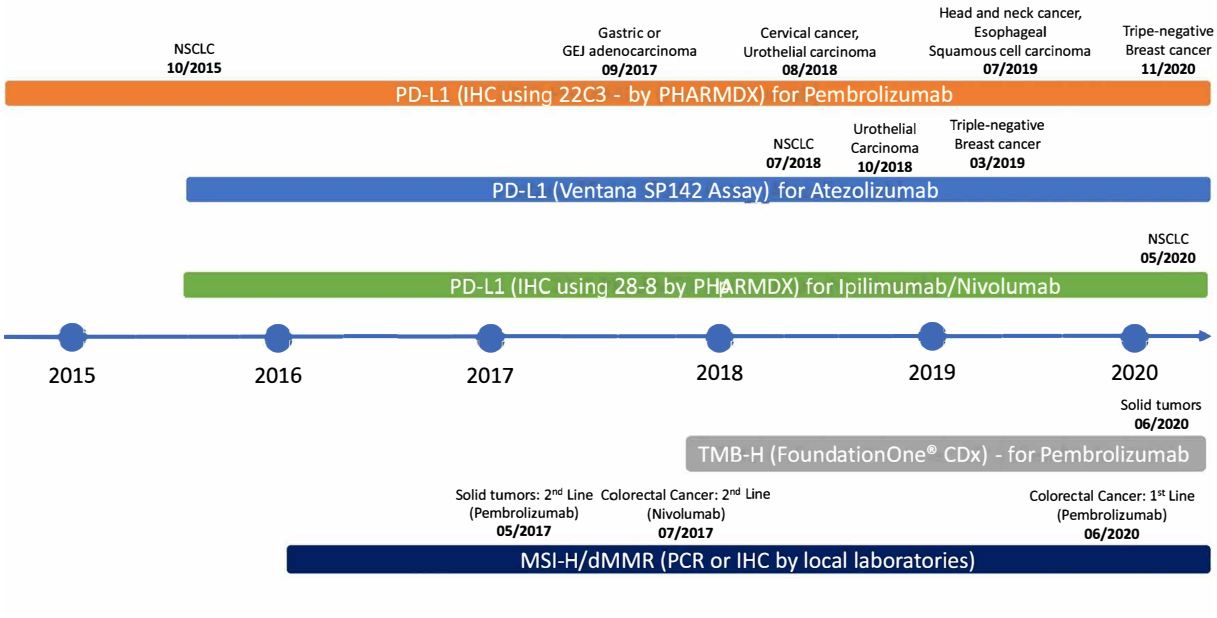


Figure 1.6. Timeline of ICB biomarker approval by the FDA. Adapted from [106] under a creative Commons CC BY licence.

1.3.1 Tumour genetic factors

Antigen presentation by tumours on MHC class I molecules is, unsurprisingly, a key determinant of anti-tumour immune responses. Tumours can present either neoantigens, mutated proteins generated as a result of non-synonymous somatic mutations, or non-mutated self-antigens[107]. Where the latter are presented in an inappropriate context (for example the tumoural presentation of gamete-associated antigens) these can lead to immune recognition. Such antigens can be referred to as cancer testis (CT) antigens and have been favoured as 'public' targets for the tumour immune response[108]. However, despite their promise, no significant outcome-associated markers have been identified and indeed some CT antigens have a negative prognostic association, such as the 'anti-CTLA-4 resistance-associated MAGEA' (CRMA) cluster. Expression of this subset of eight genes from chromosome Xq28 predicted resistance to CTLA-4 but not PD-1 blockade - thought to be due to effects on autophagy and antigen processing[109].

The number of non-synonymous single nucleotide variants within tumours - referred to as TMB - can be posited to affect the chances of generating novel antigens which become immunogenic (neoantigens). This is borne out by the observation that those tumours with very high TMB, such as melanoma or NSCLC, have some of the highest response rates to ICB (Figure 1.7). In melanoma, baseline TMB positively correlated with clinical response following ipilimumab treatment[110,111], with similar observations in NSCLC[112] and subsequently across a wide range of tumours[105]. Nonetheless, the relationship between TMB and outcome is not straightforward, with some tumours, such as mRCC, 'outperforming' their TMB - with a low mutational rate but high ICB response. Further, within individual tumour types, a high TMB does not guarantee a good response to treatment. As such, when considering biomarkers for ICB response in general, and TMB in particular, it may be that a single time-point is insufficient (so-called *static biomarkers*) and instead how markers change *over time* and in particular *following ICB* might be more informative (so-called *dynamic biomarkers*). For TMB, work by Riaz and colleagues[94] demonstrated this by showing that pre-treatment TMB only associated with OS in the ICB-naive group, whereas a decrease in TMB from pre-treatment to on-treatment, was strongly associated with outcome in all patients, with a marked decrease seen in those with a CR or partial response to treatment.

The relevance of TMB can also be taken in the context of how it is found within tumours. Work by the TRACERx consortium has influenced the field of intra-tumoural heterogeneity (ITH), solidifying the concepts of 'clonal' and 'subclonal' neoantigens[114,115]. Clonal mutations, leading to clonal neoantigens, are found in all tumour cells, whereas subclonal mutations/neoantigens are found in only a subset of tumoural cells. Notably, lung tumours enriched for clonal neoantigens were found to demonstrate improved sensitivity to PD-1 and CTLA-4 blockade compared to those with more subclonal mutations[114]. Further, infiltrating $CD8^+$ T cells primarily recognised clonal antigens, and were highly expressive of PD-1, suggesting that neoantigens that are more widespread within the tumour attract an immune response, which is then sensitive to ICB.

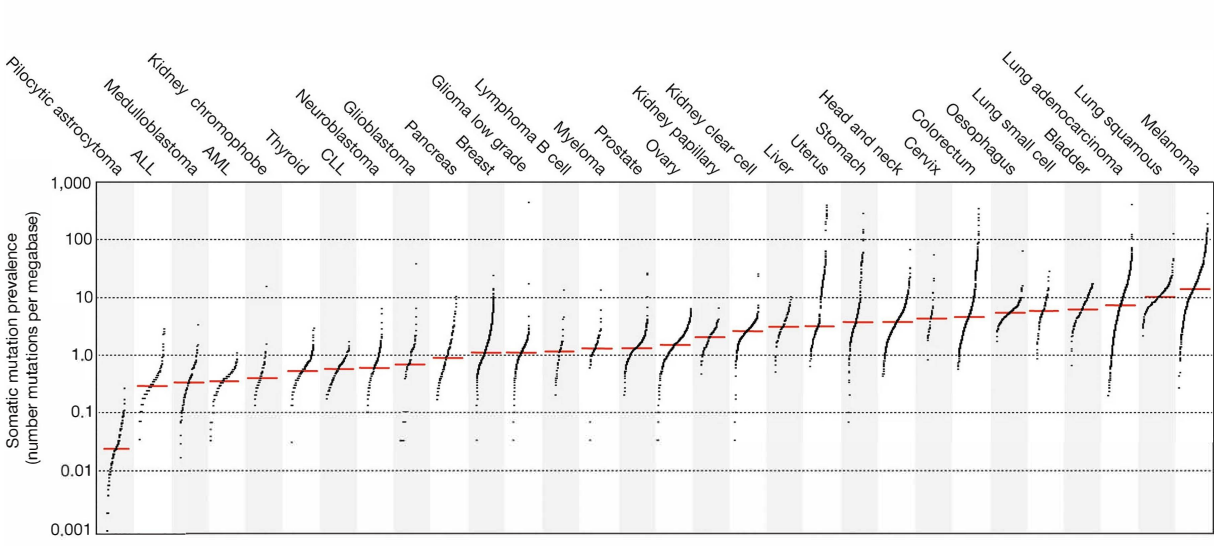


Figure 1.7. The number of somatic mutations across a number of human cancer types, with the number of mutations per megabase plotted on the y-axis. The red lines represent the median for each tumour type. Taken from [113] and reproduced with licence number 5585250647071.

As well as TMB as a general association with outcome, there are some specific mutational signatures with implications for ICB treatment. One such example is MSI caused by deficiencies in DNA mismatch repair (MMR). Of great interest is the fact that tumours with MMR are susceptible to ICB treatment regardless of tissue of origin. This was first described by Le and colleagues, who conducted a (reasonably small) clinical trial comparing outcomes following pembrolizumab in colorectal and non-colorectal tumours that were MMR-deficient versus those which were MMR-proficient[116]. They described a striking difference between groups, with 78% PFS at 20 weeks in the MMR-deficient group and 11% in the MMR-proficient group (HR progression or death 0.10, p<0.0001). Further work by the same group showed a similar effect across 12 different tumour types[117]. This paved the way for FDA approval of PD-1 blockade for MSI-positive cancers regardless of histology, and the licensing of pembrolizumab for MSI-positive colorectal cancers in the UK (NICE guidance TA709). Hence MSI has become a genetic biomarker for response to ICB (Figure 1.6).

1.3.2 Germline genetic factors

As well as tumour genetic factors, patient germline genetic factors may influence response to ICB. Supportive of this, high heritability has been described for a number of immune traits in the context of cancer, including subset abundance of $CD8^+$ T cells, NK cells, and T helper cells as well as IFN-related signatures and antigen presenting machinery[118]. Genetic variants were observed to affect IFNγ signalling and immune infiltration, with a genetic link observed between autoimmune risk loci and the tumour immune response, a finding also reported by Shahamatdar *et al.* who describe a link between a rheumatoid arthritis polygenic risk score and $CD8^+$ T cell infiltration[119]. However, these traits have yet to be validated as biomarkers for the ICB response.

Germline HLA status has also been correlated with response to ICB, with evidence that loss of heterozygosity (LoH) at one or more HLA-I alleles is associated with a poorer OS following ICB. This effect was described in a widely-cited paper from Chowell *et al.*[120] where 1535 patients were HLA-I genotyped and their outcomes ascertained. They had two cohorts of patients - cohort 1 (n=369, MM and NSCLC) and cohort 2, which served as a validation cohort (n=1166, multiple different cancer types). They found that LoH at least one locus was associated with an increased hazard for death in cohort 1 (HR=1.40, 95% CI 1.02-1.9, p=0.036), validating in cohort 2 (HR = 1.31, p=0.028). Within this same paper, they also describe that carriage of the HLA-B44 super-type had improved survival and that there was greater TCR clonality in those heterozygous at all three HLA loci. However, whilst this work does provide some of the first evidence for a germline genetic influences on the ICB response, and has also been reported elsewhere[121], many others have failed to replicate these results - most prominently Chhibber *et al*[122]. In their work, they analysed data from 17 clinical trials for pembrolizumab and did not find a significant effect of LoH at HLA-I alleles for either OS, PFS or best overall response (n=3248, 3288 and 3333 respectively). They were unable to find any significant association either when looking at

individual tumour types, or when looking across all patients. They were unable to adequately explain this failure to replicate, although they did note that the original Chowell paper[120] did not account for differences in ethnicity. Nonetheless, a number of other investigators were also unable to replicate the original findings in NSCLC[123,124], casting doubt on the importance of LoH at HLA-I loci as a biomarker for ICB response.

1.3.3 The tumour and immune microenvironment

One of the most established existing biomarkers for response to PD-1 blockade is tumoural PD-L1 levels, and it stands to reason that interruption of the PD-L1-PD-1 axis would be more effective if PD-L1 expression by tumours is a major mechanism of immune resistance. To this end, numerous studies have demonstrated associations between high levels of PD-L1 on tumours and response to ICB[27,105,125] and three such assays are now FDA-approved[126] (Figure 1.6) with clinical decision-making in NSCLC being guided by PD-L1 positivity. If PD-L1 is found on at least 50% of tumour cells, pembrolizumab can be given first line. If it is present in at least 1% of cells, it can be used second-line.

Despite these successes, however, a number of other studies have reported no association between PD-L1 staining and outcome and the relationship is therefore complex[127]. The reasons for this are multifactorial but include temporal expression of PD-L1, different methods of detection and the importance of expression on different cell types. As a result, different assays have been developed, including calculating the tumour positive score (proportion of positive tumour cells) and combined positive score (accounting for both tumour and immune cells). These are employed by the pharmDx assays (Figure 1.6). In some cancers - including urothelial and melanoma - PD-L1 expression by TILs, but not tumour cells, is associated with response to ICB[105]. The Ventana assay utilises this to calculate PD-L1 expression on TILs (Figure 1.6).

As discussed in section 1.2 (page 14), the importance of TILs is well-established and a host of investigators have tried to characterise TIL states associated with outcome. As well as T cells, the importance of other immune cells in the tumour microenvironment has been described, albeit not translated into a distinct biomarker. For example, intra-tumour myeloid cells and their derivatives have been shown to have an inhibitory effect[94,128], with an association between tumour-associated macrophages and a poor response to ICB described in MM[129]. Suggested mechanisms for this include anti-PD-1 antibody sequestration[130].

Characterisation of the tumour-immune micro-environment has led to the development of the 'Immunoscore' which is based on quantities of $CD3^+$ and $CD8^+$ T cells at the tumour core and margin[131–133]. Now available as an *in vitro* diagnostic test for colorectal cancer[134], it can aid in staging and prediction of response to some chemotherapies, although is not routinely used in clinical practice in the UK[135].

1.3.4 Peripheral blood factors

An 'ideal' biomarker would be cheap, quick and easy to sample - this is where a number of existing tumoural or genomic metrics are lacking. To repeatedly sample tumours is invasive and impractical, whilst Next Generation Sequencing (NGS)-based tests remain expensive. Further, all biomarkers currently approved are based on tumour, rather than host, factors and are static (Figure 1.6). As such, a dynamic biomarker easily obtained on existing peripheral blood assays is urgently sought.

1.3.4.1 Immune cell counts

One of the most prominent such biomarkers is the NLR - i.e. the neutrophil count divided by the lymphocyte count - with a high value generally associated with a poor prognosis, thought

to reflect an unfavourable balance between inflammation and the adaptive immune response. A meta-analysis of the utility of NLR demonstrated its relevance[136]. Here the authors analysed 27 studies across mRCC and MM, incorporating 3891 cases. They found that 'high' pre-treatment NLR was associated with poorer overall survival (pooled HR 2.18, p<0.0001). However, only four studies were trials of ICB, with the remainder examining anti-VEGF treatment. Nonetheless, the effect was present when just examining the ICB trials (HR 2.16, p<0.001). The median cut-off for NLR being 'high' was 3.02 with the mode being 3; however, changing the cut-off did not substantially affect the findings[136]. They also included two trials of other treatments (IL-2 and oncolytic viruses[137,138]) finding no association between pre-treatment NLR and outcome in their meta-analysis. As such, whilst this marker is a useful pre-treatment parameter of subsequent outcome, it is relatively non-specific across multiple cancers and treatment, and does not provide insight into biological changes following ICB.

A number of other peripheral blood biomarkers of response to ICB have been described (Figure 1.8). These include absolute proportions as well as ratios of a number of circulating immune cells. For example, a higher peripheral T_{cm}:T_{eff} ratio was observed in patients with NSCLC and MM with an inflammatory tumour phenotype. A higher ratio correlated with intra-tumoural PD-1 expression and associated with improved PFS[139]. Additionally, a lower proportion of monocytic myeloid-derived suppressor cells (mMDSCs) was associated with improved OS following ipilimumab treatment[140]. Further, a number of repertoire features of $CD8^+$ T cells have been correlated with outcome following ICB - as discussed below (section 1.5.3, page 48).

1.3.4.2 Circulating molecules

As well as levels of circulating immune cells, soluble plasma molecules can act as a biomarker of response. Similar to its correlation with irAEs (section 1.1.4.3), a fall in plasma IL-6 levels from pre-treatment to on-treatment was shown to be associated with improved PFS in a small

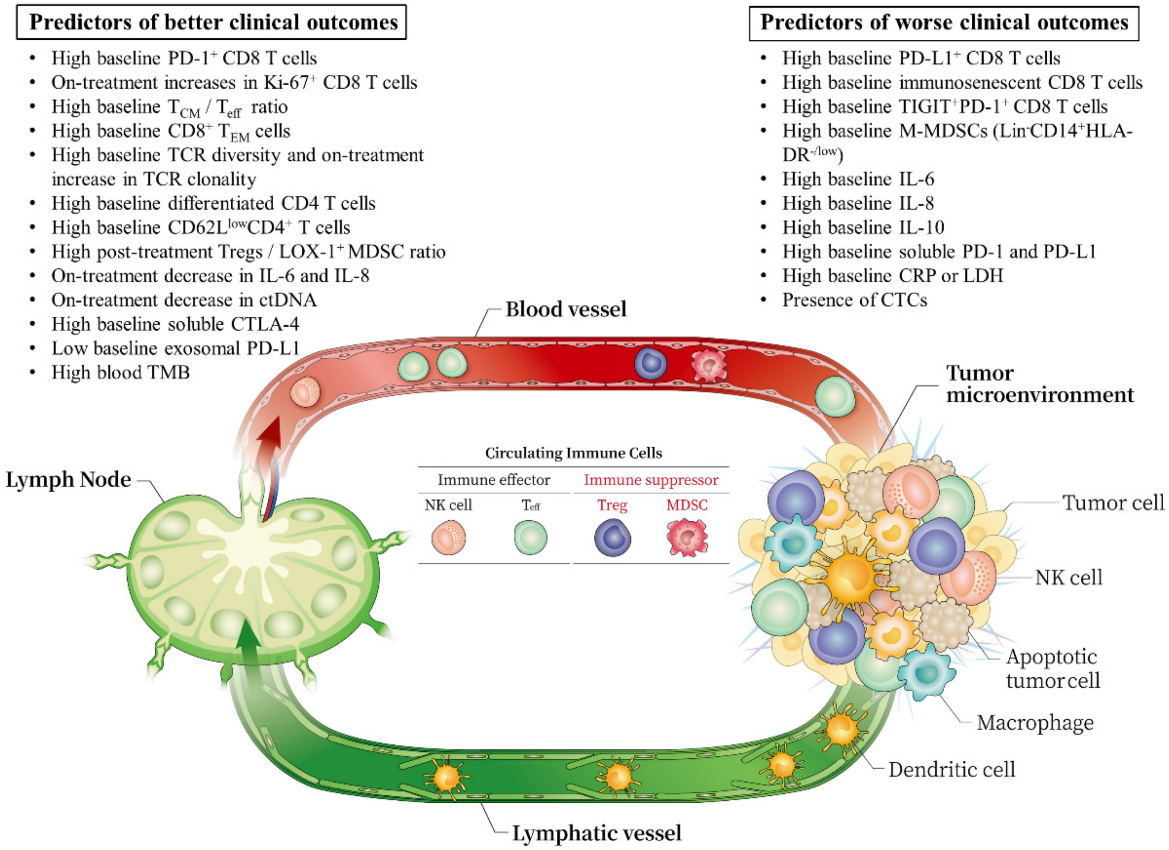


Figure 1.8. Summary of peripheral biomarkers of response to ICB, taken from [141] under a creative Commons CC BY licence. CTC - circulating tumour cell.

(n=47) cohort of patients with NSCLC (fall defined as >40% or more, PFS in those with a fall was 11 months, compared to 5 months in those without a fall)[142]. However, this was a small cohort with an extremely heterogenous range of post-treatment blood sample points (17-196 days) and no external validation was provided. Nonetheless, higher baseline IL-6 has been described as a poor prognostic factor in MM[143,144]. Similarly, IL-8 levels - a tumour-secreted molecule important for neutrophil chemotaxis and local inflammation - have been associated with outcome, with high baseline levels poorly prognostic, whilst on-treatment decreases are associated with favourable responses across multiple tumour types[145,146]. Other correlates with outcome include IL-10, C-reactive protein (CRP) and lactate dehydrogenase (LDH)[147].

Other circulating markers which have been investigated as potential biomarkers include soluble

immune checkpoints. High levels of soluble CTLA-4 at baseline correlate with OS in patients with melanoma treated with ipilimumab[148], whilst higher levels of soluble PD-1 and PD-L1 at baseline have correlated with poor response to anti-PD-1 treatment in melanoma[149]. Circulating tumour DNA (ctDNA) has also shown promise as a marker of response to pembrolizumab and other ICB across a range of tumours - both as a static, pre-treatment, biomarker and as a dynamic marker[150,151]. Similarly, circulating tumour cells (CTCs) have been investigated as a potential biomarker, with a fall in CTCs during ICB treatment for NSCLC correlating with outcome[152].

1.3.5 Other factors

The microbiome has long been demonstrated to influence immune functioning and indeed it has been demonstrated that specific GI bacteria can have an effect on ICB response with adoptive transfer in mice leading to improved treatment sensitivity. Whilst these have yet to be developed into biomarkers or adjuncts to therapy in humans, this is an exciting prospect[153–155].

1.4 The T Cell Receptor (TCR)

1.4.1 Thymic development and V(D)J rearrangement

The TCR is the functional receptor by which T cells recognise their cognate antigen. Approximately 90-95% of TCRs are composed of an α and β chain, with up to 10% of T cells carrying a γ and δ chain. $\gamma\delta$ T cells do not form a major component of this thesis and are not discussed in further detail.

The TCR is produced during thymic development, with the TCRβ chain forming first - during the double-negative stage of T cell development. The TCRβ gene locus consists of 52 variable (V) gene segments, two diversity (D) gene segments, 13 joining (J) segments and two constant

regions[156]. For TCRβ chains - which incorporate a V, D and J segment, D-J rearrangement occurs first, where a D gene segment is juxtaposed to a short J segment. This is an error-prone process with the addition of random nucleotides at the joins between gene segments, thus generating further diversity. Following this, a V segment is attached to the 5' end of the DJ segment. As the V genes are spread over a large region (∼0.7 megabases for TCRβ), the process for V gene joining occurs by looping. The mechanics of rearrangement are mediated by RAG enzymes, which introduce double strand DNA breaks at recombination signal sequences (RSS) which flank all TCR segments[157]. The result of this recombination leads to a functional VDJ_β exon, which is transcribed and spliced to a constant region, resulting in mRNA which can be translated into the TCRβ (Figure 1.9a). Following the production of a functional TCRβ, it combines with an invariant partner α chain (pTα) and CD3 molecules. This is expressed at the cell surface and stimulates rapid cell proliferation, expression of both CD4 and CD8 and progression to the double positive stage of thymocyte development. Failure to produce a functional TCRβ leads to cell death[156].

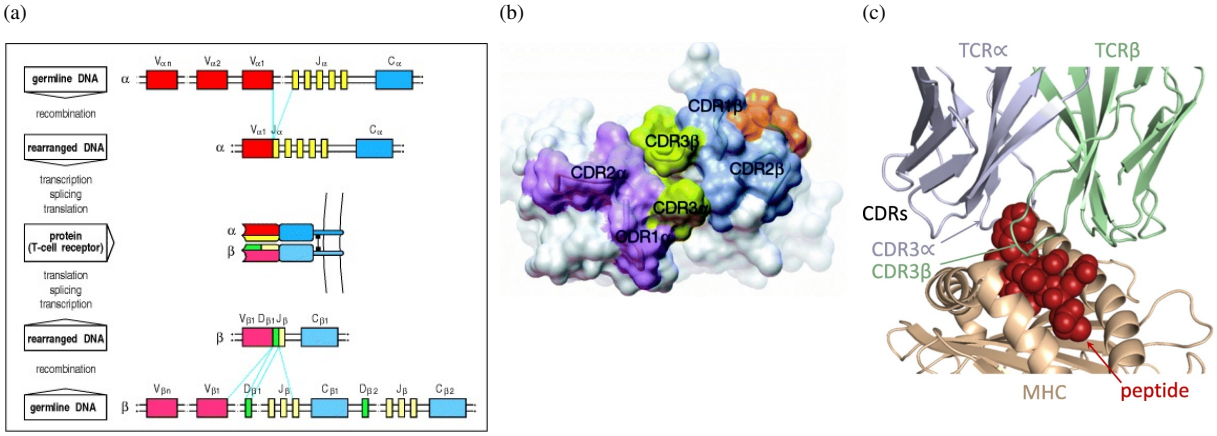


Figure 1.9. (a) Process of V(D)J recombination for TCRα and TCRβ chains. The rearranged DNA is then transcribed and spliced to produce mRNA that contains just the V and C regions. Taken from [156], NCBI Bookshelf content in the public domain (no licence required to reproduce). (b) 3D crystal structure of TCR showing CDR regions. Taken from [158] and reproduced with licence number 5585260124636. (c) 3D protein structure of TCR showing how it is the complementary determining region 3 (CDR3) region - in particular that of the TCRβ - that contacts the peptide bound to major histocompatability complex (MHC). Taken from [159] under a creative Commons CC BY licence.

In the double positive stage TCRα chain rearrangement occurs. This follows a similar process, although the alpha chain has no diversity (D) gene and so there is only VJ joining. There are over 70 V genes and 61 J genes for the TCRα chain. Notably, many T cells have in-frame rearrangements on both chromosomes and so can produce two α chains - this is possible because the generation of a productive TCR does not stop alpha chain rearrangement. However, subsequent development and positive selection (whereby only TCR that can weakly bind self-peptide:self-MHC complexes are selected) ensures that each T cell only has one specificity, even in the presence of two alpha chains[156].

Upon translation and combination of an α and β chain, the TCR enters the plasma membrane and folds - creating three loops, or complementarity determining regions. CDR1 and 2 loops - which are formed from the V genes of the TCRβ and TCRα - fold to the periphery and contact primarily with the MHC component of the peptide-MHC (pMHC) complex. The third loop - CDR3 - is highly variable and is contributed to by the D and J segments. It is this part of the TCR - and particularly the TCRβ chain - that contacts the antigen in the peptide binding groove of the peptide-MHC complex (pMHC) complex[156–158] (Figures 1.9b and 1.9c).

Diversity in the TCR is therefore achieved in a number of ways - firstly, the rearrangement and use of different gene segments; secondly, the insertion of random nucleotides during the joining events and thirdly, the combination of both the TCRα and TCRβ chain. It is estimated that there are $>10^{15}$ unique TCR in a human T cell repertoire[160].

1.4.2 The MHC and antigen recognition by TCRs

TCRs do not recognise whole proteins or antigens, but rather bind to short peptides (epitopes) expressed on MHC molecules. CD4 (and therefore $CD4^+$ T cells) binds to MHC class II - which typically is found primarily on antigen presenting cells and presents extracellular derived antigens.

CD8 binds to MHC class I which typically presents intracellular (self/viral/tumour) antigens and is found on all cell types. MHC class I molecules are comprised of an alpha chain - encoded at in the MHC genetic locus on chromosome 6p21.3 - and an invariant chain β_2 microglobulin which is encoded on chromosome 15. When folded, two domains of the alpha chain - α_1 and α_2 - form the walls of a cleft on the surface of the molecule, and it is here, in a groove, that the peptide sits. Peptides that bind to MHC class I molecules are typically between 8-10 amino acids in length, with hydrophobic or basic residues at the carboxy terminus[156]. The length of peptide that can bind to MHC class II is less constrained. Peptide-MHC binding is stable, once bound to MHC the peptide remains in place until the entire complex is degraded. Indeed, MHC class I molecules are unstable in the absence of bound protein and rapidly degrade. When the TCR binds to a peptide-MHC complex, the orientation of binding is very consistent. The variable (V) alpha and beta domains contact with the bound peptide - the V_α primarily at the amino terminus and the V_β at the carboxy terminus. Both chains also interact with the α helices of the MHC class I molecule with the CDR1 and CDR2 regions of the TCR in close contact with the pMHC complex. As such, the specificity of the TCR is for *both* the antigenic peptide *and* its presenting MHC molecule. As a result, the HLA type of the individual will have a direct bearing on the TCR repertoire present and HLA type needs to be considered when analysing TCR antigen specificity or repertoires.

1.4.3 TCR signalling

Whilst the TCR (i.e. $\alpha\beta$-heterodimer as described above) is capable of recognising antigen bound to MHC, it is unable to signal that antigen is bound. Rather, it relies on accessory proteins - these are invariant and consist of a CD3 $\gamma\delta\varepsilon$ and ζ chains - collectively making up the CD3 complex[161]. The CD3 complex has both transmembrane and immunoreceptor tyrosine-based activation motif (ITAM) domains in their cytoplasmic tails responsible for downstream signalling. The first event in TCR signalling occurs via phosphorylation of tyrosines in ITAMs via src-family kinases,

specifically Lck which is constitutively associated with the cytoplasmic domain of CD4/CD8[156]. When a T cell binds to a target cell expressing a complementary pMHC complex, receptor clustering occurs with both the TCR and the CD4/CD8 co-receptors. This brings the Lck kinase in close proximity to the ITAMs and other targets on the cytoplasmic domains of the TCR/CD3 complex, thus triggering a downstream signalling cascade mediated by phosphorylation events[156]. Whilst this process results in signalling from the TCR, a number of other signals are required for robust T cell activation - for example co-stimulation via cell surface receptors such as CD28 and a third signal such as that mediated by pro-inflammatory cytokines (e.g. IFNγ)[4].

1.5 T cell receptor repertoire analysis

The uniqueness of each TCR as generated by V(D)J recombination means that each TCR can be considered a 'molecular barcode', identifying not just a receptor but a group of cells - all sharing the same receptor - i.e. a T cell clone. Understanding receptor use, phenotypes of different clones and changes over time in different disease states and with treatment has the potential to provide deep insights into the immune response. As a result, the study of immune repertoires has gained attention as NGS and high-throughput technologies have enabled sequencing of large quantities of immune receptors - a process termed TCRseq. As this field has developed, there are an increasing array of technologies to facilitate this sequencing, as well as analytical approaches.

1.5.1 Molecular biology approaches for TCRseq

There exist multiple technologies available for TCRseq. At the most simple level, the starting material can either be messenger RNA (mRNA) or genomic DNA (gDNA), with advantages and disadvantages of each. Using mRNA is more sensitive due to the multiple copies of each transcript. Further, unique molecular identifiers (UMIs) can be added during the reverse transcription step,

thus minimising PCR biases. gDNA has the advantage that there are a stable number of copies per cell and so the number of copies of each chain directly correlates to the number of cells present in each clone. Whilst this is often assumed for mRNA approaches, it is a limitation. However, DNA approaches do not take allelic exclusion into account and so can overestimate diversity[162].

There several different approaches for generating bulk TCRseq libraries. One approach is multiplex PCR - whereby a set of forward primers for all known V genes and reverse primers for either J or C regions is used[163]. For RNA-based approaches, fewer C primers are needed due to splicing of this region. However, with multiplex PCR, the use of primer sets that target different regions of the V gene can result in shorter reads which may not capture the entire V region; although the CDR3 section is usually sequenced[164]. One of the most high-profile multiplex PCR approaches is the ImmunoSEQ platform offered by Adaptive Biotechnologies which provides 'end to end' TCRseq from biological specimens and also provides a bioinformatic pipeline for processing and analysing data. It has been used widely, and this technology features in many major publications in the field. Notably, this platform only sequences the TCRβ chain and as such has driven the general trend noted in the literature where repertoire analysis is performed solely on TCRβ data. It also comes with an extremely high per-sample financial cost.

An alternative to multiplex PCR is rapid amplification of 5' complementary DNA ends (5'RACE)[165]. Here, RNA is reverse transcribed and un-templated C nucleotides are added to the 3' end of the cDNA during this process. A template switch oligonucleotide containing a poly(G) stretch anchors to this, allowing switching of templates and extension of cDNA and addition of an adapter sequence. Therefore, subsequent PCR steps only need to include primers to the adapters and constant region. A number of commercially available as well as academic protocols use this strategy[166]. 5'RACE approaches can give longer reads and so may be more suitable if CDR1/2 analysis is desired; however, typically this approach requires higher quality RNA[164].

Qiagen has a commercially-available kit - QIAseq Immune Repertoire - which uses a similar approach to 5'RACE but without including a template-switch step. First RNA samples are reverse-transcribed to cDNA before second strand synthesis, end repair and A-tailing of the double-stranded cDNA. An adapter is then ligated to the 5' end, containing a 12-base UMI (discussed below) and a sample index. PCR can then occur using a primer specific to the C region, and one universal primer complementary to the adapter. It is this method that I have used in experiments for this thesis (Chapters 4 and 6).

All these approaches have the potential to introduce errors - either through PCR biases or sequencing errors. As such, the inclusion of UMIs is one strategy to try to mitigate this. UMIs are a sequence of random nucleotides inserted during library construction - either during reverse transcription or following adapter ligation in the example of the QIAseq approach[167]. Such an approach can reduce errors in two ways - by counting the number of occurrences of each UMI, rather than overall reads, PCR bias and amplification errors can be minimised. Secondly, by grouping together TCR with the same UMI, sequencing errors can be minimised as consensus of sequence within each group can be determined and erroneous calling of additional clones can be reduced. Indeed, the utilisation of UMI groups enabled me to troubleshoot some quality control (QC) issues I had with my TCRseq data (see section 4.3.1.1, page 116).

As discussed, all methods have their advantages and disadvantages, with variability in the repertoire information generated by each approach - there is no field 'gold standard'[168]. In a recent benchmarking, Barennes *et al.* compared multiple methods for TCRseq[166]. Whilst they found that each approach had its own unique biases, they also determined that multiplex PCR methods were more likely to skew towards a particular V gene, whilst UMI-based approaches were less able to detect rare clonotypes. They conclude that the approach used depends on the biological question, but if the object is to reconstruct a true overall representation of the repertoire, or find TCRs of

interest from clonal expansion, then 5'RACE approaches with UMI correction is likely to be most appropriate as it more accurately reports clonal frequencies than other approaches[164,166].

Finally, as well as the above methods which all generate TCRseq libraries from bulk samples, there are a range of single-cell approaches available[164]. The underlying biochemistry uses similar approaches; for example, 10X Genomics' Chromium system - one of the most widely used - uses a 5'RACE based approach on mRNA isolated from single cells[169]. During the second strand synthesis step, a template switch mechanism introduces an oligonucleotide sequence which is used for a subsequent forward primer during V(D)J amplification steps, with the reverse primer complementary to the TCR constant region[170]. Performing simultaneous transcriptome and V(D)J sequencing on single cells can provide a vast depth of insight to both the clonal identity and gene expression of T cells of interest. This technology is leveraged for both Chapters 3 and 5. Nonetheless, the directionality of the chemistry is important - 10X have two kits for producing libraries, either 3' or 5', depending on which end of the transcript is primarily captured[171]. 3' approaches (whereby the final fragmented libraries mainly represent the 3' end of the transcript) are less amenable to V(D)J sequencing due to the fact that the highly variable V(D)J reason is found at the 5' end, with the more invariant constant region found 3' (Figure 1.9a). This is important both in experimental planning and also because many newer single cell technologies - including those using array-based approaches on fixed RNA - use a 3' approach and so are less amenable to simultaneous V(D)J sequencing.

1.5.2 Repertoire metrics

Immune repertoires can effectively be considered a population - with each unique TCR a 'species'. Cells which all carry the same TCR (i.e. a 'T cell clone') can be considered individual members of the same species. As such, the study of repertoires draw on approaches from ecology or

microbiology, whereby the study of heterogenous populations - such as wildlife or bacteria - is a mainstay. The term 'repertoire metrics' describes a suite of mathematical indices, which assign a score to biological samples, thereby quantifying a metric of interest (Figure 1.10)[163]. One of the most widely-used is the Shannon entropy (Shannon; Figure 1.10a) and it is best considered a measure of *diversity*. Shannon accounts for both richness (total number of unique clones) and evenness (their relative abundance or 'distribution spectrum')[163]. As illustrated in Figure 1.11, Shannon is maximal when there are a high number of evenly distributed clones, although richness is more heavily weighted than evenness. This contrasts with Simpson's index, another metric of diversity, which places a heavier emphasis on evenness[172] and is effectively a probability of two sequences, randomly chosen, belonging to the same clone. The Gini-Simpson index (different to the Gini coefficient described below) is 1-Simpson's index, giving values approaching 1 maximal diversity and evenness (Figure 1.10b).

In contrast to Shannon and Simpson's indices - which are measures of *diversity*, it is sometimes more helpful to consider *evenness* in isolation. Metrics which do this can be considered a way of calculating 'clonal dominance' and this element is particularly helpful in my work whereby it appears that a smaller number of large - or expanded - clones may be mediating the effect of ICB[78,93]. Pielou's index is one such metric (Figure 1.10c), usually used as the complement (1-Pielou's) to get a number between 0 and 1, where 1 is a repertoire with a high level of dominance. Pielou's index takes repertoire richness into account - where dominance within a rich repertoire results in a higher score. Gini coefficient (different to Gini-Simpson index) is another metric of distribution which originates from economics (Figure 1.10d)[173]. With less emphasis on repertoire richness, Gini quantifies the 'balance' of a population and was first described in the context of wealth distribution. A score of 1 is a truly unequal distribution (one person has all the money) whereas 0 is entirely equal (everyone has the same amount of money). This concept is visualised using the Lorenz curve (Figure 1.10e). This same principle can be applied to T cell repertoires,

and hence the Gini coefficient is a reasonably accessible and comprehensible measurement of *clonal dominance* which can be applied to repertoires of varying size.

Figure 1.11 - taken from [163] - is a helpful visualisation of the four metrics discussed here. As can be seen, increasing the size of the repertoire has a large impact on Shannon (which prioritises richness) with less effect on Gini-Simpson, which is more affected by evenness. Similarly, Pielou's and Gini coefficient both measure unevenness, but Pielou's is more affected by increasing repertoire size as it is sensitive to richness, whereas Gini is less influenced by bigger repertoires, but is more sensitive to oligoclonality and 'dominant' repertoires.

Finally, there are a number of metrics which quantify repertoire overlap, including the Jaccard index, Sorensen index and Morisita-Horn index (Figure 1.10f). Of these, the latter is the most commonly-used in the analysis of T cell repertoire overlap because, unlike the Jaccard or Sorensen indices, it takes into account the relative abundance of shared clones and is also robust to different sample sizes[163,174,175].

1.5.3 Repertoire features and ICB

Understanding the T cell repertoire - and in particular the application of repertoire metrics - has the potential to generate insights into mechanisms of the anti-cancer immune response. However, findings can be contradictory and heterogeneity in the metrics used can inhibit meaningful cross-study comparisons.

1.5.3.1 Tumour-infiltrating T cell repertoires

A seminal paper describing the importance of $CD8^+$ T cells in the immune response following ICB by Tumeh and colleagues (discussed above, section 1.2 page 14) applied the complement of Shannon entropy (calculated using TCRseq of the tumour-infiltrate) to generate a 'clonality'

metric[64]. They showed that a more clonal TIL compartment was significantly correlated with response to PD-1 blockade and that following treatment, patients who responded had an order of magnitude more clones expanded than those who progressed. This work has played a crucial role in advancing the theory of the importance of intra-tumoural T cell clonality.

A number of other studies have supported this finding, demonstrating the importance of clonality in the tumour-infiltrating compartment. Roh *et al.*[176] showed that more clonal populations of TILs associated with response following PD-1 blockade (but not CTLA-4 blockade) in 56 patients with MM. In their clinical trial of neoadjuvant nivolumab for the treatment of resectable melanoma, Forde *et al.* analysed the clonality of resected tumours, finding higher clonality in those with a major pathological response[96]. Pruessman *et al.* described that the fraction of nucleated cells within a melanoma that are T cells (T cell fraction - TCFr) was able to predict probability of recurrence following complete resection of stage I-III melanoma (a TCFr of <20% was associated with a 2.5x recurrence risk)[177]. Others have also reported oligoclonal expansion of TILs in patients with melanoma following ICB[178]. Nonetheless, there is a wide heterogeneity in immune responses, as a large study of 60 patients with synchronous melanoma metastases showed[179]. In this study (n=30 treated with ICB and n=30 treated with BRAFi), deep molecular, genetic and immune profiling of synchronous metastases was performed, revealing a large degree of heterogeneity - both of the tumour genomics but also of the immune response. For example, across different metastatic sites within the same individual there was a wide variation in T cell clonality, and indeed a number of large T cell clones were restricted to individual metastases and not shared. However, metastases with a higher TMB and $CD8^+$ T cell infiltrate also had higher clonality, and although the amount of $CD8^+$ T cell infiltration did associate with tumour regression, clonality did not.

Together, there is a substantial body of literature to suggest that intra-tumoural clonality is benefi-

cial in the anti-melanoma immune response following ICB, however there is likely heterogeneity in these responses.

1.5.3.2 Peripheral blood T cell repertoires

Along with the tumour-infiltrating compartment, repertoire features of the peripheral blood and their relationship with ICB have also been described - although, again, some of these findings are somewhat contradictory and may reflect differences depending on tumour type. For melanoma, large increases in diversity and richness post-CTLA-4 blockade (with tremelimumab) have been described, with this driven by gain in total number of clonotypes found in peripheral blood mononuclear cells (PBMCs)[99,180], although it should be noted that tremelimumab has not been approved for the treatment of melanoma due to lack of efficacy. Indeed, others described this in just the $CD8^+$ T cell compartment, and in particular found that post-ipilimumab, there was a significant increase in the number of melanoma-specific $CD8^+$ T cell, but not virus-specific $CD8^+$ T cell clones[181]. These studies led to the concept of ICB - and anti-CTLA-4 in particular - 'broadening the T cell repertoire'.

However, Cha *et al.*[99] found that despite overall increases in diversity, it was maintenance of baseline high-frequency clones (i.e. large clones; defined as greater than 10^{-3} in the repertoire) that was associated with improved overall survival[99]. These results were supported by a more-recent paper from Valpione and colleagues[95], who collected peripheral blood samples from 54 patients with MM who received ICB. They too demonstrate an increase in TCR turnover three weeks post-treatment, with novel clones being found in the periphery and tumour-infiltrating compartment. Of note, they describe how patients with a good response to treatment have a more 'dynamic' repertoire, with responders either showing an increase in Gini *or* an increase in Renyi index (another diversity metric) but rarely both; whilst patients who progress had relatively static repertoires with little change in either metric[95]. Similar increases in repertoire 'flux' were

described by Forde *et al.*[96] who noted peripheral expansion and emergence of multiple T cell clones following neoadjuvant nivolumab treatment for melanoma.

Work from our group has also explored the peripheral blood repertoire features of response to ICB in MM. Notably, we did not find an association between post-ICB diversity (measured by Shannon) and outcome (Figure 1.12a) but did find that clonality - as measured by the number of large clones occupying >0.5% of the repertoire - strongly associated with clinical response (Figures 1.12b and 1.12c).

The picture in mRCC appears similar, where a reduction in diversity and increase in clonality (as calculated by the inverse of Shannon and Simpson's indices) post-nivolumab was associated with a favourable outcome[182]. However, the relative importance of TCR repertoire metrics in NSCLC is less clear. One study by Naidus and colleagues demonstrated an association between increases in TCR diversity by day 15 post-treatment with improved overall survival[183]. However, the way they calculated diversity was paradoxically by calculating and then inverting clonality, and their methodology for this was poorly described. Nonetheless, it replicated findings by Liu *et al.* who demonstrated increasing diversity (calculated by Shannon) from pre- to post-treatment was associated with improved PFS, although this was in the context of standard chemotherapy and radiotherapy. Others have also shown that increased richness (simply the number of different clones) associated with improved PFS in NSCLC[184]. However, paradoxically in this same paper the authors also find increased clonality (as measured by Pielou's index) associated with better outcome[184] and the importance of post-treatment diversity also appears contradictory to other work - for example Han *et al.*[185] - who found that whilst baseline diversity (as calculated by Shannon) was associated with improved PFS following PD-1/PD-L1 therapy, post-treatment clonality - and not diversity - also resulted in improved outcomes.

In summary, for melanoma at least, it appears that ICB results in clonal turnover with both

expansion and contraction of clones. However, the expansion and maintenance of key clones from baseline to post-treatment - along with post-treatment clonality - is consistently associated with response. The picture across different cancers - and NSCLC in particular - is less clear, although baseline diverse repertoires appear to associate with improved outcomes following ICB in this tumour type.

(a)

$$-\sum_{i=1}^{N} p_i log_b p_i$$

(b)

$$1 - \sum_{i=1}^{N} p_i^2$$

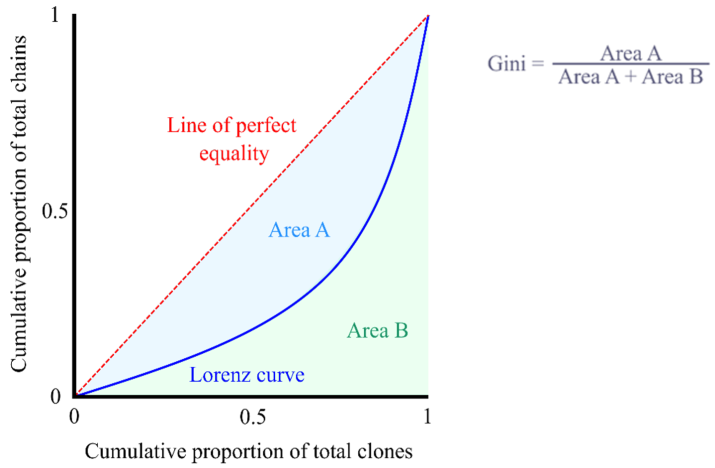
(c)

$$-\frac{\sum_{i=1}^{N} p_i log_b p_i}{log_b(\mathrm{N})}$$

(d)

$$\frac{\sum_{i=1}^{N}\sum_{j=1}^{N} |p_i - p_j|}{2N^2\bar{p}}$$

(e)



(f)

$$\frac{2\sum_{i=1}^{S} n_{1i}n_{2i}}{(\sum_{i=1}^{S} f_i^2 + \sum_{i=1}^{S} g_i^2)n_1 n_2}$$

Figure 1.10. (a) Equation for Shannon entropy - N is the total number of unique sequences p_i is the frequency of sequence i in the repertoire and b is the base of the logarithm. (b) Equation for Gini-Simpson index - definitions as per (a). (b) Equation for Pielou's index, definitions as per (a). (d) Equation for Gini coefficient. p_i and p_j are the frequency of the ith and jth clones in the repertoire and p is the average of clonal proportions. (e) Lorenz curve to visualise how Gini index is calculated - all clones are ranked by increasing proportion and plotted on the (blue) Lorenz curve. The Gini index is then the area between the line of perfect equality and the Lorenz curve, over the area under the line of perfect equality. This figure panel was produced by Bethan Storey, an FHS student who I directly supervised. (f) Equation for the Morista-Horn index with $f_i = n_{1i}/n_1$ and $g_i = n_{2i}/n_2$, n_{1i} and n_{2i} being the clone sizes of the ith sequence (i.e. entities representing a sequence) and n_1 and n_2, the total number of entities in sample 1 and 2 respectively. S is the total number of unique sequences found in both samples. Equations taken from reference [163] under a creative Commons CC BY licence.

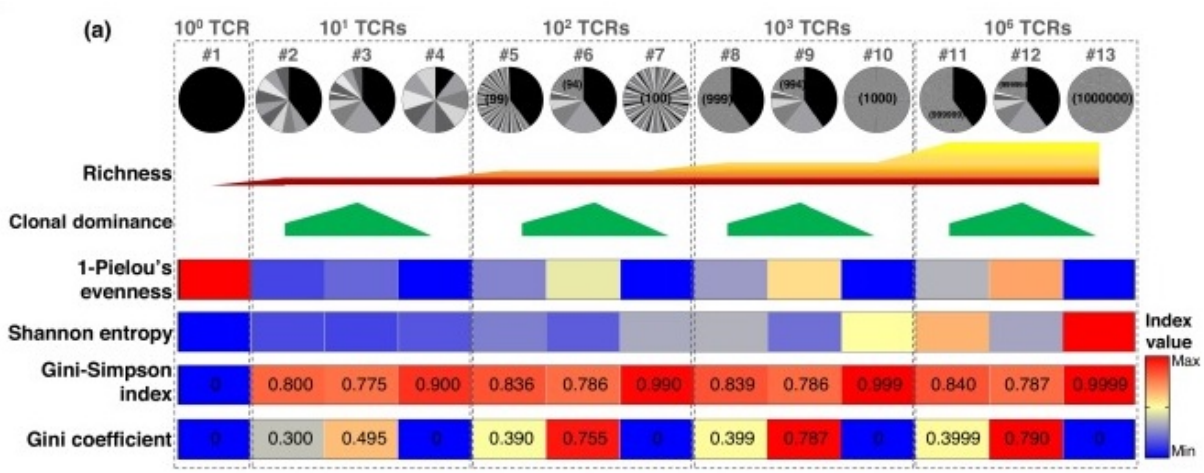


Figure 1.11. Summary of effect of repertoire size and distribution on various repertoire metrics, taken from [163] under a creative Commons CC BY licence.

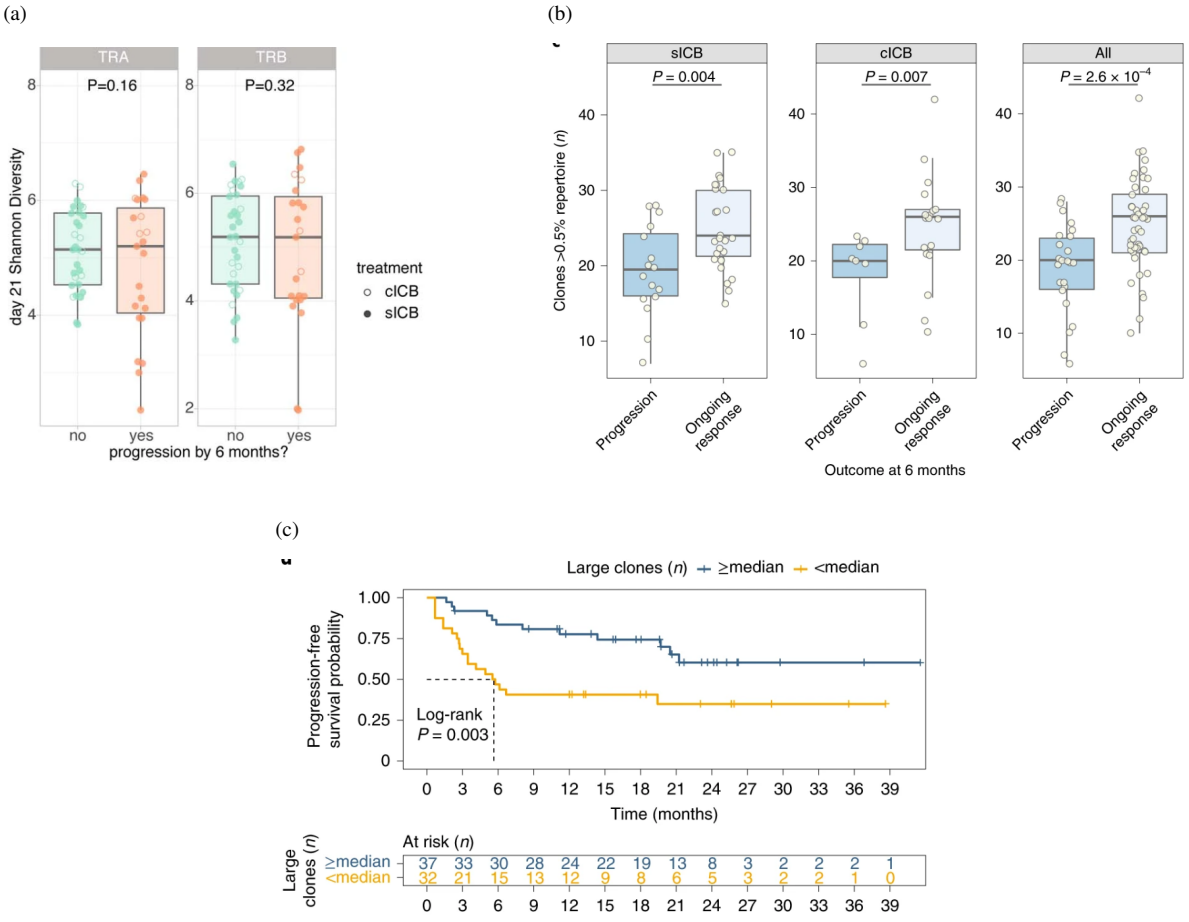


Figure 1.12. (a) Shannon diversity based on peripheral blood TCRβ chains at 21 days post treatment, coloured by clinical response. (b) Number of large clones (>0.5% of peripheral repertoire) at 21 days post treatment, coloured by clinical response and faceted by treatment. (c) Kaplan Meier survival curve for above vs below median number of large clones in peripheral blood at day 21 post treatment. Statistics with two-sided Wilcoxon rank sum test (a and b) and Log-rank (c). All figures reproduced from reference [93]; I am a contributing author.

1.5.4 T cell clustering algorithms

Whilst repertoire metrics, as described above, have generated insights into T cell responses following ICB, they are only able to describe features at a population level and are unable to describe T cell motifs - or their cognate epitopes. A number of computational approaches have thus developed to cluster T cells based on their TCR and analyse repertoires[186].

At the most basic level, it is possible to simply look at string distance between two TCR chains or perform an analysis of K-mer similarity, whereby the TCR is broken up into short sequences of K length, and common motifs identified by simple enrichment in one sample versus another. However, a range of more complicated algorithmic approaches are now established, with many working on this principle of similarity - i.e. clustering TCR based on the similarity (or dissimilarity) of their sequences.

Perhaps the best-known of these is *GLIPH* and its successor *GLIPH2*, developed by the Davis lab in Stanford[187,188]. *GLIPH* stands for Grouping of Lymphocyte Interactions by Paratope Hotspots and works on the premise - based on analysis of TCR-MHC interactions - that only short linear stretches of the CDR3 region make contact with antigenic peptide residues bound to MHC. There is always one contact with the CDR3 region of the TCRβ chain, but not always a contact with the TCRα chain. This suggested that clustering only on 'high probability contact sites' might enable deduction of shared specificity.

In the initial paper describing *GLIPH*, the authors first tetramer sorted antigen-specific T cells using MHC tetramers bound with known antigens, and sequenced the TCR in order to obtain a training dataset. Based on this, they were able to identify parameters of similarity between TCR that recognised the same antigen. Some TCRs were 'globally' similar - i.e. the CDR3 sequences against a single specificity would often differ by only one amino acid - whilst others

were similar based on 'local' motifs - i.e. enriched for amino acid motifs of 2-4 amino acids in length in the 'high probability' contact region (IMGT positions 107-116[189]). Clustering of TCR was therefore done on both global similarity (CDR3 differing by up to 1 amino acid) or local similarity (>10-fold enrichment of shared CDR3 amino acid motifs with probability <0.001 compared to a reference dataset). In all cases, just the TCRβ chain is used[187]. The authors validated their approach in a number of ways, including clustering a validation set of TCR which were stimulated by PBMCs with *M. tuberculosis* peptides. They extracted activated $CD4^+$ T cells and sequenced, then clustered them together with *GLIPH*. They subsequently then tested their TCR clusters with peptide stimulation assays (a short list of peptides was drawn up using The Immune Epitope Database (IEDB) HLA binding prediction assays). They found that all or most TCRs in a given group recognised the same peptide - thus demonstrating that their clustering in likely shared antigen specificity was valid[187].

Despite its promise, *GLIPH* was hampered by being very slow with large numbers of TCR and requiring a reference data set that was at least an order of magnitude bigger than the target dataset. As such, this led to the release and validation of version 2 (*GLIPH2*) in 2020 which improved a number of these features, markedly speeding up the processing time - thus allowing larger datasets to be clustered - and introducing a number of other smaller features to improve accuracy[188]. *GLIPH2* was recently applied to TCRseq data from patients with NSCLC, leading to the identification of key antigenic targets, and uncovering their cross-reactivity with viral epitopes[190].

Alongside *GLIPH/GLIPH2*, there are a number of other approaches which aim to cluster TCR using similarity approaches. For example, *TCRdist* generates a score based on similarity of concatenated CDR1, 2 and 3 chains using a similarity-weighted Hamming distance with a gap penalty to capture variation in length and a greater weight for the CDR3 region due to its primary

role in antigen recognition[191]. Similarly, *iSMART* (immuno-Similarity Measurement by Aligning Receptors of T cells) performs pairwise comparisons of just CDR3 regions and generates an alignment score based on the BLOSUM62 matrix for amino acid alignment.

As well as these approaches, increasing attention is being gained by the potential of deep learning/machine learning. *DeepTCR* uses deep learning and convolutional neural networks to learn patterns in TCR repertoires[192]. This tool uses both TCRβ and TCRα chain information, representing these in a continuous numerical space and extracting sequence-based features from both chains. V, D and J gene usage is also integrated as a categorical variable. The trained network will take a given TCR and represent it as a continuous numerical domain for downstream clustering[192]. Further iterations of *DeepTCR* also incorporated HLA data in order to 'contextualise' TCR sequences and allow comparisons between individuals with different HLA backgrounds.

First released in 2021, it was recently applied to T cell repertoires following ICB[193]. Here, *DeepTCR* assigned a high or low likelihood of response to ICB based on clustering TCRseq data from pre-treatment resected tumour specimens, with an ability to predict PFS (area under the curve (AUC) 0.86). They then generated 'sensitivity logos' - key amino acid residues which are highly sensitive to change in input material and thereby likely to be critical for clustering and antigen binding[192]. In their dataset of TCRseq from resected melanomas, they generated sensitivity logos for the top 50 most predictive TCR for response and progression and ran known antigen-specific TCR from a previously published dataset[70] through the repertoire classifier. They found that, rather counter-intuitively, virus-specific TCR, such as those recognising Epstein-Barr virus (EBV) or influenza, had a higher likelihood of response, whilst those recognising tumour-specific antigens such as melanoma antigen recognised by T cells 1 (MART-1) had a higher likelihood of non-response. Finally, they also describe a higher degree of turnover in tumour-specific TCR in non-responders. On the basis of these findings, they propose a model

whereby the TCR signature of responders is enriched for viral clones, whilst in non-responders it is enriched for high-turnover T cells which recognise tumour-associated antigens, suggesting that these are dysfunctional and accumulate, unable to be 'rescued' by ICB.

Whilst the use of machine learning is appealing and undoubtedly has future applications in TCR clustering, the exact mechanics of *DeepTCR* are difficult to understand. This inaccessibility creates limitations for the tool as it provides barriers to interpreting the results, how they might apply to external datasets and the exact biological implications.

1.5.5 Antigen identification

A key challenge once TCR have been identified using any one of the above approaches, is identifying the cognate antigen that each TCR recognises. The ability to do this in an accurate, robust, rapid and high-throughput manner is an area of great unmet need for the field. Identifying TCR and their cognate antigens can be approached from either end - "I know the antigen, what are the TCR that recognise it?", or: "I know the TCR, what are the antigens it recognises".

Depending on the question, the approach taken will vary. To answer the first question - that is, knowledge of the antigen and desire to find the appropriate TCR - the 'classic' approach is by fluorescent MHC tetramer screening. Simply, pMHC tetramers (loaded with the peptide of interest) are used to fluorescently tag TCR which can then be sorted by flow cytometry and their TCR sequenced by any of the methods described above (section 1.5.1)[194,195]. This approach can be conducted in a relatively high-throughput manner, and indeed many TCR have been identified in this way. Alternative approaches to identify TCR that recognise antigen of interest include co-culture experiments (where PBMCs/T cells are co-cultured with peptides or whole antigens of interest) and sorting of activated T cells (on flow cytometry against activation markers such as CD38 or IFNγ).

A number of databases have been developed to gather together TCR data generated in this manner. Most of these provide information about epitopes, cognate TCR, HLA restriction and the experiment used to identify the TCR and are referred to in this thesis, particularly Chapter 4. These are summarised as follows:

- *VDJdb*. This database gathers TCR and epitope specificity (including organism, antigen, epitope sequence) derived from published work of TCR specificity assays. On the whole, these are identified via tetramer-sort methods (as above)[196]. There are a very large number of viral antigens, however the dataset includes human cancer antigens also.

- *IEDB*. This database (the immune epitope database) is a manually-curated database of both antibody and T cell epitopes and their cognate receptors. Like the *VDJdb*, most of these are generated using tetramer experiments or similar. It has a range of disease processes that have been studied - many infectious diseases, but also autoimmune and transplant disease. The *IEDB* also has a tool, *TCRmatch*, which allows you to query sequences and find the closest matching TCR within the database. Matches do not have to be exact, and the IEDB will find matches that likely share epitope specificity - based on sequence similarity using a k-mer comparison[197]. This tool can be run in the web (this is very slow) or installed and run in BASH (allowing parallelization). However, it only queries based on TCRβ.

- *McPAS-TCR*. This database is similar to the above inasmuch as it includes manually curated TCR (both TCRβ and TCRα sequences) from the published literature[198]. The TCR are identified from experiments either using pMHC multimer, co-culture with antigen of interest or *ex vivo* identification - e.g. the top 50 most abundant clones identified by TCRseq from an end-organ of interest. However, *McPAS-TCR* is relatively small (only $\sim$5000 TCR) and the hosting website is less reliable than the above two examples.

- *TCRdb*. Unlike the above examples, the *TCRdb* does not restrict included TCR to just those

identified as binding a specific pMHC, rather it is a large database of all sequenced TCR from over 130 TCRseq experiments[199] with populated metadata outlining experimental conditions, tissues and disease processes.

- *immuneACCESS*. This database from immunoSEQ is a repository of TCR chain information generated from most - if not all - TCRseq experiments that have used Adaptive's immunoSEQ platform. As such, it is similar to *TCRdb* inasmuch as it does not give paired antigen-TCR data but rather contains a large amount of TCR data from a wide variety of experiments.

Whilst it is helpful to have identified TCR that recognise antigens of interest, the vastness of potential V(D)J rearrangements mean that such a process will never be exhaustive. What is more challenging - but arguably more important, particularly for this thesis - is the ability to start with the TCR of interest and identify the antigen it recognises. There are computational approaches that attempt this using machine learning, such as *TcellMatch*[200] or the model described by De Neuter *et al*[201]. Another example is *DeepTCR* - discussed above (section 1.5.4, page 56) - which purports to be able to identify the antigen specificity of T cells via deep learning approaches. However, both of the two papers currently using this approach rely upon published/public datasets of known antigen-specific TCR to train their model[192,193]. It does not provide a computational approach of annotating antigen-specificity of TCR *de novo*. Nonetheless, such artificial intelligence/machine learning approaches are in their infancy - currently there is not a single approach which can rapidly and robustly predict antigens given a TCR. However, it is possible that with increasing training datasets, machine learning may become increasingly powerful at predicting antigen specificity of TCR - a topic that was recently reviewed by a group at the WIMM[202].

Currently - and fundamentally - it takes molecular biology 'wet lab' experiments to convincingly 'prove' antigen recognition, rather than 'high probability' matches provided by *in silico* approaches.

One method that can be employed is that using a yeast display library, developed by Chris Garcia's group[203]. This approach has considerable advantages - given that it is unbiased and requires no *a priori* knowledge of the nature of these antigens. In short, individual yeast are DNA-encoded to express a random peptide which is bound to an HLA molecule (in this example, HLA-A*02:01)[204]. Up to 10^8 peptides can be expressed in this manner. Soluble TCR (TCRα-TCRβ pairs) are made, biotinylated and attached to streptavidin-coated magnetic MACS beads[203]. The yeast are then mixed with the TCR (where the TCR bind to the yeast expressing their complementary pMHC) and passed over a magnetic column. This process is repeated at least four times to select just those yeast that bind to the TCR. The peptides can then be identified by DNA sequencing of the yeast[203,204]. This approach has been used with good effect to identify the cognate antigen of a TCR expanded in tumours versus healthy tissue in NSCLC[190] and we are collaborating with Dr Ricardo Fernandes in Oxford (who previously worked with Chris Garcia) to use this methodology for the TCR identified in Chapter 4.

1.6 Thesis aims and objectives

This doctoral thesis aims to build on this existing body of literature and leverage emerging molecular biology and bioinformatic approaches to address current gaps and unmet need.

As such, the over-arching aim of this thesis is as follows:

By examining CD8$^+$ T cell transcriptional and repertoire changes in peripheral CD8$^+$ T cells over time, can I better describe:

1. *Molecular mechanisms of immune checkpoint blockade (ICB)*
2. *CD8$^+$ T cell clonal responses following ICB*
3. *Clinically-applicable biomarkers for response and immune-related adverse events following*

treatment with ICB

1.7 Thesis Outline

The remainder of this report is organised as follows:

Chapter 2 (page 65) — outlines the methods used in the generation of data and its analysis.

Chapter 3 (page 90) — details the results of single cell transcriptomic analyses focussing on $CD8^+$ T cell transcriptional changes to one cycle of ICB in MM and mRCC.

Chapter 4 (page 114) — details the results of T cell receptor sequencing across a cohort of 96 individuals with melanoma and 43 HDs, at multiple time points following ICB.

Chapter 5 (page 146) — details the results of a large single cell experiment examining the long term effects of ICB on PBMCs and $CD8^+$ T cell subsets and clones in patients with a CR to PD-1 blockade in metastatic melanoma.

Chapter 6 (page 197) — focusses on irAEs following ICB treatment. This chapter has two distinct halves with the first half focussing on repertoire changes found in a cluster of cases of extremely severe myocarditis and myositis. The second half describes T cell and peripheral lymphocyte effects of carriage of a novel polymorphism within the *IL7* gene.

Chapter 7 (page 224) — is a discussion of the results and how this thesis contributes to the wider field.

1.8 Scientific output thus far

As a result of work undertaken during my DPhil, I have achieved the following academic outputs.

Co-first author peer-reviewed publications

- Taylor*, Watson*, Tong* *et al.* - Nature Medicine (2022)[101]
- Watson*, Tong* *et al.* - Science Immunology (2021)[78]

Contributing author peer-reviewed publications

- Gilchrist *et al.* - Nature Communications (2022)[205]
- Ye, Olssen-Brown *et al.* - British Journal of Cancer (2021)[43]
- Fairfax *et al.* - Nature Medicine (2020)[93]

Publications during DPhil, unrelated to work presented in this thesis

- Mazet *et al.* - Nature Communications (2023)[206]
- Tsakok*, Watson* *et al.* - Radiology (2022)[207]
- Peng *et al.* - Nature Immunology (2022)[208]
- COvid-19 Multi-omics Blood ATlas (COMBAT) Consortium - Cell (2022)[209]

International oral conference presentations

- Watson *et al.* - International Oral Presentation, Tri-omics European Summit (2022).
- Watson *et al.* - International Oral Presentation, ESMO (2022). (Delivered by Ben Fairfax)
- Watson *et al.* - International Oral Presentation, VIB Leuven insights into Immuno-Oncology (2022).

Prizes

- CRUK Oxford Cancer Centre Annual Meeting - presentation award (2023)
- Association of Physicians Annual Meeting, best local poster (2021)
- British Society of Immunology Annual Conference Poster Prize; runner-up (2020)

2 | Methods

2.1 Clinical sample collection

2.1.1 Patient recruitment

The patient cohort comprises adult patients referred to receive ICB as standard of care therapy for the treatment of, or adjuvant use in, melanoma or for the treatment of mRCC at Oxford University Hospitals NHS Foundation Trust (OUHFT). Patients were prospectively and consecutively approached for recruitment by myself, along with others (see Declaration page iii). Patient recruitment of the MM cohort was established in November 2015 by Prof. Ben Fairfax. Recruitment of patients with mRCC was established by me at the commencement of this DPhil. This required submitting an amendment to Oxford Radcliffe Biobank (ORB) in order to widen the scope of the project from just patients with MM to patients with all cancers. I liaised with clinicians in the OUHFT mRCC clinic as well as the ORB in order to achieve this.

All patients who volunteered to take part provided written informed consent to donate samples to ORB (Oxford Centre for Histopathology Research ethical approval reference 19/SC/0173, project nos. 16/A019, 18/A064, 19/A114) and grant access to their routine clinical data. Patients received either cICB (ipilimumab 3 mg/kg plus nivolumab 1 mg/kg 3 weekly for up to 4 treatment cycles, followed by maintenance nivolumab of 480mg every 4 weeks) or sICB consisting of either nivolumab 480 mg monthly, pembrolizumab 2 mg/kg three weekly or pembrolizumab 4 mg/kg six weekly. For mRCC, all patients received cICB, however, the dosing is different - 3 mg/kg nivolumab and 1 mg/kg ipilimumab for up to four cycles and then 480 mg nivolumab every four weeks. Only patients who received at least one dose of treatment were included in analysis. Healthy donor participants were recruited via the Oxford Biobank (ethical approval

reference 06/Q1605/55), with written informed consent. All donors were of European ancestry.

2.1.2 Post-mortem tissue collection

In order to use post-mortem (PM) tissue in research (data presented in Chapter 6), it was necessary to obtain separate approvals. I completed a Central University Research Ethics Committee (CUREC) application and approval was granted on 17th March 2022 from Medical Sciences Interdivisional Research Ethics Committee (MS IDREC) (Ref R80630/RE001).

2.1.3 HRA approval for LSI data

In order to obtain retrospective clinical outcome data for validation of the LSI (Chapter 6, section 6.4.5, page 213), it was necessary to obtain Health Research Authority (HRA) approval. I completed the entire application process and permission to obtain and use data in this manner was granted on 18th September 2022 (Ref 22/HRA/3763).

2.1.4 Laboratory blood counts

Laboratory blood counts were obtained from the patients' electronic patient record (EPR) with pre-treatment samples being defined as those taken closest to the first cycle of ICB, but no greater than 30 days beforehand and post-treatment samples defined as the first sample taken at least 21 days following ICB, but no later than 49 days. Lymphocyte counts were generated using the Sysmex XN series analysers (Sysmex Corporation, Kobe, Japan) in an NHS clinical diagnostic laboratory.

2.1.5 Blood collection

Whole blood (30-50ml) was collected into EDTA tubes (BD vacutainer) immediately prior to the administration of ICB. This belies the nomenclature of "cycle" - e.g. cycle 2 (C2) is taken immediately before the second cycle of treatment. The blood is density centrifuged with Ficoll Paque and PBMCs obtained. These are then either immediately separated into subsets using Miltenyi MACS magnetic columns (positive selection for $CD8^+$ T cells, negative selection for $CD4^+$ T cells) according to the manufacturer's instructions, with all steps performed either at 4°C or on ice, or cryopreserved. For bulk RNAseq, post-selection cells were pelleted and resuspended in 350μl of RLT plus buffer with 1% beta-mercaptoethanol or dithiothreitol (DTT). Samples were snap-frozen at -80°C for batched RNA extraction. For cryopreservation, cells are resuspended in 90% foetal calf serum (FCS) plus 10% dimethyl sulfoxide (DMSO) at a maximum concentration of $10x10^6$ per ml before being gradually frozen at 1°C per minute (Mr Frosty) to -80°C for 24 hours before being transferred to liquid nitrogen (c.-165°C).

2.1.6 RNA extraction

Homogenization was carried out using a QIAshredder (Qiagen), followed by RNA extraction using the AllPrep RNA/miRNA kit (Qiagen). RNA was eluted into 34μl of RNase-free water, concentration quantified by Qubit, and stored at -80°C until further analysis.

2.1.7 Sequencing

All sequencing was performed by the Oxford Genomics Centre (OGC) - part of the University of Oxford. OGC were supplied with sequencer-ready pre-made libraries. They performed QC and set up sequencing reactions, returning raw FASTQ files. Further specifics of sequencing for each experiment are provided in the relevant sections below.

2.2 Single cell RNA sequencing

In this thesis, single cell data is presented from two separate scRNAseq experiments:

1. The Science Immunology ('SciImm') experiment: an experiment of 16 samples (all magnetically-sorted peripheral $CD8^+$ T cells) from 8 patients with MM, with blood sampled at baseline and 21 days later. It is referred to as the 'SciImm' experiment/samples in this thesis, as the results were published in *Science Immunology* in 2021[78]. This experiment used fresh PBMCs (i.e. not cryopreserved) as the starting material (subsequently magnetically separated by positive selection) and one sample per gel bead in emulsion (GEM) well - samples were not multiplexed at the droplet generation level. Data from this experiment is primarily presented in the first half of Chapter 3 although further analyses also appear in Chapters 4 and 5).

2. The long-term ('LT') experiment: an experiment of 136 samples (a mixture of PBMCs and magnetically-sorted peripheral $CD8^+$ T cells) from a range of patients - with MM, mRCC as well as HDs. It is referred to as 'LT' as the primary aim of this work was to examine long term changes to persistent clones in MM, however other samples were also included in the experiment for secondary analyses. This experiment used entirely cryopreserved PBMCs as the starting material (some were subsequently magnetically separated via negative selection), and multiple (n=6-9) samples were multiplexed on the same GEM well. Data from these samples is presented in the second half of Chapter 3 (primarily mRCC samples), as well as Chapter 5 (primarily long term analysis of MM samples).

There were differences in methodology - both experimental and computational - between these experiments. These are outlined in the sections that follow.

2.2.1 Sample preparation and sequencing

2.2.1.1 Sample preparation and sequencing: the SciImm experiment

Samples in the SciImm experiment were prepared from fresh PBMCs. The process for blood collection and cell separation as outlined above (section 2.1.5) was followed. $CD8^+$ T cells were counted and then immediately oil-partitioned into single cell droplets without delay, followed by cell lysis and reverse transcription (RT) on the 10x Genomics Chromium system[210]. A total of 6000 $CD8^+$ T cells were loaded into each partitioning reaction. Single-cell 5' RNA transcriptome and V(D)J libraries were constructed from the cDNA, according to the manufacturer's instructions. Due to the sequential and prospective nature of sample collection, droplet generation and RT were performed on individual samples, but library generation and sequencing were performed in two batches of pooled samples. Sequencing was performed on an Illumina HiSeq4000: 75 base pair (bp) paired-end (PE) reads for the 5' RNA libraries, 150bp PE reads for the V(D)J libraries to a depth of 50,000 reads per cell.

2.2.1.2 Sample preparation and sequencing: the LT experiment

Samples in the LT experiment were prepared from cryopreserved PBMCs. Vials of PBMCs were thawed at 37^{o}C for approximately 3 minutes. Cells were washed in Hank's balanced salt solution (HBSS) and counted. For PBMC samples: cells were pooled together based on the same number of live cells, with a minimum of $2x10^5$ cells per sample. The PBMC pool was then run over a MACS live:dead column (Miltenyi) to remove dead cells. The flow-through (i.e. live cells) were then re-counted and 60,000 live PBMCs were loaded into a partitioning reaction. For $CD8^+$ T cell samples: thawed PBMCs were incubated with both live:dead and $CD8^+$ T cell negative selection antibodies and beads (Miltenyi). In effect, this created a concoction that tagged all dead cells and all cells that were not $CD8^+$ T cells with a magnetic bead. This mixture was then run over

a magnetic column, meaning that the flow-through was depleted of dead cells and enriched for $CD8^+$ T cells. The $CD8^+$ T cells were counted and samples pooled based on the minimum number of $CD8^+$ T cells available. 60,000 cells from this pool were loaded onto a partitioning chip. All steps were performed on ice. Cell thawing, separation, pooling, GEM-cell droplet partitioning, lysis and RT were all performed on the same day. Amplified cDNA was stored at -20°C for <3 months for batched library preparation (two batches total).

Sequencing was performed on an Illumina NovaSeq 6000 S4 flow cell (150bp PE). For each pool there were five library samples - PBMC gene expression (GEX) libraries, $CD8^+$ T cell GEX libraries, PBMC origin TCR libraries, PBMC origin BCR libraries, $CD8^+$ T cell origin TCR libraries. Batch one of sequencing was the first four pools (i.e. 20 samples), which were sequenced across one lane of an S4 flow cell. This was deliberately under-sequenced in order to establish sequencing requirements across the rest of the samples. Following this sequencing run, there were a median of 18,000 reads/cell for GEX libraries (target ∼27,500) and 4,800 reads per cell for V(D)J libraries (target ∼7,000). I therefore sequenced the remaining seven pools, plus some additional sequencing of libraries from the first four pools that were under-sequenced, across three further lanes of an S4 flow cell. In total - across both runs - I achieved a median of 28,500 reads/cell for the GEX libraries, and 7100 reads/cell for the TCR libraries.

2.2.2 Pre-processing, QC and cell filtering

2.2.2.1 Pre-processing, QC and cell filtering: the SciImm experiment

FASTQ files were aligned using *Cellranger* v2.2.0. For V(D)J data, *Cellranger VDJ* was used. For QC, the R package *scater*[211] was utilised to identify single-cell outliers and *scran* used to detect doublets that were removed from analysis. After alignment and preprocessing, $CD8^+$ T cells were filtered for the presence of *CD3D* and either *CD8A* or *CD8B* reads. *Seurat*[212] was used

for additional QC, data normalization, and identification of variable features. Cells were filtered for those with >500 total UMIs, >300 detected features, and mitochondrial gene percentage <20%. Genes expressed in <5 cells were also removed. Pre-processing, QC and filtering of data in this, SciImm, experiment was performed by Isar Nassiri.

2.2.2.2 Pre-processing, QC and cell filtering: the LT experiment

Pre-processing of the data from the LT experiment was performed by me, based on a set of scripts developed by Orion Tong with input from Christina Ye. FASTQ files were aligned using *Cellranger* (v6.0.1) for GEX libraries and *Cellranger VDJ* for V(D)J libraries. For samples which had been sequenced across multiple lanes, the FASTQ files were inputted for alignment on the same *Cellranger* run. *EmptyDrops* was used to identify empty droplets (false discovery rate (FDR) ≤ 0.01)[213]. Barcodes were excluded only if they were called as empty by both *Cellranger* and *EmptyDrops*. *CellSNP-lite* was used to reconstruct genotype data from reads and then *Vireo*[214] was used to compare this to patient-level genotype in order to de-multiplex samples from pools. Doublet identification was performed during sub-clustering by identification of mixed transcriptomes of canonical markers. *Scrublet*[215] was applied to generate doublet scores, but cells were not filtered on this basis (due to difficulty in detecting doublets in enriched datasets due to a lack of variance). Doublets were retained due to potential biological significance; they were labelled as a separate cluster. Genotypic doublets (i.e. barcodes matching two genotypes, as called by *Vireo*) were removed. Cells with <300 transcripts and >20% of mitochondrial-encoded genes were removed. Cells with mitochondrial gene proportions of 10-20% were kept, but assigned as a separate dataset for downstream reference mapping. Genes were considered if they were expressed in at least 5 cells. For all analyses focussing on $CD8^+$ T cells, only cells belonging to the subset "CD8.GD.DN.MAIT.Tcells" were included. This subset was defined as described below (section 2.2.3) with canonical gene markers as visualised in Figure 5.9. For magnetically-sorted

$CD8^+$ T cells, >80% of recovered cells belonged to this cluster (Table 2.1).

Sample source	PBMC subset	Number of cells	Percentage
Healthy donor	Bcells	20	0.20
Healthy donor	CD4.Tcells	270	2.70
Healthy donor	CD8.GD.DN.MAIT.Tcells	8983	91.00
Healthy donor	Doublets	41	0.42
Healthy donor	Myeloid	35	0.36
Healthy donor	NK	480	4.90
Healthy donor	Plt_HSC	2	0.02
Melanoma	Bcells	1976	2.40
Melanoma	CD4.Tcells	4577	5.50
Melanoma	CD8.GD.DN.MAIT.Tcells	69858	84.00
Melanoma	Doublets	1006	1.20
Melanoma	Myeloid	858	1.00
Melanoma	NK	5114	6.10
Melanoma	Plt_HSC	60	0.07
Renal cell carcinoma	Bcells	642	1.60
Renal cell carcinoma	CD4.Tcells	3117	7.70
Renal cell carcinoma	CD8.GD.DN.MAIT.Tcells	33229	82.00
Renal cell carcinoma	Doublets	560	1.40
Renal cell carcinoma	Myeloid	681	1.70
Renal cell carcinoma	NK	1914	4.70
Renal cell carcinoma	Plt_HSC	418	1.00

Table 2.1. Number and percentage of each broad PBMC subset found within the magnetically-sorted $CD8^+$ T cell population. Only those annotated as "CD8.GD.DN.MAIT.Tcells" were analysed as $CD8^+$ T cells.

2.2.2.3 Clonal definitions in analysis of scRNAseq data

In both scRNAseq experiments (SciImm and LT), for analysis that relied on TCR data - e.g. clonal tracking over time or phenotypic make up of clones, only $CD8^+$ T cells with resolved TCR data was included - i.e. cells with either one TCRβ, one TCRβ and one TCRα or one TCRβ and two TCRα chains. Cells with different combinations of chains were excluded. However, some $CD8^+$ T cells did not have *any* V(D)J data - in the SciImm experiment this was the case for 4536 cells (20%); 31,030 (22% of those clustering in the subset "CD8.GD.DN.MAIT.Tcells") in the LT experiment. These $CD8^+$ T cells were still included in analyses that did not require V(D)J information. For all analysis of scRNAseq data, a clone was defined based on concatenation of

the amino acid sequence of the CDR3 region of the chains present.

2.2.2.4 Cell numbers per sample

In general, cell recovery across samples was high. However, there were a few samples with low numbers of cells (Table 2.2). I paid attention to this variability with statistical approaches, such as using a pseudobulk approach for differentially expressed gene (DEG) analysis and *MiloR* for differential abundance (DA) analysis (see sections 2.2.4.5 and 2.2.4.3).

(a)

Donor	C1 Count	C2 Count
80	1731	2273
81	439	1262
82	1993	2004
83	1028	643
84	1391	1349
85	28	2405
87	1160	1224
88	1925	1590

(b)

Donor	C1 Count	C2 Count	C4 Count
170	7	-	1990
186	2832	1970	-
187	2414	2940	1636
188	998	1241	-
212	91	-	2023
215	2209	2117	1234
216	2444	1643	1036
218	949	2376	-
237	12	1056	11

(c)

PBMCs				
Patient	Count: baseline	Count: 3-9 weeks after commencing ICB	Count: 6m - 2yrs after commencing ICB	Count: Post cessation of ICB
133	1129	3530	-	617
136	4360	1390	2413	-
155	1068	2279	-	2166
162	339	778	-	-
174	1815	919	-	806
27	59	2371	1216	3124
36	3792	229	670	2448
43	4366	1870	1032	2669
47	820	1344	1480	889
64	3638	4112	983	1497
70	2194	2186	-	3611
71	1535	4081	-	3563
79	71	3156	-	-
94	2397	4331	3504	1030
814 (HD)	1597	4159	857	-
815 (HD)	5360	1633	2019	-

(d)

CD8s				
Patient	Count: baseline	Count: 3-9 weeks after commencing ICB	Count: 6m - 2yrs after commencing ICB	Count: Post cessation of ICB
133	1433	1683	-	574
136	2209	395	2336	-
155	388	1312	-	725
162	486	148	-	-
174	1425	555	-	752
27	16	1583	2793	2792
36	1968	398	24	2116
43	1711	822	3133	1035
47	877	1409	1520	1053
64	1788	2339	2275	737
70	2053	1989	-	3037
71	-	996	-	1394
79	20	2556	-	-
80	2476	2924	-	1323
82	2314	2323	-	717
83	2219	2072	-	3867
88	2444	2022	1834	-
94	-	2475	1464	1323
814 (HD)	1406	1033	1074	-
815 (HD)	4086	1225	159	-

Table 2.2. Cell numbers per sample for scRNAseq experiments. (a) the SciImm melanoma samples, (b) the mRCC samples and (c) the MM and HD PBMC samples from the LT experiment. (d) as per (c) but for $CD8^+$ T cell samples. C1 = d0, C2 = d21, C4 = d63.

2.2.3 Dimensionality reduction and annotation

2.2.3.1 Dimensionality reduction and annotation: the SciImm experiment

For the SciImm experiment, principal component analysis (PCA) was performed on the scaled data, with the top 16 principal components selected for dimensionality reduction and uniform manifold approximation and projection (UMAP) clustering. To determine an ideal resolution value, cell clusters generated using values between 0.1 and 2.5 were compared using the R package *clustree*[216] with values between 1.5 and 2.0 showing high cluster stability. There was no observed effect of batch on principal component (PC) distribution or baseline cytotoxicity score. To assign each cell cluster generated by *Seurat* to a cell, we curated transcripts per million (TPM) normalized counts for $CD8^+$ T cells from previous public T cell cancer scRNAseq datasets[91,92,217–219]. Using *SingleR*[220], each cell was matched to one of the $CD8^+$ T cell subsets present in the reference datasets, on an individual basis, based on global gene expression similarity. Based on this annotation, subset identity for each cluster was determined. This step was performed by Orion Tong who assisted in the drafting of this section of the methods.

2.2.3.2 Dimensionality reduction and annotation: the LT experiment

Dataset integration

For integration of the two datasets (i.e. the SciImm experiment and the LT experiment) into a core single-cell RNA-seq, datasets were first pre-labelled for cell-type enrichment methods. All datasets containing whole PBMC fractions were then concatenated and the 4000 most highly variable genes selected on raw counts using 'Pool' as the batch variable and the 'Seurat_v3' implementation in *Scanpy*[221]. *scVI*[222,223] was then run on the raw counts of the 4000 most highly variable genes, using the dataset label as the batch variable. Once the core dataset was trained,

datasets containing enriched cell types or higher mitochondrial proportions (10-20%) were further referenced mapped using *scArches*[224]. The latent embedding generated by *scVI* and *scArches* was used for downstream analysis (clustering and visualization). For gene-level analyses (e.g. DEG analysis), normalised, scaled data was used.

For samples in the LT experiment, clustering was undertaken based on a nearest neighbour graph using the 30 latent dimensions that were obtained from the *scVI* and *scArches* output. Here, the number of neighbours set to k=30 and distance metric set to 'cosine'. Coarse leiden clustering was then performed on the graph with resolution r=0.03. For each of the resulting level 1 clusters, a new neighbour graph was calculated using *scVI*'s 30 latent dimensions, with the number of neighbours again set to k=30. Based on the new neighbour graph, each cluster was clustered into smaller 'level 2' clusters with leiden clustering at resolution r=0.3. Using 'level 2' clusters, broad cell type annotations were generated to split the dataset into 'Bcells', 'CD4', 'CD8NK' and 'Myeloid_Plt' datasets.

To fully capture cell type heterogeneity, each broad 'level 2' subset dataset was remodelled using *scVI*. Per 'level 2' cell type, 3000 highly variable genes were recalculated as described above. *scVI* models were then further trained using the same parameters above. Using each subset's *scVI* latent embeddings, new neighbour graphs were calculated using k=30 and 'cosine' as the distance metric.

Cell type annotation

To guide clustering, automated cell-type annotations were first performed on *scVI* embeddings with *Celltypist*[225], using the pre-trained 'Immune_All_Low.pkl'. Marker genes were calculated by performing a t-test-based differential expression analysis on a given cell type (based on *Scanpy*-normalised, log counts), compared to the rest of the cells from the same level annotation. Where

clusters were highly similar, they were merged based on hierarchical dendrograms generated on *ScVI*-derived neighbourhood graphs. For final $CD8^+$ T cell annotations used in this thesis, cross-validation was performed based on assigned annotations from the SciImm experiment. These steps were all performed by Bo Sun who assisted in the drafting of this section of the methods.

2.2.4 Downstream analysis

2.2.4.1 Defining stable/expanding clones

In order to define those clones that were stable/expanding or involuting between time-points, I applied a Fisher's test, using a nominal p value cut-off of 0.05. For example, looking at time points A to B, if the size (based on proportion of repertoire) of a clone was smaller at time point B than time point A, and the p value was significant, this was considered 'involuting'. If there was no significant difference in size, or the clone had significantly increased in size, the clone was labelled as 'stable/expanding'. If the clone was only present at time point A (and so was not found at time point B), this too was considered 'involuting', whilst those found at time point B but not at time point A were also stable/expanding. For this analysis, only clones with >1 member cell were included.

2.2.4.2 Defining clone phenotype

In order to define a phenotype per clone, the phenotype of the majority cell type was used. This definition was consistent with published work[78] but also pragmatic because there was no clear distribution of proportion of cells within clones that were a certain phenotype (Figure 2.1). Hence, any percentage cut-off would be relatively arbitrary, and I felt that a simple majority was preferable.

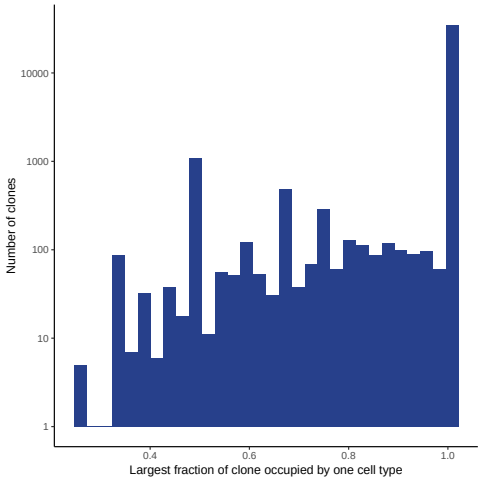


Figure 2.1. Proportion of each clone occupied by a given cell subtype by number of clones. For example, fraction=1 means that the clone is made up of 100% the same cell type (this is the case for the vast majority of clones - note the $\log_{10}$ y-axis) and fraction = 0.5 means that the most populous cell type occupied 50% of that clone.

2.2.4.3 Differential abundance analysis

In order to examine changing proportions over time, the proportion of all cells occupied by a certain subset can simply be calculated by dividing the number of cells of each subset by the total number of cells in that sample. For this analysis, only samples with >1000 cells were included. For analysis looking at proportion of cells with a positive tumour reactivity score (i.e. Figure 5.32), only samples with >1000 cells were included and proportion is the total positive over the total number of cells.

DA analysis using *edgeR*

It is possible to use *edgeR* to perform a DA analysis, as is described in this vignette (ref [226]). By using *edgeR*, it is possible to take advantage of the non-binomial generalised linear model approach to model overdispersed count data in the presence of limited replication. Simply, rather than a gene expression matrix, one constructs an abundance matrix whereby each row is cell type, each column is a sample and each data-cell contains the abundance of that cell type in that sample[227]. The standard *edgeR* workflow can then be applied, and the results are outputted in

terms of a LogFC for each cell type along with an FDR-corrected significance level.

DA analysis using *Milo*

Milo[228] seeks to address a number of issues with classical DA analysis, including variation brought about by different numbers of cells per sample and the need for an *a priori* definition of cell subsets. *Milo* utilises a *k*-nearest neighbours (kNN) approach to assign cells to partially overlapping 'neighbourhoods' (i.e. sub-cluster groups) of cells and perform a DA analysis on these neighbourhoods, generating an output with a fold change in abundance for that neighbourhood and an FDR-adjusted spatial p value which also takes into account spatial overlap between neighbourhoods. In order to apply *Milo* to my scRNAseq data, I followed the vignette created by the package authors. I used number of reduced dimensions=30, reduction method SCVI (as per dimensionality reduction outlined above), k=40 (there were too few cells per neighbourhood with k=30). For calling significant changes in neighbourhoods, FDR alpha was set to 0.2.

In order to define comparisons - i.e. the two sample sets across which to do the DA test - I utilised *contrasts*, following this vignette. Contrasts is an *edgeR* concept which keeps the entire dataset for dispersion estimation but only analyses the differences between two discrete groups. Finally, it is possible to assign neighbourhoods to a cell identity (e.g. that of a pre-defined cluster) using *Milo* to determine the most abundant cell type within each neighbourhood. For this I used cell fraction of 60% - labelling clusters as 'mixed' below this cut-off. This approach has been used to group the neighbourhoods in Figures 5.12 and 5.13.

2.2.4.4 *AddModuleScore* and *AddModuleScore_Ucell*

The *AddModuleScore* function of *Seurat* was first described by Tirosh *et al.*[68] and is extremely widely used. This function adds a score to each cell within single cell data based on expression of a gene set. However, the more recently-released *Ucell* package[229] aims to improve upon

AddModuleScore by utilising a rank-based approach of gene-expression within each cell - rather than relative expression compared to other cells as per the *Seurat* method. This leads to consistency across datasets where each cell would be assigned the same score regardless of the dataset in which it appears, unlike the *Seurat* method, which is dataset dependent. *UCell* has been highly cited and utilised. The *AddModuleScore* from *Seurat* is used throughout Chapter 3 for consistency with the published work (ref [78]). However, following the release of *UCell*, this methodology has been adopted for subsequent single-cell analysis, as presented in Chapter 5.

2.2.4.5 Differentially expressed gene (DEG) analysis

Unless otherwise stated, DEG analysis is conducted in *Seurat*[212,230] using the *FindMarkers* function on normalised and scaled data, with all filters ('min.pct', 'min.cells.feature', and 'logfc.threshold') disabled. The default statistical test (Wilcoxon rank-sum) was applied.

DEG analysis in large vs small clones

To test if the number of DEGs is modulated by clone size, to control for differences in statistical power in detecting DEGs across groups with varying cell counts, the number of cells used for analysis was standardized to the number present in the smallest group and bootstrapped 100 times to account for sampling bias. Only clones present at both time points were included, and clonal size was defined based on baseline size. For example, when comparing the number of DEGs in MM samples in large versus small effector clones (i.e. section 3.3.2 and Figure 3.3b, page 95), effector cells were first categorised as to whether they are a member of a large or a small clone (based on a 0.5% cut-off) and time point. These cells were downsampled to the size of the smallest group and a DEG analysis performed using *FindMarkers* in *Seurat* to quantify the number of significant DEGs (defined by adjusted p value of 0.05) for large clones 21 days vs large clones baseline and small clones 21 days vs small clones baseline. This was repeated 100

times (i.e. bootstrapped) and the results of each test is plotted as a box plot (e.g. Figure 3.3b).

DEG analysis with pseudobulk

To perform a DEG analysis with pseudobulking, for a given cell-type, I converted the gene-by-cell matrix to a gene-by-replicate matrix - i.e. where each row is a gene and each column is a sample (replicate) - using matrix multiplication. The values in the matrix represent the aggregated count of that gene across all cells of a given type within that sample. This is in effect a data-wrangling task, assisted by this HBC Training vignette. Differential gene expression can then be tested *DESeq2*[231] with the (default) Wald test of the negative binomial model coefficients (DESeq2-Wald).

2.2.4.6 GOBP analysis

Gene ontology biological process (GOBP) analysis was undertaken using *XGR*[232], with the following settings: ontology=="GOBP", test = "hypergeo", min.overlap=2, elim.pvalue=0.05. For some plots the minimum overlap was increased to reduce the total number of pathways displayed - where this was done, it is indicated in the figure legends. In cases where a pathway was both up- and down-regulated, the direction with the lowest p value was selected.

GOBP in large versus small clones

GOBP analysis can be affected by the number of genes inputted. To account for this, in the analysis of large versus small clones (e.g. Figures 3.4a and 3.12b), the same number of genes were taken forward to examine pathways - i.e. the top and bottom N genes by $\log_2$FC, where N was determined by the lowest number of significantly modulated DEGs. For example, if small clones only significantly differentially upregulated 10 genes, only the top 10 genes (by $\log_2$FC) were taken forward into the pathway analysis for large clones also.

2.2.4.7 Identifying annotated TCR from public data

TCRseq data of sequencing from 199 melanomas by Pruessman *et al.*[177] or viral-reactive TCR sequences were downloaded from VDJdb[233] with confidence scores >0. Cells present in scRNAseq data were annotated as being found in melanoma, or as viral-reactive, based on their ownership of a TCRβ chain (amino acid sequence alone) that was found in either the Pruessman or VDJdb dataset.

2.3 Bulk RNA sequencing and genotyping

2.3.1 Bulk RNA library preparation and sequencing

RNA was thawed (on ice) prior to mRNA isolation using NEB Next Poly(A) mRNA Magnetic Isolation Module kits. A maximum of 600ng of RNA was used to generate dsDNA libraries using NEB Next Ultra II Directional RNA Library Prep Kits for Illumina. Samples were then sequenced on either an Illumina HiSeq4000 (75bp PE) or a NovaSeq6000 (150bp PE). Reads were aligned to CRGh38/hg38 with *HISAT2*[234], and read counts generated using *HTSeq*[235] version 1.0. High-mapping quality reads were selected based on MAPQ score using *bamtools*. Marking and removal of duplicate reads were performed using *picard*, and *samtools* was used to pass through the mapped reads and calculate statistics[236]. Laboratory work and bioinformatic pre-processing of bulk RNAseq was performed by others, as acknowledged in the Declaration (page iii).

2.3.2 TCR mapping

MiXCR[237] was used to map reads on reference sequences of V, D and J genes, and to annotate TCR clonotypes from mapped reads based on the CDR3. The non-default partial alignments option (allowPartialAlignments=true) was used to preserve partial alignments for assembly. Three

iterations of read assembly were performed to increase the number of assembled reads containing the CDR3 region using assemblePartial. Downstream analysis of mapped reads is as below, *MiXCR* alignment and mapping was performed by Isar Nassiri and Orion Tong.

2.3.3 Genotyping and HLA typing

Genotyping was performed on the Illumina Global Screening Array 24 v3 (Illumina). Genotypes were aligned to b37, filtered for call frequency >0.9, cluster separation >0.3, SNP missingness <3%, minor allele frequency (MAF) >1% and Hardy-Weinberg Equilibrium (HWE) P>10-20, prior to imputation using the Michigan Imputation Server v1.2.4 with the Haplotype Reference Consortium v1 as a reference panel, using *Eagle2* and *Minimac4* for phasing and imputation. Post-imputation, SNPs were filtered for MAF >4%, HWE P>10-10 and r2 >0.7, and lifted-over to b38. The vcf file exclusively containing chromosome 6 was used as an input for the Michigan Imputation Server Genotype Imputation HLA (*Minimac4*) 1.5.8 pipeline against the Multi-ethnic HLA reference panel. Results were filtered by Class I and II genes. This work was primarily performed by others, as acknowledged in the Declaration (page iii).

2.3.4 Downstream analysis

2.3.4.1 Applying expression scores to bulk data

To calculate the geometric mean expression of a gene set in bulk data, the *DESeq2*-normalised gene expression for the genes of interest were extracted from the gene-by-sample expression matrix and the equation *exp(mean(log(expression)))* applied.

2.3.4.2 Determining clone size in bulk data

In bulk RNAseq data, a clone was defined by a concatenation of the V gene, J gene and amino acid sequence of the CDR3 region of the TCRβ. Clone size was calculated as the count for that clone (number of reads) divided by the sum of all counts in that sample.

2.4 TCR sequencing

Two separate TCRseq experiments are contained in this thesis:

1. The 'large TCRseq' experiment. This involved 384 samples - a mixture of $CD8^+$ T cell, $CD4^+$ T cell and resected tumour specimens from patients with MM and HDs sampled at multiple time points. This experiment forms the basis of Chapter 4.
2. The 'myositis TCRseq' experiment. This involved three PBMC specimens, post-mortem (PM) tissue and a fresh muscle biopsy from three patients with extremely severe myositis and myocarditis. Results of this experiment are presented in Chapter 6.

2.4.1 RNA extraction from tissue

RNA was extracted from blood cells (either PBMCs or magenetically-sorted $CD8^+$ T cells or $CD4^+$ T cells) as outlined above (section 2.1.6, page 67).

From FFPE tumour blocks

For RNA extraction from formalin-fixed paraffin-embedded (FFPE) tumour samples (for the large TCRseq experiment) blocks were identified using clinical histopathological reports. Haematoxylin and Eosin (H&E) slides for each block were microscopically inspected to identify areas of tumour deposit. Blocks were sectioned into 10μm slices in a clean and RNase-free environment.

Unstained sections were macro-dissected to obtain tumour regions. Five unstained sections were then combined and deparaffinised prior to RNA extraction using the AllPrep DNA/RNA FFPE extraction kit (Qiagen) according to manufacturer's instructions. RNA was eluted in 14 or 20 µl RNAase-free water. This work was performed by Rosalin Cooper.

From Post-mortem FFPE tissue

A similar process was followed for FFPE PM tissue (for the myositis TCRseq experiment), however the specimens were not macro-dissected as per the tumour blocks but the histopathology department (at OUHFT, working with the ORB) made slices of the most appropriate sections. These were provided as 10μm scrolls and I used four scrolls as the starting material for deparaffinisation.

From fresh muscle specimen

For RNA extraction from fresh muscle (for the myositis TCRseq experiment), the specimen was thawed on ice before being placed in a 2 ml microtube with Qiazol buffer as per the RNeasy Plus Universal Mini Kit protocol (Qiagen). A tissue disruptor was used to mechanically disrupt the tissue for $\sim$one minute. The remainder of the manufacturer's instructions for the Mini Kit were followed for RNA extraction.

2.4.2 Library preparation, sequencing and pre-processing

For both TCRseq experiments, TCR sequencing was performed using the QIAseq Immune Repertoire RNA Library Kit (Qiagen) according to manufacturer's instructions. In short, RNA (median input 80ng) was reverse transcribed to cDNA before being adapter-ligated and amplified using gene-specific primers.

For the large TCRseq experiment, sequencing was performed on an Illumina Novaseq 6000 (SP

flow cell, 250bp PE) - with read depth approximately 1.5-2 million per sample. For the myositis TCRseq experiment, sequencing was performed on an Illumina MiSeq - 300bp PE. For both experiments, alignment and mapping of FASTQ files was performed using the CLC genomics workbench (Qiagen). For the large experiment, the number of UMIs per group was left at the default setting of three. For the myositis experiment, due to the paucity of clones in the PM tissue, this was set to one. Mapped sequences were filtered for productive TCRβ chains.

2.4.3 Downstream analysis

2.4.3.1 Determining clone size

As per bulk RNAseq data, a clone was defined by a concatenation of the V gene, J gene and amino acid sequence of the CDR3 region of the TCRβ. Clone size was calculated as the count for that clone (number of reads) divided by the sum of all counts in that sample.

2.4.3.2 *GLIPH2* clustering

GLIPH2 was run according to package instructions with default parameters; the reference files were as provided. Results were filtered as described elsewhere[190] - specificity groups found in 3 or more individuals, containing 3 or more clones and with significant biases in Vb gene usage, and CDR3β clonal expansion in comparison with the reference dataset.

2.4.3.3 Defining ER clones

To identify ER clones, I compared abundance (as a normalized count) of all TCR within each specificity group pre- and post-ICB, generating a p value for the comparison using the *poisson.test* function in base *R* (alternative = 'two-sided') - as previously described[190]. Specificity groups were called as being 'responder' if >66% of individuals in which they were found did not have

progression of disease within 6 months of starting treatment. Responder specificity groups were called as 'Emergent Responder' if the Log_2FC from pre- to post-ICB was >1 with an FDR-adjusted p value of < 0.05. ER clones are all the clones contained with Emergent Responder specificity groups.

2.4.3.4 Repertoire metrics

The Shannon entropy was calculated using the *entropy* function from the *R* package of the same name. The Gini coefficient was calculated with the *Gini* function from the *DescTools* package. The accuracy of these functions was manually verified. The Morisita-Horn overlap index was calculated using the *Immunarch* package. An explanation of these indices is given in introduction section 1.5.2 (page 46), with the equations found in Figure 1.10.

2.4.3.5 TCR gene usage

For the analysis of TCR gene usage (section 4.3.4) I used the *Immunarch* package[238] 'gene usage' tool. This in effect efficiently generates a gene-by-sample matrix for ease of plotting TCR genes and applying analytical tools such as PCA.

2.4.4 External and validation datasets

2.4.4.1 Antigen-specific TCR calling

TCRβ CDR3 chains were matched to epitopes using IEDB TCRMatch tool with the highest scoring epitope match being assigned to each CDR3β chain with a minimum score of 0.90 (IEDB 'medium' confidence) used as a lower cut-off. The TCRMatch tool is very slow if used in a web browser, so the tool was downloaded and data was parallelised to increase computational power.

2.4.4.2 Tumour-associated TCR

Sequences and sample metadata from sequencing of tumour-associated TCR (TA-TCR) were downloaded from published datasets[64,94,177,239]. Chains were filtered for TCRβ with resolved information on V gene, J genes and CDR3 amino acid sequence. Clones were defined based on a concatenation of the V gene, J gene and CDR3 amino acid sequence.

2.4.4.3 Peripheral blood validation cohort

Bulk RNAseq was performed on magnetically-separated $CD8^+$ T cell samples, and V(D)J data called by *MiXCR* as detailed above (section 2.3). All patients included in the TCRseq discovery cohort were excluded from the validation cohort.

2.4.4.4 Intra tumoural validation dataset

Sequences and sample metadata were downloaded from Riaz *et al.*[94]. Clones were defined based on a concatenation of TCRβ V gene, J gene and CDR3 amino acid sequence. The number of clones that we identified as ER clones found in each tumour sample were counted, with response defined as per the original publication metadata (response = CR/PR, progression = PD).

2.5 Flow cytometry

For flow cytometry experiments, cryopreserved PBMCs were thawed at 37°C and washed once in HBSS prior to staining of $1x10^6$ cells with LIVE/DEAD Fixable Near-IR (Invitrogen). Cells were washed and subsequently stained with antibodies against CD3, CD4, CD8α, CD27 and CD45RA in 5% FCS + HBSS. After washing, cells were fixed for 10 minutes with 2% paraformaldehyde (Sigma), washed and resuspended in 5% FBS + HBSS prior to acquisition on a BD LSRII. All staining steps were performed for 30 minutes and at 4°C. The gating strategy to identify $CD8^+$ T

cells is shown in Figure 2.2. All flow cytometry data in this thesis was generated in experiments performed by Chelsea Taylor who also assisted with the writing of this section of the methods. All analyses were performed, and figures produced, by myself. For each analysis, the maximum number of samples at the time point of interest were included - these are given in the relevant results sections and figure legends.

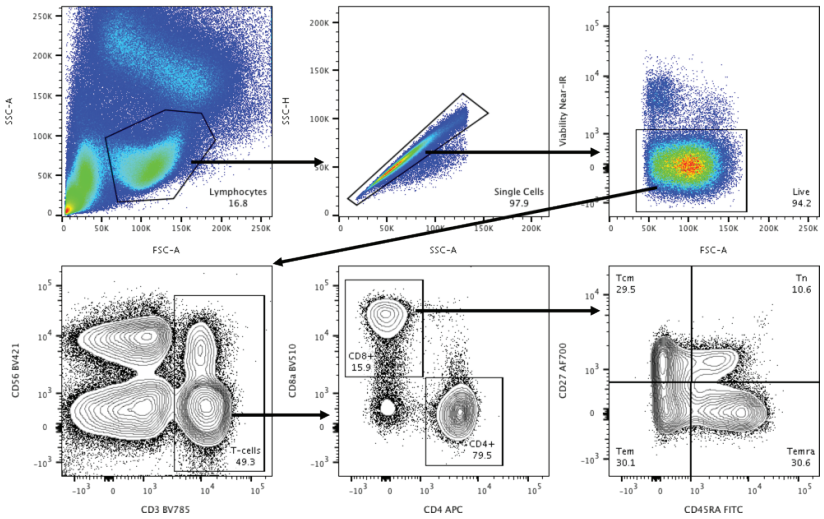


Figure 2.2. Flow cytometry gating strategy to identify $CD8^+$ T cells and four main subsets. Tcm = T central memory (central memory T cell (T_{cm})). Tem = T effector memory (T_{em}). Tn = naive T cell. Temra = T effector memory T cells re-expressing CD45RA (equivalent to T_{eff}). *This figure was produced by Chelsea Taylor.*

2.6 General statistical analysis

All statistical analysis was performed in *R* (v4.0.5). Statistical tests applied were as per the figure legends and were two-sided unless otherwise stated. Where an *R* package has been used to analyse the data - e.g. *FindMarkers* - the default statistical tests and significance thresholds have been used, unless otherwise stated. In general, the *R* package *ggpubr* and function *stat_compare_means* was used to generate all Wilcoxon test comparisons. *Fishers.test* in base *R* was used for Fisher's tests. The Kolgomorov Smirnov test compares likelihood of *A* values being found in *B* probability distribution and was performed using *R* package *Stats*, function *ks.test*.

2.6.1 Survival analysis

Survival analysis was performed using the *survival* package in *R* (for survival models and Cox proportional hazards calculations). Plots were generated with the function *ggsurvplot* (*survminer* package) and the Log-rank test used as labelled.

2.6.2 LSI analysis

Prior to survival analysis of LSI data, a number of steps were undertaken to clean, code and merge the outputs from clinical systems. The treatment was coded to mean the first ICB that was given for *metastatic* cancer. The 'diagnosis' field referred to the diagnosis for which ICB was given. Whether treatment had previously been received for another type of malignancy, or whether there were multiple diagnoses, was also recorded and included as co-variates (e.g. Table A.2). LSI was calculated based as the post-treatment lymphocyte count (defined as the first sample taken at least 21 days following ICB, but no later than 49 days) over the pre-treatment count (closest to the first cycle of ICB, but no greater than 30 days beforehand).

3 | Analysis of peripheral CD8$^+$ T cell subsets before and after ICB

3.1 Chapter-specific acknowledgements

Single-cell sequencing experiments on samples from patients with MM were performed by both myself and Rosalin Cooper. The pre-processing and QC of the sequencing data was performed by Isar Nassiri; I started my analysis at the filtered 'gene expression matrix' stage. Both myself and Orion Tong worked on downstream analysis of the data. However, presented below are only analyses that were conducted and produced by me, with the two exceptions of Figure 3.1 and Figure 3.8 which were both produced by Orion. These figures are explicitly acknowledged as Orion's in the captions.

The bulk RNAseq data was generated from blood collected by multiple colleagues, as acknowledged in the Declaration (page iii). Single cell experiments on samples from patients with mRCC were performed, pre-processed and aligned by myself, Elsita Jungkurth, Orion Tong and Bo Sun. Details of this with specific acknowledgements are outlined at the start of Chapter 5, page 146.

The work in this chapter was written up and published in *Science Immunology* in October 2021[78], with Orion and I as co-first authors. The manuscript appears as Appendix E on page 279.

3.2 Chapter-specific background

As outlined in introduction section 1.5.3.2 (page 50), analysis of bulk RNAseq data by the group demonstrated that patients with no progression of disease at 6 months of treatment had significantly more large clones in their peripheral blood than those with progressive disease

(Figure 1.12, page 55, and reference [93]), a finding I am able to replicate with TCRseq data in Chapter 4 (Figure 4.4a, page 122). I was particularly intrigued by this finding and the fact that large clones at day 21, but not baseline, associate with outcome - suggesting an interaction with ICB. Further, due to the fact that this biomarker relied on a metric at 21 days post-treatment (i.e. number of large clones at 21 days), I wished to refine this and investigate for *baseline* peripheral blood features that correlate with outcome.

To address these questions, I performed scRNAseq of both transcriptomes and TCRs of peripheral magnetically-sorted $CD8^+$ T cells from patients receiving ICB for MM at baseline and 21 days later (referred to as the SciImm experiment - see methods section 2.2, page 68). I analysed changes over time at both a subset and clonal level and was able to demonstrate that large clones are more likely to be from effector (T_{eff}) subsets. Further, ICB has a differential effect on $CD8^+$ T cells as a function of their clonal size - with larger clones differentially regulating more, and more relevant, genes post-ICB, even within the same subset. Further, more cytotoxic $CD8^+$ T cells were more likely to persist following ICB and be found within melanomas from public databases.

I wished to further expand this analysis and investigate cross-cancer comparisons and so subsequently performed further scRNAseq experiments on samples from nine patients with mRCC at three time points post ICB (part of the 'LT' experiment - see methods section 2.2, page 68). This allowed me to compare the effects of ICB on $CD8^+$ T cell clones between these two tumour types, finding some areas of divergence but overall a number of similarities.

Donor	Age	Sex	Treatment
80	82	M	sICB
81	72	F	sICB
82	57	M	cICB
83	45	F	cICB
84	43	F	sICB
85	56	M	cICB
87	68	M	cICB
88	69	M	sICB

Table 3.1. Summary of eight patients included in scRNAseq experiment.

3.3 Results

3.3.1 Single-cell sequencing of eight patients with metastatic melanoma

I generated paired baseline (day 0, d0) and on-treatment (day 21, d21) 5' scRNAseq and V(D)J profiles across magnetically-sorted peripheral $CD8^+$ T cells from eight patients with MM who received either cICB (n=4) or sICB (n=4) (Table 3.1). Following alignment and QC, (see methods section 2.2.2, page 70), there were 22,445 cells, of which 17,909 cells had TCR sequences. Following dimensionality reduction and cell annotation - performed by Orion Tong, see methods section 2.2.3 (page 74) - we identified seven distinct $CD8^+$ T cell subsets: naive, T_{cms}, T_{ems}, T_{effs}, mitotic, $\gamma\delta$ T cells and mucosal associated invariant T cells (MAIT cells) (Figure 3.1a). These were defined by key marker genes as summarised in Figure 3.1b, with key immune pathways, including IFNγ signalling and T cell activation/co-stimulation, enriched in T_{ems} and T_{effs} (Figure 3.1c). Using a gene set based on the top 50 genes co-expressed with IFNγ (Supplementary Table A.1), Orion generated a cytotoxicity score which could be applied to each cell using AddModuleScore in the *Seurat* package (see methods section 2.2.4.4, page 78). Consistent with their gene expression, T_{ems} and T_{effs} had higher cytotoxicity (Figure 3.1d).

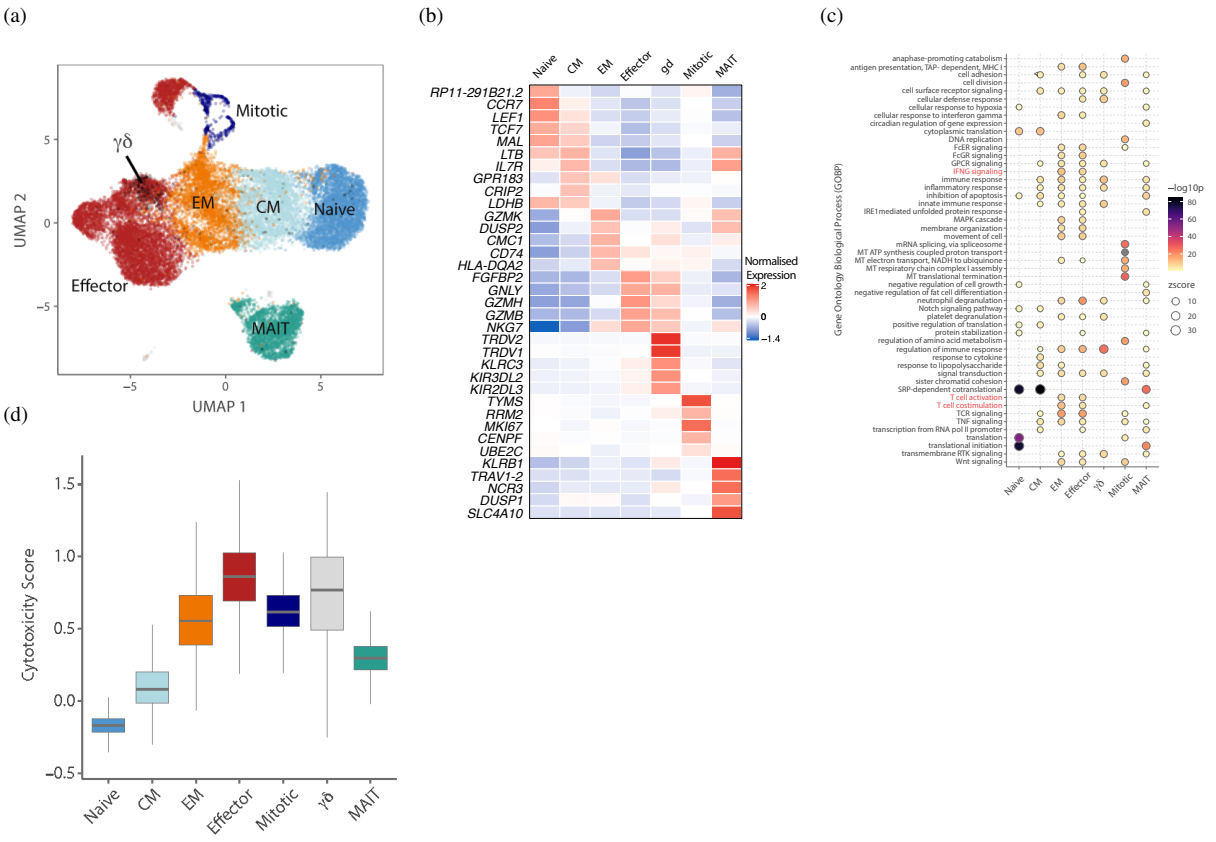


Figure 3.1. (a) UMAP clustering of 22,445 magnetically-separated peripheral CD8⁺ T cells from eight patients pre-ICB (d0) and 21 days later (d21), demonstrating seven subsets. (b) Heatmap displaying five most significant differentially expressed genes for the subsets. (c) GOBP analysis for key pathways differentially regulated by the subsets. (d) Cytotoxicity score for each subset. CM = T_{cm}, EM = T_{em}, effector = T_{eff}, $\gamma\delta$ = $\gamma\delta$ T cell. *These figures were produced by Orion Tong.*

3.3.2 CD8⁺ T cell subset distribution and gene modulation post-ICB varies as a function of clone size

Whilst we had previously described that the number of large clones was prognostic, and that these clones had a more cytotoxic gene expression profile[93], the peripheral blood phenotypes of these clones was hitherto unknown. Plotting the cell type cluster by clonal size demonstrated that at both the pre- and post-treatment time points, large clones we dominated by T_{effs}, with virtually no naive cells present (Figure 3.2).

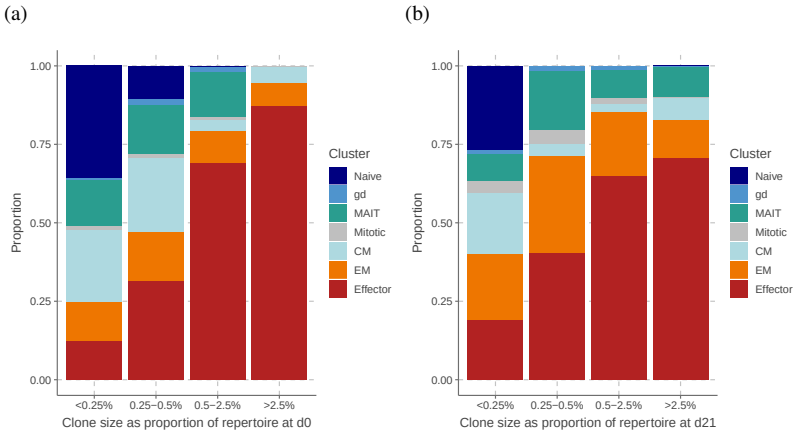


Figure 3.2. (a) clones present at baseline (d0) were categorised based on size (≤0.25%, >0.25% ≤0.5%, >0.5% ≤2.5%, >2.5%) and coloured by subset identity. (b) as per (a) but at 21 days post-ICB (d21). CM = T_{cm}, EM = T_{em}, effector = T_{eff}, gd = $\gamma\delta$ T cell

I then sought to understand the relationship between clonal size and response to ICB. I therefore filtered for just clones present at each time point and categorised these into four categories based on their clonal size (≤0.25%, >0.25% ≤0.5%, >0.5% ≤2.5%, >2.5%). I used repeated random downsampling, bootstrapping 100 times, in order to control for variation in cell number across clone size category and time point (see methods section 2.2.4.5, page 79) and examined the number of genes differentially regulated following treatment. This produced a response pattern of DE genes according to clone size, with small- and medium-sized clones having comparatively fewer DE genes than large and very large clones (Figure 3.3a). Given that this analysis is potentially

confounded by differing subset proportions in each size category, I repeated this process restricted to T_{eff} and T_{em} subsets, with clonal size simply dichotomized with a cut-off of 0.5% of the repertoire to denote large from small. The previously observed pattern was preserved within each subset, with larger clones again showing greater numbers of DE genes after ICB compared with smaller clones (Figure 3.3b). These findings were replicated when analysis was performed sequentially, each time removing a different patient, suggesting that the findings were not reflecting skew from an outlier individual (plot not shown).

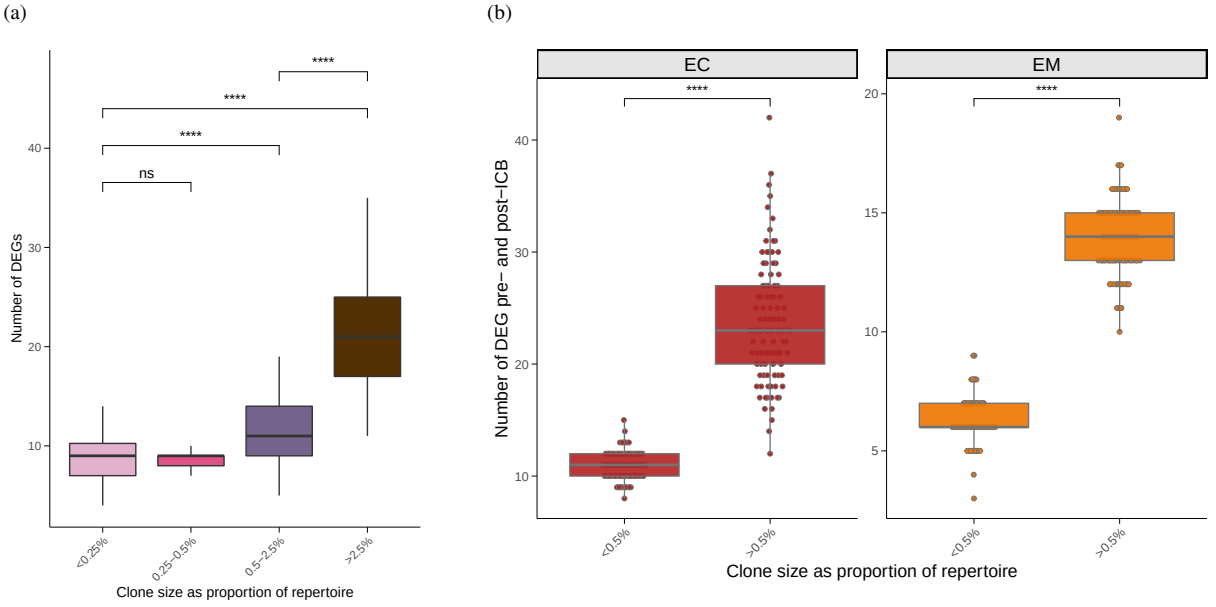


Figure 3.3. (a) Number of DE genes before and after treatment per clonal size bin. Only clones present at both timepoints were included and each clonal size bin was subsampled to a constant size and the analysis bootstrapped 100x. (b) Number of DE genes before and after treatment for large versus small T_{effs} (labelled as 'EC', red) and T_{ems} (labelled as 'EM', orange). Each cluster was subsampled to a constant size and the analysis bootstrapped 100x. Statistics with two-sided Wilcoxon rank sum test.

To understand these effects at a functional level, I performed a GOBP analysis based on the DEG sets within the T_{eff} and T_{em} subsets, controlling for differences in number of DEGs between groups (see methods section 2.2.4.6, page 80) (Figure 3.4). I noted that large T_{eff} clones had divergent gene expression following ICB compared to both small T_{eff} clones (<0.5% of the repertoire) (Figure 3.4a) and large T_{em} clones (Figure 3.4b), with pathways such as T cell activation, proliferation

and co-stimulation, TCR signalling, and IFNγ production uniquely up-regulated in large T_{effs}.

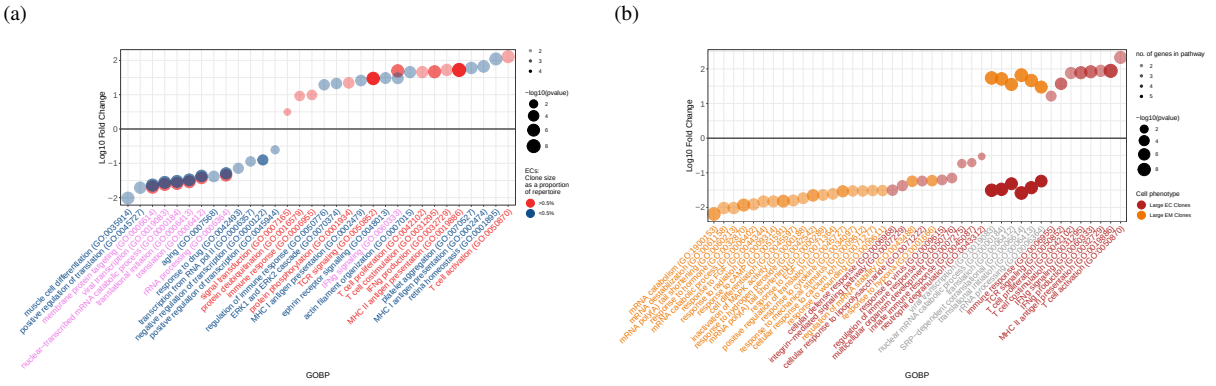


Figure 3.4. (a) GOBP analysis demonstrating pathways up- and down-regulated in large versus small T_{effs} (labelled 'EC') before and after treatment. Large T_{effs} are colored in bright red and small T_{effs} in blue. Pathways where the text is in purple represent those that are shared between both groups. (b) GOBP analysis demonstrating pathways up- and down-regulated in large T_{effs} (red) versus large T_{ems} (labelled 'EM', orange) before and after treatment. Pathways where the text is in grey represent those that are shared between both groups.

Taken together, I can conclude that the response to ICB is influenced by clonal size - both in the number and type of gene modulated. Larger clones display marked enhancement of immune gene expression after ICB treatment, with large T_{effs} uniquely up-regulating pathways crucial to the ICB response.

3.3.3 Cytotoxic CD8⁺ T cell clones persist following ICB treatment

To further understand changes to gene expression early post-ICB and follow up the observation that the number of large clones at day 21, but not baseline, correlates with outcome following ICB[93], I examined clones that expanded or persisted from baseline to 21 days, compared to those that were only found at baseline, restricting the analysis to clones composed of two cells or more. Unsurprisingly, large clones were more likely to be found at both time points, with clones only sampled at one time point predominantly belonging to smaller size categories (Figure 3.5a). Applying the previously-mentioned cytotoxicity score (Figure 3.1d), I found that although cytotoxicity was globally increased following ICB, clones present at both baseline and d21, or

only at d21, had increased cytotoxicity over those present only at d0, a consistent finding across both small and large clones (defined by a 0.5% of repertoire size cutoff) (Figure 3.5b).

To explore these observations further, I focussed on the baseline profile of clones, and categorised clones into those that significantly shrunk (as per a Fisher's exact test, see methods section 2.2.4.1, page 76) or were present at baseline but absent at d21 and those that expanded or showed no significant change in size from baseline to d21. Those which shrunk or disappeared from baseline to d21 were termed "involuting clones", whilst those which grew or did not change in size I refer to as "stable/expanding". Small clones that were stable/expanding after ICB were significantly more cytotoxic at baseline than those involuting clones (Figure 3.5c). However, this difference was not seen within larger clones, which were generally significantly more cytotoxic than smaller clones (Figure 3.5c). As such, it appears that the observed increase in cytotoxicity post-ICB is due by a combination of the persistence of pretreatment cytotoxic T cell clones, involution of clones with low cytotoxicity, and the emergence of more cytotoxic clones.

I wished to understand how these results applied to later time points, and therefore turned to bulk RNAseq data from magnetically sorted CD8$^+$ T cells sampled at day 63-106 (d63+) - which were available for six of the eight patients in this cohort. I matched single-cell and bulk clones on the basis of the TCRβ chain and found 992 clones, which comprised of 4245 cells at d21 in the single-cell data. d21 and d63+ clone size were significantly correlated (Spearman's rank ρ=0.87, p<0.0001), suggesting long term clonal stability (Figure 3.6a), a feature I subsequently follow up in Chapter 5. I classified clones at d21 in the single-cell data as those that subsequently involute by d63+ or those that are stable/expanding between d21 and d63+. Notably, those stable/expanding clones are enriched for T_{effs}, with under-representation of T_{ems} (Figure 3.6b). Further, within the T_{eff} subset, clones which are stable/expanding up to d63+ are more cytotoxic at d21 than those that involute (Figure 3.6c). This trend is true for both large and small clones, although the

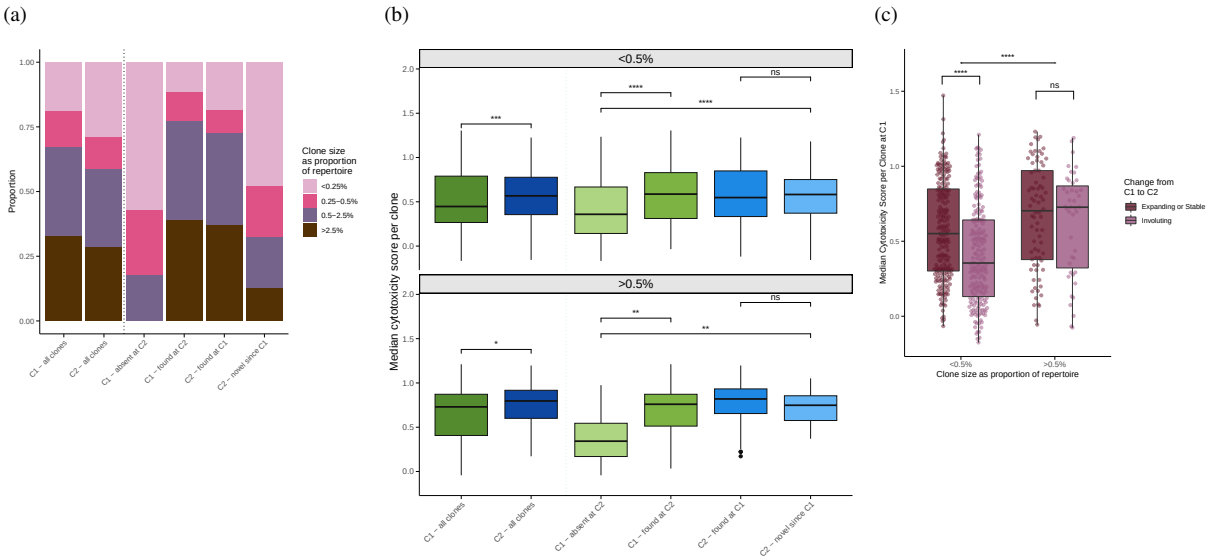


Figure 3.5. (a) Clones were categorised whether they were present or absent at one, or both, time-points and coloured by their size composition. (b) Cytotoxicity score per clone for each of the categories, faceted by clonal size (large vs small). (c) Clones were categorised into two categories - involuting for those that significantly shrunk or disappeared from baseline to d21 or stable/expanding for those that increased in size or did not change. Colours represent these categories, with median cytotoxicity per clone (at baseline) plotted against clonal size. Statistics with two-sided Wilcoxon rank sum test. C1 = d0. C2 = d21.

difference in large clones was not statistically significant (Figure 3.6d).

Finally I performed a DEG analysis on those clones that are stable/expanding from d21 to d63, compared to those that are involuting. I identify a number of genes linked to this clonal stability, which were markedly cytotoxic and typically associate with NK cells. For example, a number of killer lectin receptor genes, including *KLRF1* (killer cell lectin–like receptor F1), *KLRC2/3* (killer cell lectin-like receptor C2/3), were significantly higher in stable/expanding T_{effs} at d21 (Figure 3.6e).

It was notable that these clones which go on to persist long term were particularly cytotoxic at d21 and together, these findings suggest that pre-existing cytotoxicity associates with subsequent increased clonal persistence, with emerging clones, even if small, also having higher levels of cytotoxicity. Similarly, within the T_{eff} compartment, d21 cytotoxic clones have increased likelihood to be found at d63+ of treatment.

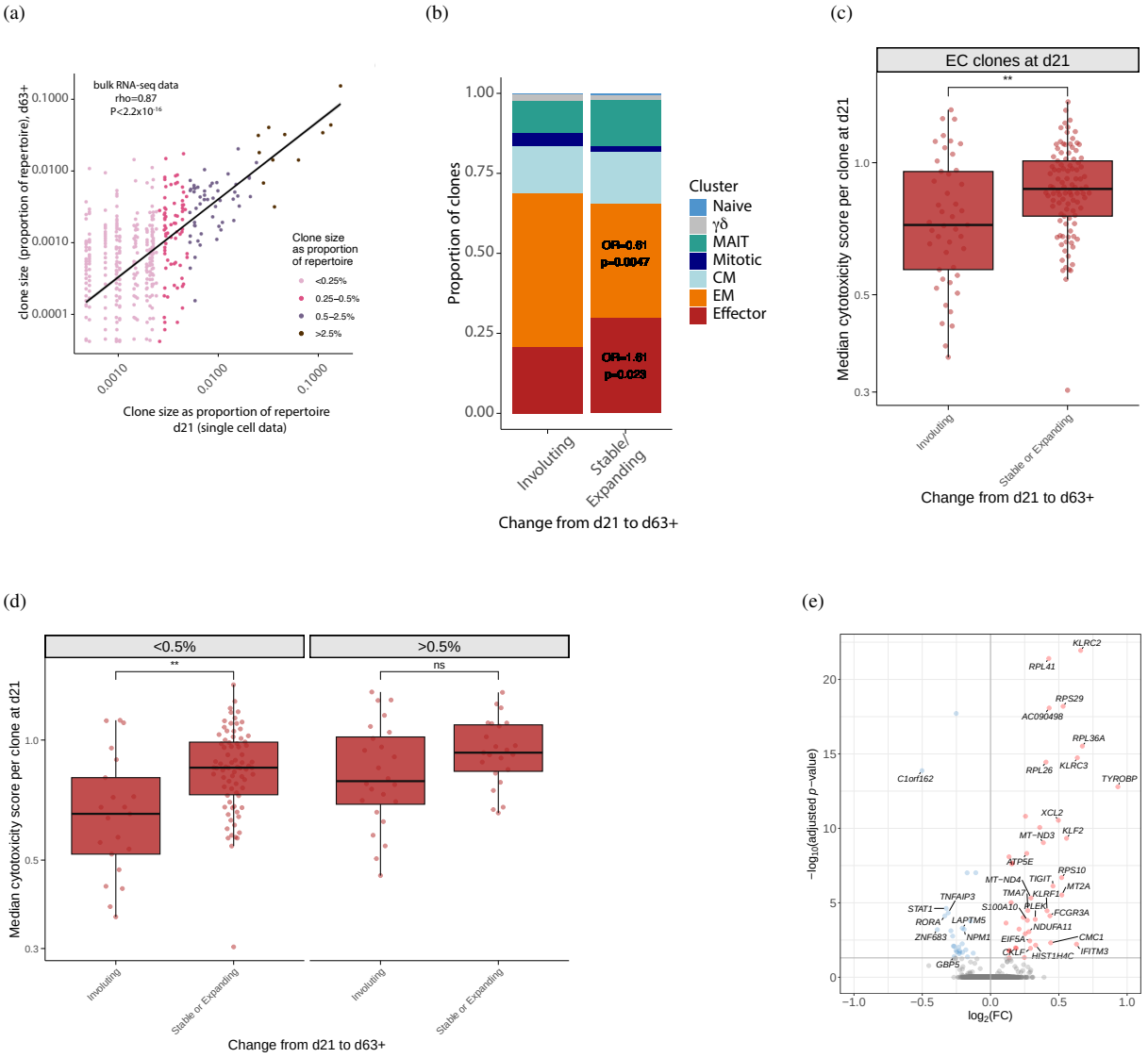


Figure 3.6. (a) Clone size at day 21 (d21, from scRNAseq) compared with size at day 63+ (d63+, from bulk RNAseq). Clones are coloured by their size as a proportion of the repertoire (at d21). (b) Clones were categorised by whether they were involuting or stable/expanding between d21 and d63+ and coloured by their subset; odds ratios (ORs) for difference between groups. (c) Median cytotoxicity score per clone for those clones at d21 that either involute or are stable/expanding by d63+. (d) as per (c) but clones faceted on their size. (e) Volcano plot showing DEGs at d21 between those clones that subsequently involute between d21 and d63+ and those clones which are stable/expanding. Genes in red are upregulated in stable/expanding clones. Statistics with Spearman's rank (a), Fisher's exact test (b) or Wilcoxon rank sum test (c) and (d). EC = T_{eff}.

3.3.4 Large, cytotoxic CD8+ T cell clones are more likely to be found within melanomas

In order to attempt to validate these findings in external data, I looked at work from Pruessman *et al.*[177] who had sequenced TCRβ chains from 199 resected melanomas. Of the 85,528 TCRβ identified in this data, 392 were present in my single cell data (see methods section 2.2.4.7, page 81). I examined the characteristics of these clones, finding that they were enriched for T_{effs} as well as large clones - at both d0 and d21 (Figures 3.7a and 3.7b for d0; d21 plots not shown). Further, those clones carrying a TCRβ found in within the Pruessman dataset had significantly greater toxicity than those not, at both baseline and d21 (Figure 3.7c for d0; d21 plot not shown). For comparison, I obtained public viral TCR data from the VDJdb[233] (see methods section 2.2.4.7, page 81), with a match of 149 cells within the single cell dataset. These were neither enriched for T_{eff} cells nor large clones and there was no difference in cytotoxicity score for those clones matching viral TCR and those not (Figures 3.7d - 3.7f).

3.3.5 Cytotoxicity score at baseline predicts outcome following ICB

In work undertaken in close conjunction with Orion Tong, we were able to apply the cytotoxicity score - which as described above appears to be a key feature of expanding and persistent clones - to our bulk RNAseq cohort (n=131 d0 samples) by taking the geometric mean of the normalised gene expression (see methods section 2.3.4.1, page 82). Classifying individuals into high or low cytotoxicity simply based on the median of this score, we could show that *baseline* cytotoxicity was predictive of progression-free survival (Figure 3.8).

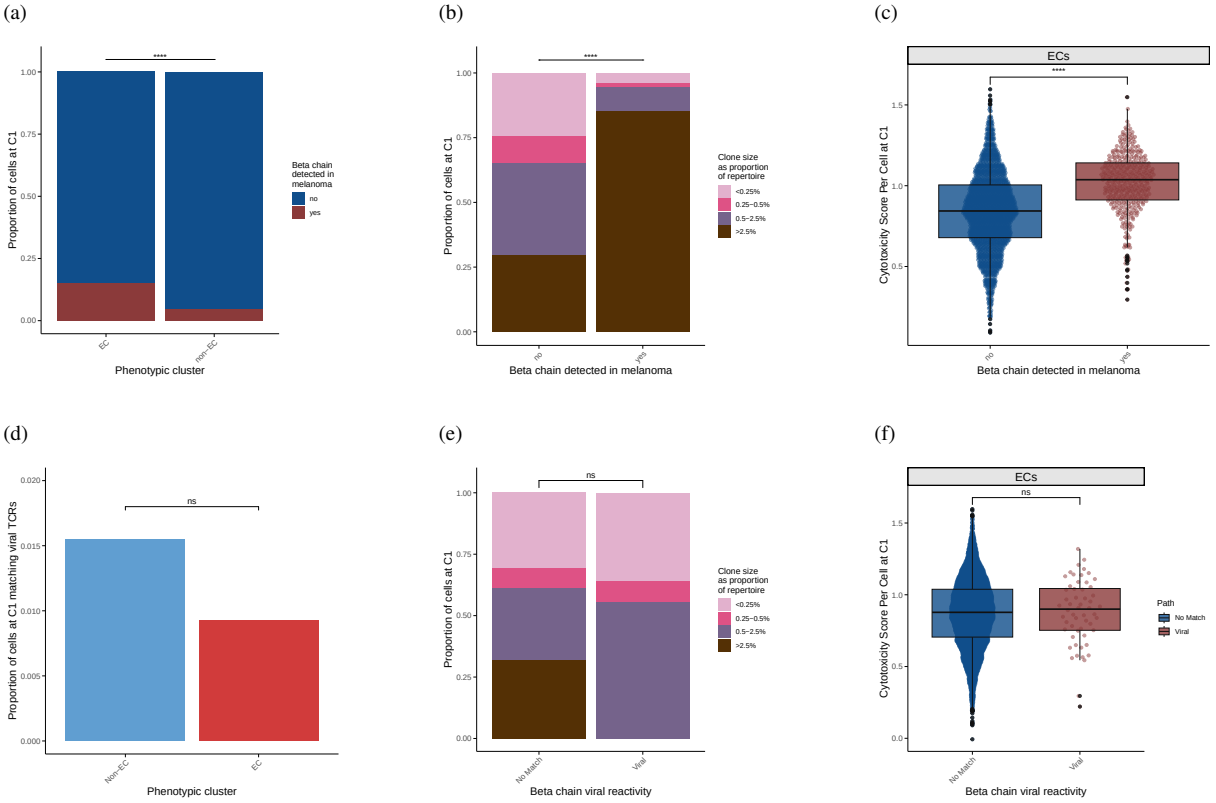


Figure 3.7. (a) Proportion of cells at baseline in single cell data coloured by whether their TCRβ matches with TCRβ found in melanomas, as per the Pruessman *et al.* dataset[177] and split by whether those cells originate from the T_{eff} cluster (labelled as 'EC'). (b) clonal size make up of cells which carry a TCRβ matching TCRβ in the Pruessman data. (c) Cytotoxicity score of those cells with TCRβ matching the intra-melanoma dataset, compared to those that don't. (d) Proportion of cells at baseline that carry a TCRβ that matches public viral TCRβ (from VDJdb[233]), for either T_{eff} (labelled as 'EC') or non T_{eff} cells. (e) as per (b) but for those cells matching viral TCRβ. (f) Cytotoxicity score per cell for those cells with a TCRβ which matches public viral TCRβ. Statistics with Fisher's exact test (a), (b), (d) and (e) and Wilcoxon rank sum test (c) and (f). The test performed in (b) and (e) was comparing the proportion of clones occupying >0.5% of the peripheral repertoire (large clones) in each group. EC = T_{eff}.

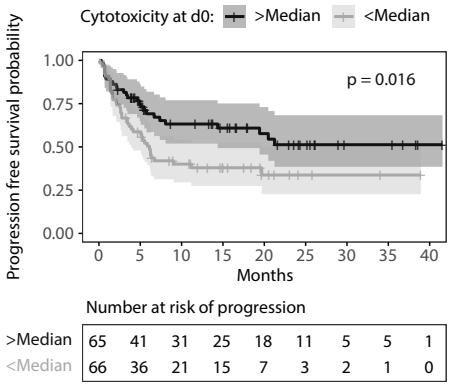


Figure 3.8. Kaplan-Meier curve showing difference in progression-free survival between those with above and below median cytotoxicity score, based on expression in bulk RNAseq pre-treatment. Statistics with log-rank. *This figure was produced by Orion Tong.*

3.3.6 Single-cell sequencing of nine patients with mRCC

In order to build on this work and perform cross-cancer comparisons, I subsequently performed scRNAseq (with paired TCRseq) of magnetically-sorted CD8⁺ T cells from nine patients with mRCC. These experiments were performed several years later, multiplexed with a number of samples from patients with MM as part of a very large single-cell experiment to examine long term changes following ICB - the 'LT experiment'. A full explanation of the different single-cell experiments and methodology used is given in methods section 2.2, page 68.

In total, I performed scRNAseq on n=22 samples from n=9 patients with mRCC, taken at baseline, d21 and d63. The patient characteristics are summarised in Table 3.2a, with the sample details found in Table 3.2b. Steps taken to perform the laboratory experiments, pre-process, align and demultiplex data are outlined in methods sections 2.2.1.2 and 2.2.2 (page 69 onwards).

(a)

Characteristic	N = 9[1]
Age	61 (7.5)
Sex is Female	1 (11%)
Treatment	
cICB	9 (100%)
Progression of disease	6 (67%)

[1] Mean (SD); n (%)

(b)

Characteristic	N = 22[1]
Source	
CD8	22 (100%)
PBMC	0 (0%)
Timing of sample (days post-treatment)	
0	9 (41%)
21	7 (32%)
63	6 (27%)
Progression of disease	15 (68%)

[1] n (%)

Table 3.2. (a) Characteristics of the patients with mRCC. (b) Characteristics of samples included in the mRCC scRNAseq experiment.

Due to the fact that these experiments were performed after a long time interval, there were progressive developments in approach. As such the pre-processing, dimensionality reduction and annotation of the LT experiment differed to the methods used in the original SciImm experiment (methods sections 2.2.2 and 2.2.3). As a result, the cell identities assigned to CD8⁺ T cell subsets

differed slightly in nomenclature to those assigned originally in the SciImm experiment.

To maximise consistency, I re-ran all SciImm samples through the entire LT experiment pre-processing pipeline. Using the same cell barcode, I was then able to compare identities between the SciImm annotation and the LT annotation. This showed that whilst the semantics were updated, there was clear consistency across cell identities as demonstrated by Figure 3.9. For example, the T_{eff} compartment in the SciImm samples (labelled as 'Effector') map to CD8.TEMRAs and CD8.TEMRA.CMC1 on the new LT annotation. For the remainder of this chapter, I will refer to cell subset identities by the newer, LT experiment, nomenclature whereby T_{cm} = 'CD8.TCM' & 'CD8.TCM.CCL5', T_{em} = 'CD8.TEM' and T_{eff} = 'CD8.TEMRA' & 'CD8.TEMRA.CMC1'.

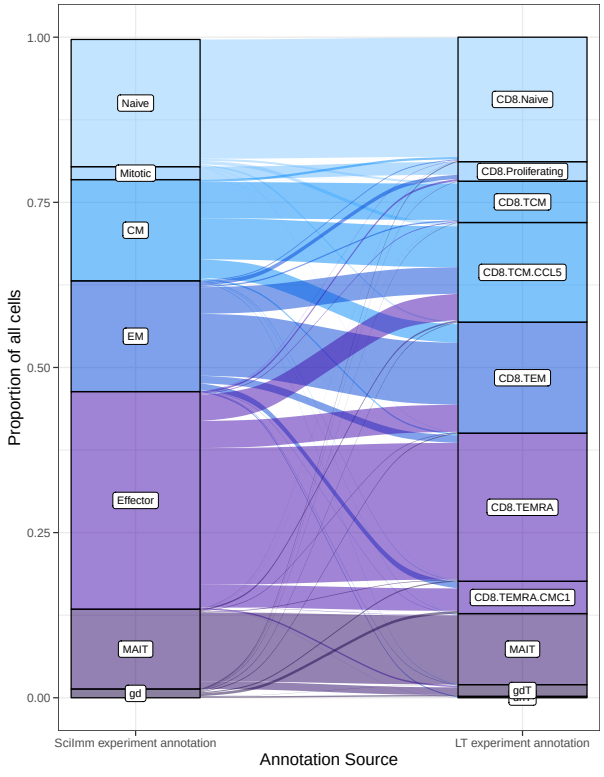


Figure 3.9. Alluvial plot showing relationship between subsets as originally annotated (SciImm experiment) and following re-annotation in 2022 (LT experiment).

Following QC, dimensionality reduction, cluster annotation and filtering for only CD8⁺ T cells (see methods section 2.2.2, page 70), there were 33,229 cells, clustering in ten major subsets.

These can be visualised on a UMAP (Figure 3.10a) and defined by maker genes as displayed in the heatmap (Figure 3.10b).

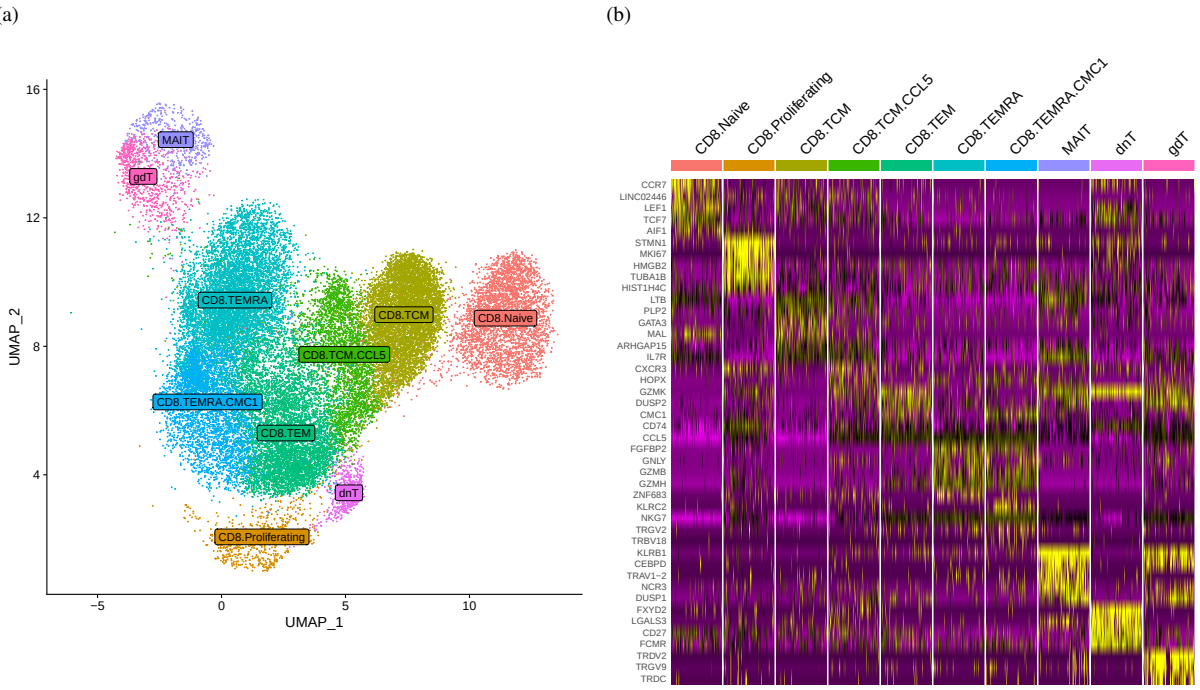


Figure 3.10. (a) UMAP plot of CD8⁺ T cell samples from n=9 patients with mRCC reveals ten distinct subsets. (b) Heatmap showing top 5 genes differentially expressed by each cluster. A yellow colour refers to differential upregulation compared to other clusters, a purple colour differential downregulation. TCM = T_{cm}, TEM = T_{em}, TEMRA&TEMRA.CMC1 = T_{eff}, MAIT = mucosal associated invariant T cells, gdT = $\gamma\delta$ T cells, dnT = double negative T cells.

3.3.7 Effect of clone size on subset distribution and gene expression in mRCC

I first repeated the analysis of subset distribution by clone size (i.e. that presented in section 3.3.2, page 94, above), categorising clones into four size groups ($\leq$0.25%, >0.25% $\leq$0.5%, >0.5% $\leq$2.5%, >2.5%) and plotting the cluster distributions within each clonal size category. The pattern mirrored that as seen for the samples from patients with MM (i.e. Figure 3.2, above) with the proportion of large clones dominated by T_{eff} subsets and all naive cells found in the smaller clone

categories (Figure 3.11). Notably the dominance of large clones by T_{eff} cells is present - and appears more marked - at C4 (63 days) (Figure 3.11c).

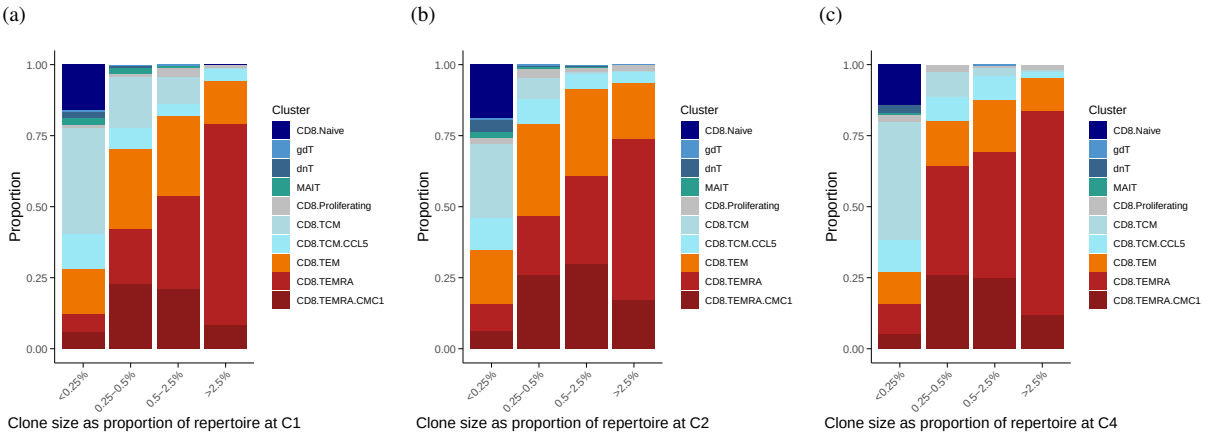


Figure 3.11. (a) clones present at d0 (labelled as 'C1') were categorised based on size ($\leq$0.25%, >0.25% $\leq$0.5%, >0.5% $\leq$2.5%, >2.5%) and coloured by subset identity. (b) as per (a) but at d21 (labelled as 'C2'). (c) as per (a) but at d63 (labelled as 'C4'). TCM = T_{cm}, TEM = T_{em}, TEMRA&TEMRA.CMC1 = T_{eff}, MAIT=mucosal associated invariant T cells, gdT=$\gamma\delta$ T cells, dnT=double negative T cells.

I next wished to see if the finding that large T_{eff} clones have a greater number of DEGs pre- and post-ICB was the case in mRCC. I therefore repeated the analysis (as presented in section 3.3.2, page 94, above) whereby I downsampled T_{eff} cells (i.e. the CD8.TEMRA and CD8.TEMRA.CMC1 cluster combined) from large and small clones to a fixed number and quantified the number of DEGs pre- and 21 days post-ICB, bootstrapping this 100x (see methods section 2.2.4.5, page 95). This finding replicated for the mRCC samples (Figure 3.12a).

I subsequently looked at pathways differentially modulated between large and small clones in the mRCC samples of T_{effs}, again restricting the number of significant genes to the the minimum across groups to control for differences in number of genes affecting the results (see methods section 2.2.4.6, page 80). Unlike in MM, there was not marked divergence in the type of pathway differentially regulated in large versus small clones (Figure 3.12b). Whilst small clones uniquely upregulate a type I interferon pathway, suggestive of a more innate/inflammatory response, both large and small clones also upregulate the similar 'defense response to virus' gene pathway

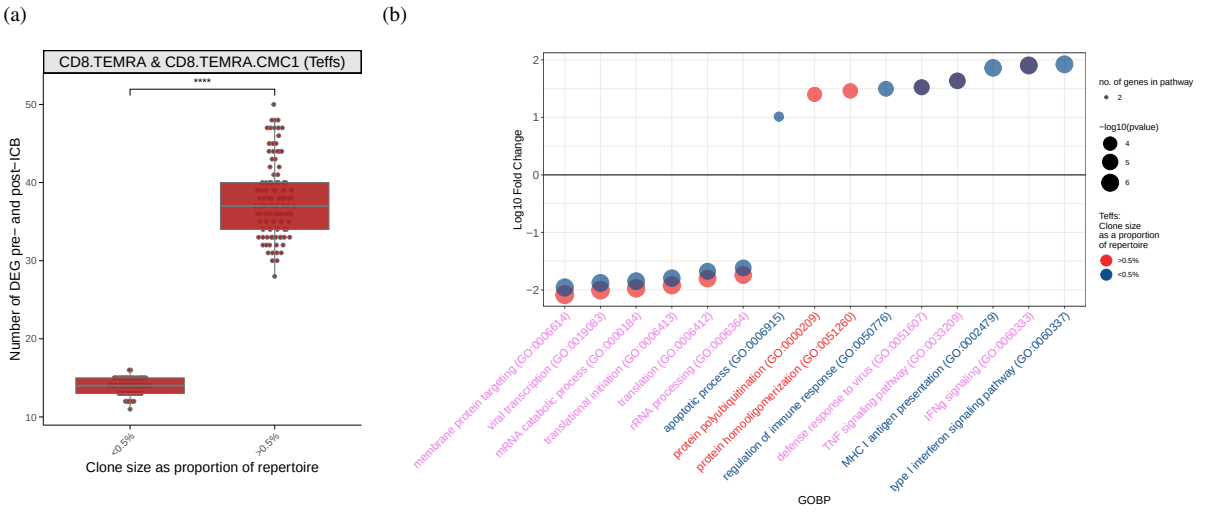


Figure 3.12. (a) Number of DE genes before and after treatment for large versus small T_{effs} (i.e. CD8.TEMRA and CD8.TEMRA.CMC1 combined). Only clones present at each time point were included. Each cluster was subsampled to a constant size and the analysis bootstrapped 100x. Statistics with two-sided Wilcoxon rank sum test. (b) GOBP analysis demonstrating pathways up- and down-regulated in large versus small T_{effs} before and after treatment. Large T_{effs} are coloured in bright red and small in blue. Pathways where the text is in purple represent those that are shared between both groups.

(Figure 3.12b). Notably, all T_{effs} upregulate IFNγ signalling, suggestive of increased cytotoxicity in this compartment post-ICB.

3.3.8 Cytotoxicity of persistent CD8⁺ T cell clones in mRCC

I wished to investigate clonal persistence from 21 days post-treatment (d21, cycle 2, 'C2') to 63 days post-treament (d63, cycle 4, 'C4'). Due to the rates of progression of mRCC and toxicity to treatment, only a minority of patients with mRCC get four cycles of ICB. Hence, there were only three samples with sufficient cell numbers at d21 and d63 (see Table 2.2b). Again, I restricted the analysis to clones composed of two cells or more. There was stability in clone size between d21 and d63 with large clones at d21 remaining large by d63 (Figure 3.13a).

Similar to findings in MM, those clones that persist are mostly of T_{eff} and T_{em} phenotype (each clone phenotype being based on its majority cell membership (see methods section 2.2.4.2) (Figure 3.13b). In contrast to the findings in MM (i.e. Figure 3.6c), clones that are stable/expanding

between d21 and d63 are not more cytotoxic than those clones which subsequently involute for either the T_{em} or T_{eff} subsets (Figure 3.13c).

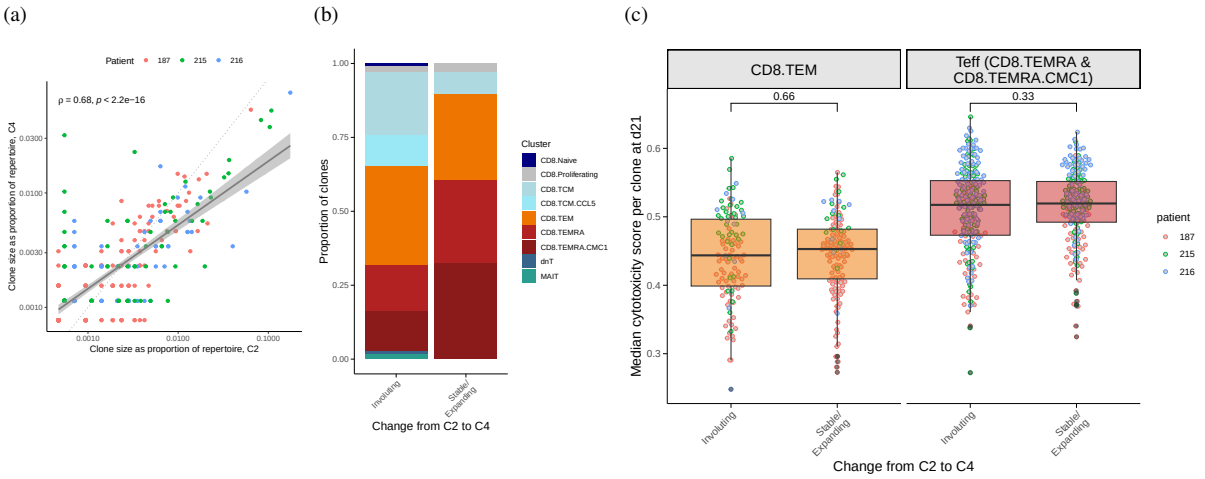


Figure 3.13. (a) Clone size at d21 ('C2') compared with size at d63 ('C4'). Clones are coloured by the patient. The solid line is the correlation line of fit, the dotted line is x=y. (b) Clones were categorised by whether they were involuting or stable/expanding between d21 and d63 and coloured by their cluster. (c) Median cytotoxicity score per clone for those clones at d21 that either involute or are stable/expanding by d63, faceted by cluster. Each dot is clone, coloured by patient. Statistics with Spearman's rank (a) or Wilcoxon rank sum test (c). C2 = d21, C4 = d63, CD8.TEM = T_{em}, CD8.TEMRA&CD8.TEMRA.CMC1 = T_{eff}.

3.3.9 Comparison of effector CD8⁺ T cell gene expression between MM and mRCC

Intrigued by the contrast between clones found in mRCC and MM at day 21, I was keen to explore differences in gene expression in these two conditions. Due to the fact that the SciImm experiment and LT experiment had been performed several years apart with very different experimental conditions (see methods section 2.2, page 68) direct comparisons between these datasets would likely be confounded. However, as part of the LT experiment, I performed scRNAseq on 18 patients with MM under the same experimental conditions as the samples from patients with mRCC. This cohort is described and presented in Chapter 5. The vast majority of these patients received pembrolizumab sICB (see Chapter 5, table 5.1) meaning that post-ICB comparisons with

the patients with mRCC (who universally received cICB) would also be confounded. I therefore opted to focus on a pre-treatment, baseline, comparison of $CD8^+$ T cells between the two cancer types, with all samples used for comparison derived from the LT experiment.

3.3.9.1 DEGs pre-treatment between samples from patients with mRCC and MM

Comparing T_{effs} between samples from patients with mRCC and MM at pre-treatment, most DEGs with the greatest magnitude of difference between tumour types were ribosomal or mitochondrial in origin (Figure 3.14a). This was increasingly evident with a GOBP analysis, whereby most pathways with significant differences between tumour types were related to translation. There were very few differentially regulated immunological pathways and those that were present - such as TCR or NFκB signalling - have a very low fold change difference (Figure 3.14b). I did note, however, that there appeared to be a number of differentially regulated TCR genes - as can be seen on the volcano plot (Figure 3.14a). To investigate this further, I analysed differences in TCR gene usage between the tumour types (Figures 3.14c and 3.14d) - noting that there was a wide range of inter-individual variation for many genes (as evidenced by the error bars) and only one V gene with significant differences in use between tumour types - TRBV6-5 (albeit with an uncorrected p-value; Figure 3.14c). Reassuringly, this was upregulated in patients with MM, the same direction as per the DEG analysis (Figure 3.14a). Nonetheless, taken together, there was limited evidence for differences in immunological gene expression pre-treatment between MM and mRCC.

Whilst there is an enormous body of literature describing DEGs discovered with *Seurat* and the *FindMarkers* function, as used above, some commentators have critiqued with this approach, suggesting that it is biased towards highly variable genes and leads to false discoveries of DEGs that do not exist[240]. The root cause of this is that each single cell is treated as a separate sample - with the potential to inflate p values and false positives. As such, an alternative is to pseudobulk

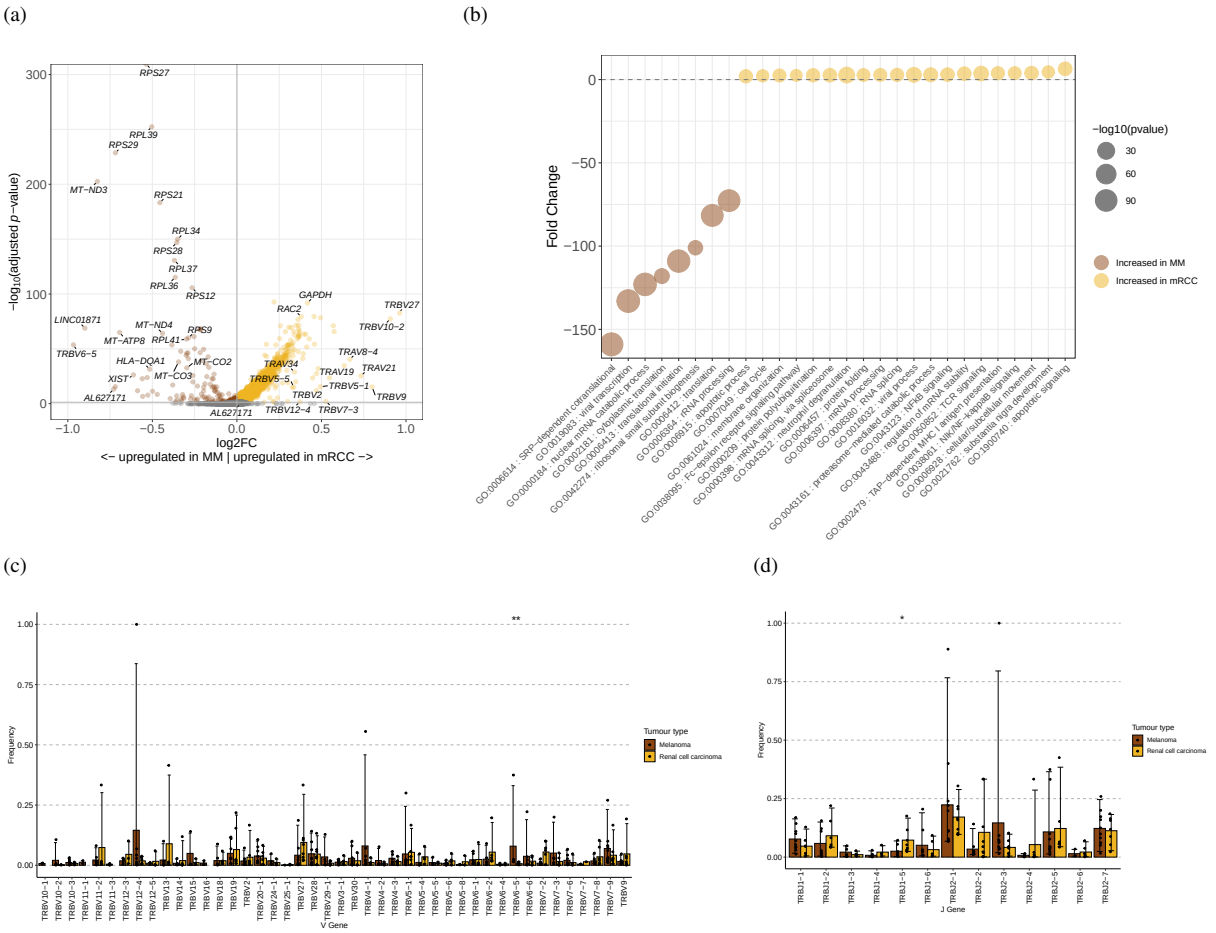


Figure 3.14. (a) Volcano plot showing DEGs between T_{effs} from patients with MM and mRCC at the pre-treatment time point. Genes to the right of the plot (coloured gold) are upregulated in mRCC whilst those to the left (coloured chocolate) are upregulated in MM. DEG analysis done with *Seurat FindMarkers*. (b) GOBP analysis of DEGs from (a). (c) TCRβ V gene usage across tumour types. (d) as per (c) but for J gene usage. Statistics with (uncorrected) Wilcoxon rank sum test (c) and (d).

the data - i.e. combine counts for all genes in a given cell-type within the same sample - and perform DEG analysis using *DESeq2* (see methods section 2.2.4.5, page 80). The disadvantage of this latter approach is a reduction in statistical power.

I performed a pseudobulk analysis on the same data - i.e. comparing pre-treatment T_{effs} from patients with MM and mRCC. Following conversion of the gene-by-cell matrix into a gene-by-sample matrix of raw counts, a DEG analysis was performed. This showed that there was no significant difference in gene expression on the basis of tumour types at pre-treatment, following p value adjustment. In order to corroborate this, I performed a PCA of gene expression and found

no separation of tumour types in the first 10 PCs (Figure 3.15, first six PCs shown).

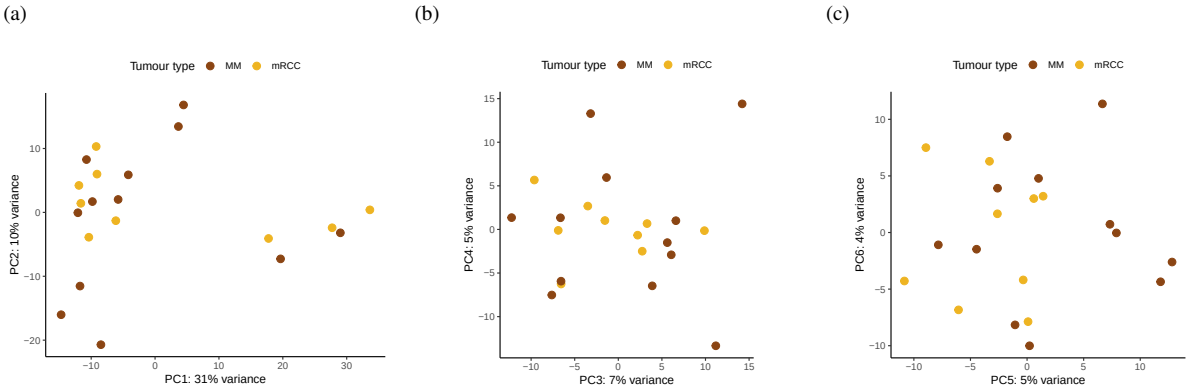


Figure 3.15. (a-c) First six principal components of normalised gene expression for T_{effs} from patients MM and mRCC at pre-treatment, coloured by tumour type.

3.3.9.2 Cytotoxicity scores in MM and mRCC

Finally, I applied the cytotoxicity score across tumour types to compare between mRCC and MM. Globally, there was a higher cytotoxicity in samples from patients with MM than mRCC at baseline (Figure 3.16a). However, this was not the case when looking on a subset-by-subset basis, with both T_{eff} and T_{em} clones having higher baseline cytotoxicity in mRCC. As such, it is possible that the globally higher cytotoxicity seen in MM was due to differences in subset proportion - whilst I found no significant difference in subset proportions between tumours for any subset (Figure 3.16d for T_{effs}, other subsets not shown), this data is likely underpowered due to the small sample size (n=6 mRCC and n=7 MM samples after filtering for only samples with >1000 cells at baseline - see methods section 2.2.4.3 and Table 2.2d). In this context, the trend suggests that patients with MM might have more T_{effs} - which could potentially explain the overall higher global cytotoxicity at baseline. Finally, the association of clone size and cytotoxicity was also identified in mRCC samples, with larger clones having greater cytotoxicity than smaller clones across cell subtypes (Figure 3.16c).

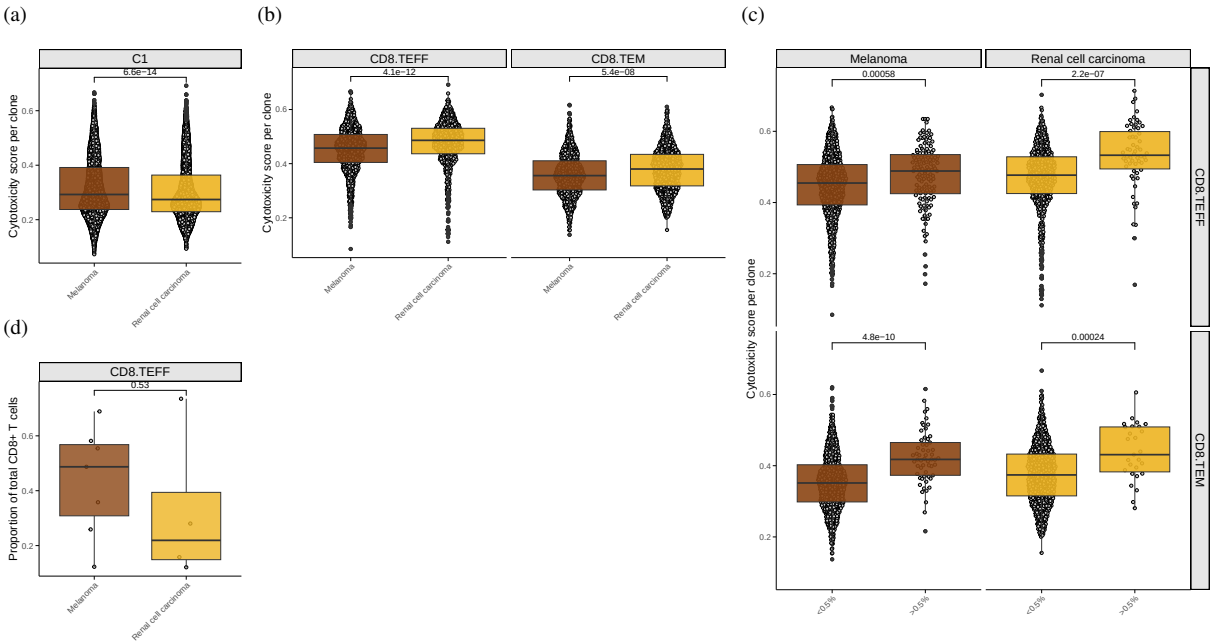


Figure 3.16. (a) Global cytotoxicity score pre-treatment, coloured by tumour. (b) Cytotoxicity score pre-treatment, coloured by tumour and faceted by subset. (c) Cytotoxicity score in large versus small clones, faceted by tumour. (d) Proportion of total CD8⁺ T cells occupied by T_{effs} coloured by tumour. For panels (a) to (c), each dot is a clone with the median cytotoxicity score per clone displayed. For panel (d) each dot is an individual, with the proportion of total CD8⁺ T cells occupied by T_{effs} displayed. Statistics with two-sided Wilcoxon rank sum test.

3.4 Discussion

In this chapter, I have explored early changes following ICB on both a subset and clonal level across both metastatic melanoma (MM) and metastatic renal cell carcinoma (mRCC). Following up our observation that the number of clones occupying >0.5% of the peripheral repertoire (large clones) at day 21 post-ICB significantly associates with clinical outcome in MM[93], I was able to demonstrate that large clones are predominantly made up of effector (T_{eff}) subsets - a finding that replicated in mRCC. Further, large clones are more sensitive to ICB and following treatment, modulate significantly more genes compared to small clones. In MM, there is a divergence not just in the quantity of DEGs but in the pathways modulated, with large clones over-expressing a range of highly relevant immunological processes, compared to small clones. Further, T_{effs} are more likely to persist to beyond 63 days than other cell subsets, and in MM those clones that do

persist are more cytotoxic than clones that involute over time. This was not the case in mRCC with the day 21 cytotoxicity equivalent between persistent and involuting clones. A comparison of gene expression of peripheral T_{effs} pre-treatment in MM and mRCC demonstrates relatively little difference between the two cancer types and whilst there are some differences in cytotoxicity - with T_{eff} clones in the context of mRCC being more cytotoxic - the magnitude of difference was small. Finally, applying the cytotoxicity score across bulk samples demonstrated that this metric, at baseline, was associated with clinical outcome in MM.

The finding that large clones responded to ICB in a divergent manner to small clones provides insight into the mechanistic underpinnings of our previous observations linking large peripheral $CD8^+$ T cell clone count with clinical outcome. It is notable that these clones appear particularly sensitive to ICB which may be because their expansion is due to tumour ligation and they are therefore 'exhausted' and susceptible to the effects of checkpoint inhibition. The fact that clones matching intra-tumoural TCRβ in public datasets were larger, more cytotoxic and from T_{eff} subsets lends credence to this theory. Further, that clones which persist from d0 to d21 are as cytotoxic as those which emerge at d21, along with the fact that baseline cytotoxicity correlates with PFS, strongly suggests that the baseline immune landscape is a crucial factor in determining subsequent response to ICB. Without the 'correct' clones present pre-treatment - i.e. those capable of recognising or responding to antigen - the likelihood of responding to ICB may be diminished.

Comparisons between MM and mRCC demonstrate that the importance of large clones is a pan-cancer phenomenon, with these clones having greater cytotoxicity, as well as differentially regulating more genes post-ICB in both tumour types. There were limited differences in gene expression of T_{effs} at the pre-treatment time point across cancers, with the majority of differences detected using the more sensitive single-cell DEG approach of *FindMarkers*, ribosomal and mitochondrial. This is perhaps unsurprising because both tumour types are immuno-sensitive

with good outcomes reported post-ICB. One might therefore expect a similar profile in their main effector compartment. Nonetheless, such similarities are relevant because they suggest that approaches to improve response or stratify patients in melanoma may be translatable to other tumours - in this case renal cell carcinoma - due to comparable *a priori* peripheral immune profiles.

Whilst this work is strengthened by its use of human samples, concomitant transcriptome and V(D)J sequencing and validation in bulk RNAseq data and external datasets, there are several limitations. Firstly, the number of individuals at each time point is low, reducing statistical power and increasing the chance that observed differences are influenced by inter-individual variation. Whilst this is a general issue for the entire field of scRNAseq, it is particularly the case in this experiment. For MM I was able to extrapolate findings to a much larger bulk cohort (e.g. 131 for the survival analysis) but due to low numbers of recruited patients with mRCC this wasn't possible in this tumour type. Further, this is observational data and so causation cannot be directly inferred and there is an assumption that presence of mRNA will result in protein expression - a correlation of functional phenotype with gene expression would strengthen the results.

In summary, the effect of ICB is determined by clonal size, with larger clones appearing more sensitive to checkpoint inhibition. Those clones that persist appear more cytotoxic in MM, as do clones that are found within public intra-tumoural datasets. Cross cancer comparisons replicate many of these findings in mRCC and whilst there are some subtle differences in gene expression between immune cells in MM and mRCC at baseline, there are many similarities.

4 | Clonal analysis of CD8$^+$ T cell repertoires following ICB

4.1 Chapter-specific acknowledgements

Experiments to generate T cell receptor sequencing (TCRseq) data were conducted alongside Chelsea Taylor, who also did the flow cytometry experiments (analysis thereof included in Figure 4.16). We worked closely to design the TCRseq experiment, select samples, perform the library preparation and pre-process the sequencing data. Rosalin Cooper identified suitable areas of tumour blocks and extracted RNA from FFPE-preserved specimens. All bulk RNAseq data was produced as part of group-wide collaboration, as outlined and acknowledged in the Declaration (page iii).

In 2021, the lab hosted Bethan Storey - a Final Honours School (FHS) student - and I was responsible for her day-to-day supervision. She undertook a project focussing on broad repertoire metrics of response; data similar to her analysis is presented below in section 4.3.2 - however all her work was directly supervised and checked by me, with figures herein all generated by myself. I performed all downstream analysis in other sections.

4.2 Chapter-specific background

A number of sections of Chapter 1, Introduction, are relevant to this chapter. Firstly, section 1.2 (*The role of CD8$^+$ T cells in the response to ICB*) details the importance of CD8$^+$ T cells in the immune response to MM and why I have sought to characterise their repertoire characteristics in more detail here. Further, sections 1.4 and 1.5 (*The T Cell Receptor (TCR)* and *T cell receptor*

repertoire analysis) explore the development of TCR repertoire diversity, how this can be analysed and the insights possible from such analysis.

As per the above, the importance of CD8+ T cells and analysis of their repertoires is established, with peripheral CD8+ T cell repertoire features correlated with response to ICB in MM and other tumours[99,182–184,241]. Further, as per Chapter 3, we have previously shown that within the peripheral CD8+ T cell fraction, pre-treatment clonal size and expression of cytotoxic genes is associated with response to treatment and OS[78], whilst the number of clones occupying >0.5% of the peripheral repertoire (large clones) 21 days post-treatment also correlates with outcome[93]. However, whilst the association between broad repertoire features and a response to ICB is now established, a description of key CD8+ T cell clones based on their TCR sequence is currently lacking. Further, most work thus far has focussed solely on insights gained from sequencing of the TCRβ with the TCRα generally not included in analysis - a phenomenon partially driven by the fact that Adaptive Biotechnologies' *ImmunoSEQ* platform only sequences the TCRβ.

In this chapter I describe work using deep TCRseq of sorted peripheral CD8+ T cells and CD4+ T cells from both healthy donors and a large cohort of patients undergoing ICB treatment for MM, alongside resected tumour samples. I aim to first describe broad repertoire features before going on to characterise and define key public CD8+ T cell TCRs which are putatively driving the anti-melanoma immune response following ICB. I investigate associations of these TCR with outcome, describe the molecular features of these clones, and attempt to validate these findings in external datasets.

4.3 Results

4.3.1 Deep sequencing of the T cell receptor

In conjunction with Chelsea Taylor, I performed TCRseq on 372 peripheral blood samples and 12 resected tumour specimens taken from 144 individuals (see methods section 2.4, page 83).

4.3.1.1 Resolution of index hopping and QC

Following sequencing, the data was initially aligned to TCR genes by using *MiXCR*[237]. However, during an initial exploration of the data we became aware of a high level of overlap of the repertoires between some samples (median overlap as proportion of clones 0.2%, inter-quartile range (IQR) 0.11-0.57%). I therefore sought to quantify this and plotted a heatmap of the proportion of the repertoire shared between two samples (Figures 4.1a and 4.1b). This displayed a large degree of overlap between certain samples, which appeared to follow a regular pattern. On further examination, samples where there was a high degree of overlap shared an index sequence (samples had been only uniquely single-indexed). We therefore suspected 'index hopping' - a phenomenon whereby samples can be mis-assigned during index sequencing[242]. Whilst this is an issue that affects bulk RNAseq in general, it is particularly exacerbated with multiplexing of single-indexed samples on a patterned flow-cell. This was not an issue we had been aware of prior to sequencing.

In order to trouble-shoot, we initially attempted to 'dehop' the data, removing sequences with the same UMI and CDR3 region if they were found in two separate samples. This was based on the premise that identical molecules (with technical additions in the form of UMIs) should not be present in two samples. This was performed by Isar Nassiri and to a certain extent worked inasmuch as evidence of index hopping was much diminished; however, it resulted in an unacceptably high

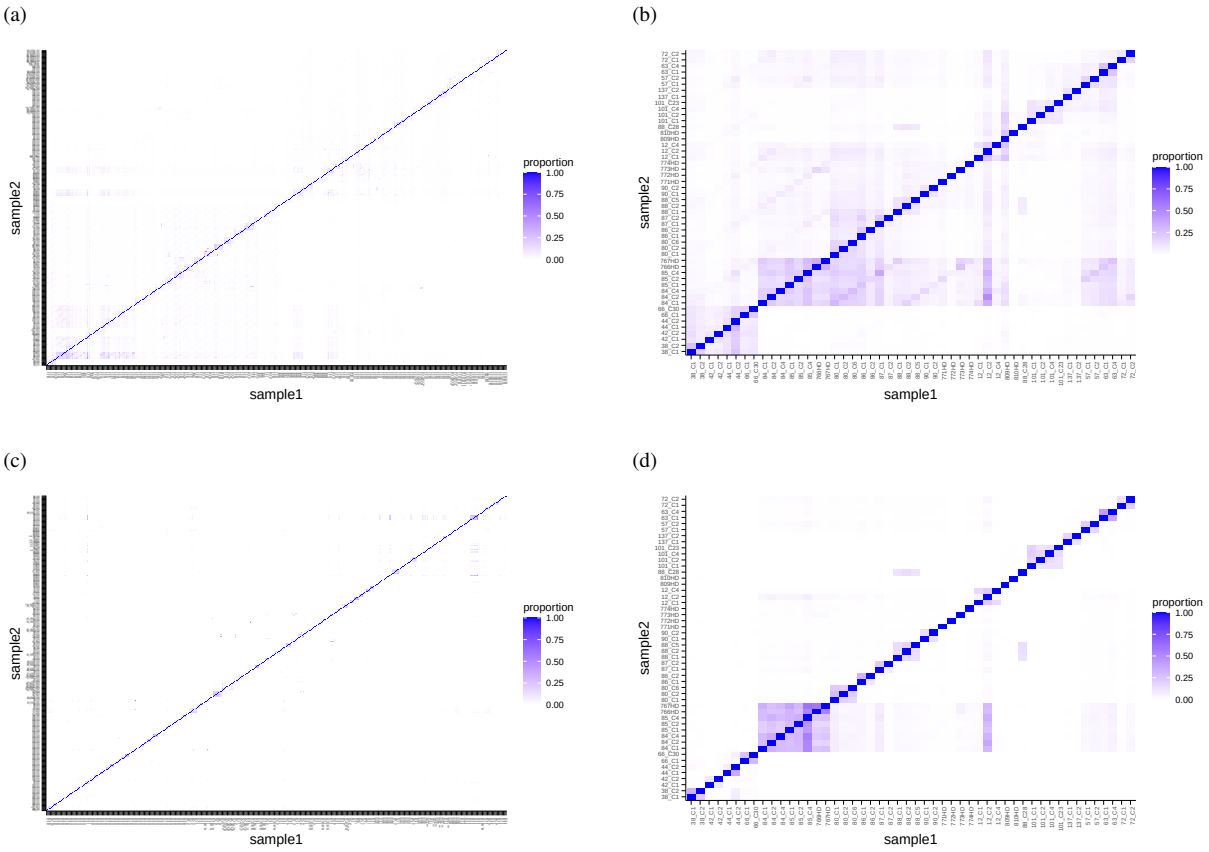


Figure 4.1. (a) Heatmap demonstrating repertoire overlap between samples in the raw TCRseq data aligned by *MiXCR*. Overlap is quantified by proportion of shared clones. (b) enlarged version of first fifty samples in (a). Regular patterns of overlap can be seen, which clearly demonstrates index hopping. (c) and (d) as per (a) and (b) but for data that was processed using the Qiagen *CLC Genomics* workbench; appearances of index hopping much improved.

loss of chains. I therefore utilised the Qiagen *CLC Genomics* workbench tool which introduces 'UMI groups' - whereby if a chain+UMI is present < N number of times it is removed. On applying this approach with N=3 (which is also the default setting), the clearly-visualised hopping on the heatmap substantially improved, although there were still some samples which had ongoing overlap (Figures 4.1c and 4.1d). Nonetheless, Qiagen technical support were satisfied with this approach and felt that the extent of repertoire sharing was consistent with other samples of this type and indeed we had reduced the proportional overlap versus the *MiXCR* data by an order of magnitude (median proportion of clones shared between two samples from unrelated individuals 0.041%, IQR 0.018-0.083%, $p<2.2x10^{-16}$, two-sided Wilcoxon rank sum, Figure 4.2a).

Nonetheless, I was keen to further explore this issue and to ensure that there was no high aberrant technical repertoire overlap. I therefore took an orthogonal approach and calculated the Morisita-Horn index (MH) - a measure of repertoire overlap - across all samples (i.e. comparing each sample with every other sample). There was a relatively bimodal distribution, with some samples having very high MH (Figure 4.2b). Visualised on a log-normalized scale, the distribution was positively skewed (Figure 4.2c). I therefore decided to then exclude those samples whereby the MH between two samples from different individuals was greater than the MH of two samples from the same individual. Applying this approach led to the exclusion of 20 samples. When these were removed, there was no longer a positive skewing of MH distributions (Figures 4.2d and 4.2e), the appearances of the heatmap were further improved (Figures 4.2f and 4.2g) and the proportion of clones shared between two samples from unrelated individuals was significantly - albeit slightly - lower (median 0.038%, IQR 0.016-0.074%). This amount of overlap is below that (but broadly in line with) the amount of overlap seen in repertoires from bulk RNAseq data, and in which there was no evidence of index-hopping (Figure 4.2a).

In summary, whilst there were some technical issues with this dataset as a result of index hopping, by working to understand the issue with Qiagen technical support we were able to mostly resolve this by using the well-established *CLC Genomics Workbench*. By then further excluding samples with anomalous levels of overlap, I was confident that this issue was minimised as far as possible.

4.3.1.2 Post-QC dataset

Following the above quality control, we were left with 364 samples from 139 individuals. The characteristics of these samples are summarised in Table 4.1. As can be seen, the majority of samples were CD8+ T cells with most pre and 3 weeks post-treatment. However, we sampled a range of time points as well as CD4+ T cells to allow comparisons.

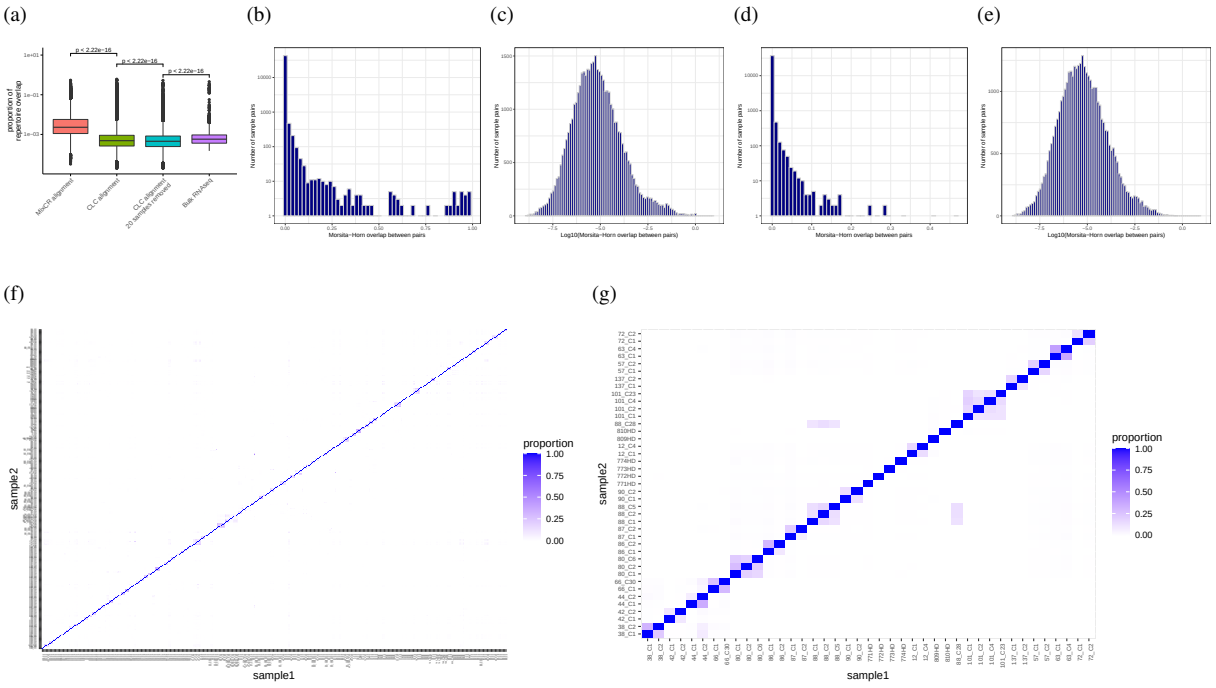


Figure 4.2. (a) Box plots representing proportion of repertoire overlap (percentage of clones shared) between raw data aligned by *MiXCR* (orange), data from 384 samples aligned with Qiagen's *CLC Genomics Workbench* (green), data from 364 samples aligned with Qiagen's *CLC Genomics Workbench* (blue) and data from bulk RNAseq (purple). All groups as significantly different from each other. (b) Distribution of MH index by sample pairs in data from 384 samples aligned using the *CLC genomics* workbench. (c) same data as (b) but log-normalised. (d) and (e) as per (b) and (c) but for 364 samples (20 samples with anomalously high MH index removed). (f) Heatmap demonstrating repertoire overlap between 364 samples aligned by *CLC Genomics Workbench*. Overlap is quantified by proportion of shared clones. (g) Enlarged version of first fifty samples in (f). Statistics with two-sided Wilcoxon rank sum test (a).

4.3.2 CD8+ T cell repertoire metrics

To first explore this dataset, I applied commonly-used repertoire indices - Shannon entropy (Shannon) and Gini coefficient (Gini)[172]. The basis and rationale of these metrics is discussed in detail in introduction section 1.5.2 (page 46). However, in short, Shannon can be considered a measure of "diversity" whilst Gini can be considered a measure of "inequality" - i.e. "clonality". The higher the Gini, the more the repertoire is *dominated* by one or a few clones.

As described in introduction section 1.5.3 (page 48), whilst a number of studies have correlated repertoire metrics with outcome following ICB in the context of different cancers, there is

(a)

Characteristic	Healthy volunteer, N = 43[1]	Patient, N = 96[1]
Age	47 (8.7)	66 (14.0)
Sex is Female	22 (51%)	40 (42%)
Treatment		
Adjuvant	0 (NA%)	4 (4.2%)
cICB	0 (NA%)	48 (50%)
sICB	0 (NA%)	44 (46%)

[1] Mean (SD); n (%)

(b)

Characteristic	CD4m, N = 25[1]	CD4n, N = 26[1]	CD8, N = 301[1]	tumour, N = 12[1]
Donor Type				
Healthy volunteer	3 (12%)	3 (12%)	42 (14%)	0 (0%)
Patient	22 (88%)	23 (88%)	259 (86%)	12 (100%)
Treatment				
Adjuvant	0 (0%)	0 (0%)	12 (4.6%)	0 (0%)
cICB	9 (41%)	7 (30%)	112 (43%)	8 (67%)
sICB	13 (59%)	16 (70%)	135 (52%)	4 (33%)
Timing of sample				
Pre-treatment	9 (41%)	7 (30%)	92 (36%)	11 (92%)
14-28days	8 (36%)	6 (26%)	77 (30%)	0 (0%)
29-98days	1 (4.5%)	5 (22%)	57 (22%)	0 (0%)
99-365days	2 (9.1%)	3 (13%)	16 (6.2%)	1 (8.3%)
>365days	2 (9.1%)	2 (8.7%)	14 (5.5%)	0 (0%)

[1] n (%)

Table 4.1. Characteristics of the 364 samples included in the full TCRseq cohort by demographic information (a) and treatment and time-point; divided by cell type (b). CD4n = naive $CD4^+$ T cell, CD4m = memory $CD4^+$ T cell, CD8 = $CD8^+$ T cell.

generally a lack of consensus as to what repertoire changes constitute an effective response and some results are contradictory and inconsistent. Hence, I sought to characterise, for our dataset, the two key repertoire metrics of diversity and clonality (i.e. Shannon and Gini) and correlate these with clinical outcome.

Both age and cytomegalovirus (CMV) status are known to skew the immune repertoire[243,244], with these factors each driving expansion of large clones and reducing overall diversity. I was able to observe this in our data with reduced Shannon and increased Gini in older individuals and those with higher CMV antibody titres, representing reduced diversity and increased clonal expansion, respectively (Figure 4.3). The correlation of plasma CMV antibody titre and repertoire metrics is striking, with a higher viral burden having a significant association with repertoire skewing (Figures 4.3c and 4.3d). As such, it is important to control for these co-variates when analysing associations with repertoire metrics.

Whilst I was able to replicate the group's previous finding of an association between clinical

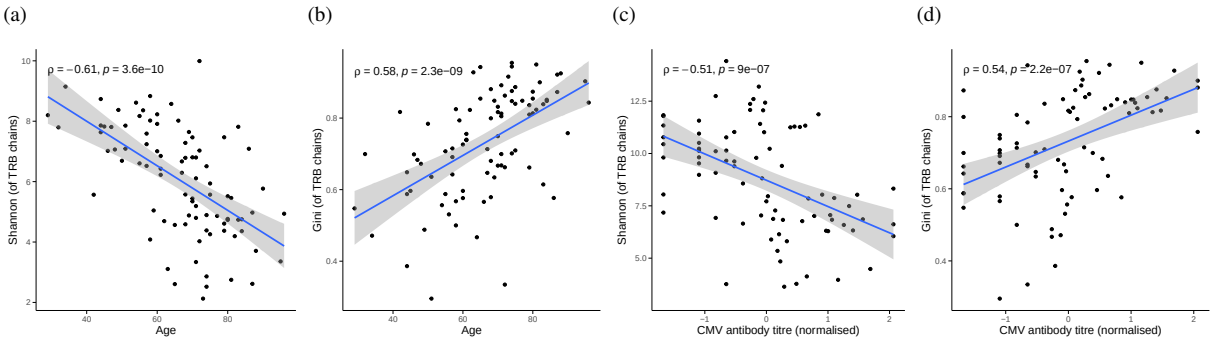


Figure 4.3. (a) Correlation between Shannon and age. Each dot is a patient sample at pre-treatment time point. Shannon is calculated on TCRβ chains. (b) as per (a) but for Gini. (c) Correlation of Shannon and CMV antibody titre in plasma (inverse normal transformation). (d) as per (c) but for Gini. Statistics with Spearman's rank.

progression at 6 months of treatment and the number of clones occupying >0.5% of the peripheral repertoire (large clones) in the peripheral blood 14-28 days after starting ICB[93] (Figure 4.4a), there was no evidence of an association between outcome and Gini at baseline or 14-28 days using a Wilcoxon test (Figure 4.4b). However, when looking at the Gini coefficient of just large clones there was a borderline significant association (Figure 4.4c). There was no difference when looking at Shannon of all clones (Figure 4.4d) or just large clones (data not shown).

As per the above observations, however, it is important to control for age and CMV status when assessing for associations of repertoire metrics. Using a linear model to control for these covariates reveals a significant association for Gini and clinical response at 6 months (those with no progression of disease have Gini 0.074 higher, on average, p = 0.019), as well as a significant association for Gini of large clones. No significant association for Shannon was observed (Table 4.2).

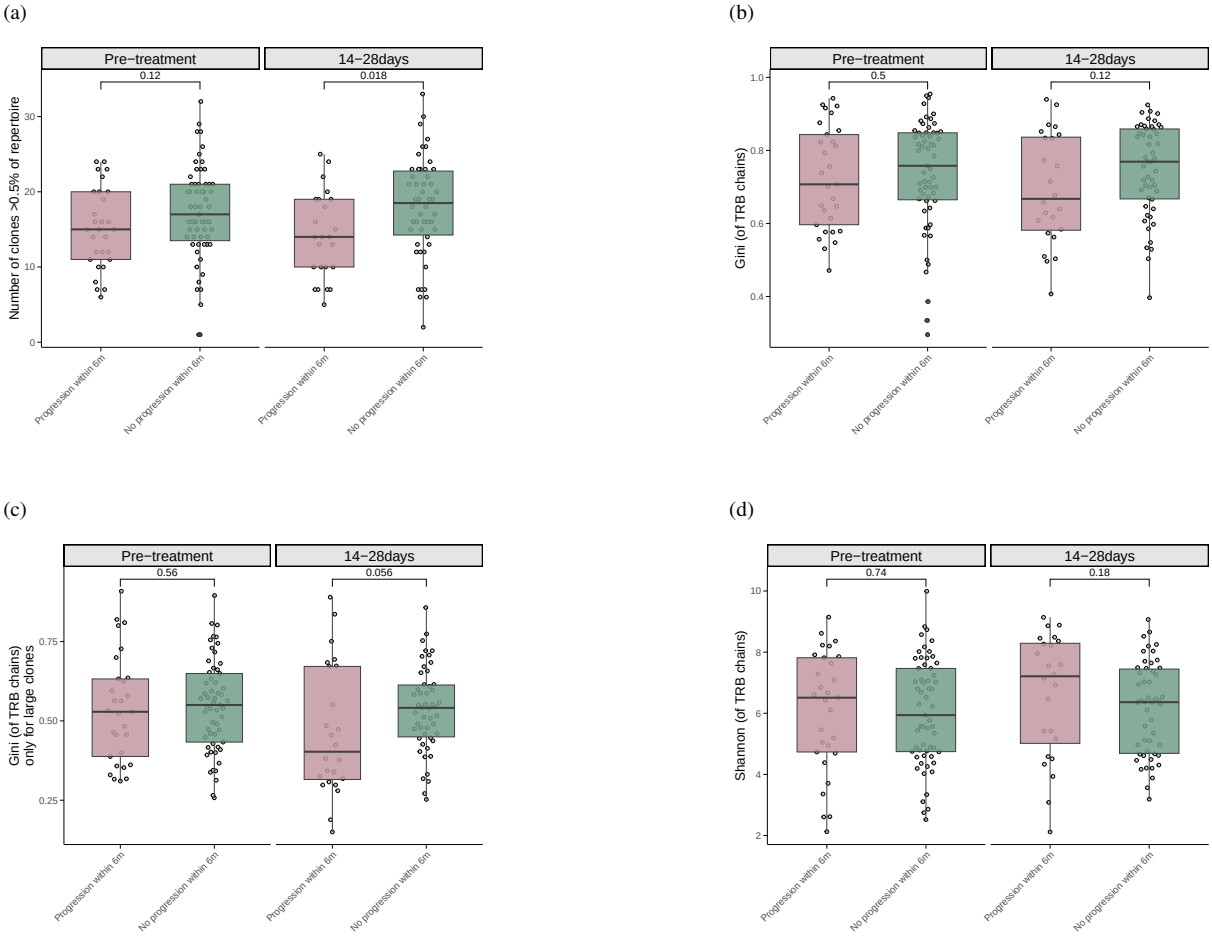


Figure 4.4. (a) Replication of finding from [93] demonstrating the association of number of large clones post-treatment in the peripheral blood and response to ICB. (b) Gini per individual coloured by clinical outcome at six months and faceted by time point of sample. (c) and (d) as per (b) but for Gini just for clones occupying >0.5% of the peripheral repertoire (large clones) and Shannon, respectively. Statistics with Wilcoxon rank sum test.

Comparator	Coefficient	Standard error	p value
Shannon	-0.62	0.34	0.075
Shannon of just large clones	0.14	0.15	0.35
Gini	0.074	0.031	0.019
Gini of just large clones	0.084	0.038	0.029

Table 4.2. Association of Shannon/Gini (measured at 14-28 days post ICB) with outcome using a linear model. The model is comparator $\sim$ progression of disease at 6 months + age + CMV serostatus. The coefficient gives the average change in those with *no* progression of disease at 6 months.

4.3.3 Comparison of CD8⁺ T cell alpha and beta chain repertoires

As would be expected, there is an extremely close correlation between repertoire metrics of the TCRα and TCRβ chains (Figure 4.5a and 4.5b). Further, it is possible to replicate the association between number of large clones and clinical outcome just on the TCRα chains alone.

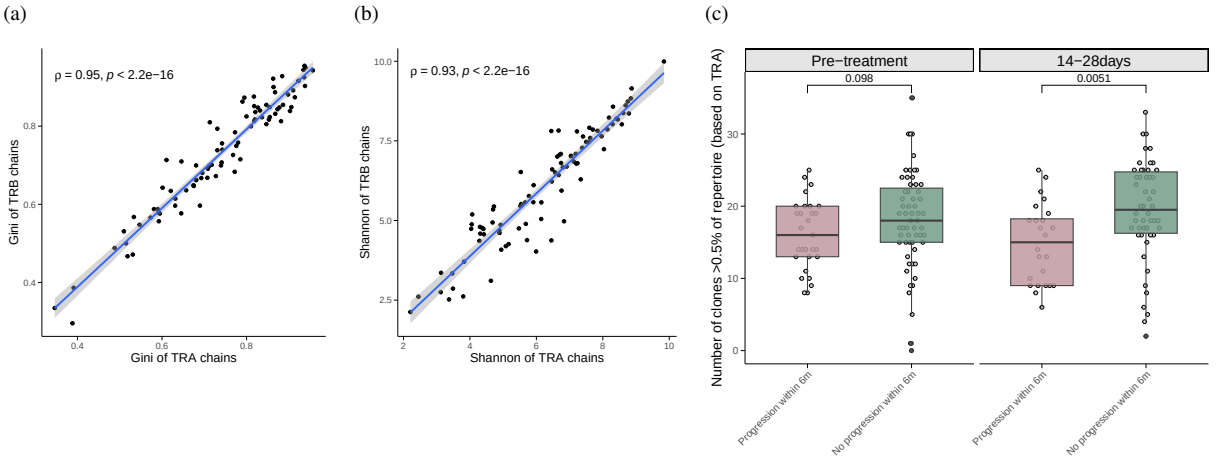


Figure 4.5. (a) Gini for TCRα and TCRβ chains at the pre-treatment time point. Each dot represents a single sample. (b) as per (a) but for Shannon. (c) Association between number of clones occupying >0.5% of the peripheral repertoire - as defined by the TCRα chain - and progression of disease at 6 months. Statistics with Spearman's rank (a) and (b) and Wilcoxon rank sum test (c).

4.3.4 Comparison of CD8⁺ T cell with CD4⁺ T cell repertoires

Within this experiment, we performed TCRseq on 25 memory CD4⁺ T cell (CD4m) and 26 naive CD4⁺ T cell (CD4n) samples, primarily at pre-treatment and immediately post-treatment (Table 4.1). Whilst Gini of CD4m correlated with that of CD8⁺ T cells (Figure 4.6a), there was no evidence of a correlation of Shannon, and no correlation for either metric between CD4n and CD8⁺ T cells (Figures 4.6b, 4.6c and 4.6d). This was the case when removing outliers (Figures 4.6e-h). Of note, the Shannon of the CD8⁺ T cells was much lower than that of the CD4⁺ T cells, whilst the Gini was markedly higher (Figure 4.6).

A correlation was observed between the number of large CD8⁺ T cell clones and large CD4⁺ T cell clones for CD4ms, persisting even with the removal of outliers (Figures 4.7a and 4.7b.

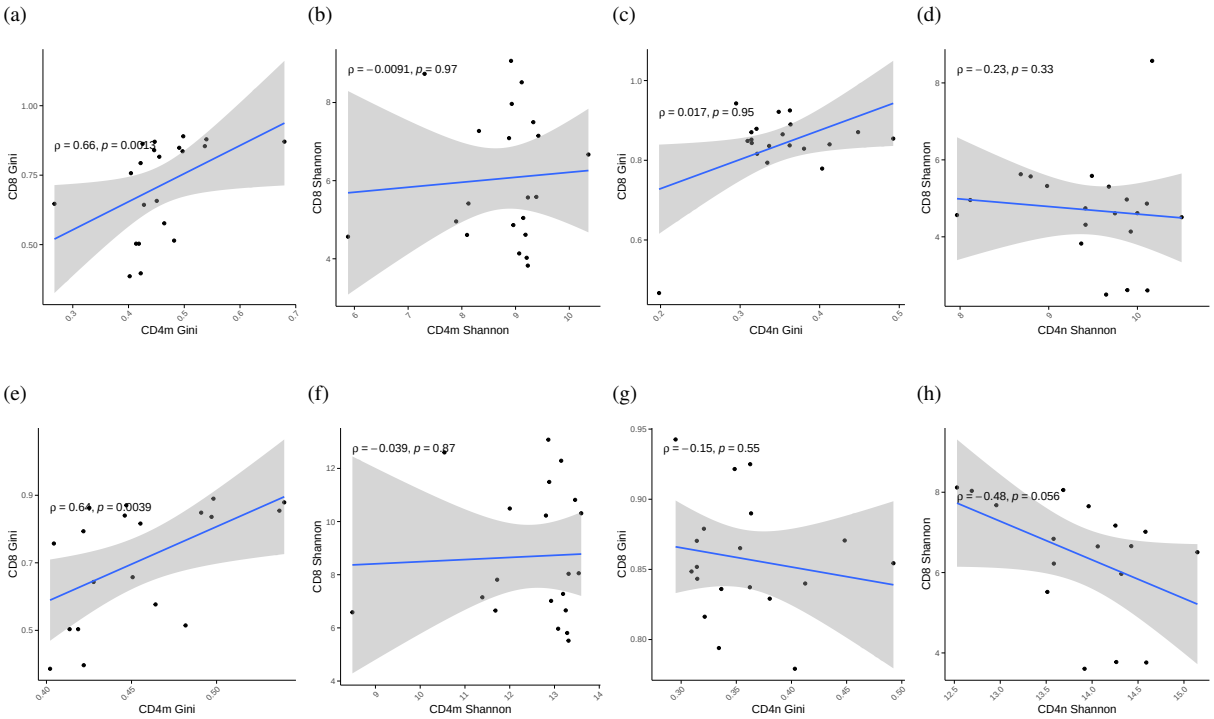


Figure 4.6. (a) Correlation between Gini of memory CD4+ T cell (CD4m) and CD8+ T cells. Each dot represents a sample for which there were paired CD4+ T cells and CD8+ T cells (multiple time-points represented). (b) As per (a) but for Shannon. (c) and (d) as per (a) and (b) but for naive CD4+ T cell (CD4n). (e)-(h) as for (a)-(d) but excluding outliers. Statistics with Spearman's rank correlation.

However, there was no evidence of a correlation with CD4ns (Figure 4.7c). Whilst the sample size here is likely underpowered for testing association with outcome, there was no significant difference in the number of large CD4+ T cell clones between those with and without progression at 6 months of treatment, although the direction of difference did appear to favour those with a good response having more large CD4+ T cell clones (Figures 4.7d and 4.7e).

Finally, I compared baseline TCR gene usage across CD4n, CD4m and CD8+ T cell samples from the same individuals (see methods section 4.3.4, page 124). Whilst there were some differences in V and J gene usage between cell types at baseline, on the whole there was notable concordance, with only 11 out of 58 V genes and 6 out of 13 J genes significantly different between the three cell subtypes (Figures 4.8a and 4.8b). Further, on performing a principal component analysis (PCA) of the gene usage, there is no clear separation across the first ten principal components on

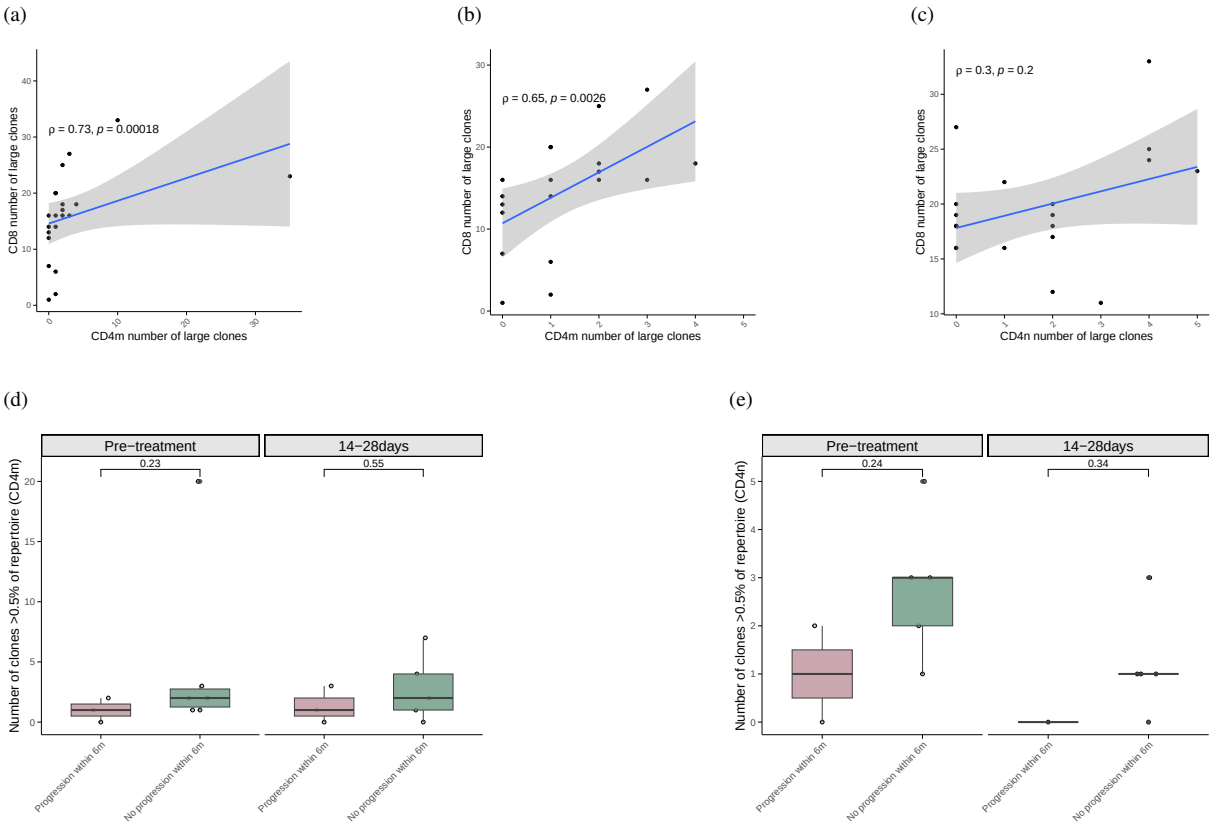


Figure 4.7. (a) Correlation between number of clones occupying >0.5% of the peripheral repertoire (large clones) between CD4ms and CD8+ T cells. (b) As per (a) but removing two outliers. (c) as per (a) but for CD4ns. (d) and (e) number of large clones coloured by progression of disease at 6 months and faceted by outcome for CD4ms and CD4ns respectively. Statistics with Spearman's rank (a) - (c) and Wilcoxon rank sum (d) and (e).

cell type (Figure 4.8c shows the first two). Whilst the CD8+ T cell samples do all have similar PC1 values, these are interspersed with CD4m and a number of CD4n samples have comparable values along PC1. This is therefore suggestive of repertoire concordance across both CD4+ T cells and CD8+ T cells.

4.3.5 Identification of key response groups of CD8+ T cells

I now shifted my focus to examine the CD8+ T cell response due to the pivotal role played by these cells. I was particularly intrigued by the finding from our previous work[93] that the number of large clones at 14-28 days, but not baseline, associated with outcome - a finding I am able to replicate

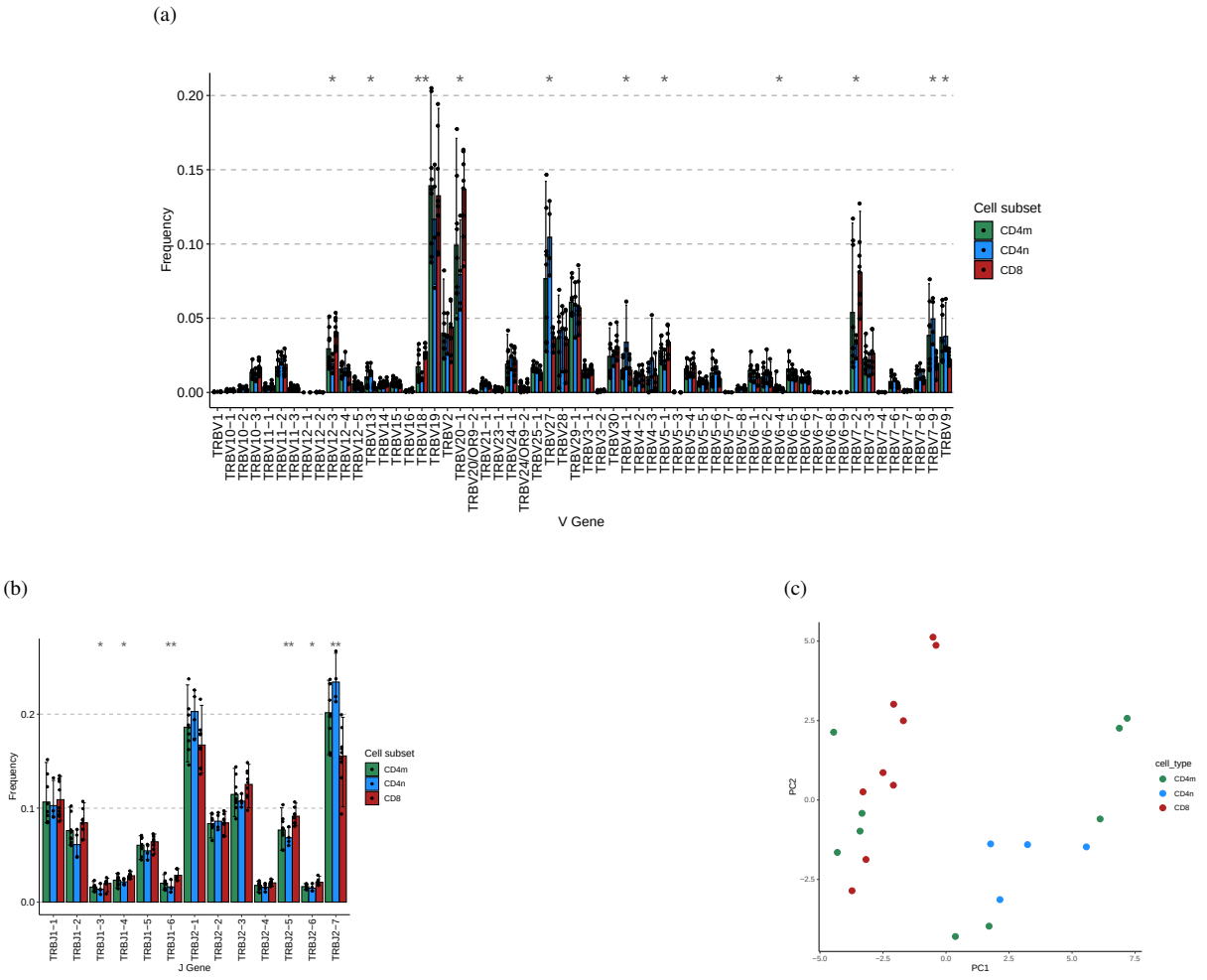


Figure 4.8. (a) TCRβ chain V gene usage coloured by cell type. The height of bars represents the median proportion of the repertoire that gene occupies across samples of that cell type. The dots are the proportion per sample, with the error bars representing 95% CI. (b) As per (a) but for TCRβ J gene usage. (c) PCA of V gene usage across cell types displaying the first two PCs, coloured by cell type. Statistics with Kruskall-Wallis test (a) and (b).

with this present dataset (Figure 4.4a). I therefore hypothesised that I might be able to identify key clones which 'emerge' following ICB. To investigate this further, I used the *GLIPH2* algorithm[188] to arrange TCRs into 'specificity groups' of putative shared antigen recognition (see methods section 2.4.3.2, page 85). I filtered these using similar thresholds as previously described[190] (see methods section 4.3.5), with a resultant 13,450 highly-public, expanded, specificity groups identified - termed 'public specificity groups' (Figure 4.9a).

Within my cohort, 85 individuals had paired pre- and post-treatment blood samples (pre-treatment

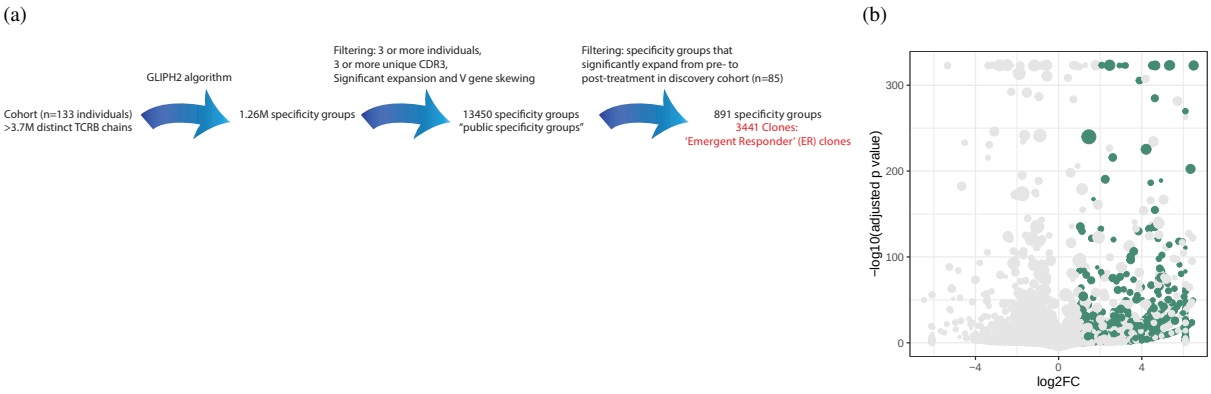


Figure 4.9. (a) Flow diagram depicting data filtering and post-processing of *GLIPH2*-clustered data. (b) Volcano plot showing change in size of public specificity groups from pre- to post-treatment with ICB. ER specificity groups are coloured in green.

samples taken immediately prior to the first dose of ICB, post-treatment samples taken a median of 21 days (IQR 7 days) following the first dose of ICB). These 170 samples were used as a "discovery cohort" to identify specificity groups, found primarily in those with a good response to treatment at six months, that significantly increased in size following ICB (see methods section 2.4.3.3, page 85) (Figure 4.9a). I found 891 specificity groups, comprising 3441 different clones, that minimally doubled in size and were primarily found in individuals with a positive response to ICB (Figure 4.9a and 4.9b). I term the clones within these specificity groups 'Emergent Responder' (ER) clones, i.e. those clones which are in emerging/enlarging groups post-treatment in individuals with a clinical response to ICB.

I found that there was no relationship between the proportion of the repertoire occupied by ER clones with either age, sex or CMV antibody titre (Figures 4.10a, 4.10b and 4.11a). However, I did note a relationship with CMV serostatus, with CMV positive patients having a proportionally lower repertoire occupancy by ER clones at all time-points (Figure 4.11b). Consistent with this, ER clones were not enriched for CMV or EBV clones as called by IEDB when compared to clones found in public specificity groups. Indeed, there is a depletion of clones recognising CMV within ER clones as well as all other viral epitopes (Figure 4.11c). In keeping with this, I found

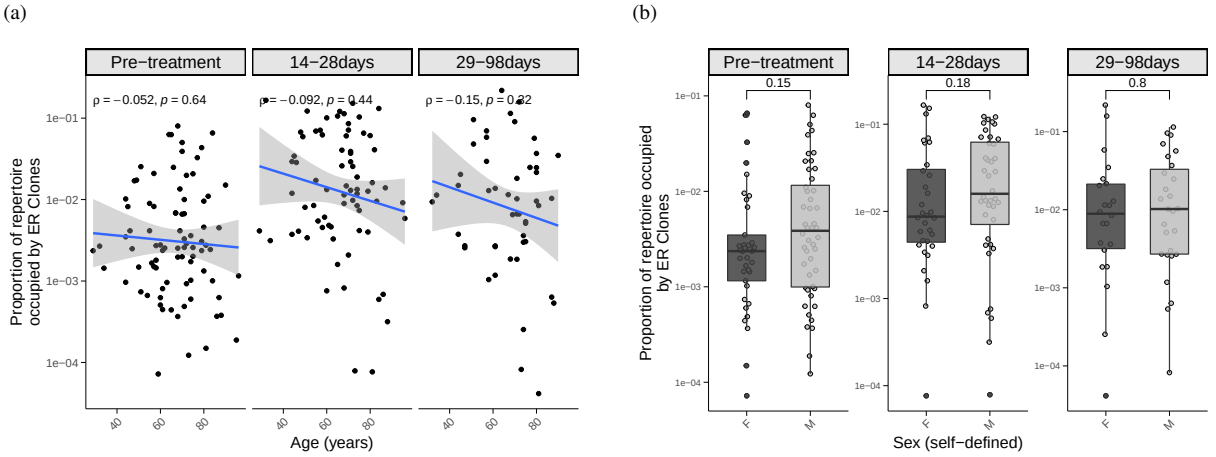


Figure 4.10. Proportion of repertoire occupied by ER clones by age (a) or sex (b). Each dot is an individual, statistics with Spearman's rank (a) or two-sided Wilcoxon rank-sum test (b).

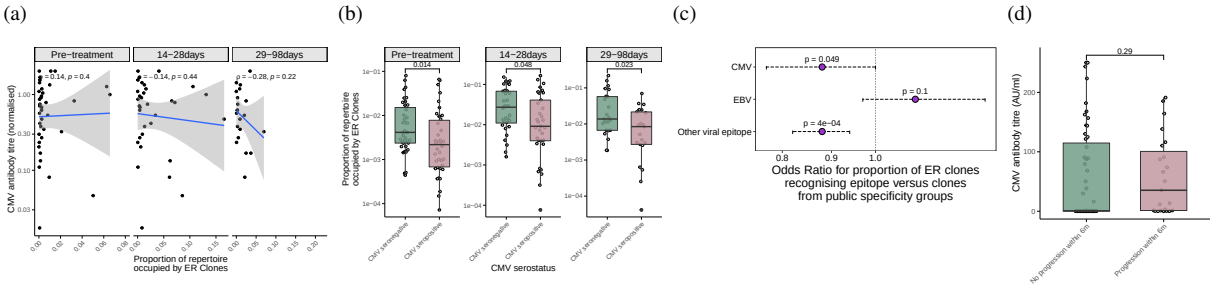


Figure 4.11. (a) Proportion of repertoire occupied by ER clones by CMV antibody titre. (b) Repertoire occupancy by ER clones by CMV serostatus. (c) Odds ratio for putative antigen recognition of ER clones compared to recognition of the same antigen by clones from public specificity groups. (d) CMV antibody titre coloured by clinical response at 6 months of treatment. Statistics with Spearman's Rank (a), two-sided Wilcoxon rank-sum test (b) and (d) or Fisher's exact test (c).

no association between CMV antibody titre and clinical outcome (Figure 4.11d).

4.3.6 ER clone repertoire occupancy corresponds with clinical response and is HLA specific

Having identified groups of TCR which significantly expand following ICB in those with a positive response to treatment (i.e. ER clones) I wished to verify that the presence of these key clones corresponded with clinical outcome. I found that the proportion of the repertoire occupied

by ER clones significantly expanded with treatment in both ICB responders and non-responders (Figure 4.12a), although when I dichotomised by treatment type this expansion in non-responders was more marked in recipients of cICB (Figure 4.12b). However, surprisingly, this was also observed across both pre- and post-treatment time-points - individuals who responded to treatment demonstrated a significantly higher proportion of ER-clone repertoire occupancy (Figure 4.12c). This is in keeping with the baseline clonal repertoire being key to mediating ICB responses, consistent with previous findings[78].

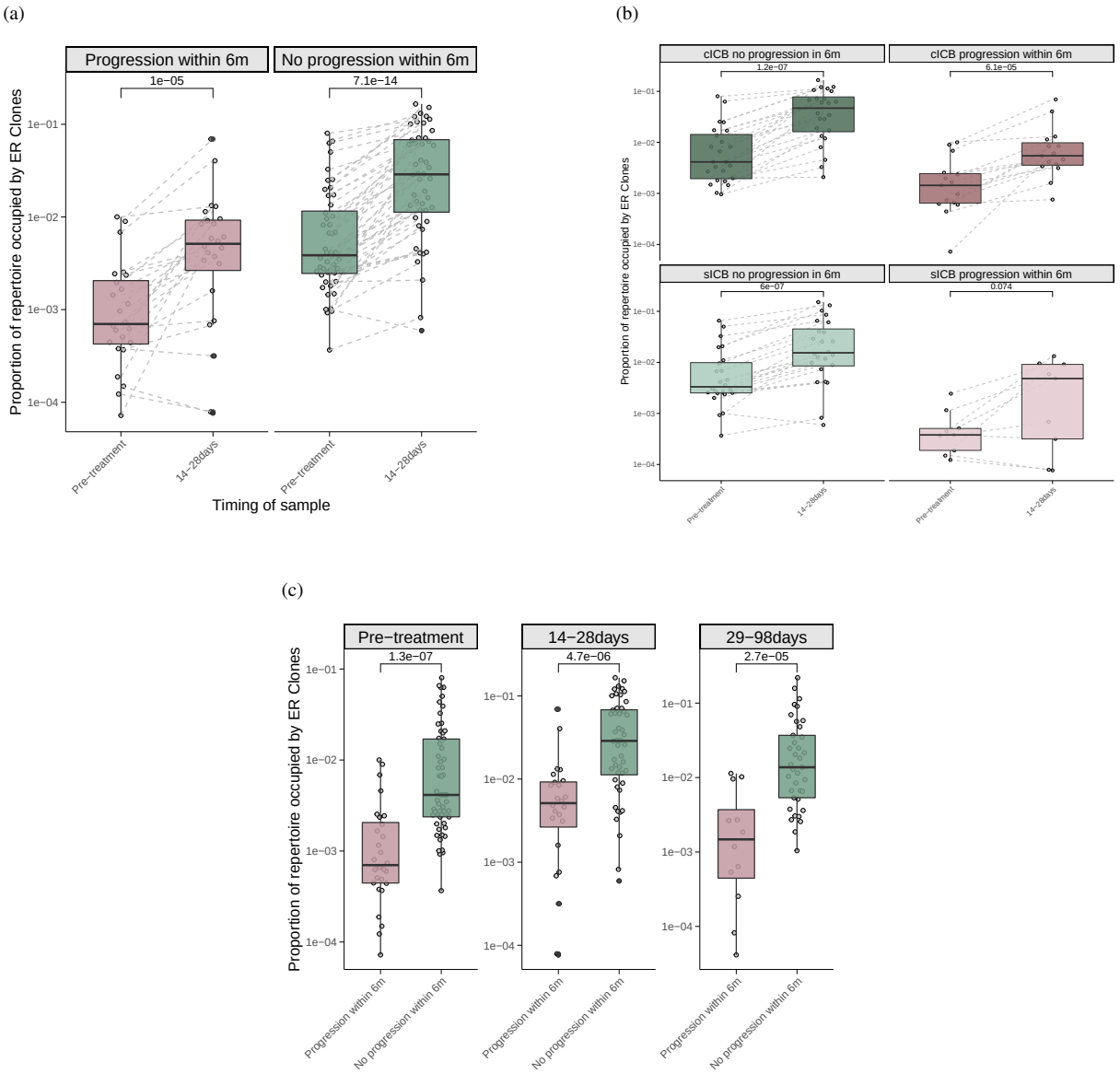


Figure 4.12. (a) Proportion of repertoire occupied by ER clones by time point and coloured and faceted by outcome (disease progression at 6 months) (b) Proportion of the repertoire occupied by ER clones by time point, faceted by treatment and clinical outcome. (c) Proportion of repertoire occupied by ER clones by clinical outcome and faceted by time point. Statistics with Wilcoxon signed rank test (a) and (b) or two-sided Wilcoxon rank-sum test (c).

Given specificity groups may demonstrate HLA type restriction[188], we explored the relationship between MM specificity groups and HLA class I type. We identified specificity groups associated with HLA allele carriage (Figure 4.13) and thus were able to find corresponding HLA-specific ER clones.

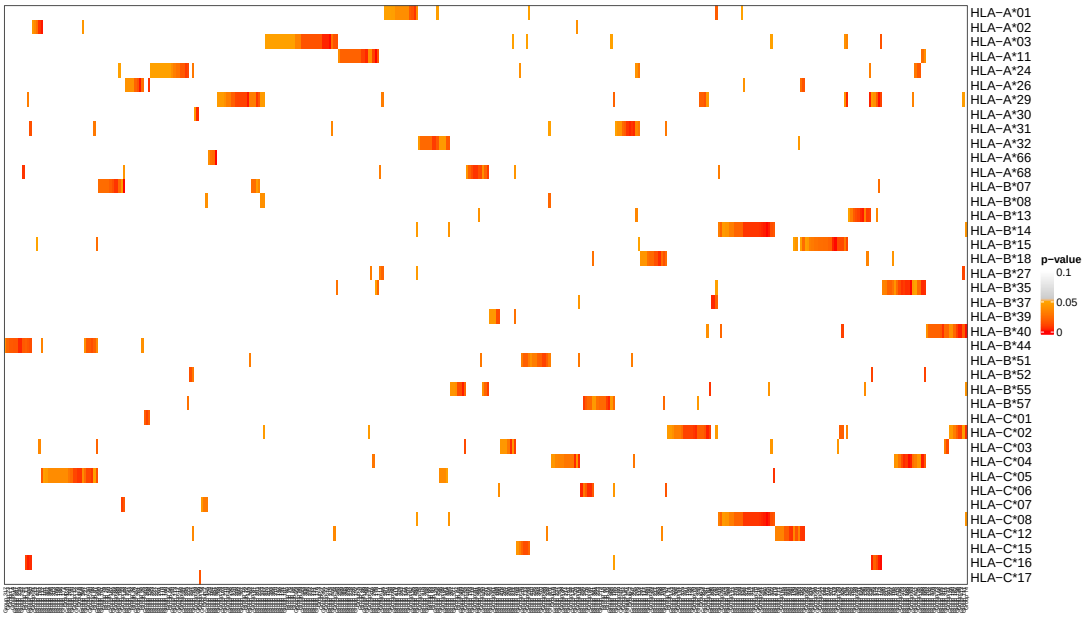


Figure 4.13. ER specificity groups (x-axis) associate with HLA types (y-axis) - colours represent adjusted p values from a Fisher's exact test generated by GLIPH2 for the proportion of individuals that each specificity group is found in with each HLA allele. Coloured boxes denote significant associations.

Notably, for several HLA types, I was powered to observe outcome associations when ER clones were restricted to those that are members of specificity groups that significantly associate with an HLA allele. In HLA-A*01 carrying patients, this reduced the 3441 clones to just 68. Remarkably, the proportion of the repertoire occupied by these HLA-A*01-restricted ER clones associated with clinical outcome in both pre- and post-treatment samples, but restricted to individuals carrying an HLA-A*01 allele (Figure 4.14a). Likewise, I was able to repeat this observation for HLA-B*07 (71 clones) and HLA-C*05 (108 clones) restricted ER clones, two of the most common HLA types (Figures 4.14b and 4.14c).

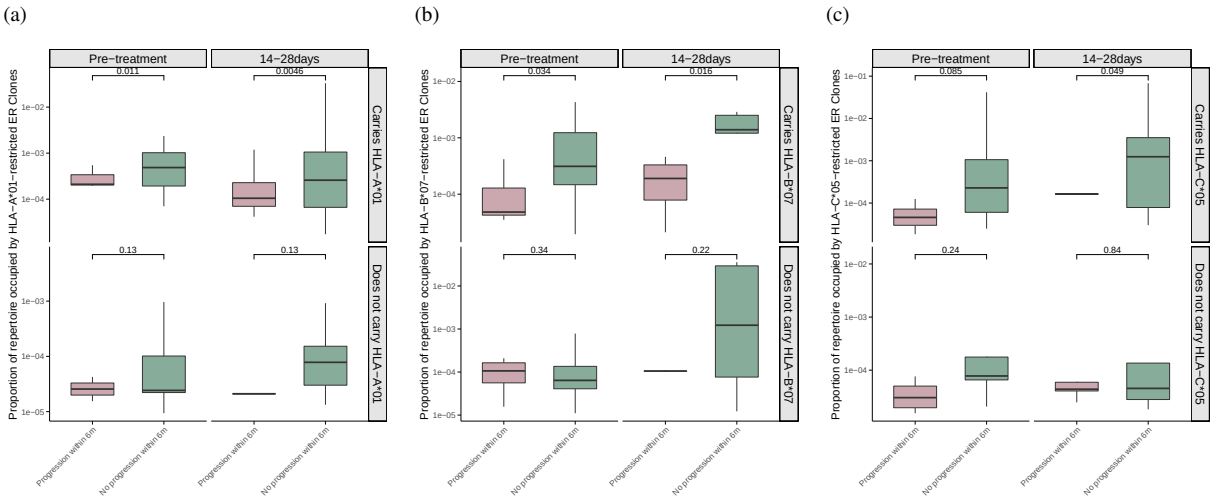


Figure 4.14. (a) Proportion of repertoire occupied by HLA-A*01-restricted ER clones associates with outcome, but only in individuals carrying an HLA-A*01 allele. (b) and (c) - as per (a) but for HLA-B*07 and HLA-C*05 respectively.

4.3.7 ER clones are large, persistent and of memory phenotype

As previously reported, the number of large (>0.5% of the repertoire) CD8+ T cell clones present in the peripheral blood correlates with clinical response (Figure 4.4a, [93]), and large clones show increased sensitivity to ICB[78] (Chapter 3). I therefore examined the relationship between ER clone size and ICB response, noting that significantly more large clones are also ER clones in those who responded to ICB compared to those who progressed within six months (Figure 4.15).

In order to examine the phenotypic subset of ER clones, I looked at scRNAseq data of peripheral CD8+ T cells taken pre-treatment and 21 days post-treatment in patients receiving ICB for MM - as previously presented in Chapter 3[78]. I was able to identify 444 cells from 63 clones within this dataset that carry an ER clone ID (identical TRB V gene, J gene and CDR3 amino acid sequence). These cells were significantly enriched for both effector memory T cell (T_{em}) and central memory T cell (T_{cm}) subsets both pre- and post-ICB (Figures 4.16a and 4.16b). Notably, T_{effs} were under-represented in ER clones (OR 0.65, 95% CI 0.50-0.85, p=0.001).

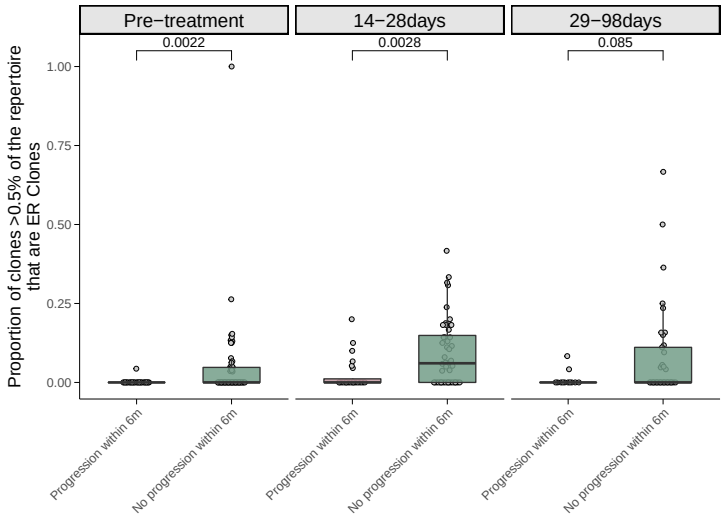


Figure 4.15. Proportion of large clones (those occupying >0.5% of the repertoire) that are ER clones, split by clinical response and faceted by time point.

To corroborate this, I analysed flow cytometry data from PBMCs from a subset of individuals in the discovery cohort (n=72) (experiments previously performed by Chelsea Taylor - see methods section 2.5, page 87). I noted a positive correlation between the proportion of $CD8^+$ T cells 14-28 days post-treatment that were T_{cm} on flow cytometry and the proportion of the repertoire occupied by ER clones; there was an anti-correlation for T_{effs} (Figure 4.16c).

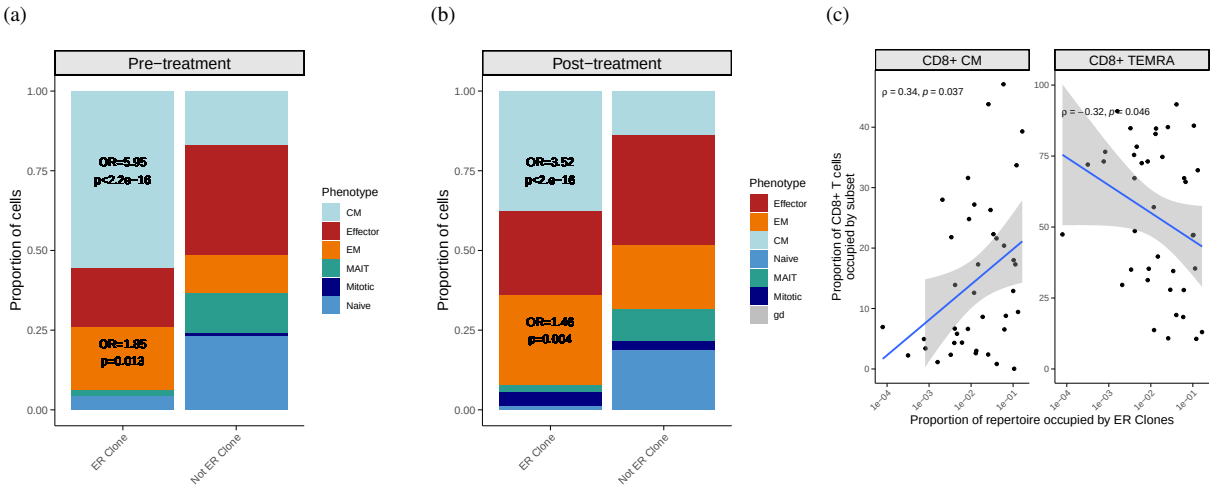


Figure 4.16. (a) Proportion of cells by phenotype as defined by scRNAseq from Chapter 3, split by whether the cell is an ER clone - pre-treatment time point. (b) as per (a) but for post-treatment time point. (c) Correlation between proportion of repertoire occupied by ER clones and T_{cm} (lablelled as 'CM', left panel) or T_{eff} (labelled as TEMRA, right panel) subsets as determined by flow cytometry at 14-28days post-treatment; n=72 individuals. Statistics are via a Fisher's exact test (a, b) or Spearman's rank correlation (c). CM = T_{cm}, EM = T_{em}, effector = T_{eff}, TEMRA = T_{eff}, $\gamma\delta$ = $\gamma\delta$ T cell.

Based on the memory phenotype of ER clones, I then explored the persistence of these clones in the peripheral blood. I looked at samples taken over two years following commencement of ICB and noted that the proportion of the repertoire occupied by ER clones was relatively stable compared to baseline (Figure 4.17a). In order to equate long-term changes with outcome, I grouped time-points into categories and faceted individuals by progression at 6 months. Notably, whilst across both groups there is an initial increase in the proportion of the repertoire occupied by ER clones (as described above), this is short-lived for those with progression - with ER clone repertoire occupancy returning to pre-treatment levels within 63 days. However, in those with no progression within the first six months of treatment, early expansion of ER clones is more marked and subsequently maintained, with repertoire occupancy staying significantly above pre-treatment levels for at least six months (Figure 4.17b). This could potentially suggest ongoing expansion of key tumour-reactive clones, possibly due to ongoing antigen ligation.

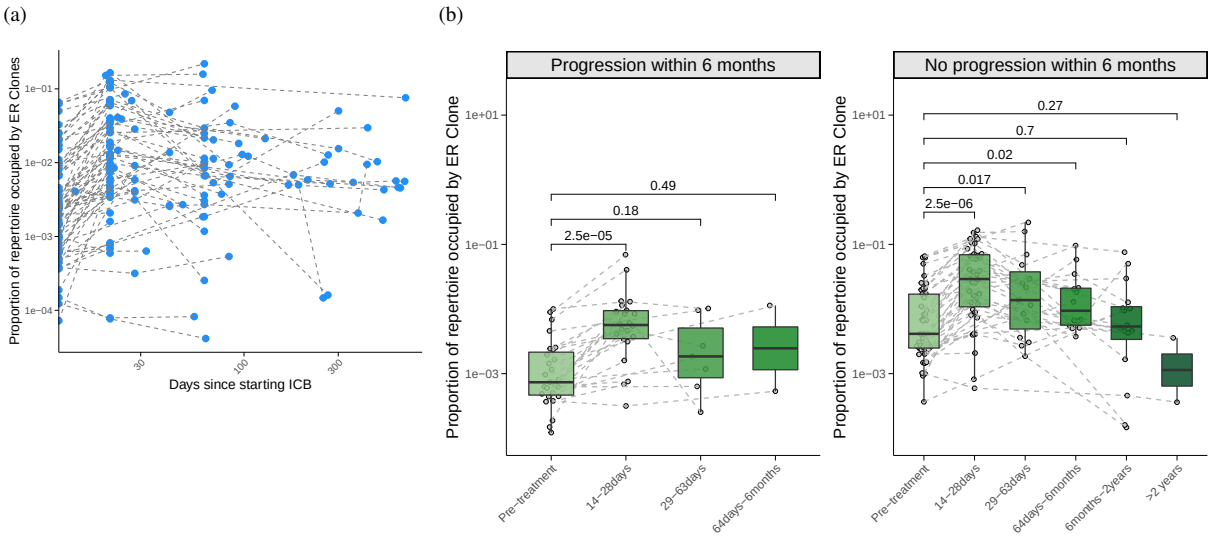


Figure 4.17. (a) Proportion of the repertoire occupied by ER clones over time - each dot is an individual. (b) Same data as per (a) but samples grouped into time bins and faceted by clinical response. Statistics with two-sided Wilcoxon rank sum test.

4.3.8 ER clones are enriched and expanded within tumours and are cytotoxic in the peripheral blood

In order to investigate whether ER clones are tumour associated, I extracted RNA from ten tumour blocks (n=7 patients) which were resected prior to ICB and which had associated paired pre- and post-ICB peripheral blood data. Tumour specimens were resected a median of 6.4 months prior to the commencement of immunotherapy (range 3.5 weeks to 16.4 months). Remarkably, I found multiple ER clones within the tumours prior to commencement of ICB, in excess of that expected by chance based on the numbers present in peripheral blood (Figure 4.18a). Further, when restricting only to clones found in both the tumour and peripheral blood at baseline in the same patient, ER clones were significantly expanded in the tumour versus the peripheral blood when compared to clones from public specificity groups (Figure 4.18b). Given the tumour blocks will have contained both CD4⁺ T cells and CD8⁺ T cells, the actual tumour-enrichment and expansion will be greater than inferred given the blood comparison is with the proportion of

CD8⁺ T cells only.

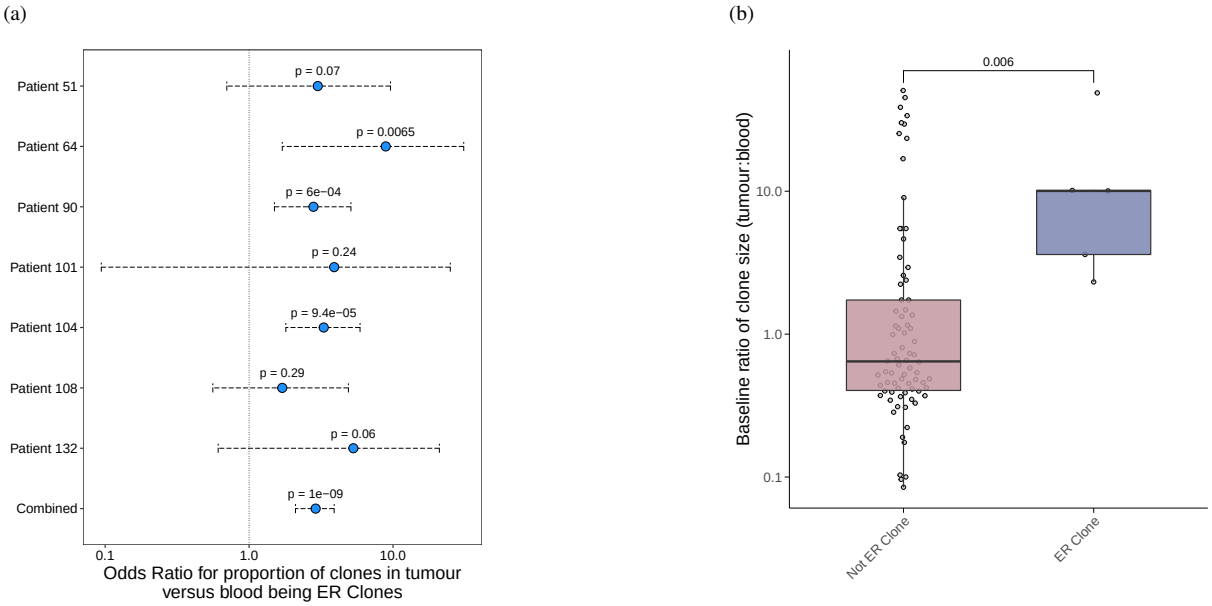


Figure 4.18. (a) Odds ratio and 95% CI for proportion of all clones within resected tumour specimens that are ER clones, compared to proportion of clones within peripheral blood of the same patient. (b) Size of clones that are found within the peripheral blood and tumour of the same patient, coloured by whether they are ER clones. Statistics with Fisher's exact test (a) and two-sided Wilcoxon rank sum test (b).

I then looked at the gene expression of those CD8⁺ T cells which are ER clones in the scRNAseq dataset (Chapter 3). Applying a previously-defined cytotoxicity score (see section 3.3.1, page 92), reveals that cells that are ER clones are more cytotoxic than non-ER clone cells within both T_{cm} and T_{em} CD8⁺ T cell clusters (Figure 4.19a). Specific genes differentially upregulated within ER clones include the central memory marker *SELL*, encoding CD62L, and *CCL5* encoding chemokine ligand 5, as well as cytotoxic molecules such as *GZMK* (Figure 4.19b). GOBP pathway analysis reveals upregulation of adaptive immune pathways and translation, with downregulation of innate responses (Figure 4.19c).

Taken together, these findings suggest increased tumour-reactivity of ER clones which - in the peripheral blood - are more cytotoxic with upregulation of key immune pathways, including those involved in tissue trafficking.

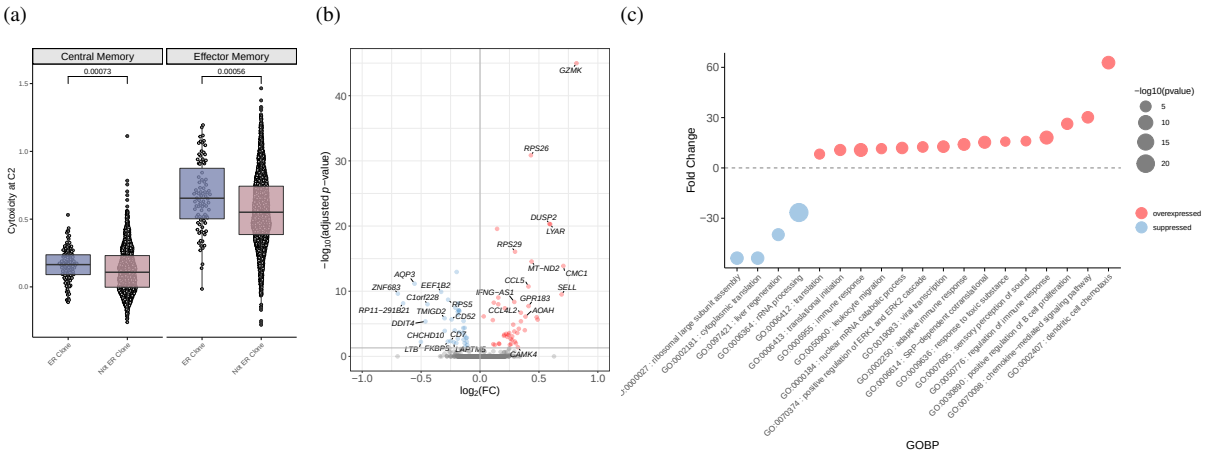


Figure 4.19. (a) Cytotoxicity as determined by single cell sequencing, coloured by whether cells are ER clones and faceted by cell phenotype. (b) Volcano plot for DEGs between cells from ER clones and all other cells. (c) GOBP for genes in (b). Statistics with two-sided Wilcoxon rank sum test (a). In (c), minimum overlap set to >2. C2 = d21.

4.3.9 ER clones are found within the repertoires of healthy donors

ER clones are defined on the basis of being highly-public, i.e. found in at least three different individuals. I therefore wished to understand their occurrence within the T cell repertoires of healthy donors. Surprisingly, ER clones are found within healthy donor repertoires, although they occupy a smaller proportion of the repertoire to patients with MM pre-treatment (median proportion in patients pre-treatment 0.26%, median proportion in healthy donors 0.057%, p<0.0001, Figure 4.20a). This is due to the fact that patients with MM have both more and larger ER clones (Figures 4.20c and 4.20b). However, when patients were dichotomized according to response to ICB within the first six months of treatment, I noted that only patients with disease control for over six months had a greater proportion of their pre-treatment repertoire occupied by ER clones than HDs (Figure 4.20d). Those individuals with progressive disease had a similar proportion of their repertoire occupied by ER clones compared to HDs. These results suggest that failure to respond to ICB could be a result of a lack of expansion of key CD8⁺ T cell clones at baseline, indicating the proportion of repertoire occupied by ER clone at baseline has prognostic utility.

For comparison, I took known TA-TCR which had been derived from sequencing of TCRβ chains

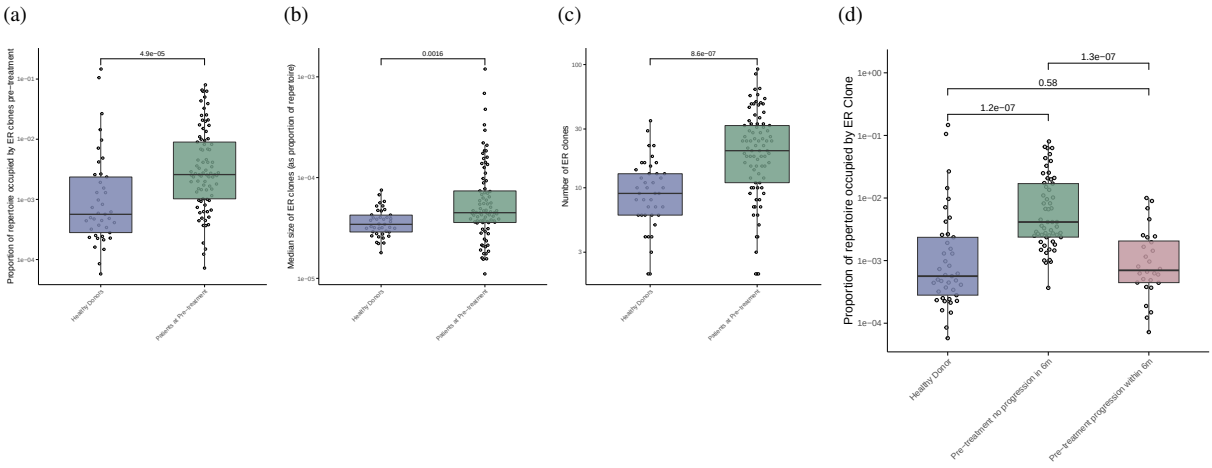


Figure 4.20. (a) Proportion of the repertoire occupied by ER clones in healthy donors and patients pre-treatment. (b) Median size of ER clones in healthy donors and patients pre-treatment. (c) Number of ER clones found in the repertoires of healthy donors and patients pre-treatment. (d) Repertoire occupancy by ER clones, comparing healthy donors to patients with no progression of disease in 6 months (green) and progression of disease within 6 months (red). Statistics with two-sided Wilcoxon rank sum test.

extracted from resected melanomas, within published literature[64,94,177,239]. Within my dataset, 20,553 unique TA-TCR were present. However, unlike ER clones, there is no effect of treatment on TA-TCR, with no evidence of expansion post-ICB in either those individuals who respond or progress (Figure 4.21a). Further, I noted that the repertoire occupancy of TA-TCR is similar between patients with MM pre-treatment and healthy donors - with those who have a good response actually having less of their repertoire occupied by TA-TCR than HDs (Figure 4.21b). Finally, I looked within the TA-TCR found in our dataset and identified that 91 are also ER clones. These clones - which are both TA-TCR and ER clones - are expanded in the baseline of individuals with a response to treatment - akin to all ER clones but in contrast to the rest of the TA-TCRs (Figure 4.21c).

Taken together, these findings suggest that most TA-TCR are not expanding with ICB and therefore may not be being ligated by antigen. Indeed, it is very possible that a great deal of TA-TCR are so-called "bystander clones" whereas, in contrast, those identified as being ER clones are, in fact, likely mediating an anti-tumour response[245].

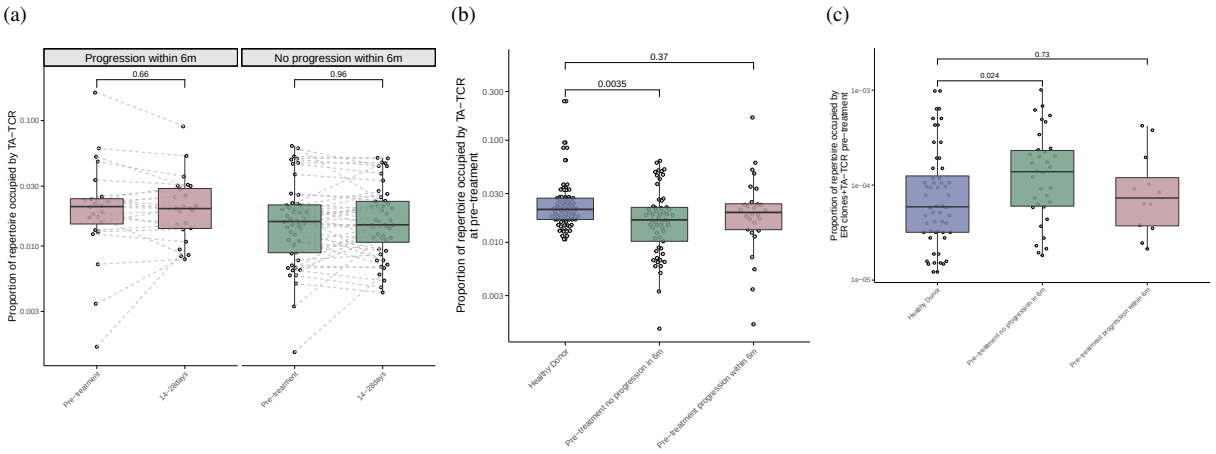


Figure 4.21. (a) Proportion of the repertoire occupied by TA-TCR by clinical response over time. (b) Repertoire occupancy by TA-TCR comparing healthy donors to patients with no progression of disease in 6 months (green) and progression of disease within 6 months (red). (c) as per (b) but for TA-TCR that are also ER clones (n=91). Statistics with two-sided Wilcoxon signed-rank test (a) or rank sum test (b and c).

4.3.10 Importance of ER clones replicates in validation datasets

Finally, I sought to validate the relevance and importance of ER clones in external datasets. In order to replicate the observation that the proportion of the peripheral blood CD8+ T cell repertoire occupied by ER clones correlated with outcome, I took bulk RNAseq data on sorted peripheral CD8+ T cells from a further 95 individuals with MM (peripheral blood validation cohort, n=91 individuals pre-treatment and n=57 individuals post-treatment, n=53 individuals paired pre- and post-ICB, Table 4.3). V(D)J data was mapped from the bulk RNAseq output using *MiXCR*[237] - hence this dataset of separate individuals comprised of TCR repertoire data generated using an alternative method.

Within this dataset, I identified 139 unique ER clones, with at least one clone being found in 73/95 individuals. I was able to replicate the finding that the proportion of repertoire occupied by ER clones associated with outcome both at pre-treatment and post-treatment time points (Figure 4.22). Furthermore, the proportion of the repertoire occupied by ER clones in the peripheral blood at both the pre-treatment and 14-28 day time-point resulted in both a progression-free and overall

Characteristic	N = 148[1]
Age	62 (14.6)
Sex	
Female	73 (49%)
Male	75 (51%)
Treatment	
cICB	83 (56%)
sICB	65 (44%)
Timing of sample	
Pre-treatment	91 (61%)
14-28days	57 (39%)
[1] Mean (SD); n (%)	

Table 4.3. Characteristics of validation cohort produced by bulk RNAseq. n=95 individuals total, n=53 paired pre- and post-ICB

survival benefit (Figure 4.22). After confining analysis to the validation cohort, individuals with greater than the median proportion of their repertoire occupied by ER clones at 14-28 days were 63% less likely to progress within six months and 56% less likely to die than those with less than the median of their repertoire occupied by ER clones after controlling for age, although the association with death was of borderline significance (HR for progression 0.37, 95% CI 0.17-0.84, p=0.018; HR for death 0.44, 95% CI 0.21-1.00, p=0.051; Cox proportional hazards). I then looked at bulk RNAseq data (aligned using *MiXCR*) and included all patients from both the discovery and validation cohorts. This resulted in 178 patients total, 173 pre-treatment and 128 14-28 days post-treatment (82 of the 85 discovery cohort patients had available bulk RNAseq data pre-treatment and 71 post-treatment, plus 91 validation patients pre-treatment and 57 patients 14-28 days post-treatment). Across this bulk data, there was a highly significant association between proportion of the repertoire occupied by ER clones, both pre- and post-treatment, and clinical outcome (Figures 4.22h and 4.22i).

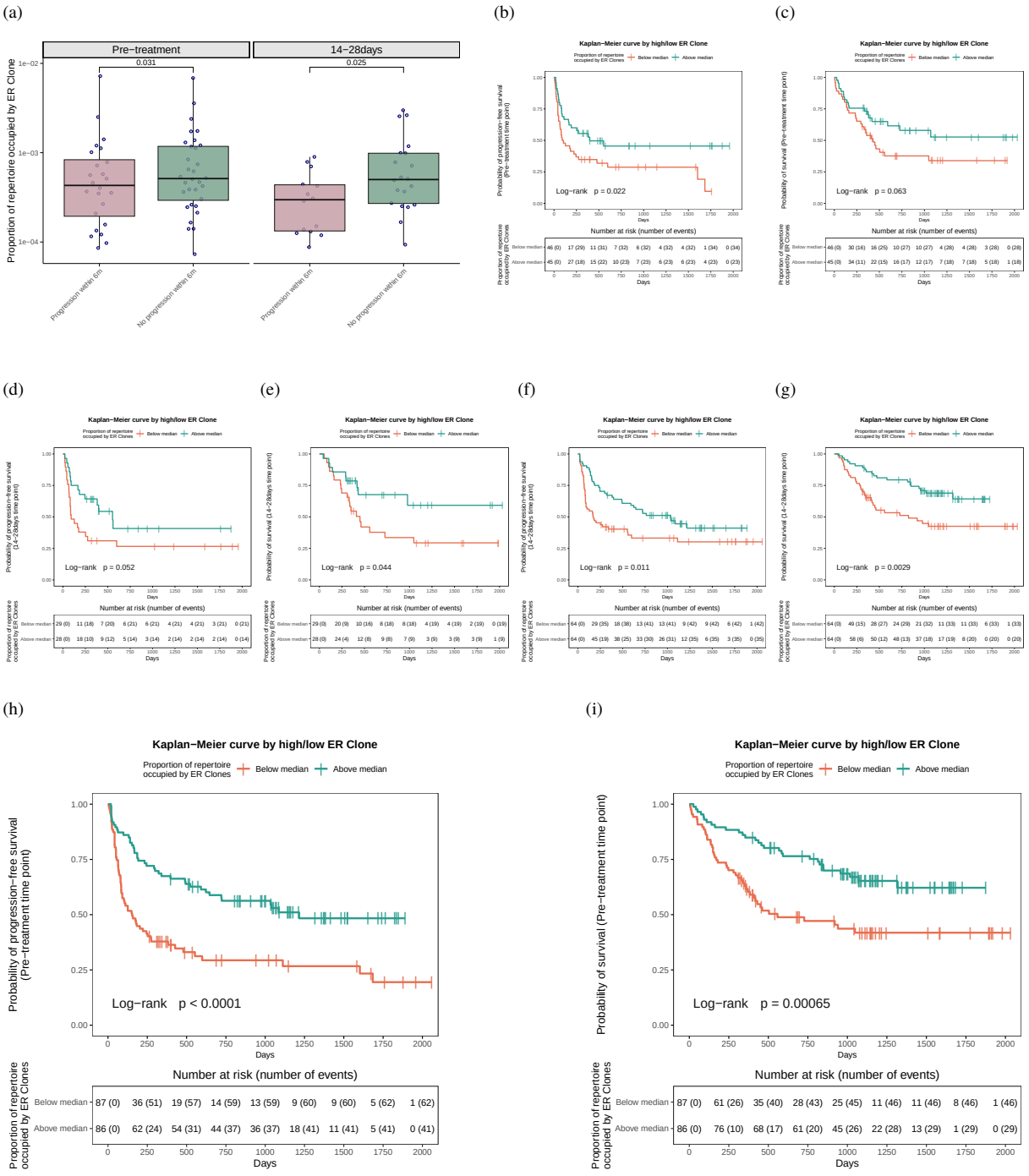


Figure 4.22. (a) Proportion of the repertoire occupied by ER clones by clinical response over time in the validation cohort (bulk RNAseq data, aligned with *MiXCR*, no overlapping individuals with discovery cohort). (b) Progression-free survival curves based on above or below median proportion of the repertoire occupied by ER clones at pre-treatment in validation cohort. (c) as per (b) but overall survival. (d) Progression-free survival curves based on above or below median proportion of the repertoire occupied by ER clones at 14-28 days post-treatment in validation cohort. (e) as per (d) but overall survival. (f) Progression-free survival curves based on above or below median proportion of the repertoire occupied by ER clones at 14-28 days in pooled discovery and validation cohort (bulk RNAseq data, aligned with *MiXCR*, including all individuals from both validation and discovery cohorts). (g) as per (f) but overall survival. (h) Kaplan-Meier curve (KM) for overall survival based on above or below median proportion of repertoire occupied by ER clones pre-treatment in pooled bulk RNAseq cohort. (i) as per (h) but overall survival. Statistics with one-sided Wilcoxon rank sum test (a) or Log Rank test (b-i).

In order to corroborate our findings of the intra-tumoural relevance of these clones, I explored the dataset from Riaz *et al.*[94] who sequenced TCR from resected melanomas pre- and post-sICB therapy. I find that the number of ER clones found within the tumours in post-treatment samples correlated with outcome in this study too (Figure 4.23a). Further, there appeared to be trafficking of ER clones into the tumours in patients that responded to PD-1 blockade, but not in those with progressive disease (Figure 4.23b). Such a difference was not observed in non-ER clones.

These results suggest that ER clones as defined in the discovery cohort are highly-public and of broad disease relevance across multiple datasets in MM.

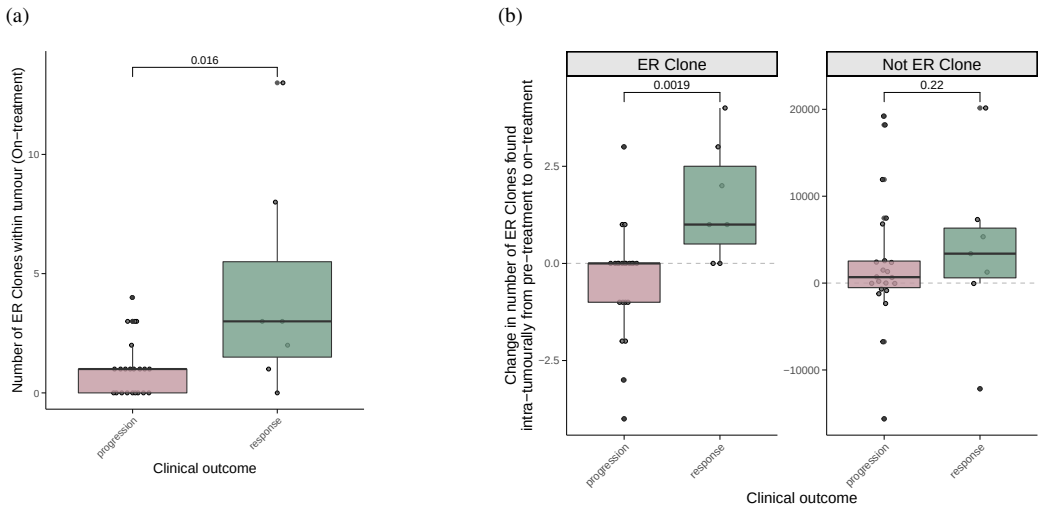


Figure 4.23. (a) Number of ER clones found within tumours at the on-treatment time point from Riaz *et al.*[94], coloured by clinical response. (b) Change in the number of clones found within tumours, coloured by clinical outcome and faceted by whether clones are ER clones. Statistics with one-sided Wilcoxon rank sum test.

4.4 Discussion

In this chapter, I have used deep sequencing of the TCR of peripheral T cells - with a specific focus on CD8⁺ T cells - to draw insights into short and long-term repertoire changes following ICB. Notably, when controlling for age and CMV status, the Gini coefficient (Gini) at 14-28 days post treatment correlated with clinical outcome, suggesting that 'clonal dominance' post-ICB is

an important feature of response. There was correlation in repertoire metrics between CD8+ T cell TCRα and TCRβ chains, as well as between memory CD4+ T cells and CD8+ T cells. V and J gene usage between CD4+ and CD8+ T cells was also strikingly similar.

Focussing on the CD8+ T cell compartment, I utilised unsupervised clustering of T cells with the *GLIPH2* algorithm[188] to identify highly-public CD8+ T cell clones which strongly associate with response to ICB treatment in MM. Whilst this work was performed agnostic to HLA type, HLA associations with respect to outcome could be found. These clones, termed 'Emergent Responder' (ER) clones, are large, cytotoxic and of a memory phenotype. ER clones show a tendency to upregulate tissue-trafficking chemokines and are found to be enriched and enlarged within tumours. Further, ER clones persist long-term in the peripheral blood, with durability of this expansion being associated with a sustained response. Whilst ER clones can be found in the blood of HDs, they occupy a significantly greater proportion of the repertoire in patients with a good response to ICB. Finally, these findings validate in two replication cohorts - one peripheral blood dataset from our group and a second, public, intra-tumoural sequencing dataset[94].

The finding that day 14-28 Gini correlates with outcome aligns with work by others, such as Cha *et al.*[99] and Valpione and colleagues[95] (as summarised in introduction section 1.5.3.2, page 50), as well as work from our own group[93] which describes the importance of increasing clonality post-ICB in 00determining clinical outcome. Here, however, I have looked beyond repertoire metrics and described, for the first time, TCR from peripheral CD8+ T cells which strongly correlate with outcome in MM.

These findings have important implications. Firstly, these TCR have clear potential as a peripheral host immune biomarker for response to ICB. The fact that their presence in the repertoire corresponds with clinical outcome in both the discovery and validation datasets at multiple time points suggests that they could be used following either pre- or on-treatment blood sampling to

stratify patient response.

Secondly, this work provides further mechanistic insight into the importance of the *a priori* CD8+ T cell repertoire in the response to ICB in MM. The fact that low numbers of these key TCR pre-treatment associates with poor outcomes suggests that one mechanism of treatment failure is insufficient antigen recognition, consistent with previous findings[78,99]. Further, the finding that many of these key TCR are found in healthy individuals suggests that key response T cells may be cross-reactive and not restricted to private neo-antigens, as has been suggested for NSCLC[190]. Given that those with disease progression had a lower proportion of their repertoire occupied by ER clones than healthy donors suggests a role for a failure of general immune surveillance in those with a poor response to treatment.

Thirdly, for both cancer vaccines and autologous cell therapies, the identification of public neoantigens - tumour targets relevant to multiple individuals - is of great importance for both logistical and clinical reasons[246]. By identifying highly public groups of key response TCR in an unsupervised manner, there is great potential to subsequently advance this current work and identify cognate antigens with possible import in these therapeutic fields. My work indicates that responsivity in terms of change in clonal size to ICB is vital in determining public clonotypes with prognostic and potentially therapeutic utility - the absence of response to ICB of clonotypes corresponding to public TA-TCR, as well as the lack of prognostic association of such clones, indicates that focusing on tumours in isolation at a single time point is likely to be of relatively low return. Moreover, my data are in keeping with the majority of clones within tumours forming bystanders - the relative depletion of such clones in the blood of responding individuals potentially indicating that these may be non-benign in effect[66]. Finally, the fact that ER clones demonstrate prognostic association according to HLA type facilitates downstream attempts to identify their cognate antigen and reinforces the importance of the peripheral immune response in identifying

key immunological mediators of tumour rejection.

A recent study[193] has also attempted to describe TCR motifs associated with a successful response to ICB (discussed in introduction section 1.5.4, page 56). Using a deep learning approach, this work described motifs associated with viral antigens corresponding with a higher likelihood of response, whilst tumour-specific TCR corresponded with a higher likelihood of non-response. This finding is in contradiction to our description of ER clones which are depleted of viral-recognising TCR. However, Sidhom *et al.*'s study is based on the intra-tumoural, rather than peripheral, repertoire, and they describe that the viral signature associated with response may be relative to background TCR. The approach described here - which agonistically identifies groups of TCR expanding post-treatment in people with a good response to treatment - suggests that, despite being highly public, key response TCR appear to be depleted for virally-reactive clones.

I recognise the limitations of this work. Firstly, the study design primarily allows for associations to be described, rather than causality to be assigned. Secondly, as with most studies of T cell repertoires using bulk data, I am unable to pair TCR beta and alpha chains and therefore identify the entire TCR. Thirdly, as is standard practice for all RNA-based TCRseq, there is an underlying assumption that number of reads correlates closely with clonal size. However, given that I have used multiple modalities including bulk sequencing, single cell sequencing and flow cytometry and that findings validate in multiple external datasets using differing samples and technologies, I am confident in the robustness, relevance and high applicability of my findings.

In conclusion, I can identify highly-public groups of key peripheral CD8+ TCR which closely correspond with clinical outcome following ICB treatment for MM across multiple datasets. These TCR are present in the baseline and clones carrying them are expanded, more cytotoxic, tumour-reactive and of a memory phenotype. This work is of broad relevance to biomarker development and targeted immunotherapeutic development.

5 | Long term effects of ICB on peripheral $CD8^+$ T cell subsets

5.1 Chapter-specific acknowledgements

For work presented in this chapter, I would like to acknowledge Elsita Jungkurth who assisted with all the wet-lab experiments. Further, consistent with work throughout this thesis, the blood samples on which these experiments were based were collected and isolated with a wide range of colleagues, as specified in the Declaration (page iii).

The raw sequencing data was pre-processed by myself (see methods sections 2.2.2) - however, this relied heavily on a pipeline developed primarily by Orion Tong, also in conjunction with Christina Ye.

Finally, the dimensionality reduction and cell annotation was performed by Bo Sun (see methods section 2.2.3), in order to unify all single cell data that had been produced as part of four separate projects within the Fairfax lab into one consistent 'atlas'. I used the reduced and aligned data for downstream analysis. All analyses and figures presented here were generated by me.

5.2 Chapter-specific background

A number of sections of the introduction, Chapter 1, are relevant to this chapter. Firstly, section 1.2.5 (page 27) summarises the current work on understanding long term clonal responses to ICB. As discussed in this section, there is relatively limited understanding of the phenotype, temporal changes and importance of clones that persist long term in the peripheral blood and this chapter seeks to explore these cells further. In particular, I was intrigued to follow up on a

key observation that was made in the analysis of the TCRseq data - particularly in section 4.3.7 (page 132) - whereby I noted the long-term persistence of ER clones and, notably, in those with a complete response to treatment (CR) the proportion of the repertoire occupied by these putatively key clones remained elevated beyond 100 days (Figure 4.17b, page 135).

Whilst it has been established that key T cell clones can be found in the peripheral blood many months after commencing treatment for ICB, a detailed understanding of the long term gene expression profiles, along with temporal changes, is currently lacking. In particular, there exists a gap in the understanding of what happens following a CR to ICB. Whilst it is widely accepted that tumour regression occurs primarily as a result of direct cytolysis by $CD8^+$ T cells - a process that relies on antigen recognition and ligation (see section 1.2) - what is unclear is how these clones behave in the absence of ongoing antigenic stimulation. If a patient has a CR, technically they no longer have any tumour present. In the 'traditional' model of T cell immunology - for example a response in the event of an acute infection - following removal of antigen, cytotoxic effector T cells which have expanded subsequently involute, with a minimal number of memory cells remaining. Indeed, this dogma is clearly spelled out in the famous textbook *Janeway's Immunobiology*, where the authors write - *"in the absence of... stimulus, [effector cells] undergo 'death by neglect', removing themselves by apoptosis"*[247]. However, on the basis of existing evidence regarding long term persistence - as outlined above - this does not appear to be the case. This dogma has also recently started to be challenged with the description of a relatively novel cell type - termed long-lived effector cells (LLECs) - which retain properties of effector cells (rapidly responsive and cytotoxic) and yet have the longevity of memory $CD8^+$ T cells[248].

In order to investigate long term changes to $CD8^+$ T cells following a CR to ICB, I designed a large single-cell experiment using peripheral blood samples taken at multiple time points - including post-cessation of ICB - from patients with a CR (n=12) and with PD (n=6). This single

cell experiment is referred to as the 'LT' (for long-term) experiment (see methods section 2.2, page 68).

5.3 Results

5.3.1 Single cell sequencing of individuals with a complete response to PD-1 blockade

5.3.1.1 Sample cohort

I examined the cohort of cryopreserved PBMCs that have been collected, isolated and stored by members of the Fairfax lab (myself included) since December 2015. I identified patients within that cohort who had:

1. Had been treated with PD-1 blockade
2. Subsequently had a CR to treatment
3. Were no longer receiving any form of ICB
4. On whom we had pre- and post-treatment PBMCs cryopreserved.

I subsequently approached these individuals and sought consent for a further blood sample. In addition to this, I re-examined the individuals included in my previous single cell experiment (as described in Chapter 3) and identified four on whom it was possible to obtain a further blood sample. I also included nine individuals with mRCC and two healthy donors (HDs) on whom we had blood samples three weeks apart. For these HDs, I approached them one year later in order to get a third, long-term, sample.

For all samples from patients with MM and HDs, I performed single cell sequencing of PBMCs

as well as a second replication sample of magnetically-sorted CD8⁺ T cells. The exception to this was those from patients in the original single cell cohort (termed the 'Science Immunology' (SciImm) cohort and presented in Chapter 3). Since the SciImm experiment used magnetically sorted CD8⁺ T cells and not PBMCs, I used sorted CD8⁺ T cells for these four individuals. For those with mRCC (see Chapter 3), I only sequenced magnetically sorted CD8⁺ T cells in order to maximise the number of these cells.

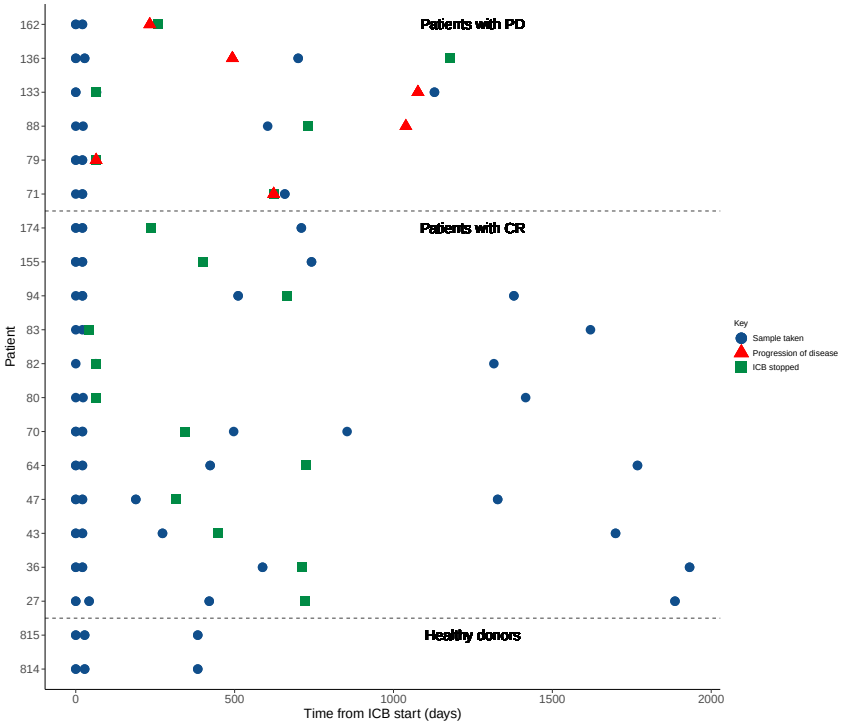


Figure 5.1. Schematic of timing of samples for melanoma patients and healthy donors.

In total, this experiment included 136 samples - 52 of which were PBMC samples, all except three (due to poor recovery following magnetic bead separation) repeated as isolated CD8⁺ T cell samples (n=49), along with a further 35 samples of just CD8⁺ T cells (n=22 mRCC, n=12 from SciImm patients (n=4 samples processed as part of this experiment and n=8 data added from previously performed experiment), and n=1 sample from patient 70 on whom PBMCs were not sequenced due to lack of space on GEM pools) (Table 5.1).

These 136 samples originated from n=29 individuals, n=18 MM, n=9 mRCC and n=2 HDs. In terms of melanoma patients (n=18), there are 65 samples (n=52 PBMC, with n=49 duplicated as CD8⁺ T cells with n=13 additional CD8⁺ T cell samples, not duplicated as PBMCs) at a range of time points (Figure 5.1). The demographics and sample mix of the melanoma patients and HDs are outlined in Tables 5.1a and 5.1b. In total, there were 12 patients with complete response to treatment (CR) on whom I had a sample after the cessation of ICB; 10 of these were treated with single-agent pembrolizumab (sICB). The median time from stopping ICB to the sample being taken was 1165 days (3.2 years), IQR 511-1250 days (1.4-3.4 years). For one patient (70) there were two samples taken after the cessation of ICB, one year apart; these were merged for simplicity of analysis. The mRCC cohort is described in Chapter 3, with results of analysis of this cohort also presented there. Samples were multiplexed on the same GEM well - mode 6 PBMC samples and 8 CD8⁺ T cell samples. Steps taken to pre-process, align and demultiplex data based on genotype, along with dimensionality reduction and cell annotation, are outlined in methods section 2.2.2 (page 70).

(a)

Characteristic	N = 20[1]
Age	73 (12.2)
Sex is Female	7 (39%)
Treatment	
cICB	2 (11%)
sICB	16 (89%)
Progression of disease	6 (33%)
status	
HD	2 (10%)
MM	18 (90%)

[1] Mean (SD); n (%)

(b)

Characteristic	CD8, N = 62[1]	PBMC, N = 52[1]
Timing of sample		
baseline	18 (29%)	16 (31%)
3-9 weeks post-commencing ICB	20 (32%)	16 (31%)
6m-2yrs post-commencing ICB	10 (16%)	9 (17%)
post	14 (23%)	11 (21%)
Progression of disease	15 (27%)	13 (28%)
status		
HD	6 (10%)	6 (12%)
MM	56 (90%)	46 (88%)

[1] n (%)

Table 5.1. Characteristics of the melanoma patients and healthy donors (a) and samples (b) included in the scRNAseq experiment.

5.3.1.2 PBMC annotation reveals classical subsets

Following QC and removal of low quality cells (see methods section 2.2.2), dimensionality reduction and annotation, there were 109,502 PBMCs (from n=16 individuals, n=14 with MM - i.e. n=18 minus the 4 SciImm patients - and n=2 HDs) which could be categorised into classical subsets with canonical gene markers, clearly visualised on a UMAP plot (Figure 5.2, Table 5.2), and easily differentiated by their top ten canonical markers (Figure 5.3). There was homogeneity of distribution of samples across all subsets - which correspond with both individuals and time points (Figure 5.4). Genotypic doublets (i.e. doublets formed of two or more cells from different individuals) were removed, however other doublets (defined by either gene expression or V(D)J evidence) were retained due to potential biological significance (see methods section 2.2.2).

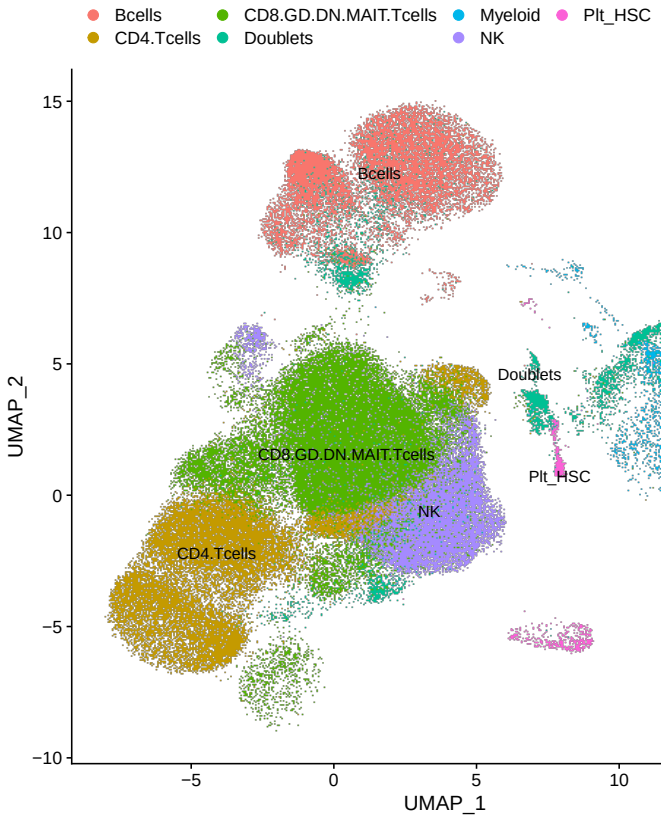


Figure 5.2. UMAP plot of PBMC samples reveals clear classical subsets. CD8.GD.DN.MAIT.Tcells is a cluster which contains 'classical' CD8⁺ T cells, along with MAIT cells, $\gamma\delta$ T cells, and double negative T cells (DN T cells). NK = natural killer, Plt_HSC = platelets/haematopoietic stem cells.

Subset	Cell number
Bcells	15247
CD4.Tcells	21643
CD8.GD.DN.MAIT.Tcells	41085
Doublets	5706
Myeloid	7882
NK	16839
Plt_HSC	1100

Table 5.2. Number of cells in PBMC subsets. CD8.GD.DN.MAIT.Tcells is a cluster which contains 'classical' CD8$^+$ T cells, along with MAIT cells, $\gamma\delta$ T cells, and DN T cells. NK = natural killer, Plt_HSC = platelets/haematopoietic stem cells.

.

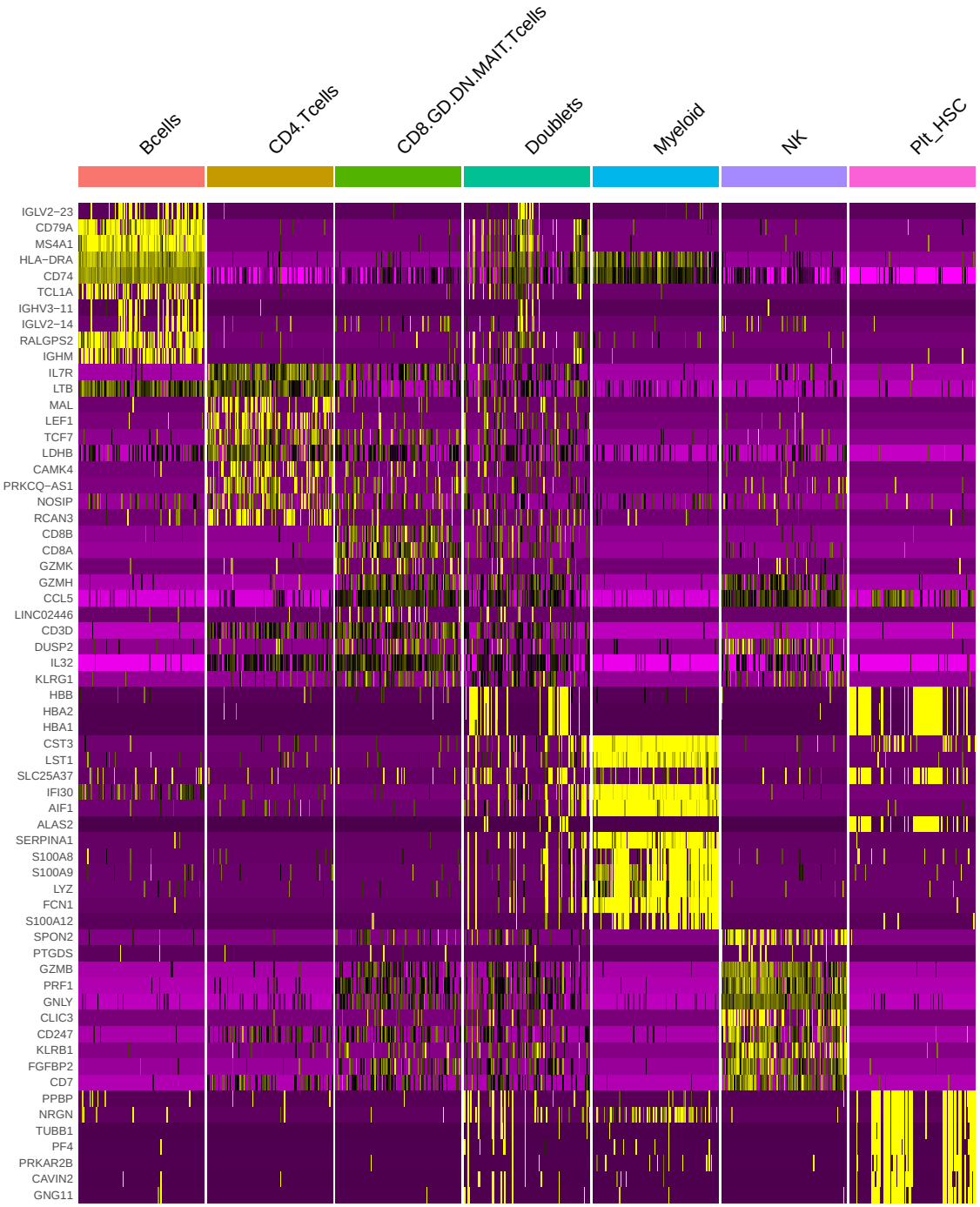


Figure 5.3. PBMC subsets can be defined by their canonical gene expression - the heatmap shows the top ten genes for each subset. A yellow colour refers to differential upregulation compared to other clusters, a purple colour differential downregulation.

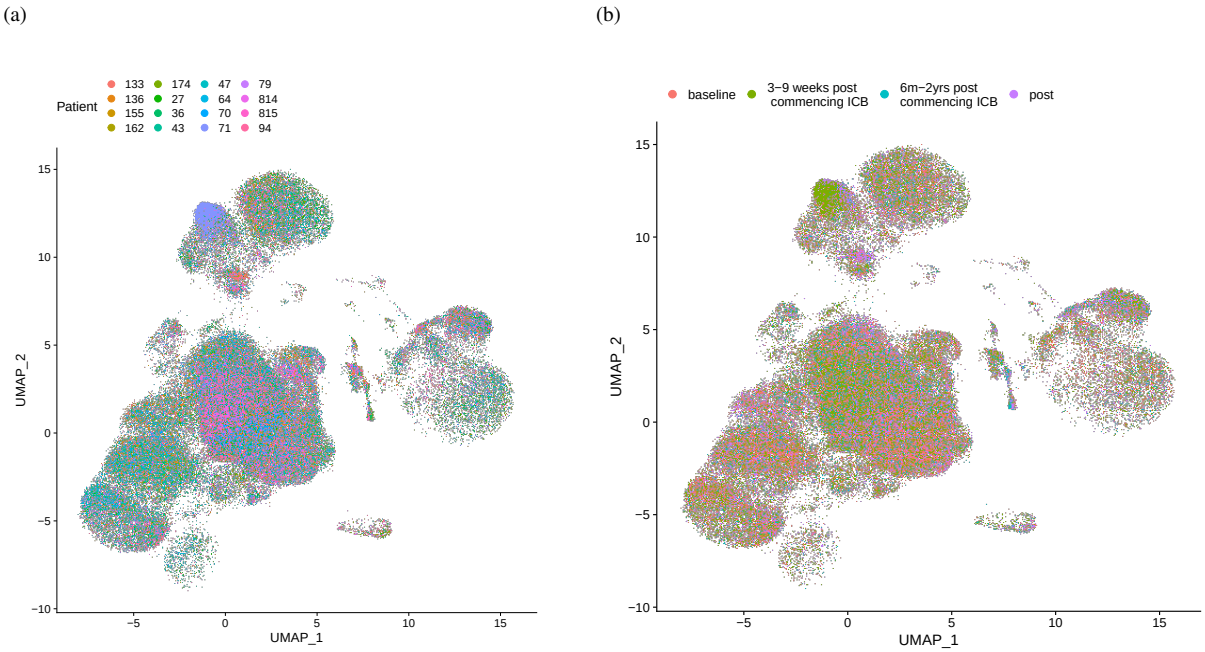


Figure 5.4. UMAP plot of PBMC samples coloured by patient (a) or time point of sample (b).

5.3.1.3 CD8⁺ T cell cohort

There were three sources of CD8⁺ T cells for analysis - those isolated as part of the PBMC experiments, those which were magnetically sorted prior to GEM generation in this experiment and those which were performed as part of the previous SciImm experiment, reported in Chapter 3 (see methods section 2.2, page 68). From the current (LT) experiment using magnetically sorted CD8⁺ T cells, there were 112,070 cells post QC, of which 78,841 were from patients with melanoma or HDs. Pooling these together with those from the PBMC experiment (n=41,085) gave a total of 119,926 cells.

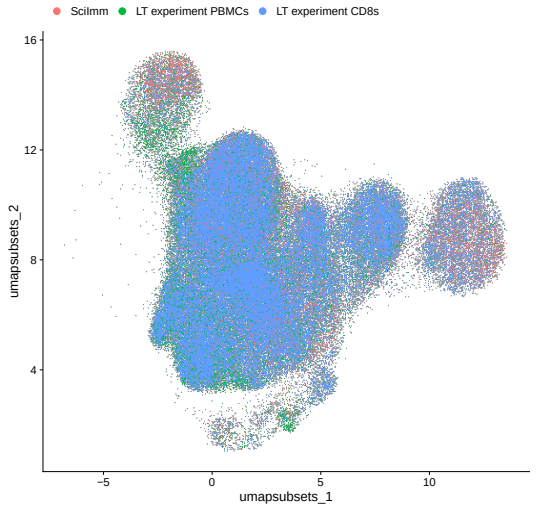


Figure 5.5. UMAP plot of CD8⁺ T cell samples coloured by experiment showing diffuse clustering of those cells from the SciImm samples and from the whole PBMCs.

As stated above, there were four individuals who were included in the previous SciImm experiment (detailed in Chapter 3) on whom I was able to get a further blood sample and hence compare their previously-sequenced d0 and d21 samples (the 'SciImm samples') with a further late sample. In order to integrate the previous sequencing data (i.e. the SciImm samples) into these current results, I re-ran the FASTQ files from the SciImm samples through the same pre-processing pipeline (see methods section 2.2.2) as used for all the other samples, and they were also put through the same

dimensionality reduction and annotation process to ensure consistent annotations (see methods section 2.2.3). Following all QC and filtering, I noticed that these eight SciImm samples (d0 and d21 from four patients) gave a total of 18,794 cells. This was notably higher than the 13,187 post-QC cells from these samples in the original work.

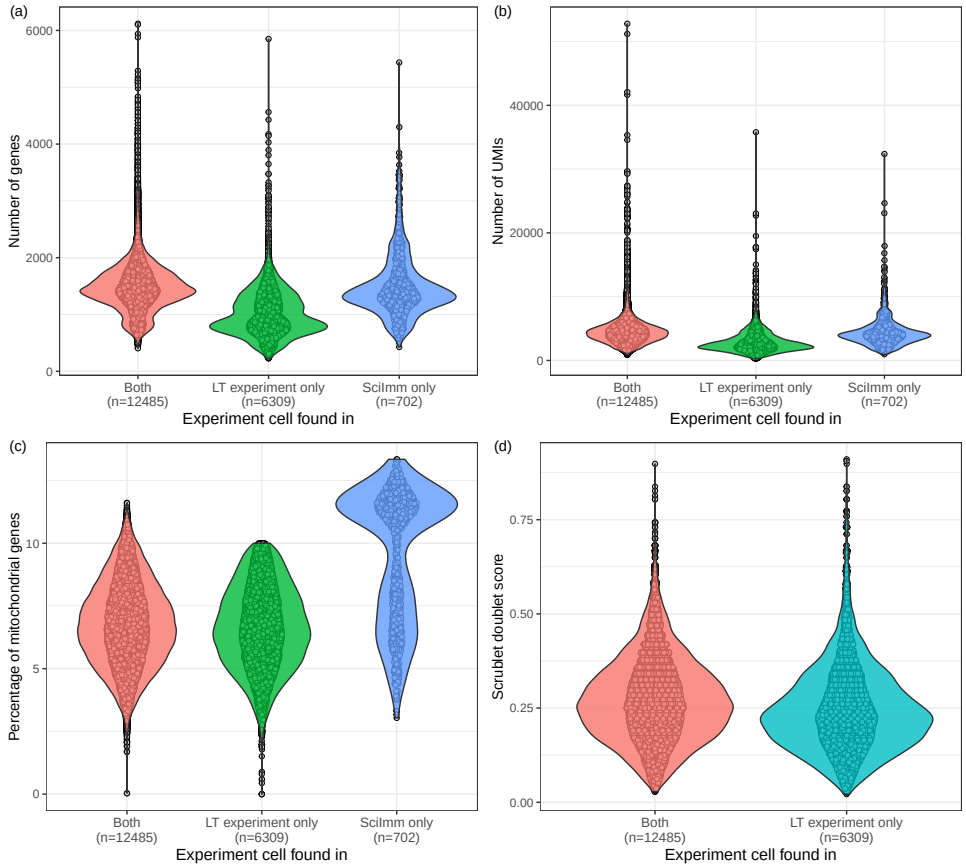


Figure 5.6. A comparison of cells which were found exclusively in the original alignment (Chapter 3) - "SciImm only" - those cells found only in the repeated alignment for this experiment - "LT experiment only" - and those found in both alignments. The number of genes (a), number of UMIs (b), percent of mitochondrial genes (c) and the doublet score (d) - which was only available for the repeat alignment and pre-processing - are displayed.

I wanted to understand if there were any differences in these cells which were not included first time. However, I was not able to identify any major differences in where they clustered on the UMAP (Figure 5.5), nor in their number of genes, number of UMIs, percent of mitochondrial genes or *Scrublet* score (Figure 5.6). The reasons for this discrepancy are likely to result from different pre-processing steps. In the original, SciImm, single cell experiment, all the pre-processing and

QC was performed by Isar Nassiri (see methods section 2.2.2, page 70) who passed me the expression matrices for downstream analysis. He filtered cells for inclusion only if they expressed *CD3* and *CD8A*; filters that were not subsequently applied for CD8⁺ T cell selection in the LT experiment (see methods section 2.2.2, page 70). Further, the SciImm samples were aligned in 2018 using *CellRanger* v2.2.0, whereas the alignment for the current, LT experiment, samples was performed in 2022 using v6.0.1. It is probable that some of the differences are accounted for by changes to the alignment software.

Nonetheless, I was reassured that on these QC metrics (Figure 5.6), the re-aligned SciImm samples appeared consistent and hence have included them in downstream analysis. As a result, pooling all CD8⁺ T cell samples gave a total of 138,720 cells.

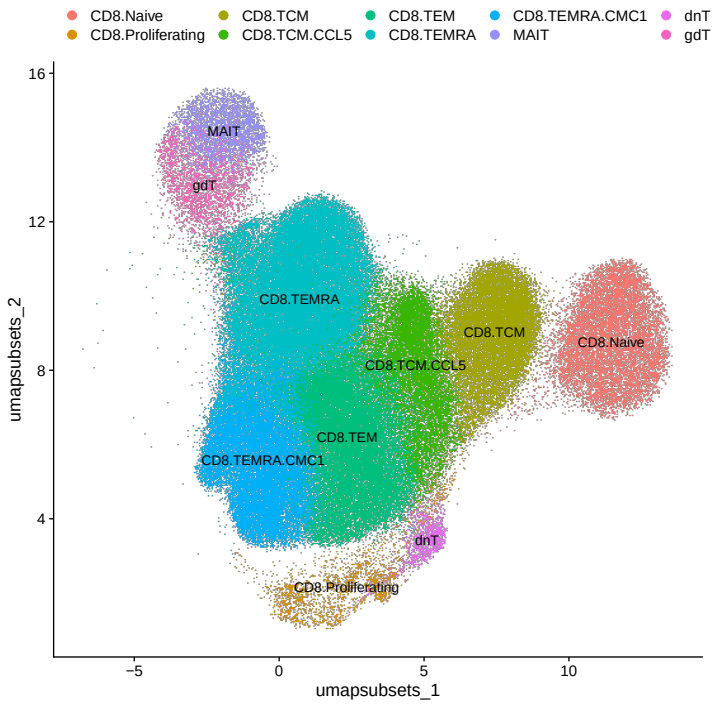


Figure 5.7. UMAP plot of CD8⁺ T cell samples reveals ten distinct subsets. TCM = T_{cm}, TEM = T_{em}, TEMRA/TEMRA.CMC1 = T_{eff}, MAIT=mucosal associated invariant T cells, gdT=$\gamma\delta$ T cells, dnT=double negative T cells.

The CD8⁺ T cells could be clustered according to canonical gene expression, giving ten main clusters - visualised on a UMAP and with a heatmap of top ten genes (Figures 5.7 and 5.9;

Table 5.3). As previously described, these LT experiment annotations mapped consistently to cluster names originally used for the SciImm samples (see Chapter 3, section 3.3.6 - particularly Figure 3.9, page 103). The CD8.TEMRA cluster can be considered analogous to T_{effs}. As is visualised, there is a separate cluster of CD8.TEMRAs that highly expresses *CMC1*, encoding COX assembly mitochondrial protein homolog. This has been shown to markedly enhance the stability of newly synthesized COX1 prior to assembly with other respiratory chain complex IV proteins[249] - and hence could be considered a component of respiration. Notably, this subset also differentially regulated a number of cytotoxic genes, which are also commonly found in NK cells - such as *KLRC2, KLRC3, KLRF1* and *TIGIT* compared to other clusters (Figure 5.9). Multiple cells in this cluster also upregulated granulysin, granzymes and *PRF1*, suggestive of a highly cytotoxic phenotype, consistent with the requirement for increased respiration. Further, *CMC1* was identified as being associated with T_{ems} in our previous single cell work[78] - hence this cluster may represent a highly cytotoxic T_{eff} group with elements of T_{ems}.

Subset	Cell number
CD8.Naive	8374
CD8.Proliferating	1778
CD8.TCM	12206
CD8.TCM.CCL5	12164
CD8.TEM	29161
CD8.TEMRA	43580
CD8.TEMRA.CMC1	24813
MAIT	3211
dnT	858
gdT	2575

Table 5.3. Number of cells in $CD8^+$ T cell subsets. TCM = T central memory (T_{cm}), TEM = T effector memory (T_{em}), TEMRA = T effector memory T cells re-expressing CD45RA (equivalent to T_{eff}), MAIT=mucosal associated invariant T cells, gdT=$\gamma\delta$ T cells, dnT=double negative T cells

As per the PBMCs data, spread of patients and time points were homogenous (Figure 5.8).

(a) (b)

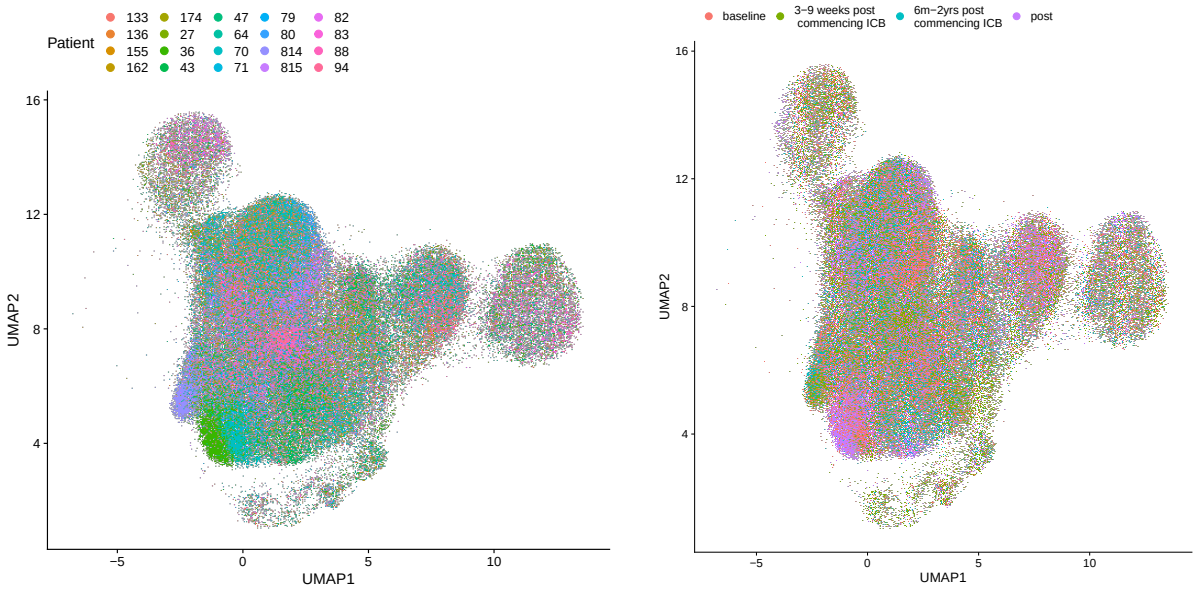


Figure 5.8. UMAP plot of CD8⁺ T cells samples coloured by patient (a) or time point of sample (b)

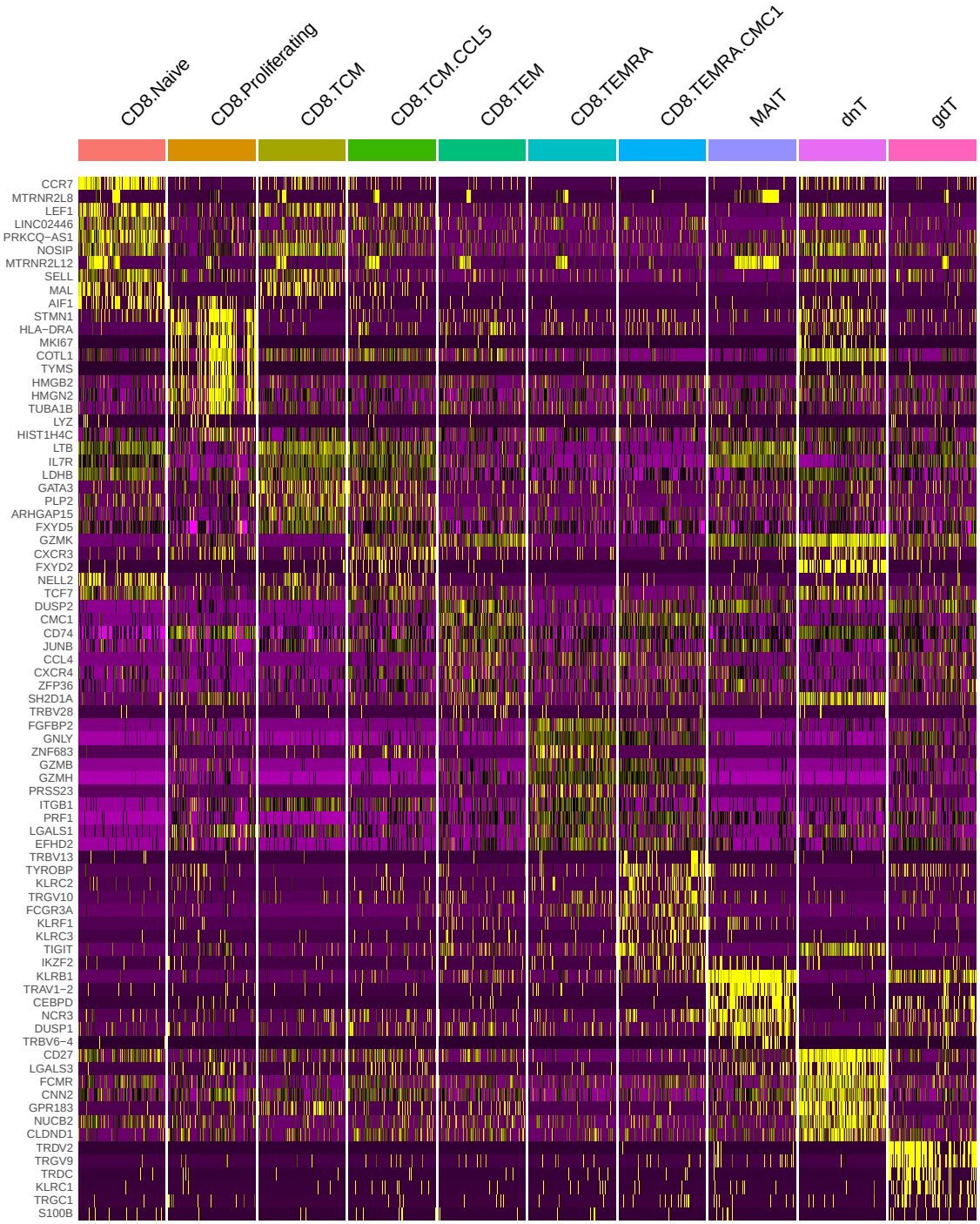


Figure 5.9. CD8⁺ T cell subsets can be defined by their canonical gene expression - the heatmap shows the top ten genes for each subset. A yellow colour refers to differential upregulation compared to other clusters, a purple colour differential downregulation. TCM = T_{cm}, TEM = T_{em}, TEMRA/TEMRA.CMC1 = T_{eff}, MAIT=mucosal associated invariant T cells, gdT=$\gamma\delta$ T cells, dnT=double negative T cells.

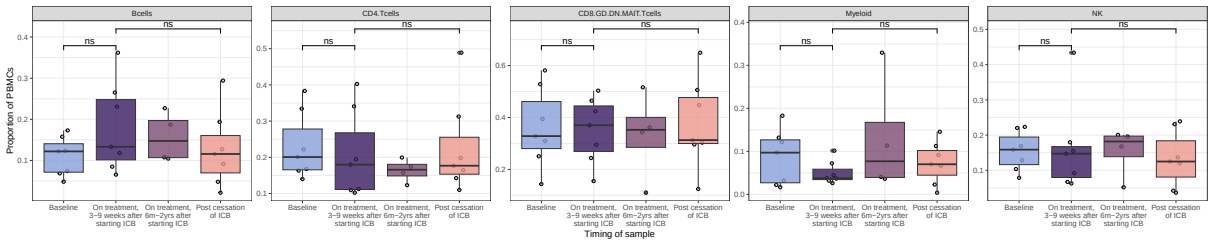
5.3.2 Changes to subset abundances over time

I was intrigued to explore how PBMC subsets changed over the long term in those with a CR. I therefore selected patients with an ongoing CR on whom I had post-treatment samples, opting to focus on the ten individuals who were treated with sICB (pembrolizumab).

I first simply looked at the proportion of each PBMC subset by individual, excluding those samples where there were <1000 cells. We have previously used such an approach to examine differences in B cell proportions in scRNAseq data (e.g. Figure 3h from reference [101]). Of note, there were no significant differences in either the PBMC or CD8$^+$ T cell subsets from baseline to 3-9 weeks on treatment or from 3-9 weeks on treatment to post treatment (Figure 5.10), except for CD8.Proliferating cells, although this difference is no longer significant once p value correction for multiple testing is taken into account. The data presented is using an unpaired Wilcoxon test as in order to use a paired test, only samples present at each time point compared can be included. There were five samples with >1000 cells and every cell type at each time point - when comparing proportions in these samples using a paired test (Wilcoxon signed rank), there were no significant differences either (plots not shown).

An alternative approach to simply calculating subset proportions is to treat proportions like a gene expression matrix and perform a differential abundance analysis using *edgeR*[226,227] (see methods section 2.2.4.3, page 77). With this approach, there were similarly no significant changes to abundance of PBMC subsets from baseline to 3-9 weeks on treatment or from 3-9 weeks on treatment to post-cessation of ICB (Figures 5.11a and 5.11b). The only significant changes in CD8$^+$ T cell subsets were seen in the CD8.Proliferating compartments, which increase in abundance from baseline to 3-9weeks and then decrease to post-treatment (Figures 5.11c and 5.11d). This is consistent with the changes to raw subset proportions (i.e. Figure 5.10) and indeed the direction of change across all subsets was consistent across both approaches.

(a)



(b)

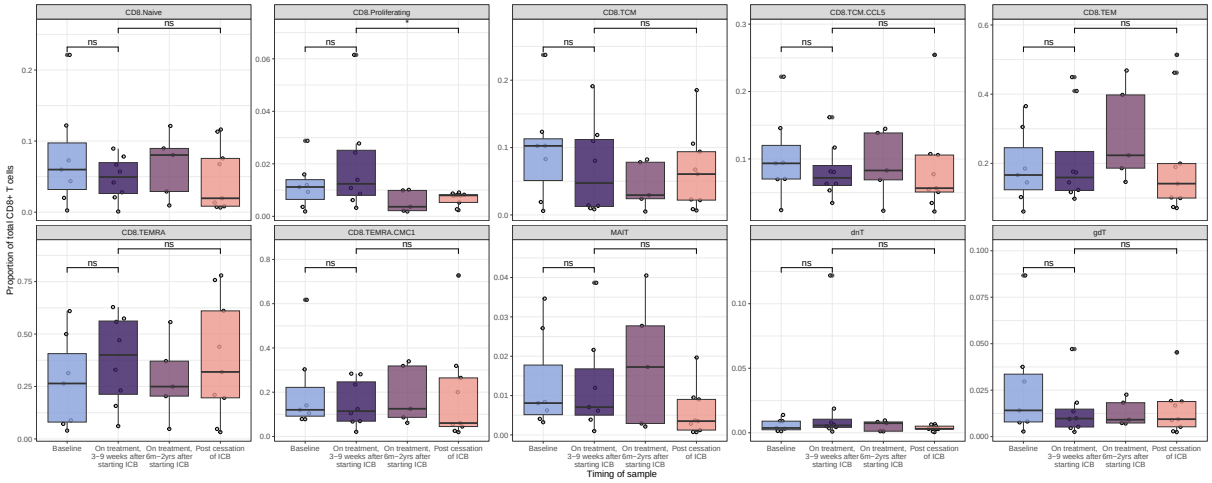


Figure 5.10. (a) Proportion of total PBMCs occupied by each subset in 10 patients with CR to pembrolizumab over time. (b) as per (a) but for CD8⁺ T cell subsets. Only those samples with >1000 cells (total) were included. Statistics with Wilcoxon rank sum test. No significance was observed when restricting to paired samples with a Wilcoxon signed rank test (not shown).

5.3.3 Differential abundance with *Milo* - PBMC subsets

Whilst it is possible to simply quantify differences in pre-defined clusters and analyse changes over time either on a per-individual basis or using a pseudobulk approach such as with *edgeR* as outlined above (section 5.3.2), a challenge with this approach is that it does not take into account continuous differentiation trajectories of cells and depends on *a priori* defined cell groups which will always, to a certain extent, be arbitrarily defined. Further, such pre-defined groupings of cells are relatively 'coarse' and so such an approach may miss nuanced changes in smaller groups of cells over time. In order to register as a significant change in proportions at a coarse subset level,

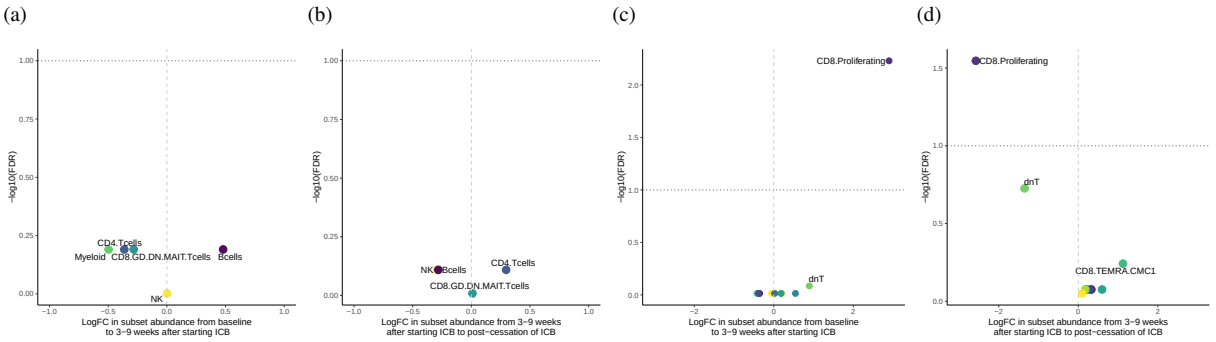


Figure 5.11. (a) Changes to PBMC subset abundance from baseline to 3-9 weeks post-commencing ICB. Each dot represents a subset, with placement on the x-axis determining if that subset increases (LogFC > 0) or decreases (LogFC < 0) from baseline to 3-9 weeks. The horizontal line represents an FDR of 0.1 and so any point below this is non-significant. (b) as per (a) but for 3-9 weeks post-initiation of ICB to post-cessation of ICB. (c) and (d) as per (a) and (b) but for CD8⁺ T cells. Statistics with a non-binomial generalised linear model as per *edgeR*[226].

the changes would have to be substantial. *Milo* - a statistical approach available as an R package - set out to address these issues by utilising a kNN approach to assign cells to partially overlapping 'neighbourhoods' of cells and perform a DA analysis on these groups (neighbourhoods)[228]. *Milo* has been validated, utilised and widely cited as a tool for DA analysis[228] and the methods used here are found in section 2.2.4.3, page 78.

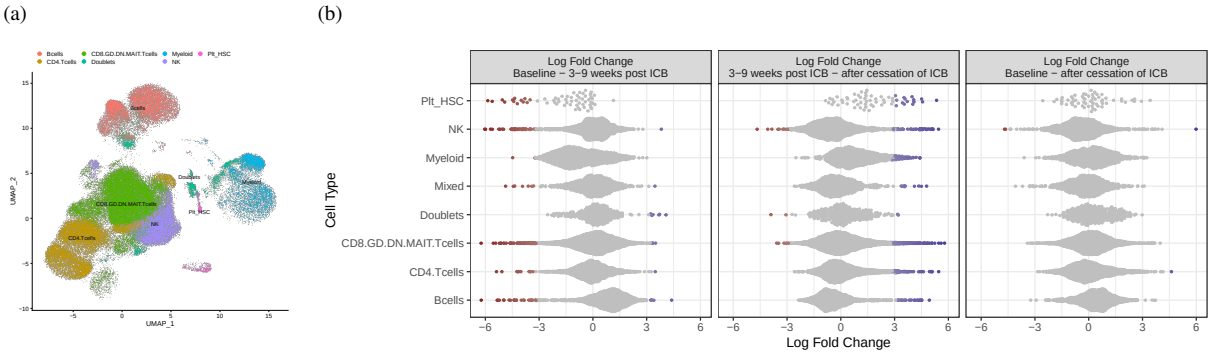


Figure 5.12. (a) UMAP of PBMC subsets for reference. (b) differential abundance (DA) of PBMC subsets by time points as labelled in facet headings. Each dot is a neighbourhood of cells, with blue neighbourhoods significantly increasing in abundance across time points and red neighbourhoods significantly decreasing.

I first wanted to simply examine changes to PBMC subsets. As can be seen, there is a reduction in the abundance of most cell types from d0 (baseline) to 3-9 weeks post-ICB (Figure 5.12). This was somewhat surprising, particularly the initial reduction in abundance of CD8⁺ T cells which,

as per the literature, are thought to be mobilised post-ICB. However, the reduced abundance in the peripheral blood after the first cycle of ICB may represent tissue trafficking of these cells and, of note, following the cessation of ICB there is a significant increase in abundance of many subsets, including CD8+ T cells. When comparing the overall change from baseline to after cessation of ICB there is grossly no change in abundance across most cell types - suggesting that changes seen from baseline to 3-9 weeks subsequently normalise.

To understand these changes in more detail, I looked at DA changes within annotated subsets of CD8+ T cells, CD4+ T cells, NK cells, monocytes and B cells (Figure 5.13). Similar to the PBMC subsets, the majority of cell types decrease in abundance from pre-treatment to 3-9 weeks post treatment, most notably T_{em} (Figure 5.13d), naive B cells (Figure 5.13f), classical monocytes (Figure 5.13h) and NK cells (Figure 5.13j). Conversely, all of these subtypes increased from 3-9 weeks post-treatment to post-cessation of ICB, save for classical monocytes. The underlying cause for the initial dip in abundance followed by the long term increase in abundance is unclear - however, as hypothesised above, it may represent turnover of cells or trafficking to tissue sites initially, followed by long term recirculation of key subtypes. Again, the relative stability identified in the long-term (i.e. baseline to after cessation of ICB) suggests that short-term shifts in abundance with ICB normalise with time.

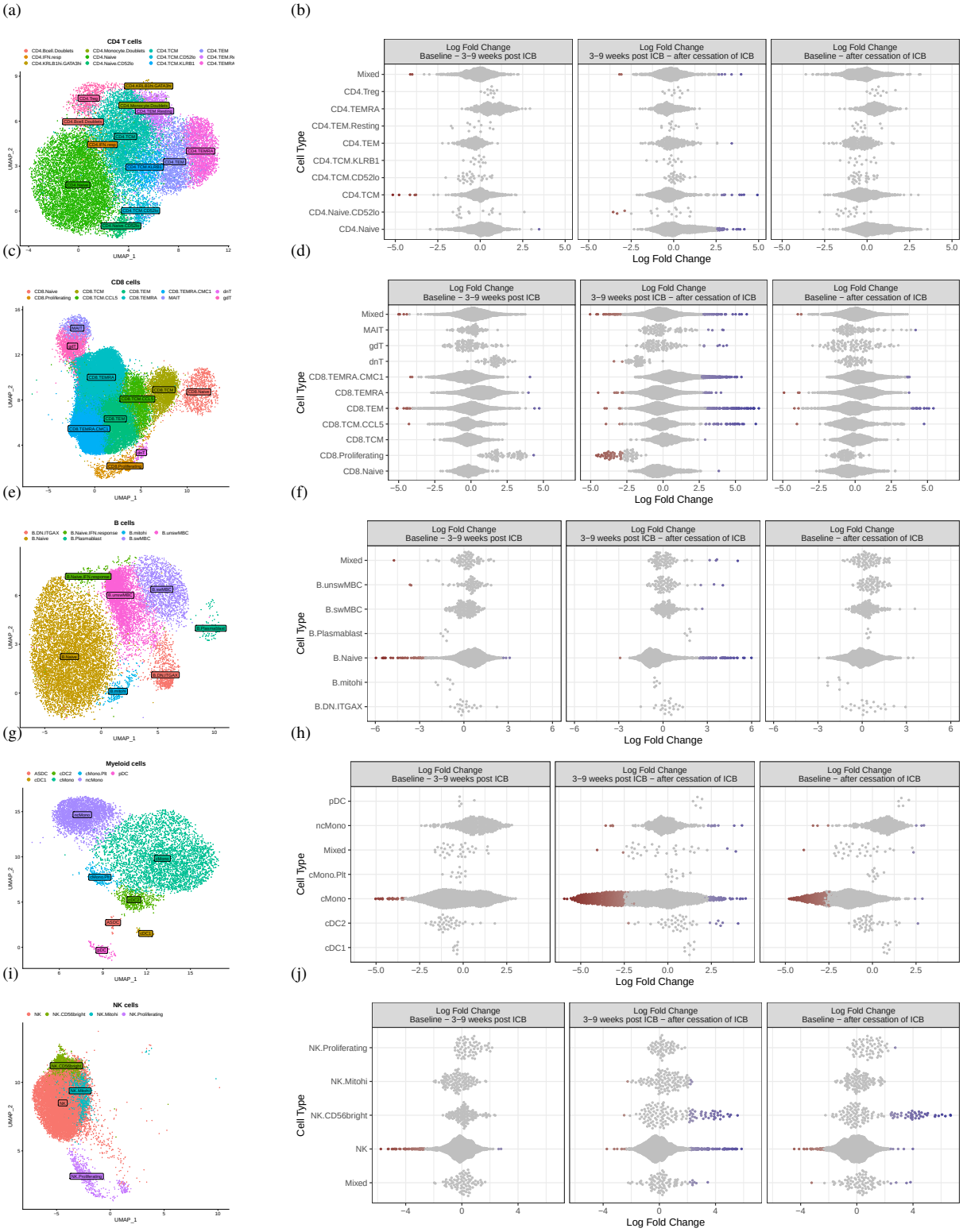


Figure 5.13. (a) UMAP of CD4⁺ T cell subsets for reference. (b) differential abundance (DA) of CD4⁺ T cell subsets by time points as labelled in facet headings. (c-d) as for (a-b) but for CD8⁺ T cells. (e-f) - B cells; (g-h) - myeloid cells; (i-j) - NK cells. Each dot is a neighbourhood of cells, with blue neighbourhoods significantly increasing in abundance across time points and red neighbourhoods significantly decreasing.

The biggest changes in DA from 3-9 weeks post-starting ICB to after cessation of ICB were observed in the CD8⁺ T cell compartment (Figure 5.13d), where significant increases in abundance are seen in not just T_{em} cells but also T_{cm}, T_{eff} (i.e. CD8.TEMRA&CD8.TEMRA.CMC1) and MAIT cell cells. It is notable that there are increases in abundance of these cell types - one might expect an increase in memory T cells following clearance of antigen, but it is curious that there are significant increases in the T_{eff} compartment - suggesting ongoing presence of cytotoxic cells.

5.3.4 Differential abundance with *Milo* - CD8⁺ T cell neighbourhoods

Due to the focus in this thesis on CD8⁺ T cells, I was keen to explore changes to their DA in more depth using *Milo*. As well as annotating neighbourhoods with pre-determined labels - as per the above (Figure 5.13) - it is possible to agnostically group neighbourhoods together based on "community detection". *Milo* uses three metrics to do this - the number of shared cells between two neighbourhoods, the direction of fold change for DA neighbourhoods and the difference in fold change[250]. These parameters can be altered to change the resolution and obtain greater or fewer groups of neighbourhoods - which are put together on the basis of their similarity rather than their cell type of origin.

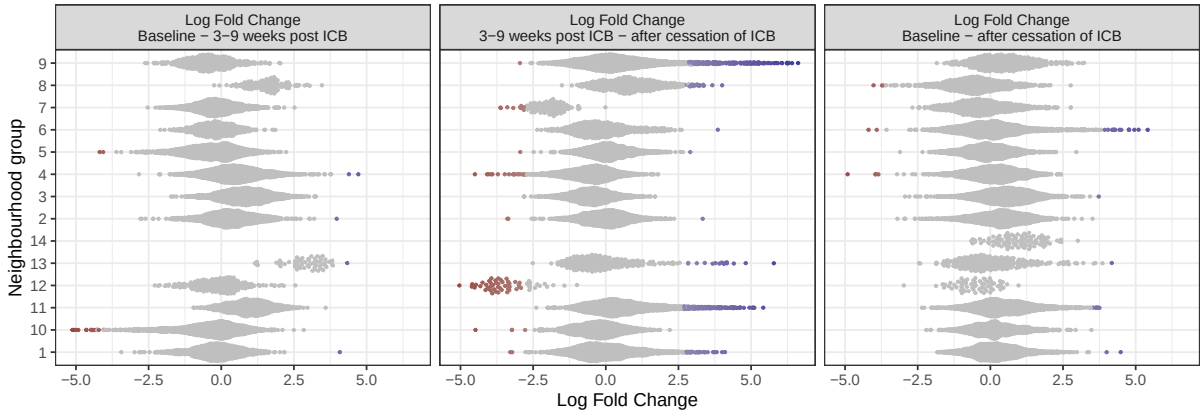


Figure 5.14. DA of CD8⁺ T cells with neighbourhoods grouped in an agnostic manner faceted by time points. Resolution is set to maximum difference of LogFC 2 and minimum overlap between neighbourhoods of 5.

Taking a resolution of max.lfc.delta - i.e. difference in LogFC - of 2 and a minimum overlap between neighbourhoods of 5, for the CD8$^+$ T cells I was able to generate 14 groups of neighbourhoods that demonstrated a varying level of DA between 3-9 weeks post-treatment and post-cessation of ICB. These groupings appeared 'clean' - i.e. the significant direction of change was only in one direction for each group (Figure 5.14). Interestingly there was minimal change in abundance of these neighbourhoods from baseline to 3-9 weeks with by far the largest increases in abundance seen from 3-9 weeks post-commencement of ICB to after cessation, potentially suggesting these changes are due to the long-term effects of ICB. Nonetheless, the overall trend from baseline to post-cessation was similar, although there were fewer significant neighbourhoods increasing in abundance over this time-course (Figure 5.14).

It is possible to plot the location of these groups on top of the UMAP to understand where they locate (Figure 5.15b) and this can be done just to highlight those groups which significantly increase in abundance (Figure 5.15c). Alternatively, instead of highlighting the whole group, it is possible to highlight simply the exact neighbourhoods which significantly change in abundance (Figure 5.15d). Notably, many of the neighbourhoods showing significant increases in DA from 3-9 weeks post-treatment to post-cessation of ICB sit over the CD8.TEMRA.CMC1 cluster (i.e. neighbourhood group 11, coloured in orange in Figure 5.15c), which differentially regulate a number of NK genes (section 5.3.1.3 and Figure 5.9) and display both T_{eff} and T_{em} markers.

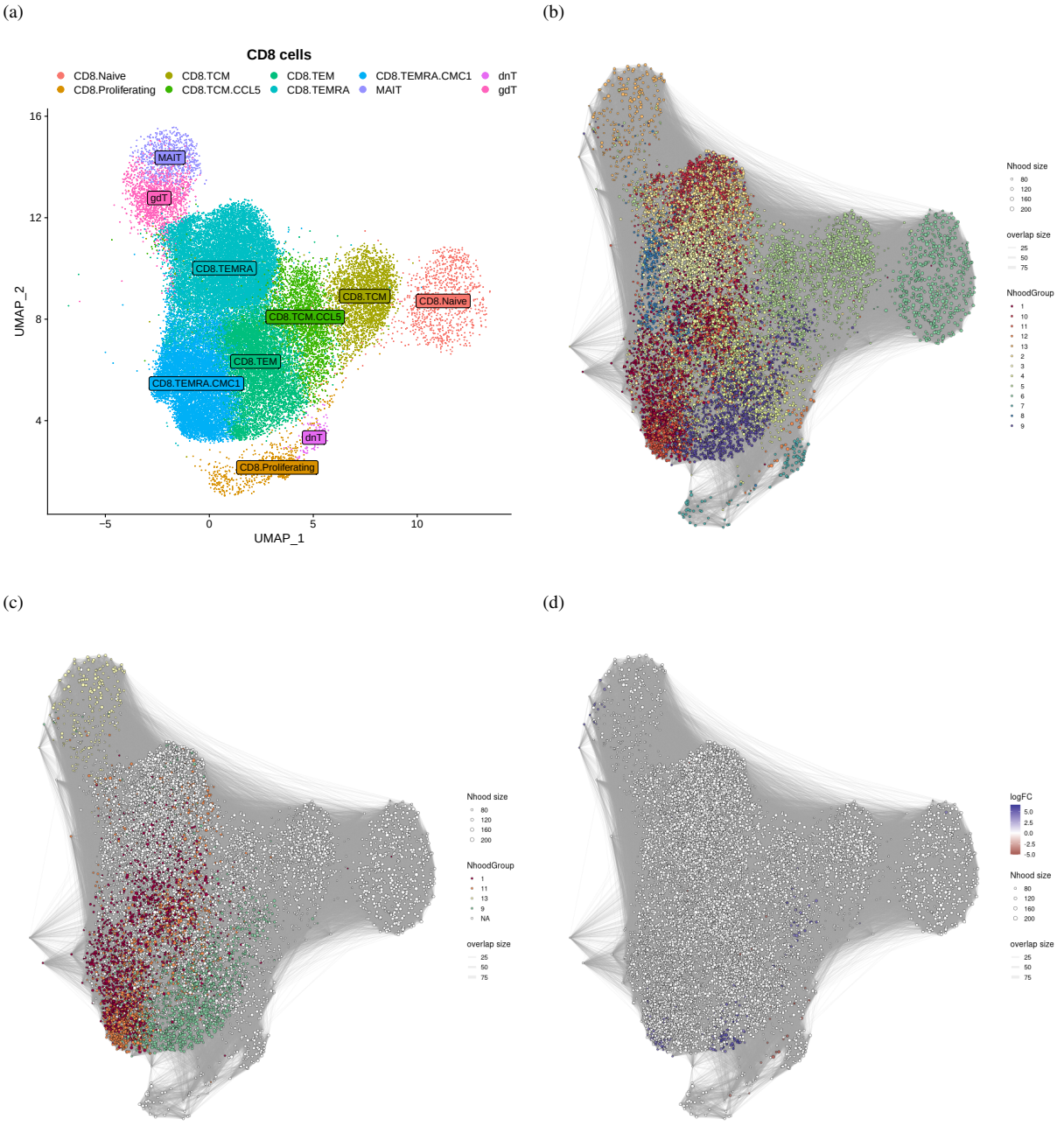


Figure 5.15. (a) UMAP of CD8⁺ T cell subsets for reference. (b) Projection of all neighbourhood groups - as shown in Figure 5.14 - onto UMAP. (c) Projection of neighbourhood groups onto UMAP but just those which significantly increase in abundance from 3-9 weeks post-treatment to post-cessation of ICB are coloured (groups 1, 9, 10 and 11). (d) Projection of neighbourhood groups onto UMAP, but only those neighbourhoods that significantly change in abundance are coloured. As can be seen, a number of significantly upregulated neighbourhoods sit at the seven O'clock position on the UMAP - overlying the tip of the CD8.TEMRA.CMC1 cluster.

I next performed a DEG analysis to understand how cells in neighbourhood groups 9 and 11 (coloured green and orange in Figure 5.15c) - which overly the CD8.TEM and CD8.TEMRA.CMC1 clusters respectively - differ from all other groups. The top 25 genes upregulated in each of these neighbourhood groups are given in Table 5.4. As can be seen, there is an overlap of 10 genes between both groups - including *CCL5*, a tissue trafficking marker, and *NKG7* - Natural Killer cell granule protein 7 which regulates exocytosis of cytotoxic granules[251]. Differentially regulated genes are displayed as volcano plots with their associated Gene ontology biological process (GOBP) in Figure 5.16. Of note, both neighbourhood groups downregulate translational pathways, whilst also upregulating key immune pathways such as "cellular response to IFNγ" and "cellular defense response".

In summary, most cell subsets decrease in abundance from pre-treatment to 3-9 weeks post-ICB. However, in the long term - from 3-9 weeks to post-cessation of ICB - there is an increase in abundance across a number of cell types, most notably T_{effs} and T_{ems}. Agnostic grouping of neighbourhoods which significantly increase in abundance reveals a particular increase in cells with a highly cytotoxic gene expression profile, similar to NK cells.

Gene	LogFC for neighbourhood group 11	Adjusted p value group 11	LogFC for neighbourhood group 9	Adjusted p value group 9
MALAT1	6.28	0.00		
NKG7	4.33	0.00	0.83	0.00
CCL5	3.64	0.00	2.50	0.00
GNLY	2.22	0.00		
CST7	1.97	0.00	1.55	0.00
CMC1	1.22	0.00	0.88	0.00
RPS26	0.93	0.00		
TYROBP	0.84	0.00		
GZMH	0.73	0.00		
GZMB	0.69	0.00		
KLRD1	0.54	0.00		
KLRC2	0.51	0.00		
DUSP2	0.50	0.00	3.47	0.00
TXNIP	0.47	0.00		
CTSW	0.45	0.00	0.46	0.00
CD74	0.44	0.00	2.00	0.00
PRF1	0.37	0.00		
SRGN	0.36	0.00	0.92	0.00
CCL4	0.36	0.00	0.78	0.00
FCGR3A	0.35	0.00		
AOAH	0.32	0.00		
SH2D2A	0.31	0.00		
PIK3R1	0.31	0.00	0.93	0.00
CD8A	0.30	0.00		
KLRG1	0.29	0.00		
JUNB			3.01	0.00
FTH1			2.23	0.00
ZFP36			1.89	0.00
ZFP36L2			1.73	0.00
CXCR4			1.57	0.00
BTG1			1.53	0.00
GZMK			1.52	0.00
TSC22D3			0.97	0.00
JUND			0.89	0.00
KLF2			0.75	0.00
CD69			0.62	0.00
DUSP1			0.59	0.00
ARL4C			0.58	0.00
SARAF			0.54	0.00
DNAJB1			0.52	0.00

Table 5.4. Top 25 upregulated genes in neighbourhood groups 9 and 11, excluding mitochondrial, ribosomal and TCR genes.

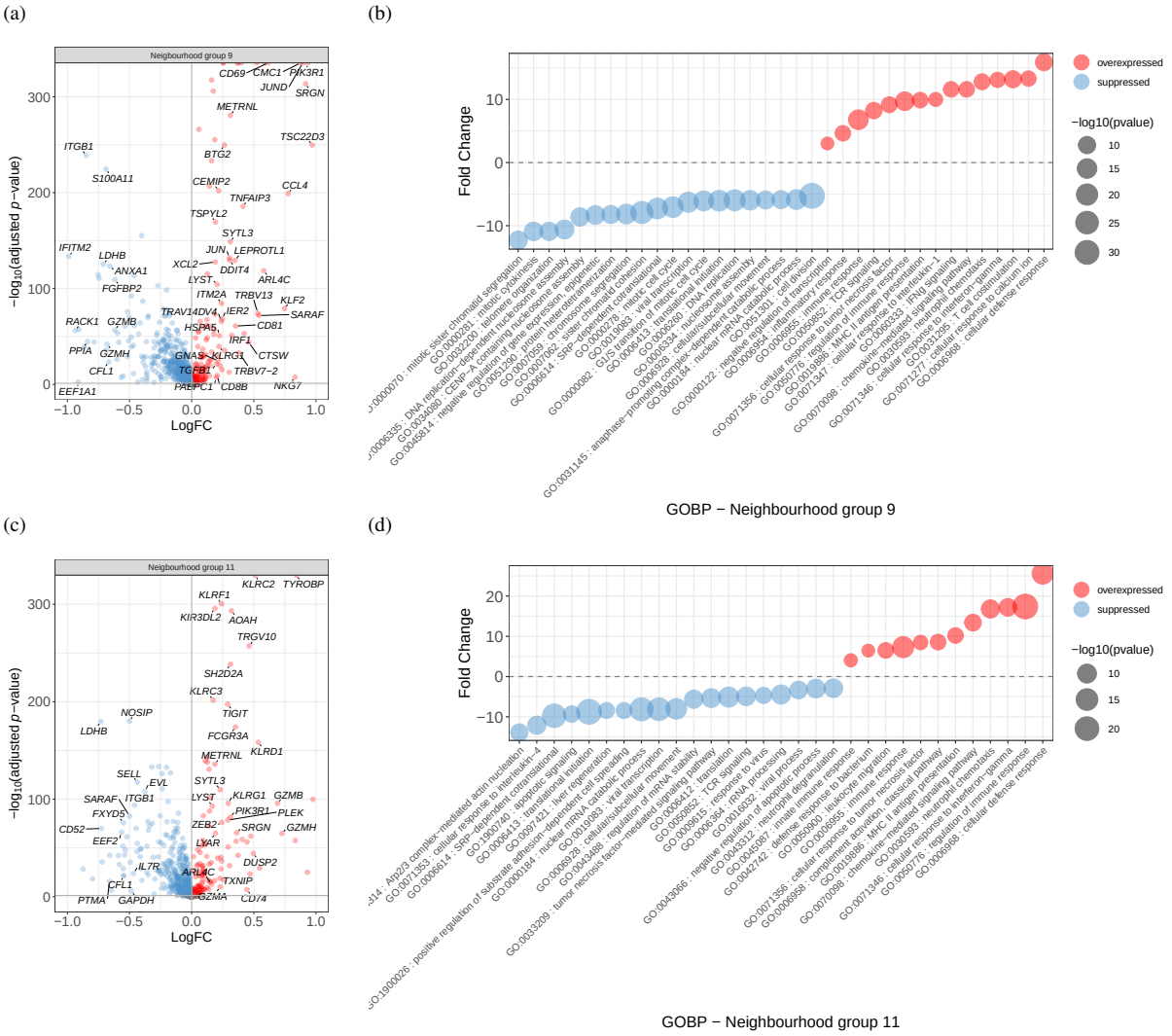


Figure 5.16. (a) Volcano plot of DEGs in neighbourhood group 9 compared to all other neighbourhood groups. (b) GOBP analysis for genes differentially regulated by neighbourhood group 9. (c) and (d), as per (a) and (b) but for neighbourhood group 11. For GOBP analysis, minimum overlap set to >6.

5.3.5 A Killer-like expression profile in CD8+ T cells persists in those with a CR to ICB

Based on the above observations, I was keen to explore to what extent a killer-like expression profile is associated with a CR to sICB in MM. I therefore took the top 25 genes differentially upregulated by neighbourhood 11 - which clusters with the CD8.TEMRA.CMC1 subtype - excluding mitochondrial, ribosomal and TCR genes (Table 5.4). I then utilised the AddModuleScore_UCell function from the *UCell* R package[229] (see methods section 2.2.4.4, page 78), annotating each cell with a 'killer score' based on expression of these 25 genes. I calculated the median killer score per *clone*. Notably, in those with a CR, there is a significant increase in killer score over time for both T_{eff} (i.e. CD8.TEMRA&CD8.TEMRA.CMC1) and T_{em} clones for those with a CR (Figure 5.17).

The primary aim of the current analysis is to examine long term changes to CD8+ T cells in patients with a CR - it was not designed or powered to perform meaningful comparisons between those with good and a poor response to ICB. Those with progression of disease included in this study also mostly (4/6 patients) progressed after eighteen months of treatment, and therefore may not be representative of early progression. Nonetheless, it is notable that in those whose disease did progress, an opposite trend is visible, with either no change (T_{em}) or a decrease in killer score (in T_{eff} subsets) over time. In HDs there is no consistent trend over time (Figure 5.17).

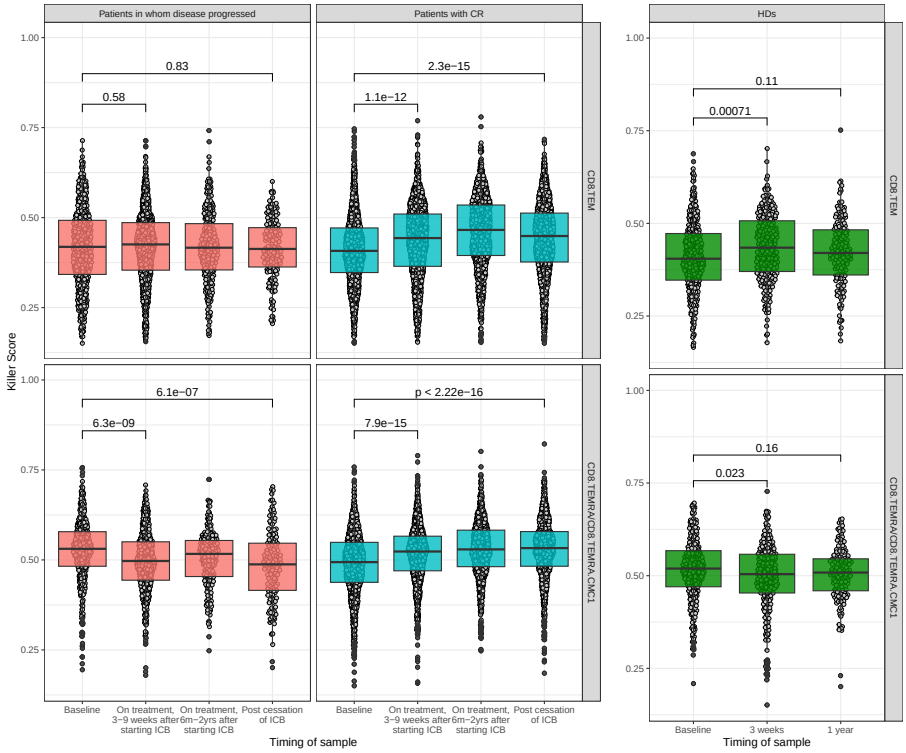


Figure 5.17. Changes to killer score over time faceted by sample type (those who have progression of melanoma (red), those with an ongoing CR to ICB (blue) and healthy donors (HDs - green)) and clonal phenotype. Each dot represents a clone, with the phenotype of the clone determined by the dominant phenotype in all cells present in the clone. The value plotted is the median killer score for that clone. Statistics with Wilcoxon rank sum test. CD8.TEM = T_{em}, CD8.TEMRA/CD8.TEMRA.CMC1 = T_{eff}.

Rather than looking on a *per-clone* basis, it is possible to look on an individual basis. Focussing on just those cells from the CD8.TEMRA/CD8.TEMRA.CMC1 (i.e. T_{eff}) clusters, and taking the median killer score per *sample*, I noted a similar trend, whereby over time there is an increase in killer score in those with a CR - evident with either time as a continuous variable or as time point categories (Figures 5.18a and 5.18b).

Finally, to compare patients with a CR to those with PD (all patients only treated with sICB), I downsampled the same number of cells from each outcome group, and calculated the median killer score per clone and the median of these scores per group, bootstrapping this 100 times. This demonstrated that, at baseline, those with CR had a lower killer score whilst at post-treatment time points, the killer score was higher (Figure 5.19). This could potentially reflect differences in

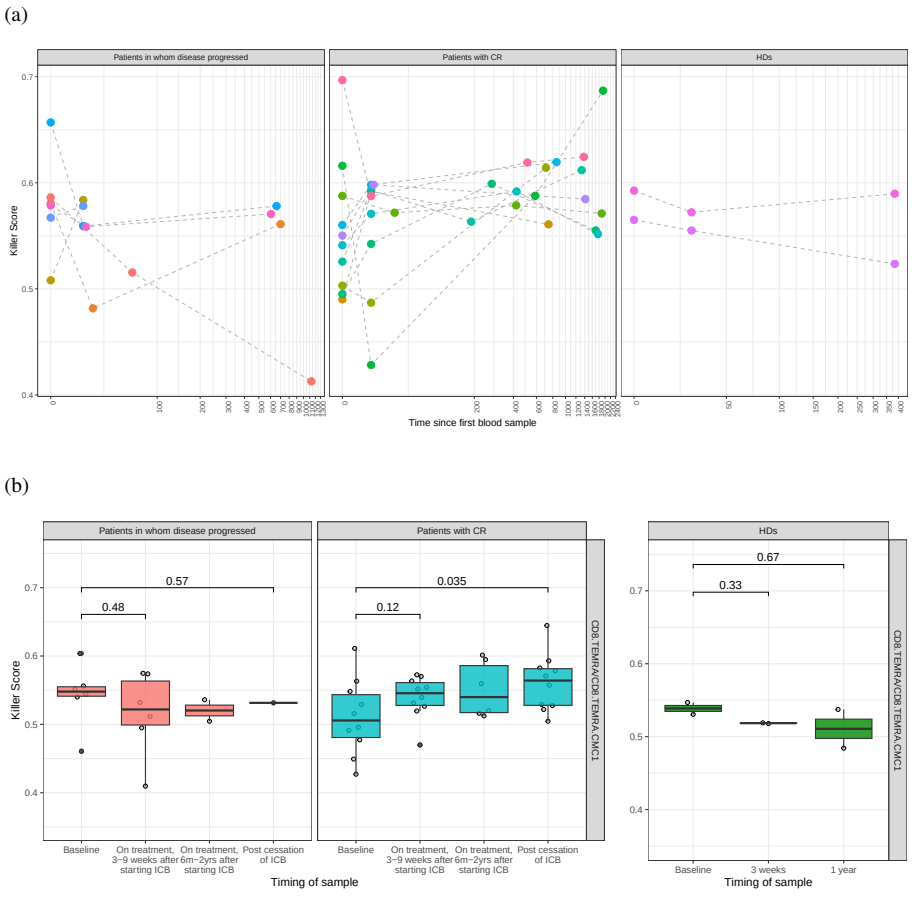


Figure 5.18. (a) Changes to killer score over time, faceted by sample type. Each dot represents a sample, with the value plotted the median score per sample, restricted only to T_{effs} (labelled as 'CD8.TEMRA/CD8.TEMRA.CMC1'). (b) as per (a) but rather than time as a continuous variable, it is categorised into time points.

tumour burden pre-treatment, with a differential response post-ICB, although I do not have data to corroborate this.

In order to validate these findings from scRNAseq, I decided to examine the wider cohort using bulk RNAseq data. Taking 90 patients treated with sICB for MM, I calculated the geometric mean of the normalised expression of the top 25 genes associated with neighbourhood group 11 ('killer genes', Table 5.4 and methods section 2.3.4.1) within magnetically sorted peripheral CD8⁺ T cells. In this bulk RNAseq data, there was no association with outcome (Figure 5.20a). However, importantly, I noted that in those without progressive disease, there was a significant increase in killer score expression as time passed, with those samples taken after the cessation of

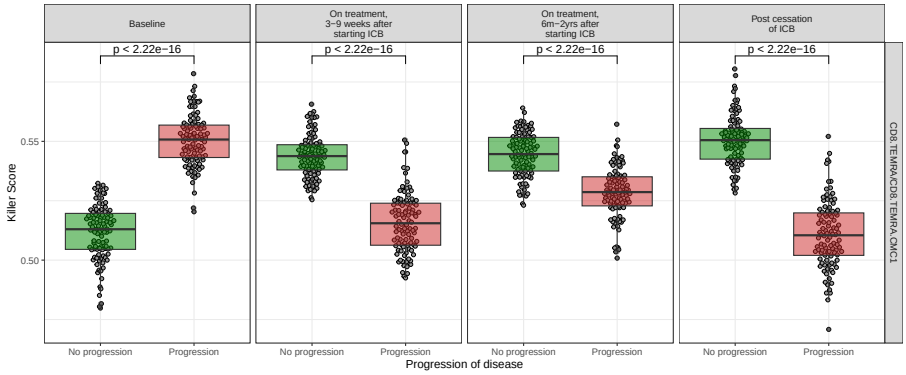


Figure 5.19. Killer score between those with progressive disease and those with CR faceted by timing of sample. Only T_{effs} were included (labelled as 'CD8.TEMRA/CD8.TEMRA.CMC1'). The number of cells in each outcome group was downsampled to a constant size (150) and the median killer score per clone calculated. This was repeated 100 times and each dot represents the median killer score of all clones in each outcome group. Statistics with Wilcoxon rank sum test.

ICB having significantly higher killer score than those at earlier time points (Figure 5.20b). This corroborates my previous findings in the scRNAseq data of this signature occurring with long term response.

(a) (b)

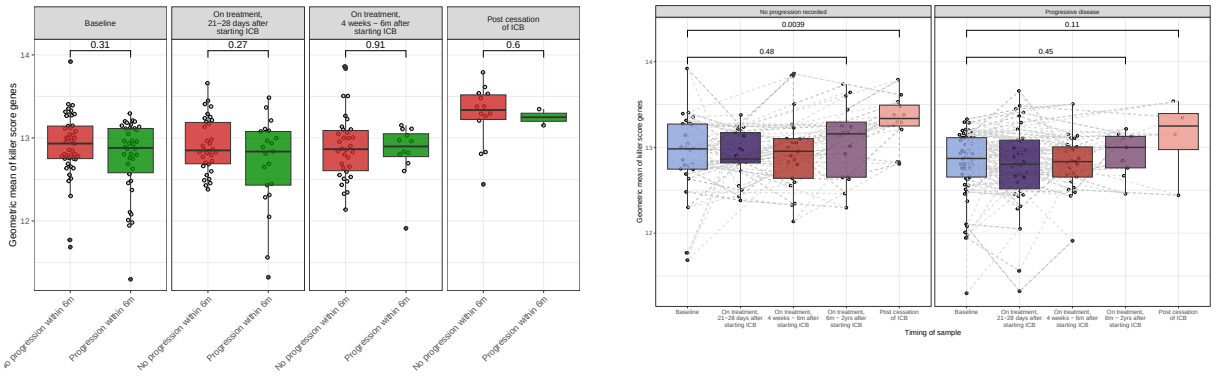


Figure 5.20. (a) Killer score from bulk RNAseq calculated using the geometric mean of normalised expression of top 25 genes differentially upregulated by neighbourhood group 11 (Table 5.4) from 90 patients treated with sICB for MM, faceted by time point and coloured by response. (b) Killer score as per (a) but over time across all samples, with significant increases seen at later time points but only in patients without progressive disease. Statistics with two-sided Wilcoxon rank sum test.

5.3.6 Killer score subsection summary

To summarise the above results, by performing an agnostic abundance analysis I identified the increase in abundance of a group of cells which highly express a number of 'killer-like' genes,

commonly found in NK cells. By applying scores of these gene sets across both scRNAseq and bulk RNAseq datasets, I could corroborate that a feature of long term complete response to ICB is increased expression of these killer-like genes within the effector T cell compartment.

5.3.7 Clonal dynamics following a complete response to ICB

5.3.7.1 Changes to clonal size over time

I next wanted to examine the clonal dynamics following a CR to ICB in order to build on previous observations of long term clonal stability as described in Chapter 4, section 4.3.7 (page 132). I first plotted the size of each clone by time point, colouring clones by whether that clone is found at all sampled time points (Figure 5.21). The extent of clonal stability is extremely high. In a number of patients with a CR, there is persistence of the same hyper-expanded clone for many years post-complete response and cessation of ICB. For example for patients 70, 80 and 155, the largest clone at baseline - often occupying >10% of the peripheral repertoire - remains the largest clone, of a similar size, up to five years after starting ICB and long after the cessation of treatment (Figure 5.21). Interestingly, a similar pattern is seen in those who had PD, however all four patients with PD progressed at least eighteen months after starting ICB and so may not be representative of those with early progression. Finally, it is notable that whilst individual 27 had very few cells recovered at baseline (see methods section 2.2.2, page 73) two of the clones detected are resampled at all time points and remain hyper-expanded.

I was interested to understand in particular those hyper-expanded clones at baseline that persist long term in those with a CR. I opted to focus on the ten individuals treated with sICB to remove any confounding effects of treatment. I selected clones that 1. were present at every time point in patients with a CR to sICB and 2. occupied >5% of the peripheral repertoire at every time point sampled. There were eight clones from seven patients fitting these criteria. I examined the

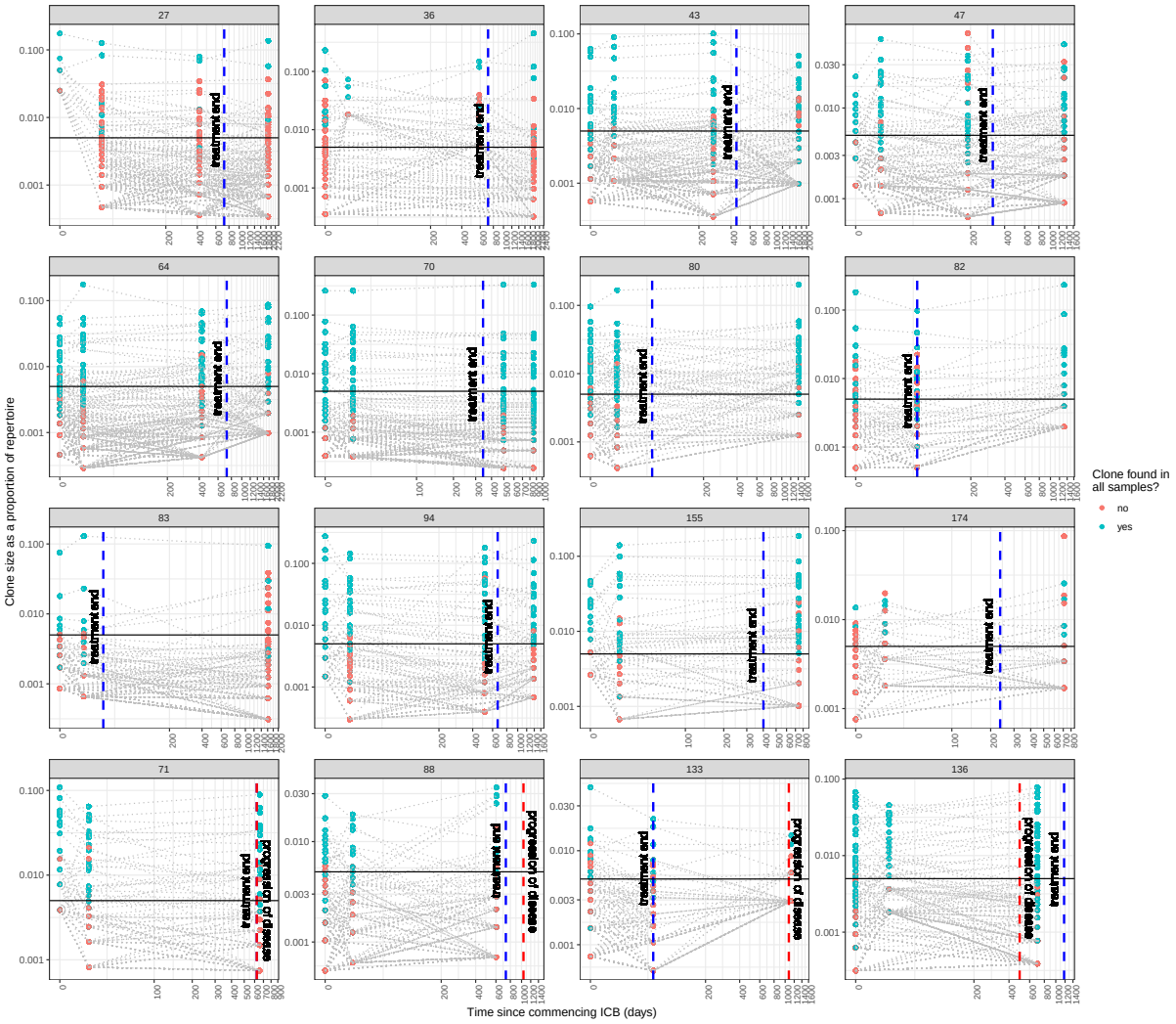


Figure 5.21. Proportion of the repertoire occupied by each clone over time, faceted by individual. Each point represents a clone, coloured by whether or not that clone is found in all samples for that individual. The top three rows of patients all had a complete response to treatment, the bottom row all had late progressive disease. The horizontal black line represents a size of 0.5% - considered a large clone. The vertical blue and red lines represent the time of treatment ending or disease progressing, respectively. Note that the x-axis is pseudo-log scale.

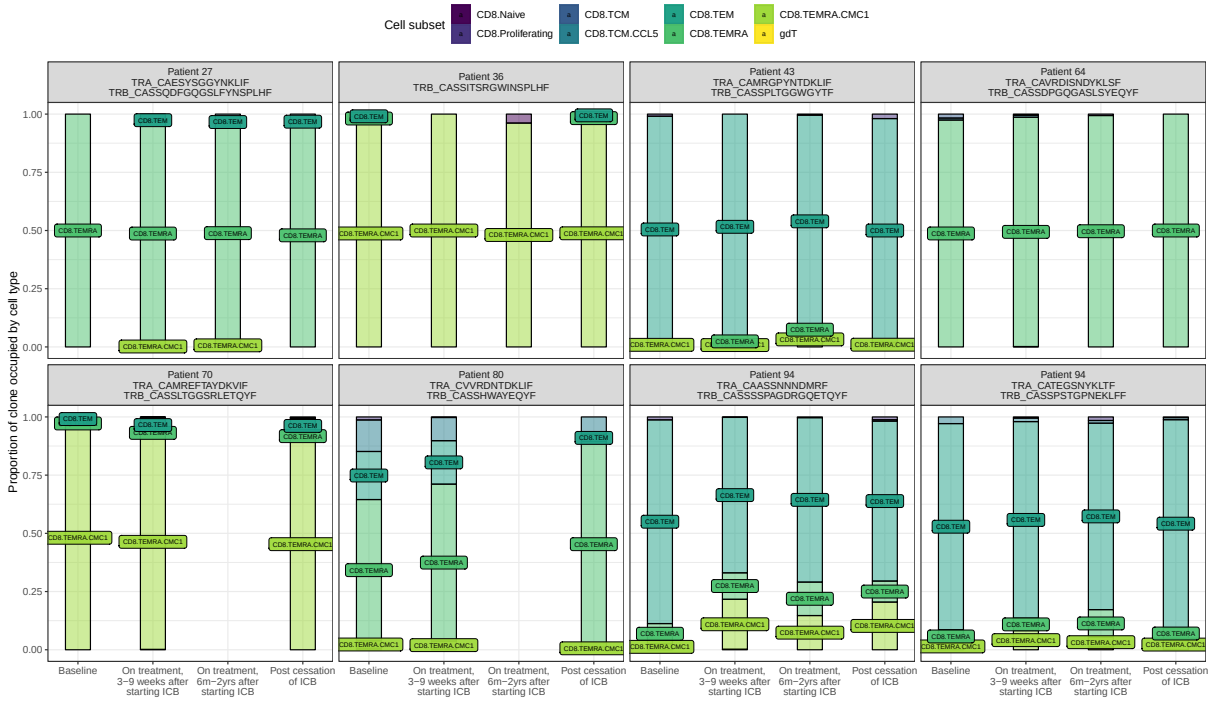


Figure 5.22. Phenotypes of hyper-expanded clones over time. Clones that were 1. were present at every time point in patients with a CR to sICB and 2. occupied >5% of the peripheral repertoire at every time point were chosen. Displayed is the proportion of each clone occupied by cells of each cluster by time point and faceted by clone.

cellular make-up of each clone - five had a majority phenotype of T_{eff} (labelled as 'CD8.TEMRA' or 'CD8.TEMRA.CMC1'), whilst the other three had a majority T_{em} (CD8.TEM). Notably, the cellular make-up of each clone was relatively stable over time (Figure 5.22).

Due to the high representation of T_{eff} and T_{em} cells in these hyper-expanded clones (Figure 5.22), and their proximity to neighbourhood group 11 on the UMAP (Figure 5.15), I wondered if some of these cells had a killer-like phenotype (as described above - see section 5.3.5, page 172). I therefore sought to annotate a 'killer-like' cluster. Plotting the distribution of killer scores across all cells revealed a bimodal distribution (Figure 5.23a). A cut-off of 0.64 was chosen to lie to the right of this second peak and aligned with the 85th centile (marked on Figure 5.23a with a red vertical line). As such, any cell with a killer score > 0.64 was assigned to this cluster - termed 'killer-like'. These cells primarily cluster together where neighbourhood group 11 was found at the bottom of the T_{eff} and T_{em} subsets (Figure 5.23b).

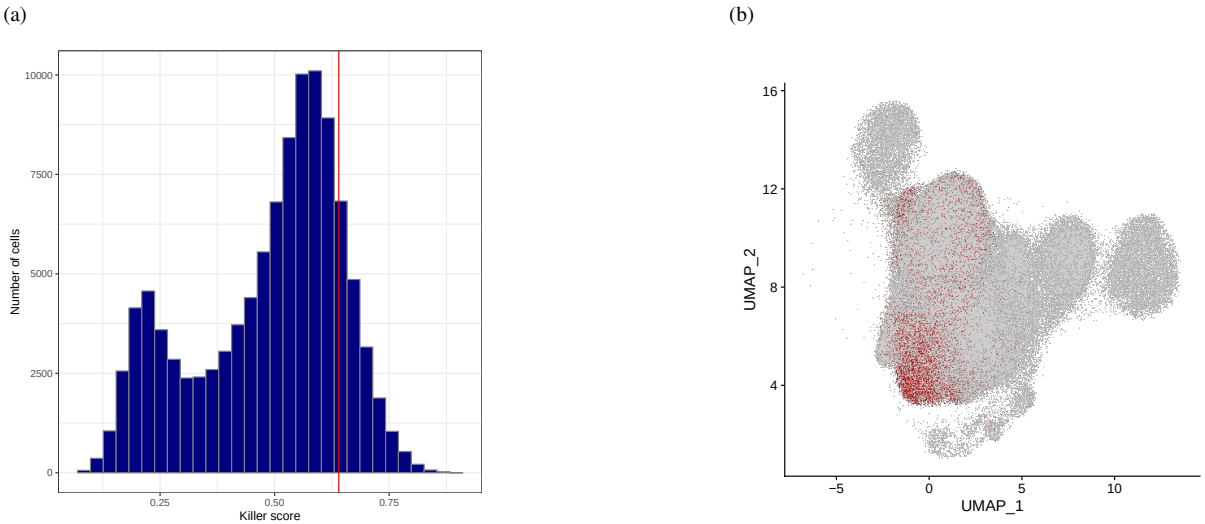


Figure 5.23. (a) Distribution of killer score (calculated as described in section 5.3.5) across all cells. The red line represents the cut-off for the killer-cluster of 0.64, at the 85th centile. (b) UMAP with cells with a high killer score (>0.64) coloured in red.

Repeating the above clonal phenotyping for eight hyper-expanded clones reveals that a large proportion of the CD8.TEM cells are indeed from the killer-like cluster (Figure 5.24).

5.3.7.2 Defining large expanding persistent (LEP) clones

As displayed in Figure 5.21, there is clonal stability over time, with multiple hyper-expanded clones present at all time points in multiple samples. Indeed, across all samples, a very large proportion of the repertoire at the post cessation of ICB time point comprises clones that are found in every sample (Figure 5.25a).

I was keen to identify those clones which may be most important in mediating the response to ICB, and therefore applied criteria found to associate with key clones in my previous work. As such, I filtered for those which are stable/expanding from pre- to post-treatment (i.e. d0 to 3-9 weeks) using the same methodology as described for Chapter 3 and ref [78] (methods section 2.2.4.1). As described, these clones had a higher cytotoxicity score at the post-treatment point. Further, I filtered clones occupying >0.5% of the peripheral repertoire (large clones) at the first post-treatment time point (also shown to correlate with response - ref [93], Figure 4.4a).

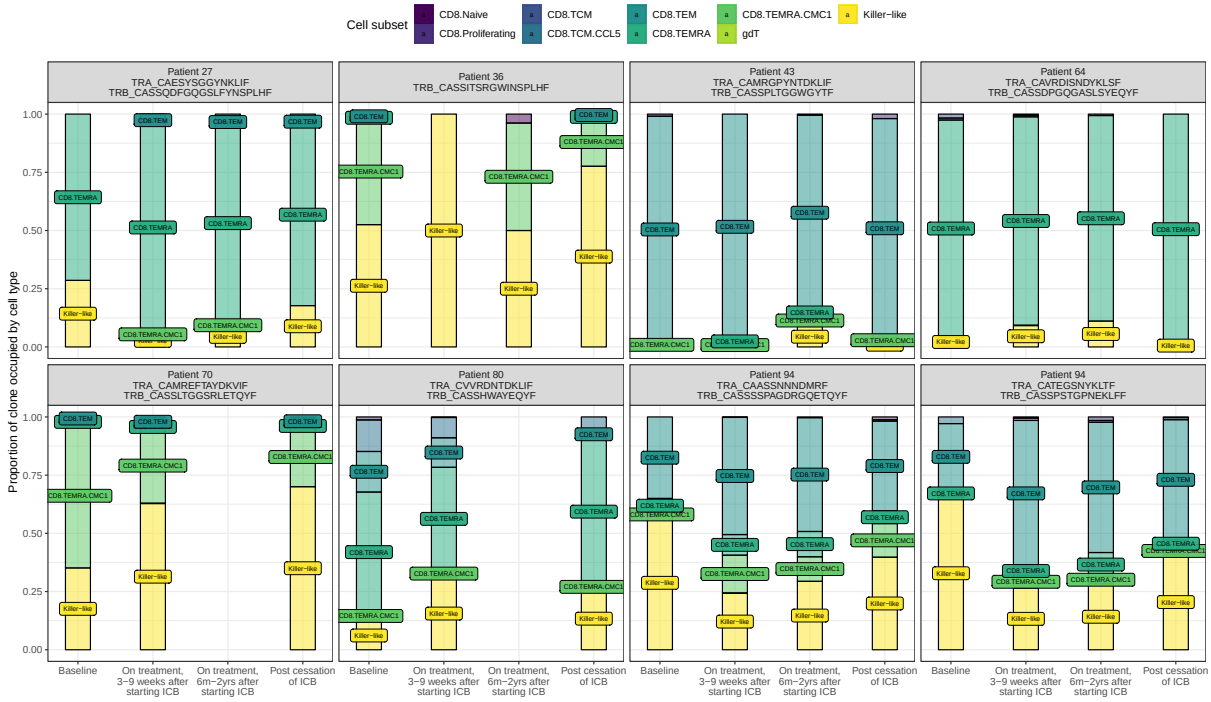


Figure 5.24. Data is the same as per Figure 5.22, but including the killer-like cluster.

Finally, I looked for those clones which persisted to the post-treatment time point. I termed these clones large, expanding, persistent (LEP) clones. Across the 10 patients with CR, there were 192 LEP clones, with a median of 22 per individual (Table 5.5). Despite the relatively low numbers of clones per individual, these still represent a significant proportion of the repertoire at the post-cessation of ICB time point (Figure 5.25b).

Patient	Number of clones
155	23
174	12
27	22
36	4
43	18
47	23
64	23
70	13
80	28
94	26

Table 5.5. Number of LEP clones per individual with CR.

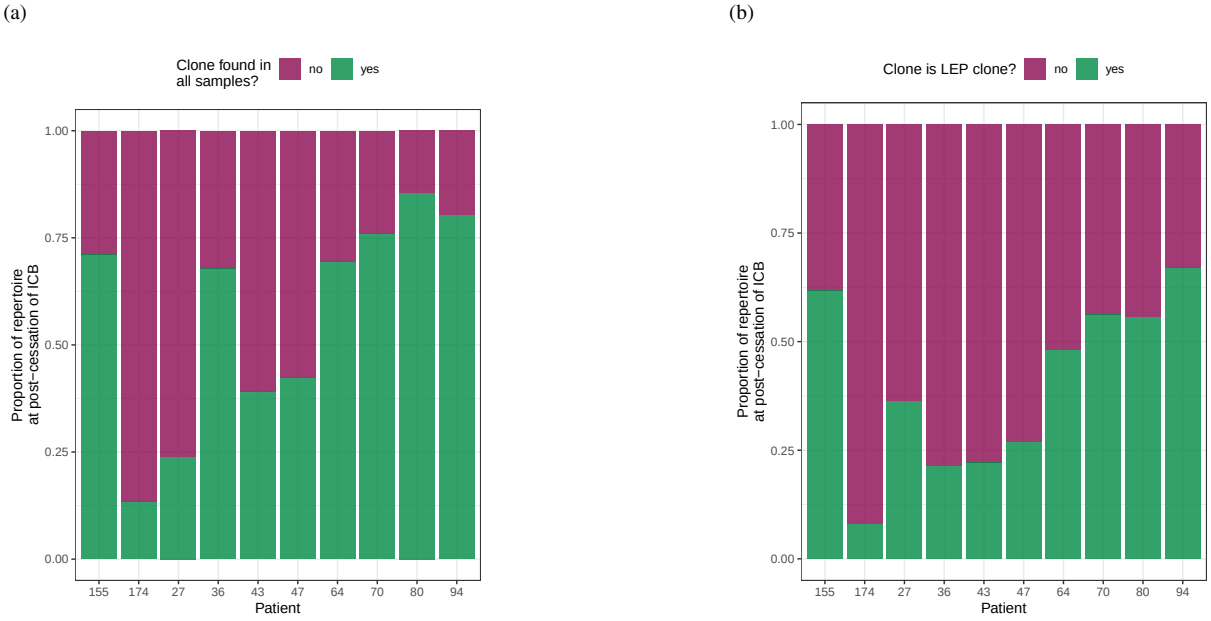


Figure 5.25. Proportion of the repertoire occupied by persistent clones. (a) Proportion of the repertoire post-cessation of ICB occupied by clones that are present in all samples (green) per patient with a CR. (b) as for (a) but for large expanding persistent clones (LEP clones).

5.3.7.3 Changes to clonal phenotype over time

To further understand how clones change phenotype over time, I plotted an alluvial plot showing the subset flow (including the killer-like subset) of all clones (Figure 5.26a), restricting the analysis to just patients with CR to sICB (n=10). Here, clones are given a phenotype based on their majority cell type. As can be seen, when looking at all clones, there is the expected mixture of all cellular subtypes. Notably, there is no clonal persistence in the naive ('CD8.NAIVE') subset, with minimal persistence in the T_{cm} ('CD8.TCM' and 'CD8.TCM.CCL5') subsets. Most of the persistent clones are either T_{em} ('TEM') or T_{eff} ('CD8.TEMRA', 'CD8.TEMRA.CMC1' and 'killer-like') in phenotype (Figure 5.26a).

I next looked at just those clones present at all time points. When compared to all clones, these clones have more of a T_{em}/T_{eff} phenotype, as expected, with about 50% of clones at all time points from a memory subset (T_{cm} or T_{em}), and the remaining half from a T_{eff} subset (Figure 5.26b). There is a reasonable degree of clonal flux, with clones changing their overall phenotype

from one time point to the next. Generally from baseline to the first time point post-ICB this tends to be memory clones becoming more effector; at later time points there is more flux from effector back to memory (Figure 5.26b).

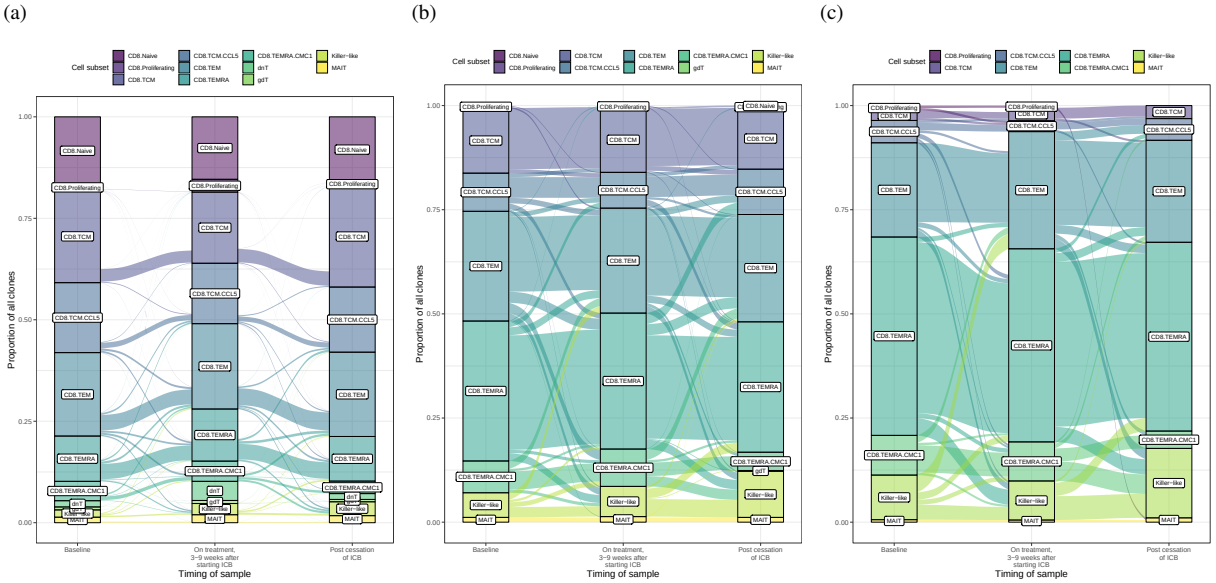


Figure 5.26. Alluvial plots of long term persistent clones in just patients with a CR to sICB (n=10). (a) Flow of subset proportions over time for all clones. (b) As per (a) but only for clones which are found at all time points. (c) as per (a) but only for large expanding persistent clones (LEP clones).

I filtered just those LEP clones and repeated the analysis. This resulted in an overall increase in clones from T_{eff} subtypes, suggesting that, consistent with previous observations, clones defined as LEP clones are more cytotoxic than other clones. Whilst most clones retain their phenotypes over time, qualitatively there is again flux towards increased effector function from baseline to the first time point post ICB with T_{em} becoming T_{eff} (i.e. 'CD8.TEMRA', 'CD8.TEMRA.CMC1' and 'killer-like') and an increase in the number of T_{eff} subsets that gain a killer-like phenotype (Figure 5.26c). Subsequently, there is more of a flux back to memory phenotypes, although notably the proportion of clones that are killer-like increases over time, consistent with above observations (see section 5.3.4, page 166).

Finally, I examined the phenotypic make-up of LEP clones at the post-cessation of ICB time point across individuals. Whilst there was a relative degree of heterogeneity across individuals, consis-

tently these clones were made up of cells from T_{eff} clusters ('CD8.TEMRA', 'CD8.TEMRA.CMC1' or 'killer-like') (Figure 5.27a). This was in stark comparison to those clones that were *only* found at the post-cessation time point - i.e. novel clones following the end of treatment (Figure 5.27b). These novel clones were dominated by cells from naive and memory clusters.

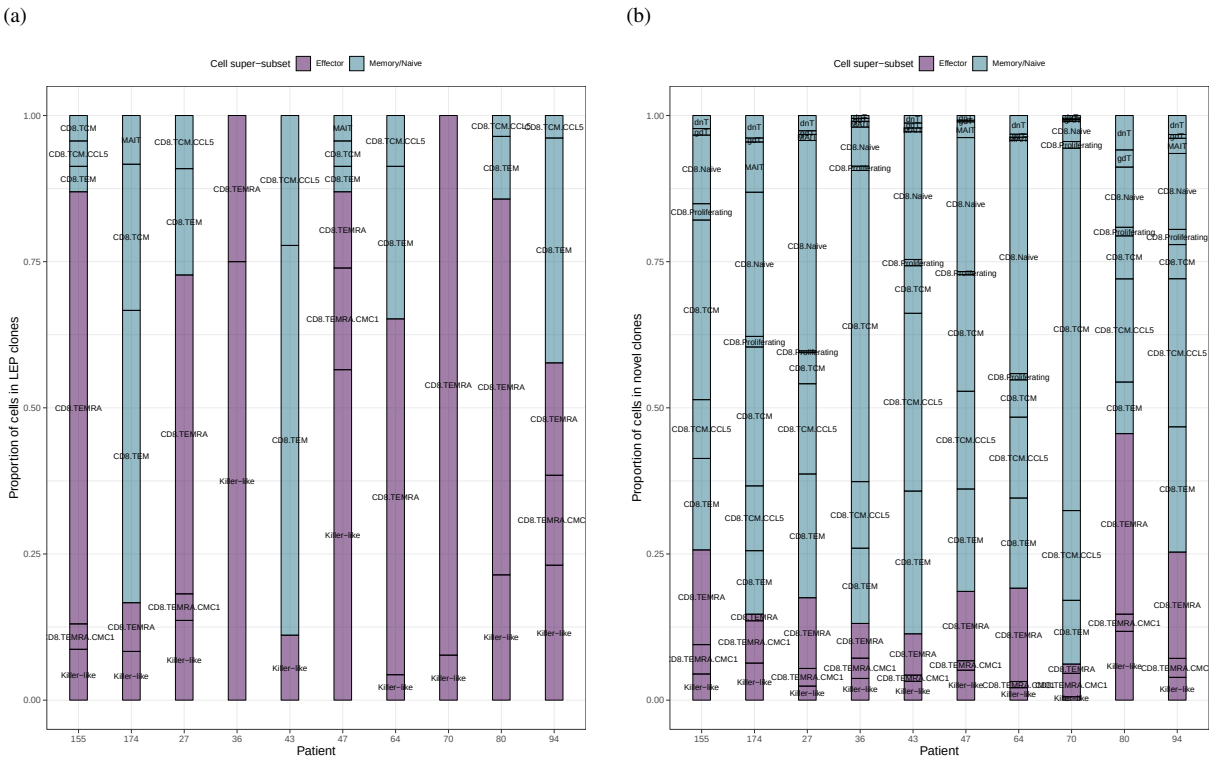


Figure 5.27. Cellular make up of post-treatment clones in patients with a CR to sICB (n=10). (a) Make up of large expanding persistent clones at the post-cessation of ICB time point in those patients with a CR. The y-axis represents the proportion of all LEP clones for that individual, coloured by their cellular makeup - either naive/memory (blue) or effector (purple). Labels are the cluster name. (b) as for (a) but for *novel* clones post cessation of ICB - i.e. clones not found in any prior samples.

5.3.7.4 Comparison with healthy donor samples

For comparison, I examined the long term changes that occurred in two healthy donor samples. Interestingly, in these samples there was also observable long term clonal stability (Figure 5.28a), and the proportion of the repertoire that was occupied one year after the first sample by clones which were stable/expanding and large between first sample and 3 weeks later was also comparable to that observed in patients (Figure 5.28b). Finally, the phenotypic make-up of LEP

clones from HDs was similar to that from patients, with a predominance in cells from effector subsets, although subjectively there was less phenotypic flux of clones (this is not possible to quantitatively compare) and no overall increase in killer-like clones with time (Figure 5.28c).

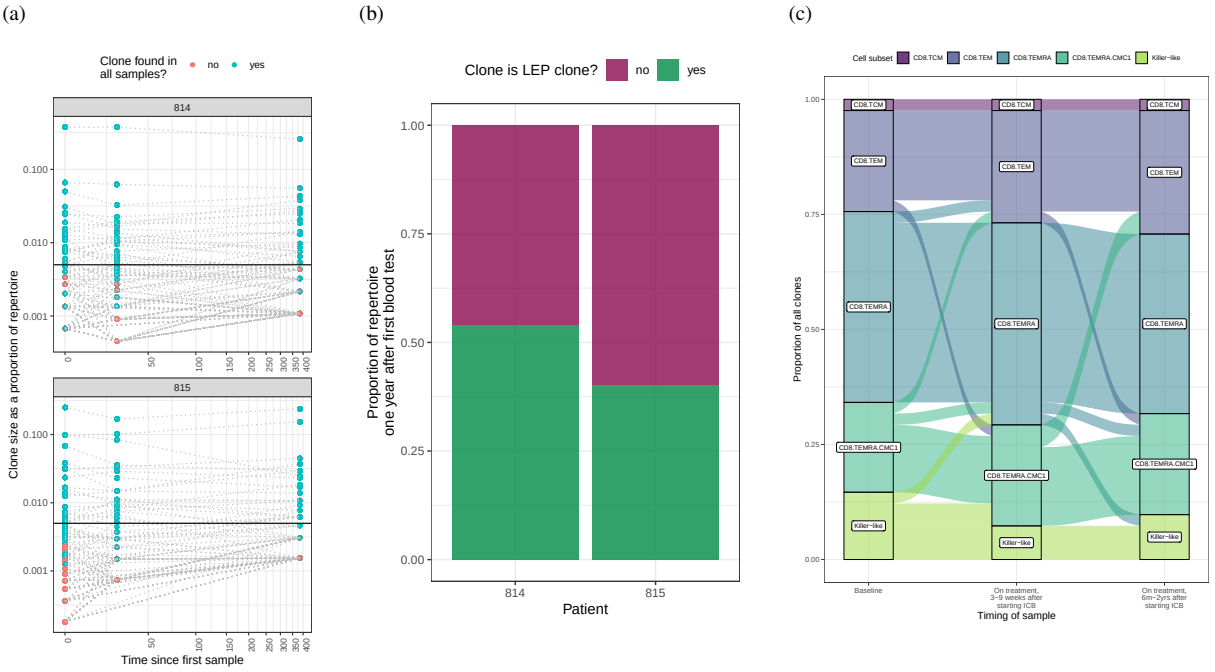


Figure 5.28. (a) Clonal stability over time for HD samples (n=2) - each dot represents a clone with the y-axis showing the proportion of the repertoire occupied by that clone and the dots coloured by whether or not the clone is found at each sampled time point. (b) Proportion of the repertoire at one year occupied by LEP clones for the two HDs. (c) Alluvial plots of phenotypic change over time for LEP clones in HD samples.

5.3.8 Clonal dynamics subsection summary

In summary, there is remarkable clonal stability with large, expanded clones detectable early in treatment with ICB remaining in the peripheral blood long term - including many years after cessation of ICB. Clones that persist long term have a predominance of effector phenotypes and, whilst there is some flux over the course of treatment and with time, on the whole retain their phenotype in the long term. The extent to which these changes are influenced by ICB is unclear, as a similar pattern can be observed in longitudinal samples from HDs, albeit in fewer numbers and without statistical power to make confident comparisons. I hypothesise that LEP clones -

being expanded and large - are likely reacting to cancer antigens and the presence of similar expanded, cytotoxic, clones in HD samples may be due to phenocopying of anti-viral clones found in the absence of malignancy.

5.3.9 Transcriptomic description of large expanding persistent clones

5.3.9.1 Differentially expressed genes of large expanding persistent clones

Whilst the gross phenotypic changes in HDs appeared comparable to that seen in patients with a CR, I wished to understand any differences at the expression level. I therefore performed a differentially expressed gene (DEG) analysis on large expanding persistent clones (LEP clones) from patients with a CR to sICB versus LEP clones from HDs (Figure 5.29). Notably, those clones from CRs upregulated a greater number of immunologically relevant genes and pathways - including IFNγ signalling, T cell co-stimulation, T cell activation and TCR signalling (Figure 5.29b).

5.3.9.2 Expression scores of large expanding persistent clones

In order to explore expression profiles of large expanding persistent clones (LEP clones), I applied a range of different expression scores using gene sets previously defined in the literature[70,77,78,92,98] - included as supplementary table A.1. Again, I gave each single cell an expression score using *AddModuleScore_UCell* (as described above in methods section 2.2.4.4, page 78) and then calculated the median score per *clone* at each sampled time point for each individual. As can be seen, LEP clones demonstrate substantial and significant increases in tumour-specific score[70], cytotoxicity - as defined by us[78], dual-expansion (i.e. clones found both in tumour and peripheral blood)[92] and cytotoxicity as defined by others[98]. Increases are most marked from day 0 to 3-9 weeks post-treatment but notably, for all scores, post-cessation of ICB expression remains above

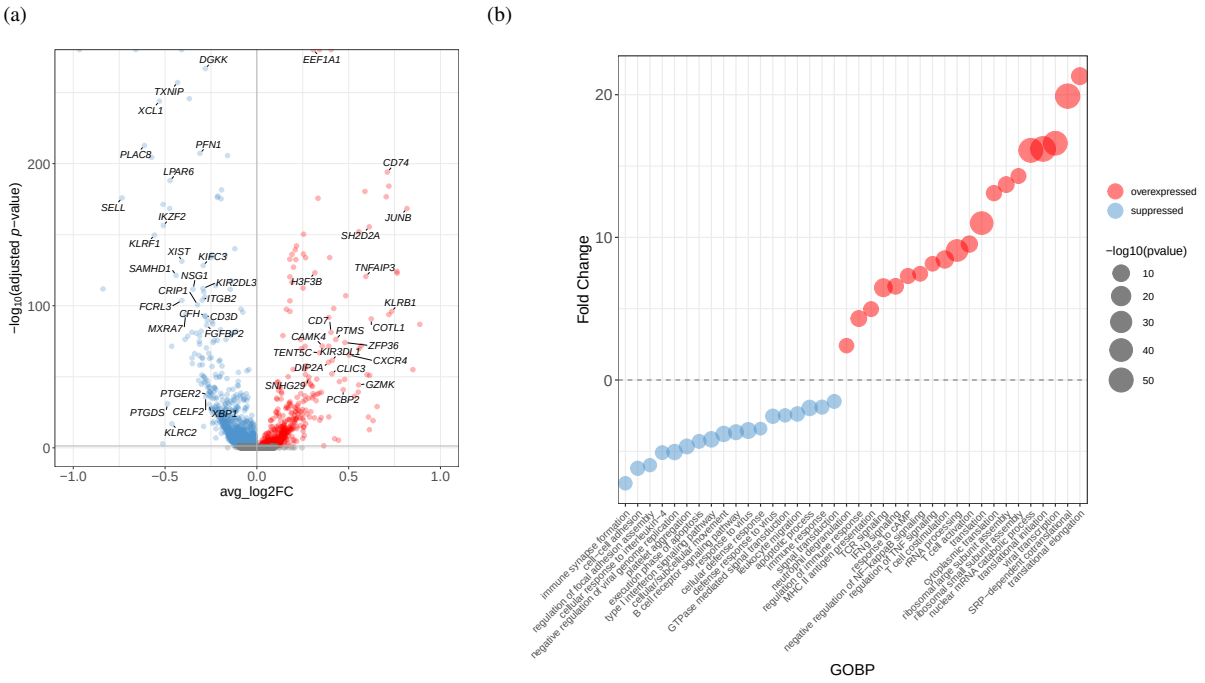


Figure 5.29. (a) Volcano plot of DEGs for LEP clones from patients with CR versus HDs. (b) GOBP analysis of the DEGs. Red dots represent genes (a) and pathways (b) significantly differentially upregulated in cells from LEP clones in patients with CR, whilst blue dots are those genes/pathways downregulated, when compared to cells from LEP clones in two HDs. For (b), minimum overlap set to >3.

that of baseline. There are minimal and borderline significant changes to peripheral proliferation genes - as defined by the seminal paper by Huang *et al.*[77] - and there is only a modest increase in exhaustion as defined by Lucca *et al*[98] (Figure 5.30). Of note, there are no trends seen in healthy donor samples, suggesting that the increases demonstrated are the result of ICB treatment (Figure 5.30).

Comparing expression in LEP clones versus all other clones demonstrates that these clones - i.e. clones which persist long term in the peripheral blood having expanded from pre- to post-treatment - have significantly higher expression of tumour-specific, cytotoxic and dual expanded genes when compared to all other clones (Figure 5.31). They also have significantly higher expression of exhaustion and peripheral proliferating gene sets, although the magnitude of difference is less for these scores. These differences were significant and of a similar magnitude at all sampled time points, but only data for the post-cessation of ICB time point is included in Figure 5.31 for

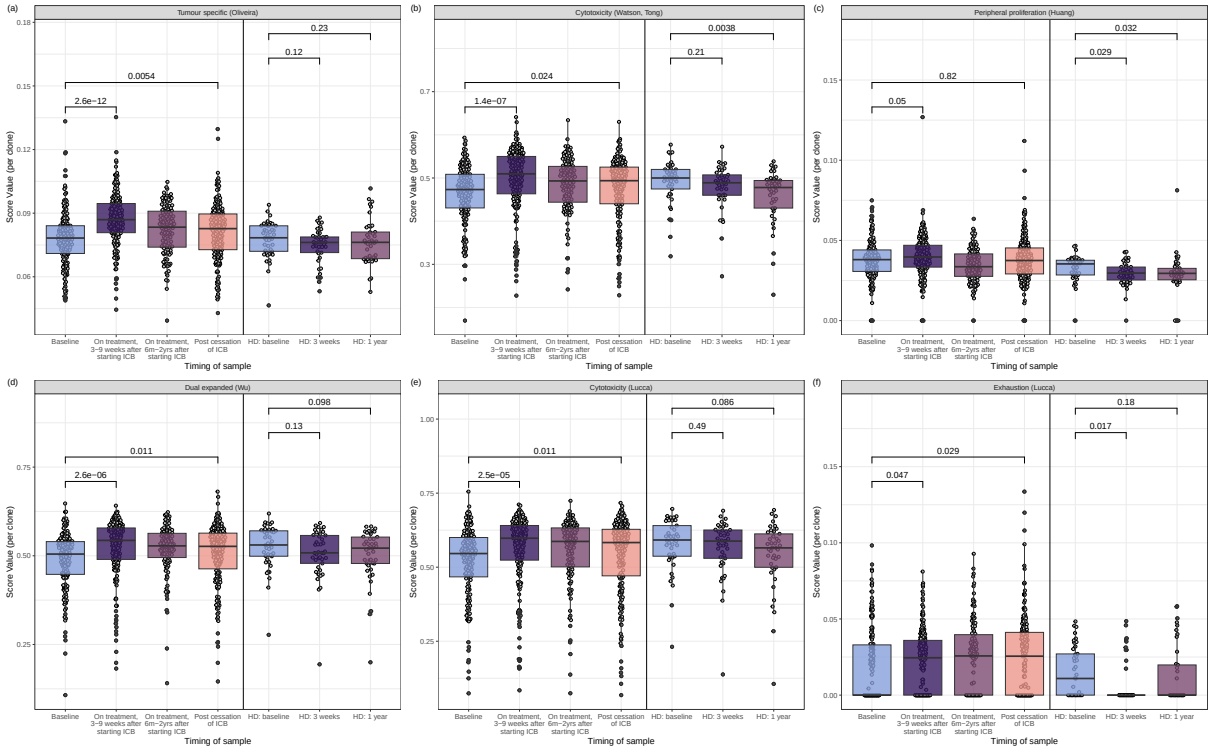


Figure 5.30. (a-f) Expression scores over time for LEP clones in patients with CR (left hand side of plot) and HDs (right hand side of plot). Each dot represents a clone, with the median score per clone plotted. Scores are as per facet labels. Scores are based on gene sets as tabulated in Supplementary Table A.1. References - Oliveira [70]; Watson, Tong [78]; Huang [77], Wu [92], Lucca [98]. Statistics with Wilcoxon rank sum test. Note that the y-axis is not fixed.

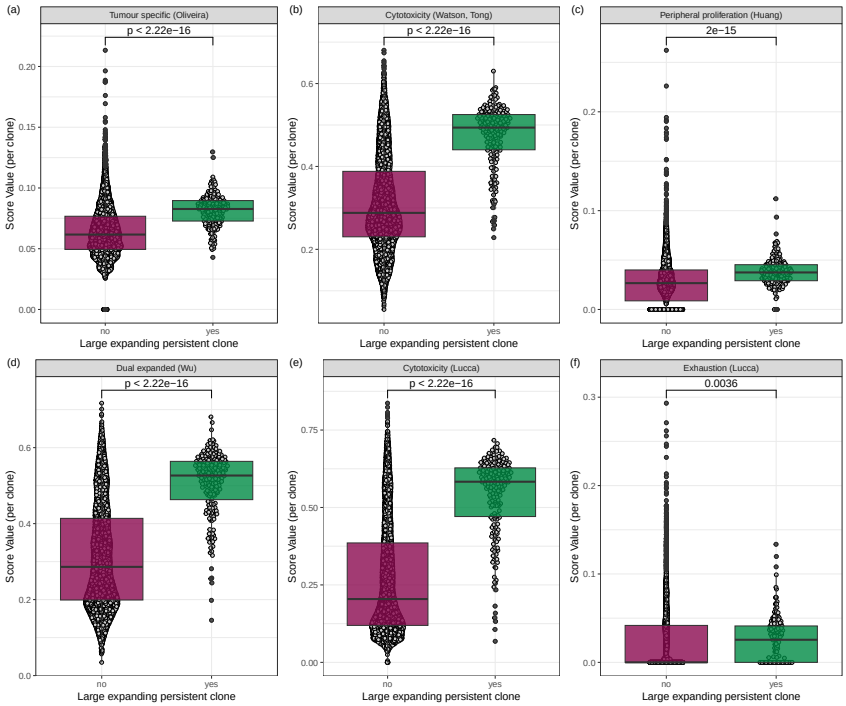


Figure 5.31. (a-f) Expression scores for LEP clones vs all other clones in patients with CR at the post-cessation of ICB time-point. Each dot represents a clone, with the median score per clone plotted. Scores are as per facet labels and are as described in Figure 5.30. Statistics with Wilcoxon rank sum test.

conciseness.

In addition to these scores, I looked at expression of a gene set associated with 'tumour reactivity' as outlined in a recent review led by Ton Schumacher[67] (discussed in introduction section 1.2.3, page 18; gene set in Table A.1). This phenotype has been described to be associated with TILs that are reactive to the tumour (as opposed to bystander cells). Looking at the distribution of cells that have a positive score for this gene set, I note that the majority score 0, possibly reflective of the fact that this gene set was defined on TILs (Figure 5.32a). I therefore defined each cell as 'tumour reactive' if the score was >0 and looked at how the proportion of positive cells changed over time. Notably, patients with a CR to sICB have an increase in the proportion of tumour reactive cells post-treatment (Figure 5.32b). Due to the low sample size, it is hard to draw firm comparisons with PD but it does appear that those samples from patients whose disease subsequently progresses have a higher proportion of tumour reactive cells at baseline (p=0.033,

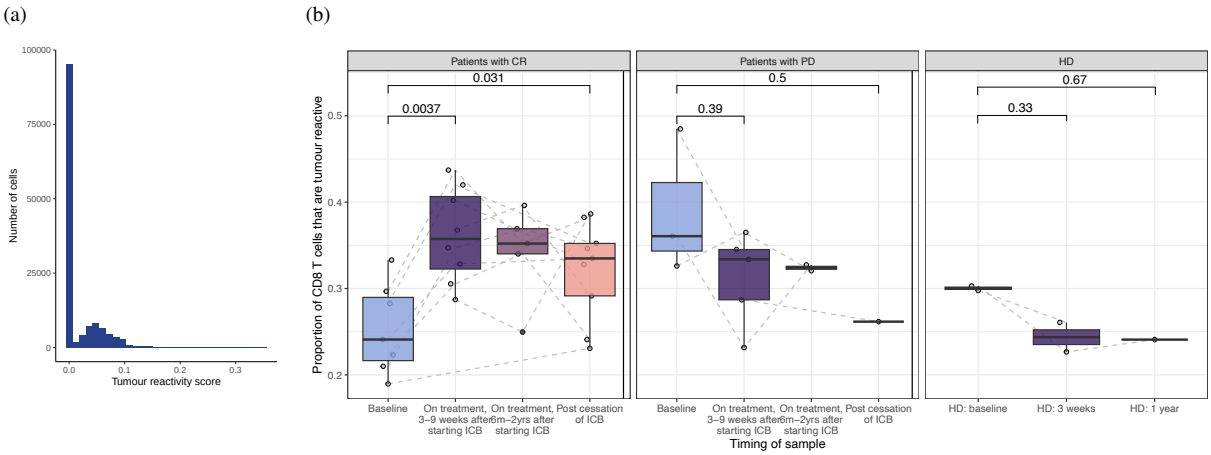


Figure 5.32. (a) Distribution of tumour reactivity score as defined by a gene set from [67] (see Table A.1). (b) Proportion of all CD8⁺ T cells with a tumour reactivity score >0 coloured by time point and faceted by outcome. Only samples with >1000 cells were included. Statistics with Wilcoxon rank sum test due to different sample numbers per time point.

not plotted) but do not have an increase in tumour reactivity with ICB. There is no relationship over time in HDs (Figure 5.32b).

Finally, I looked at expression of key genes which have been shown to be associated with long-lived effector cells (LLECs). These cells were first described in 2020 by Renkema *et al.*[248], and are discussed in more detail in the discussion below (section 5.4, page 191). However, in short, this cell type has features of both effector and memory function - retaining longevity along with cytotoxicity and rapid functionality. This cell type is KLRG1⁺, CX3CR1⁺, T-bet⁺ (encoded by TBX21), CD27^{lo}, SELL^{lo} and CD127^{lo} (IL7R)[248]. Notably, LEP clones have a similar expression profile (Figure 5.33).

5.3.9.3 Antigen specificity of large expanding persistent clones

In order to investigate the antigen specificity of LEP clones, I ran all TCRβ sequences through the IEDB *TCRmatch* tool, as described in methods section 2.4.4 (page 86). For both patients with a CR to sICB and HDs, there was no significant enrichment in either CMV, EBV or other virally-associated TCR (Figures 5.34a and 5.34b). Interestingly, when looking at clones that are

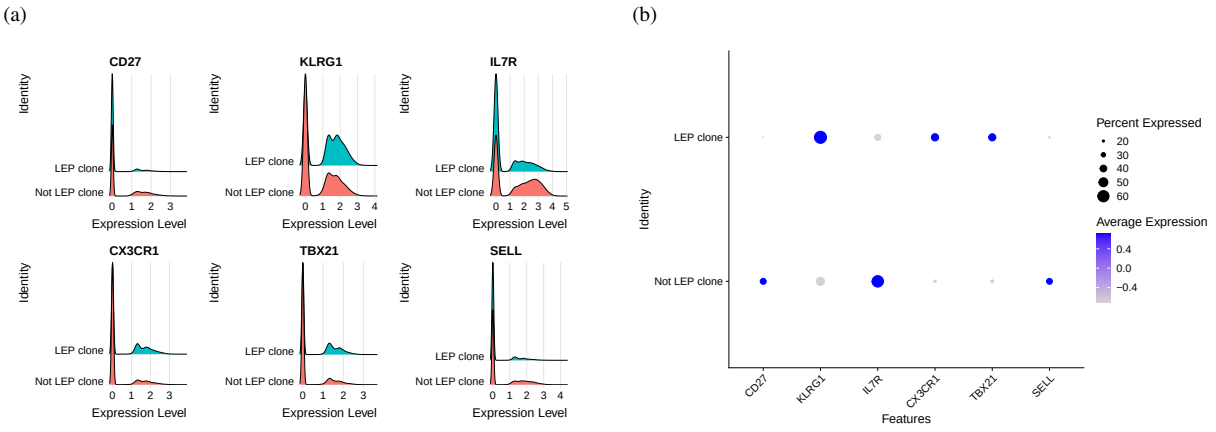


Figure 5.33. (a) Ridge plot and (b) dot plot showing differences in gene expression of cells belonging to LEP clones compared to all other clones. The genes chosen are those used to define LLECs as per reference [248], whereby LLECs have a KLRG1^{+}, CX3CR1^{+}, T-bet^{+} (encoded by TBX21), CD127^{lo} (IL7R), CD27^{lo} and SELL^{lo} expression profile. Notably, large expanding persistent clones (LEP clones) have a similar expression profile.

present at all cycles in patients with a CR (not restricted to those that expand and are enlarged at 3-9 weeks post-ICB) there is a significant enrichment for CMV-associated TCR and TCR associated with other viral epitopes (Figure 5.34c). This could provide an explanation for these fixed, long term clones.

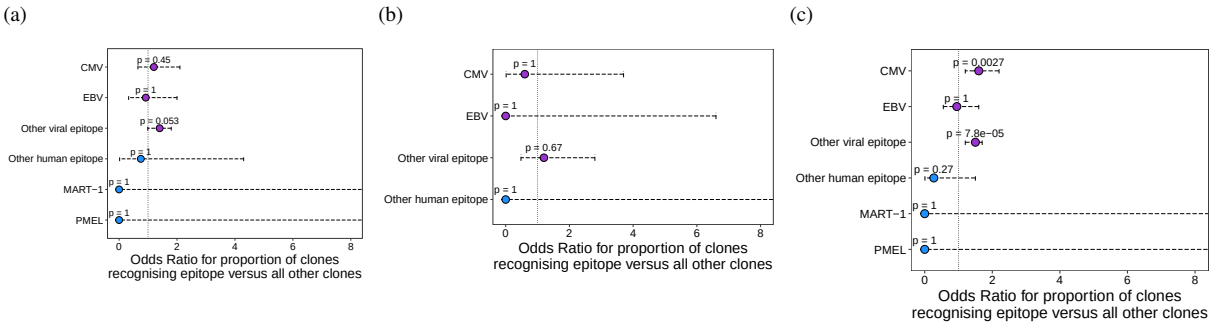


Figure 5.34. Antigen specificity of LEP clones. (a) Odds ratio for LEP clones being enriched for TCRβ associated with the named antigen in patients with a CR to sICB. (b) as per (a) but for HDs. (c) as per (a) but for clones present at all time points. Statistics with Fisher's exact test.

Finally, within this single cell dataset, there were 17 clones which had TCR which were known to be associated with melanoma antigens - MAGE-1, MAGE-10, MART-1, NY-ESO and PMEL. I examined the characteristics of these clones and identified that they were very small (maximum 2 cells, maximum 0.1% of the repertoire) (Figure 5.35a). Further, they were found in a similar

number in those with and without progression of disease (Figure 5.35a) and are primarily comprised of cells from naive and central memory clusters (Figure 5.35b).

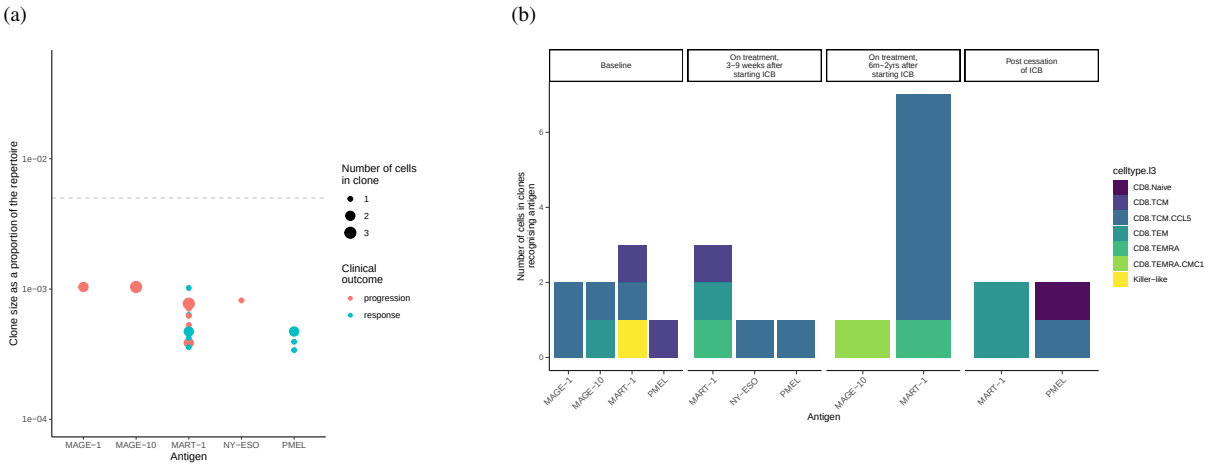


Figure 5.35. Characterisation of clones which carry TCRβ associated with melanoma antigens. (a) size of clone by antigen that the TCRβ chain is associated with, coloured by clinical outcome and sized by the number of cells in that clone. The horizontal line is at 0.5% - the threshold for 'large' clones. (b) Phenotype of cells found within clones that carry a melanoma antigen-associated TCRβ, faceted by time point of sample.

In conclusion, LEP clones do not enrich for TCR associated with known antigens in the IEDB, although they may recognise relevant antigens which have not been annotated in this data.

5.4 Discussion

Here I have performed a large single cell experiment in order to understand the long term consequences on ICB on peripheral immune cells, with a primary focus on CD8⁺ T cells. In the long term, following cessation of ICB and a complete response to treatment (CR), there is an increase in abundance of a subtype of CD8⁺ T cell which highly expresses a number of NK-associated genes, termed a killer-like subset. Using the top 25 genes upregulated by this subset to generate a 'killer score', I was able to show that in patients with CR to sICB, but not those with progressive disease (PD) or healthy donors (HDs), there is a broad increase in killer gene expression over time across both T_{em} (annotated as 'CD8.TEM') and T_{eff} (annotated as 'CD8.TEMRA' and 'CD8.TEMRA.CMC1') subsets. This finding was validated in bulk RNAseq

where I was able to show increased expression of these top 25 killer genes following a CR to sICB.

I next explored long term clonal dynamics following a CR to sICB, identifying that a number of clones which are expanded prior to treatment with ICB remain expanded throughout treatment and persist post-cessation of ICB - so-called hyper-expanded ubiquitous clones. In order to identify clones which are most likely to be mediating the anti-tumour response, I selected those which are stable or expanding from pre-treatment to 3-9 weeks post treatment (based on findings described in Chapter 3 and reference [78]), occupy >0.5% of the repertoire at 3-9 weeks post treatment (based on findings in reference [93] and Chapter 4) and are persistent post-cessation of ICB. I term these large expanding persistent clones (LEP clones). Both hyper-expanded ubiquitous clones and LEP clones have a greater proportion of T_{effs} than all clones; however, the ratio of effector to memory clones is greatest for LEP clones. It is of great interest - and has not previously been described to this extent - that these long-term persisting clones have a predominantly cytotoxic, effector, gene expression profile.

Finally, I went on to describe the gene expression and TCR profile of these large expanding persistent clones. LEP clones are not enriched for TCRβ that recognise known melanoma antigens, but similarly are not enriched for CMV or EBV TCR. LEP clones from patients differentially upregulate more immunological pathways when compared to those clones from HDs. Utilising a range of scores from previously-published papers, I was able to demonstrate that in long-term persistent clones, there is a large increase in cytotoxicity, tumour reactivity and dual expansion (i.e. a signature of expanded CD8$^+$ T cell clones in both blood and tumour) from baseline to 3-9 weeks post-treatment. Over time, the levels of cytotoxicity and tumour-reactivity do then subsequently decrease - however, strikingly, they remain significantly in excess of pre-treatment levels many years post-cessation of ICB. Notably, LEP clones have higher levels of cytotoxicity,

tumour reactive and peripheral proliferation than other clones at all time points.

A 2020 paper by Renkema *et al.* described a population of KLRG1^{+}, CD27^{lo} CD8^{+} T cells which persist into the memory phase and display a protective function against both bacteria and viruses[248]. They term this cell group "long-lived effector cells" (LLECs) and describe that these cells form a unique subtype that retain functions of both effector and memory T cells. These LLECs have less reliance on IL-15 for their survival than classical KLRG^{+} effector cells, despite appearing to be derived from this subset - suggesting that so-called short-lived effectors can subsequently develop into stable and long-lived memory cells, which retain dual roles of rapid functionality and longevity. A number of the cell neighbourhoods that demonstrated DA in the long term following ICB share transcriptomic features of LLECs. For example, KLRG1 is significantly upregulated by the cells in both neighbourhood groups 9 and 11 and appears in the list of the top 25 differentially upregulated genes for group 11 (logFC for group 11: 0.29, p<0.0001; logFC for group 9: 0.22, p < 0.0001), whilst CD27 is significantly downregulated by both groups (logFC for group 9: -0.05, p<0.01; logFC for group 11: -0.22, p<0.0001). Further, those clones which expand and then persist (i.e. LEP clones) share a gene expression profile very similar to LLECs as previously described[248] (Figure 5.33).

In their work from 2021, Lucca *et al.*[98] described that T cell clones shared between melanoma lesions and peripheral blood had a particularly cytotoxic gene expression profile. Further, the cytotoxic profile of tumours increased following ICB, suggesting that key clones involved in tumour rejection are easily identifiable in the peripheral blood. The LEP clones described here score very highly for Lucca *et al.*'s cytotoxic gene set and comparatively less for an exhausted gene set from the same paper (Figures 5.31d and e) suggesting that they are possibly the key clones mediating tumour rejection[98].

LEP clones have an increased peripheral proliferating score - based on gene set including *MKI67*

(encoding Ki67) from Huang *et al.*[77] (Table A.1) - when compared to all other clones. This observation is unsurprising because to 'maintain' a large clone, there is a degree of turnover of member cells and ongoing cell division is required. However, what is notable is that there are no significant increases in this score following ICB, despite the fact that these clones are selected because they are stable/expanding from baseline to 3-9 week after starting ICB. This suggests that the expansion/maintenance of the size of these clones, as sampled in the peripheral blood, could be due to mechanisms other than simply mitosis - for example a reduction of cell death of these clones in the tumours, or mobilisation from lymphoid tissue.

Previous work by Han *et al*, discussed in introduction section 1.2.5 (page 27), described the peripheral phenotype of clones which persist long term and are found to be previously TI and resident in skin[100]. Whilst they describe this phenotype as T_{em}, and are only able to do this for four clones in one individual, the list of genes upregulated in these clones is strikingly similar to my list of 'killer genes' ('C1' cluster in supplementary table 4 in ref [100] versus Table 5.4, above) with shared upregulation of *NKG7*, *CMC1*, *GZMH*, *CCL5* and *PRF1*, for example. Hence my findings are consistent with this previous work, but substantially expand this description across 10 individuals, demonstrating similar changes in multiple clones across a long time course of peripheral blood samples.

What is notable from this current work is that long-term persistent clones not only gain cytotoxicity and tumour-specific gene expression features following treatment with ICB but that this gene expression profile is preserved in the very long term. Even many years following cessation of ICB, and in the case of CR where there is no radiologically-discernible tumour, certain clones continue to maintain a killer-like programme of gene expression. The causal link for this cannot be explained by the current experiment, but there are potentially two reasonable explanations. Firstly, it is possible that even in the case of a "complete response" there is still a degree of

"residual disease" which may or may not be detected on standard clinical imaging. Secondly, it is possible that treatment with ICB and a successful eradication of cancer results in the generation of LLECs - which then have substantial longevity.

In very recent work from Antoni Ribas' group, neo-antigen specific T cells and their TCR were isolated from patients with MM with and without a good response to PD-1 blockade[252]. In patients with a long-lasting clinical response, the T cell responses were polyclonal (i.e. multiple clones all recognising a restricted set of antigens), detected in both the tumour and peripheral blood and - importantly - targeted the same antigens recurrently over time (up to 9 months)[252]. This is suggestive that repeated and prolonged exposure to antigen, with recurrent TCR ligation, is maintaining ongoing clonal expansion. Additionally, work in chimeric antigen receptor T cell (CAR T cell) therapy in liquid tumours has described that, up to 10 years post-infusion, CAR T cells remain detectable in the peripheral blood[253]. Interestingly, these long term CAR T cells have a cytotoxic profile but are predominantly $CD4^+$ T cells and, compared to normal T cells, display upregulation of antigenic signalling pathways, again suggestive of ongoing antigen ligation[253].

However, in the case of chronic exposure to antigen, one might expect the expression profile of long term persistent clones to be more exhausted. The fact that large, possibly tumour-reactive, clones remain cytotoxic for many years is of great interest. It is possible that, rather than elimination, there is immunological cancer 'containment' with treatment success being defined by ongoing *cytotoxic* T cell responses that keep tumours in check. How this process, whereby there is persistence of large killer clones without significant increases in exhaustion, even long after the cessation of ICB, is maintained, is an important question which remains to be determined.

This current work has several limitations - again, being retrospective and observational in nature means that I can only describe associations, not causation. Further, a lack of tumour sequencing in this case means that I am unable to identify those clones which are also tumour-infiltrating.

Additionally, all my work is on RNA, rather than protein, expression and so it is an assumption that the surface expression and/or function of the clones described correlate with their transcriptome. Nonetheless, this work has several advantages - pairing V(D)J with gene expression sequencing allows clonal identity to be tied to phenotype, an element that has been lacking from all previous studies describing long term clones in the context of ICB. Further, scRNAseq allows exact pairing of the TCRα and TCRβ - facilitating the identification of complete key TCR.

5.4.1 Conclusions

Clones that persist long term - up to several years following cessation of ICB - retain, and in many cases, increase the level of expression of highly cytotoxic, killer-like genes. This long term phenotype has not previously been described in the context of human cancer, and an understanding of mechanisms underpinning this process has important implications for a wide range of immuno-oncology applications.

6 | $CD8^+$ T cell features associated with immune-related adverse events

6.1 Chapter-specific acknowledgements

A number of colleagues contributed to the work described in this chapter. For the work on myocarditis with myositis (section 6.3), the experimental work was undertaken by myself, assisted by Elsita Jungkurth. For the work on the characterisation of the mechanisms underpinning the association between a polymorphism at *IL7* and irAEs (section 6.4), this was a Fairfax group-wide project with major contributors Chelsea Taylor and Orion Tong. The data presented in this thesis was entirely analysed by me, however the experimental work undertaken to generate bulk RNAseq and flow cytometry data was primarily performed by Chelsea, Orion and Alba Verge de los Aires. Clinical data for section 6.4 was collected primarily by myself, with major contributors from Ben Fairfax and Christina Ye. Clinical data collection for validation of the LSI was obtained through a collaboration with NHS staff (Grant Vallance and Brian Shine, Oxford cohort, and Anna Olssen-Brown, Liverpool cohort).

6.2 Chapter-specific background

A number of sections of Chapter 1, Introduction, are relevant to this chapter, primarily section 1.1.4 (*Immune-related adverse events*) which details the clinical syndromes and epidemiology, molecular mechanisms, biomarkers, management and unanswered questions of irAEs.

In this chapter, I present results from two separate work streams that each investigate underlying mechanisms of irAE following ICB. Firstly, I report three extreme cases of myositis with

myocarditis that we observed in early 2022 during the Covid-19 booster campaign. Secondly, I report my contributions to the characterisation of the molecular effects of a novel polymorphism associated with irAEs (rs16906115) which was published in *Nature Medicine* (Appendix F)[101]. As part of this work, I followed up the observation that a stable lymphocyte stability index (LSI) was associated with clinical outcome, expanding this finding to multiple cancers.

6.2.1 Myositis and myocarditis in the context of PD-1 blockade and vaccination for Covid-19

Whilst myositis and myocarditis are recognised irAEs following ICB, the occurrence of these particular toxicities is very rare, being observed in <1% of cases with fatalities reported in <0.01% of recipients of anti-PD-1 alone[42,254,255]. Similarly, infection with SARS-CoV-2 can lead to both myositis and myocarditis[36]. Whilst the underlying mechanisms remain undetermined, indirect virally-triggered autoimmune reaction or direct epitope cross-reactivity are posited[256]. There is also an association between SARS-CoV-2 vaccination with mRNA vaccines and myocarditis. This is rare, appears to be driven by a younger patient population, and the underlying mechanisms are currently unclear[257–260].

In the first part of this chapter, I describe three cases of critical acute myositis with myocarditis occurring within 22 days of each other, all within one month of receiving the initial cycle of pembrolizumab. All patients had recently received a Covid-19 mRNA booster vaccine prior to treatment and were positive for SARS-CoV-2 Spike antibody. I summarise the clinical cases before presenting an analysis of T cell receptor (TCR) repertoires from peripheral blood and tissues. This revealed a high degree of clonal expansion and public clones between cases, with several T cell clones expanded within the skeletal muscle putatively recognising viral epitopes.

6.2.2 The molecular effects of rs16906115 and importance of peripheral lymphocyte stability

One of the idiosyncrasies of ICB is the high variability of occurrence of irAEs between patients. Additionally, whilst on the whole there is an association between development of irAEs and positive clinical outcomes[43], this is neither necessary nor sufficient. We have long hypothesised that germline genetics have an important role in determining clinical phenotypes of response to ICB, although a large GWAS in the context of ICB has not previously been performed. However, we were made aware of the results of the first GWAS to examine genetic associations with irAEs, discovering that carriage of the minor allele at rs16906115 (intronic to *IL7*) strongly correlated with the development of toxicity - now published[56]. Colleagues and I set out to replicate this finding within our own data, and explore the underlying molecular mechanisms. This was a collaborative effort co-led with Chelsea Taylor and Orion Tong, with a key finding that carriers of this minor allele have increased expression of B cell *IL7* (see Appendix F).

In the second part of this chapter, I present my contributions to this work, in particular focussing on the effects of carriage of this allele on CD8+ T cells and peripheral lymphocyte counts. I also further investigate an observed association between a stable lymphocyte count from pre- to post-treatment and clinical outcome, describing this relationship across multiple cancers.

6.3 Results: T cell receptor analysis of three cases of myositis with myocarditis

6.3.1 Clinical case reports

The full clinical case histories are found in Appendix D (page 276). In summary, we identified three patients, one male aged 72 (patient 1) and two females aged 82 and 81 (patients 2 and 3 respectively) who had all received single-agent pembrolizumab but suffered from severe ICB-related myositis and myocarditis within 3 weeks of each other. All three patients were previously fit and well (ECOG performance status 0). Patient 1 received pembrolizumab for adjuvant treatment and was subsequently admitted as an emergency with respiratory failure due to muscle weakness. He spent four weeks in intensive care and his condition was diagnosed with a skeletal muscle biopsy and due to characteristic blood markers (raised cardiac and skeletal muscle enzymes - troponin and creatine kinase (CK)) (Figure 6.1). Patient 2 was admitted due to very high troponin (cardiac enzymes) and collapse. She, too, had a raised CK. Myositis with myocarditis was diagnosed clinically and whilst she was managed on a ward and subsequently discharged, she had a prolonged and incomplete recovery and required repeat admissions for supportive care due to ongoing fatigue and muscle weakness. Patient 3 was admitted due to fatigue and had grossly elevated serum CK and troponin. Despite steroids and an initial improvement, she sadly acutely deteriorated and died whilst in hospital. A post-mortem examination confirmed the diagnosis of both myositis and myocarditis. Figure 6.1 displays the blood test results for all three patients, with grossly elevated troponin and CK, alongside example histopathology slides. We were struck by the severity and temporal closeness of these three cases and set out to investigate the TCR associations.

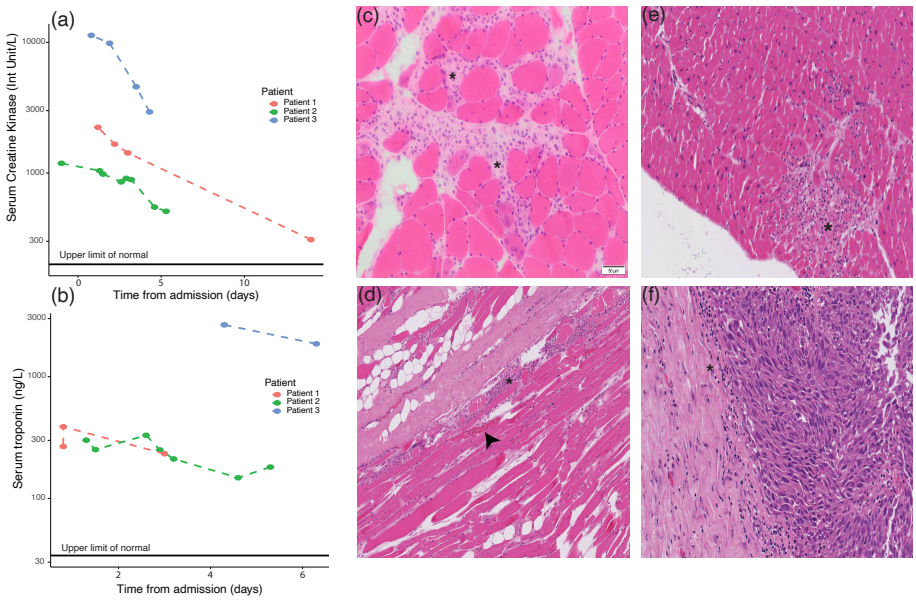


Figure 6.1. (a) Serum creatine kinase (CK) by day post-admission for each of the three patients. (b) as per (a) but for troponin. (c) H&E slide of fresh skeletal muscle biopsy taken from patient 1. Widespread leukocyte infiltration can be seen (e.g. at asterisks). (d) H&E stained slide of PM skeletal muscle sample taken from patient 3. The asterisk indicates infiltrating lymphocytes, with the arrowhead denoting myocyte necrosis. (e) H&E slide of post-mortem cardiac muscle from patient 3, demonstrating widespread leukocyte infiltration. (f) as per (e) but for tumour deposit taken from the small bowel serosa.

6.3.2 Clinical sample collection

In order to investigate any underlying TCR repertoire features of these cases, I obtained tissue specimens from all three patients. Patients 1 and 2 were recruited after the occurrence of the irAE and therefore I collected post-treatment blood and, in the case of patient 1, the fresh skeletal muscle biopsy. For patient 3, she had been recruited to the cohort prospectively, and so we had pre-ICB blood samples; however, we did not manage to obtain post-treatment bloods. Nonetheless, I submitted a CUREC application (see methods section 2.1.2, page 66) in order to access post-mortem tissue, and I analysed samples of cardiac muscle, skeletal muscle and a metastatic tumour resected from the jejunum. TCRseq was performed on these specimens as outlined in methods section 2.4 (page 83). The samples sequenced are detailed in Table 6.1a.

For control samples, I liaised with Benjamin Larman's group (Johns Hopkins) who kindly pro-

vided full sequencing data from their paper examining TCR repertoires in idiopathic inflammatory myositis (IIM)[261]. Here they performed TCRseq of TCRβ chains using RNA from 146 muscle samples - 124 from patients with IIM (the majority, n=49, of whom had immune-mediated necrotising myositis (IMNM)), 9 from healthy controls and 13 from non-IIM controls (i.e. symptomatic patients but histopathologically normal) (Table 6.1a - henceforth referred to as the Johns Hopkins samples). Further, I used resected melanoma specimens which were sequenced as part of my large TCRseq experiment (as presented in Chapter 4) as controls for the post-mortem resected melanoma deposit (Table 6.1b, n=11 specimens from n=8 individuals).

(a)

Reported (index) cases		Myositis controls (Montagne) - Fresh Frozen Muscle Biopsies
Patient 1	PBMCs (post treatment)	IMNM
	Fresh muscle biopsy (post treatment)	DM
Patient 2	PBMCs (post treatment)	IBM
Patient 3	PBMCs (pre treatment)	ASyS
	PM heart (post treatment)	Non-IIM
	PM muscle (post treatment)	Healthy
	PM tumour (post treatment)	

(b)

Tumour block	Specimen resection date	Specimen detail
T51	19/01/2017 x2	Excised melanoma from skin (x2 lesions)
T61	22/02/2017	Excised melanoma from skin
T64	07/04/2017	Melanoma deposit within lymph node
T90	10/03/2017	Melanoma deposit within lymph node
T101	19/02/2018	Excised melanoma from skin
T104	23/02/2017,12/05/2017, 04/01/2018	Excised melanoma from skin (x1 lesion) and melanoma deposit within lymph node (x2 lesions)
T108	27/06/2017	Excised melanoma from skin
T132	07/08/2018	Excised invasive melanoma from muscle

Table 6.1. (a) Samples on which TCRseq was performed. PBMC - peripheral blood mononuclear cell; PM - post-mortem; IMNM - immune-mediated necrotising myositis; DM - dermatomyositis; IBM - inclusion body myositis; AyS - anti synthetase syndrome; IIM - idiopathic inflammatory myositis. Myositis control samples came from Montagne *et al*[261]. (b) Resection date and pathological detail for 11 resected melanoma specimens (from 8 individuals) - data from which is presented in Chapter 4.

6.3.3 Analysis of occurrence of irAEs within existing cohort

I examined the incidence of myositis and myocarditis across our existing cohort of patients receiving ICB for melanoma and mRCC from end 2015 - end 2021 (n=135 who received cICB and n=102 who received sICB). In line with published incidence[254], only two of the 237 patients suffered biochemically-proven myositis and no myocarditis cases were recorded. Both patients had received two doses of *combined* PD-1/CTLA-4 blockade (cICB) (Table 6.2). After the occurrence of the three index cases which form this series, I identified a further individual in our cohort who developed clinical myositis with an asymptomatic troponin rise after his second cycle of cICB for

mRCC, 66 days post-booster (BNT162b2). This culminates in four cases of myositis with likely myocarditis within 28 days over the winter of 2021-2022, on a background of only two cases of myositis without myocarditis occurring within the same patient cohort over the preceding six years.

	Patient	Type	Time period	Treatment	Day post-treatment	Number of cycles received	Peak CK	Peak Troponin	Received steroids?	Admitted?	Overlap
Index cases	Patient 1	Myositis with myocarditis	Late 2021	PD-1 blockade alone	28	1	2236	388	Yes	Yes	Hepatitis, myaesthenia gravis
	Patient 2	Myositis with myocarditis	Early 2022	PD-1 blockade alone	39	1	1186	2101	Yes	Yes	Colitis, Hepatitis, myaesthenia gravis (clinical)
	Patient 3	Myositis with myocarditis	Late 2021	PD-1 blockade alone	23	1	11301	2664	Yes	Yes	Hepatitis
Prior to index cases		Myositis alone	Early 2018	PD-1 + CTLA-4 blockade	49	2	8938	N/A	Yes	Yes	Hepatitis
		Myositis alone	Late 2018	PD-1 + CTLA-4 blockade	28	2	5733	N/A	Yes	No	No
After index cases		Myositis with myocarditis	Early 2022	PD-1 + CTLA-4 blockade	43	2	1229	90	Yes	Yes	Hepatitis and nephritis

Table 6.2. Summary of cases of myositis or myocarditis, comparing index cases (top section) to those found within a cohort of 237 patients from end 2015-end 2021 ('prior to index cases', bottom section) and a further case identified after the index cases in early 2022.

6.3.4 Analysis of T cell repertories reveals a high degree of overlap between samples

TCRseq of peripheral blood and tissue samples from all three patients identified a high degree of clonal sharing both within individuals (different tissue sites) and between individuals. For example, clonally-expanded TCR present in the muscle biopsy from patient 1 were found similarly expanded within the peripheral blood, with a trend towards greater muscle expansion (Figure 6.2a). Looking across all three individuals, there was a high degree of clonal sharing in the PBMCs (Figure 6.2b).

Notably, there was high clonal overlap between TCR found in the PM tumour specimen from patient 3 and the other sampled tissue sites - both the skeletal muscle and cardiac muscle of

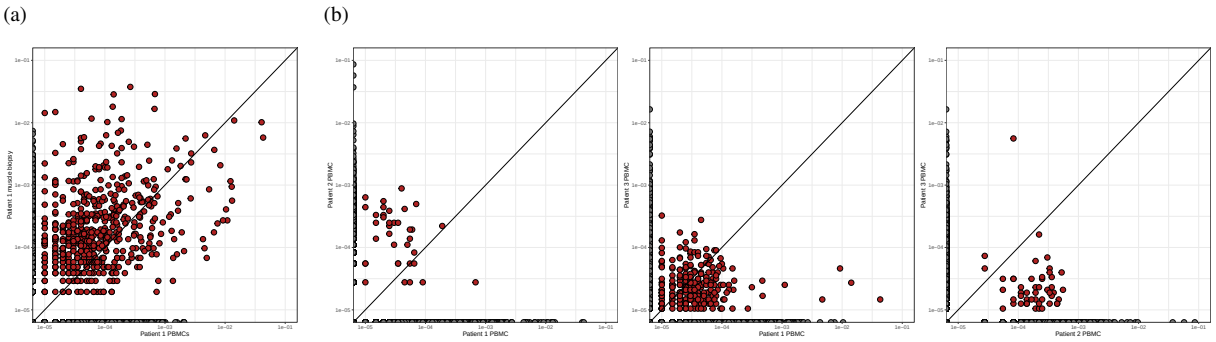


Figure 6.2. (a) Dot plot showing proportion of repertoire occupied by T cell clone in peripheral blood versus muscle biopsy from patient 1. Each dot represents a clone, with shared clones coloured red and clones present in one sample only on the x and y-axis. The axis values represent the proportion of the repertoire occupied by that clone in that sample (as labelled). The line is x=y. (b) as per (a) but for overlap between PBMC samples as labelled.

the same patient, as well as the skeletal muscle of patient 1 (Figures 6.3a and 6.3b). Of the 13 TCR found within the PM cardiac muscle of patient 3, 5 matched those found within the skeletal muscle biopsy of patient 1 (Figure 6.3b) and one was found in the peripheral blood of patient 2 (not shown).

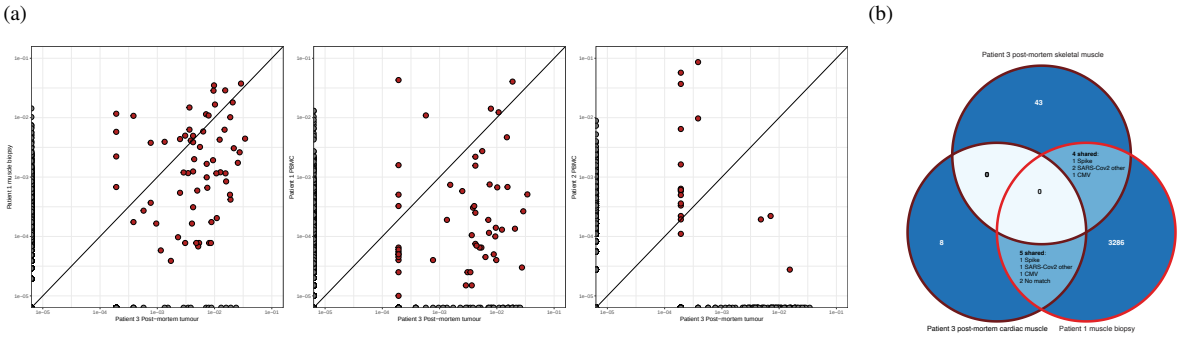


Figure 6.3. (a) Dot plot showing clonal overlap (as per Figure 6.2) for PM tumour from patient 3 (on x-axis all panels) and skeletal muscle of patient 1 (left), PBMCs of patient 1 (middle) and PBMCs of patient 2 (right). (b) Venn diagram of the TCR overlap between cardiac and skeletal muscle of patient 3 and skeletal muscle of patient 1. The antigen specificity of the overlapping clones as determined by IEDB *TCRmatch* tool is listed.

To quantify repertoire overlap, I applied the Morisita-Horn index (MH) similarity index (see methods section 2.4.3.4, page 86)[262]. This confirmed high overlap between the TCR repertoire from the PM tumour sample from patient 3 and the fresh muscle biopsy from patient 1 (MH 0.328) (Figure 6.4a). This was several orders of magnitude greater than any overlap between the PM tumour from patient 1 and TCR repertoires sequenced from muscle biopsies taken from

either controls or patients with IIM (the Johns Hopkins samples)[261] (median MH for IIM samples 0, IQR 0-8.72e-7, p=0.008) (Figure 6.4a). For a further comparison, I explored the overlap of the TCR repertoires from resected melanomas (all resections pre-2020, Table 6.1b) and the skeletal muscle samples of patient 1 and the Johns Hopkins cohort. There was limited overlap and clonal sharing between these tumours and the muscle of patient 1, which was the same as their overlap with the Johns Hopkins IIM samples (Figure 6.4b). A similar finding was noted when comparing the TCR found in the cardiac tissue - the MH for overlap between cardiac muscle (patient 3) and skeletal muscle (patient 1) was significantly greater than the overlap with any of the control muscle samples (Figure 6.4c) whilst the overlap between cardiac muscle (patient 3) and resected tumour (patient 3) was greater than the overlap between the cardiac muscle and any previously-resected tumour specimens (Figure 6.4d).

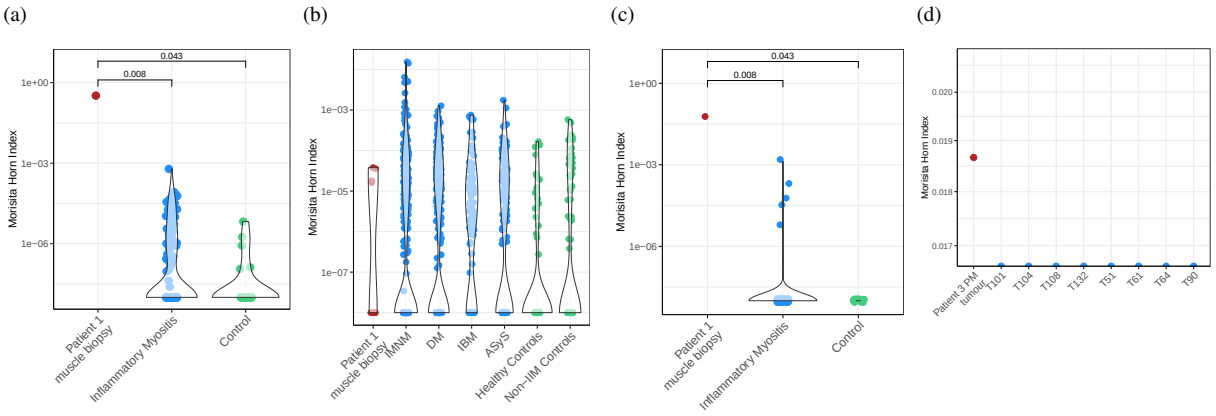


Figure 6.4. (a) Morisita-Horn index (MH) index for the repertoire overlap between the resected tumour from patient 3 and the skeletal muscle of patient 1 (red), and samples taken from patients from the Johns Hopkins cohort with IIM[261].(b) MH index for the TCR repertoire overlap between resected melanomas from eight patients from the original cohort (table 6.1b) and skeletal muscle biopsies as labelled. (c) MH index for TCR repertoire overlap between PM cardiac muscle from patient 3 and muscle biopsies as labelled. (d) MH index showing TCR repertoire overlap between the PM cardiac muscle from patient 3, the PM tumour from patient 3 (red) and resected melanomas (blue) from eight patients pre-2020. Statistics with the Kolgomorov Smirnov test (a) and (c).

6.3.5 Evidence of expansion of Spike-specific TCR within skeletal muscle

Finally, I examined the nature of putative TCR epitopes - as derived from the IEDB (see methods section 2.4.4, page 86) from specimens taken from patient 1, focussing on clones that were found

in both the peripheral blood and skeletal muscle. These shared clones matched a range of viral epitopes. I tested for the enrichment of each clone within the muscle versus the peripheral blood, finding that although no significant differences in total unique clones recognising specific epitopes (Figure 6.5b), when taking into account clone size, TCR putatively recognising the SARS-CoV-2 Spike protein were enriched within the muscle (OR 1.37, 95% CI: 1.30-1.40, p<0.0001), along with TCR reactive to other viral epitopes (Figure 6.5).

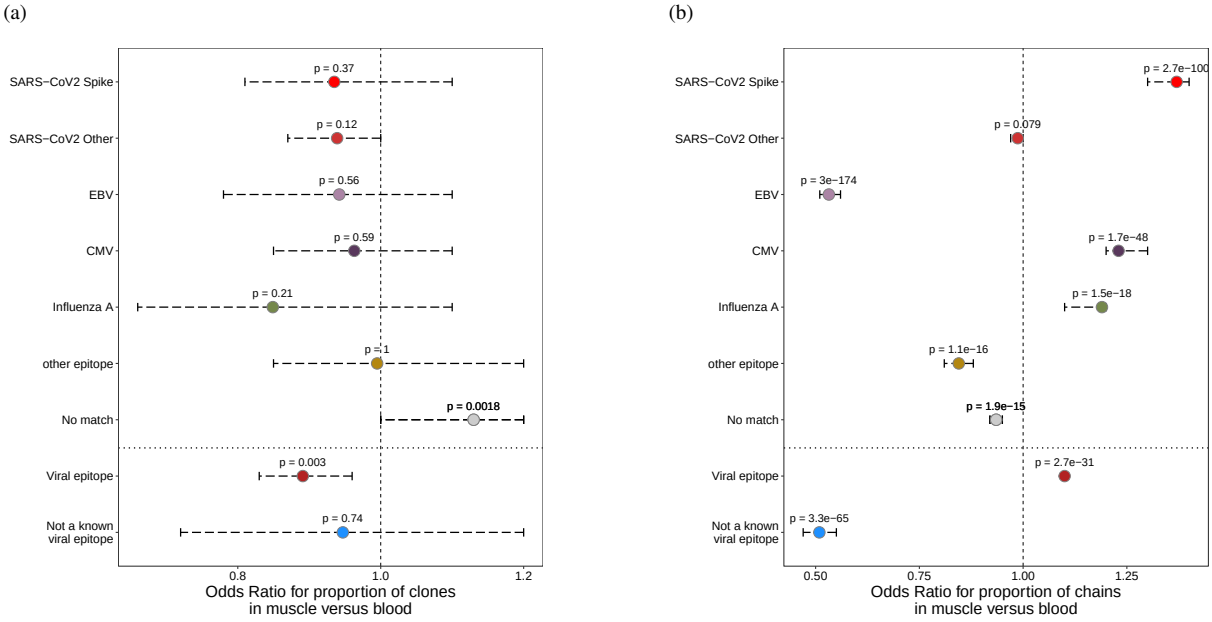


Figure 6.5. (a) Odds ratio for occurrence of epitope-specific clones (TCR) - as called by the IEDB - found in the muscle versus the peripheral blood of patient 1. (b) As per (a) but taking into account number of copies of each clone (thereby considering clonal expansion). Statistics are via a Fisher's exact test.

6.3.6 Section summary

I describe a cluster of three highly unusual cases presenting with clinically significant and life-threatening acute myositis with cardiac involvement within a three-week window, post-receipt of the first six-weekly dosage of pembrolizumab. None of the attending physicians had witnessed such rapid-onset and severe myositis with respiratory, cardiac and bulbar involvement post-ICB over many previous years of practice. Specifically, there are no reported cases severe enough to

precipitate acute respiratory failure after just one cycle of single-agent PD-1 blockade.

Analysis of TCR sequencing reveals expansion of similar clones across multiple samples. The similarity between TCR found in the PM cardiac muscle, skeletal muscle and tumour of patient 3 and the skeletal muscle of patient 1 is significantly higher than when compared to the TCR repertoires sequenced from muscle biopsies of IIM or than seen between these tissues and resected melanomas from pre-2020. As such, this suggests clonal expansion of a subset of public clones not found in other forms of myositis, indicating possible recognition of a distinct set of antigens common to both muscle and tumour. Some of these TCR are known to be Spike-reactive, and muscle-infiltrating TCR are enriched for this epitope compared to the peripheral blood of the same patient.

6.4 Results: The effect of B cell *IL7* on peripheral T cell repertoires and lymphocyte counts

6.4.1 Replication of association between carriage of risk allele at rs16906115 and irAEs

As discussed above, we became aware of the discovery of an association between a SNP at rs16906115 - intronic to *IL7* - and the development of irAEs following ICB, an observation which has now been published[56]. I first sought to replicate this finding in our data. Taking the 214 patients within the cohort who had been genotyped, we detected a minor allele frequency of 7.4% for the risk allele (a G to A change), I found that carriage of the minor allele (one or two copies) was associated with an increased likelihood of developing severe (CTCAE grade 3 or above) irAEs requiring corticosteroids prior to the fifth cycle (C5) of treatment (a metric

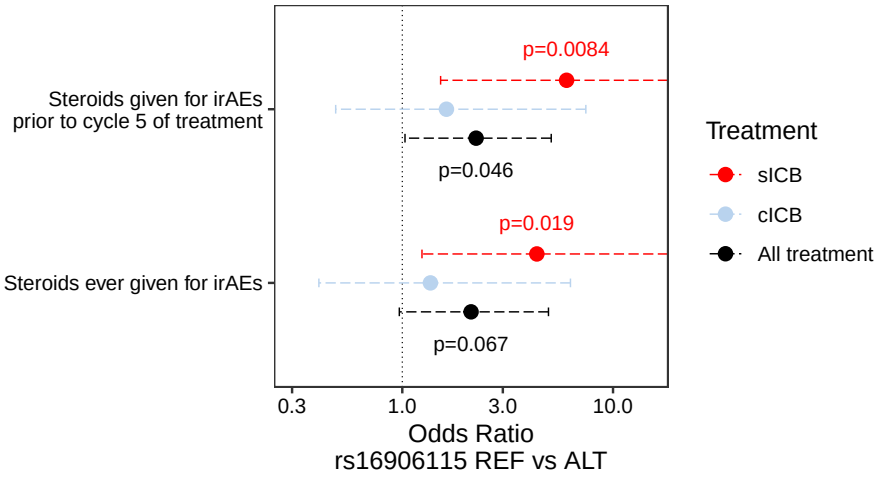


Figure 6.6. ORs for odds of developing irAEs requiring steroid treatment prior to the 5th cycle of treatment (top) or ever (bottom), coloured by treatment. Whiskers are 95% CI. Statistics with logistic regression.

previously used[43]) across all patients, with an OR of 2.24 (95% CI 1.03-5.09, P=0.046) (Figure 6.6). In the original discovery cohort[56], the vast majority (>90%) of patients were treated with sICB which carries only a 10-20% risk of irAEs when compared to cICB. On analysing the risk of developing irAEs by treatment, the genetic effect was much more marked in recipients of sICB: OR 6.0 (95% CI:1.5-23.0, p=0.0084) of developing corticosteroid-requiring irAEs prior to C5, as well as increased risk of requiring steroids at any time point on treatment (OR 4.4, 95% CI:1.2-15.1, p=0.019) (Figure 6.6). This is likely a result of the increased sensitivity to detect genetic effects with this more moderate treatment.

6.4.2 Carriers of the minor allele at rs16906115 have skewed CD8+ T cell subsets and repertoires

In work primarily performed by Chelsea Taylor and Orion Tong, we were able to demonstrate that one of the key mechanisms underpinning this is that carriers of the risk allele have increased expression of *IL7* by B cells (see [101] and Appendix F, page 280). Given the pivotal role of IL-7 in lymphopoiesis as well as the maintenance of peripheral T cells[263–265], I wished to further

explore the carriage of this polymorphism on both peripheral CD8⁺ T cell subsets and clonal repertoires.

Taking flow cytometry data from 54 patients (experiments previously performed by Chelsea Taylor, see methods section 2.5, page 87), I looked at the change to naive and T_{eff} (labelled TEMRA) subsets from pre-treatment (d0) to the first post-treatment sample (median day 21). Notably, whilst in those not carrying the risk allele there is virtually no change to either subset (blue boxes, Figure 6.7a), for those carrying the polymorphism there is a net loss of naive T cells, with a net gain of T_{effs} (orange boxes, Figure 6.7a). This is primarily driven by CD8⁺ T cells - whilst a similar trend is seen for CD4⁺ T cells, there is no significant difference between those with and without the SNP (Figure 6.7a).

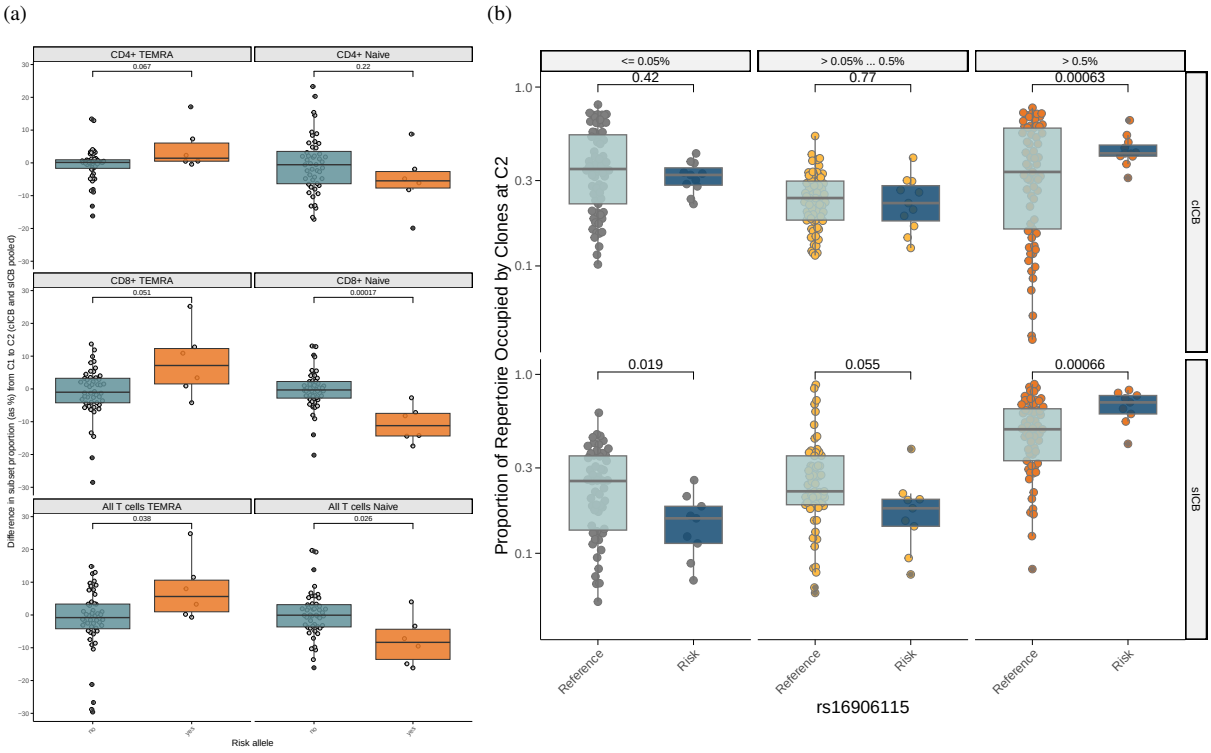


Figure 6.7. (a) Change in T cell subset proportion (percentage of total CD4⁺/CD8⁺/all T cells) from pre-treatment (d0, labelled as 'C1') to first blood test post-treatment (median d21, labelled as 'C2'), faceted by subset and coloured by genotype (presence/absence of risk allele). (b) Proportion of the repertoire occupied at first blood test post-treatment (median d21, labelled as 'C2') by clones of the size category as labelled (horizontal facets), coloured by genotype and faceted by treatment (vertical facets). Each dot is an individual (n=54). Statistics with Wilcoxon rank sum test. TEMRA = T_{eff}.

To examine effects of clonality, I examined the proportion of the repertoire occupied by clones of different sizes (>0.5% (i.e. large clones), 0.05-0.5% and $\leq$0.05% of the repertoire). In those individuals with the risk allele, there were significantly more large clones, and fewer smaller clones (Figure 6.7b). Whilst this trend was present across those individuals treated with both sICB and cICB, the effect was only significant for small clones in recipients of sICB (Figure 6.7b).

Together these findings suggest that those individuals carrying this polymorphism - who express more *IL7* in their B cells - have more mature, large CD8⁺ T cells in their peripheral repertoires.

6.4.3 rs16906115 affects lymphocyte stability post ICB

Given these effects, and the known action of IL-7 as discussed, I investigated whether carriage of the risk allele resulted in any detectable effects of ICB on the peripheral lymphocyte count as detected on routine hospital blood counts. Looking at the pre-treatment lymphocyte count (test closest to receiving treatment, and less than 30 days prior) and the first post-treatment lymphocyte count (at least 21 days but less than 50 days post ICB), I found that sICB, but not cICB was associated with a fall in lymphocyte count (Figure 6.8a). Of interest there was a genotype effect, with those carriers of the wild-type allele having significantly reduced lymphocyte count post-sICB (median pre-treatment value 1.82x10^9 cells/L, IQR 1.26-2.33; post-treatment 1.52x10^9 cells/L, IQR 1.07-2.11, p=0.00044, Figure 6.8a, top row), a reduction not observed in risk allele carriers (median pre-treatment value 1.35x10^9 cells/L, IQR 1.11-2.72; post-treatment 1.53x10^9 cells/L, IQR 1.34-1.90, P=0.68; Figure 6.8a, bottom row). Correspondingly, rs16906115 status was associated with the magnitude of change in lymphocyte count post-sICB but not cICB (for sICB: non-carriers: -0.15x10^9 cells/L; IQR -0.38:0.02 versus carriers: -0.025x10^9 cells/L; IQR -0.11:0.36, p=0.023; Figure 6.8b).

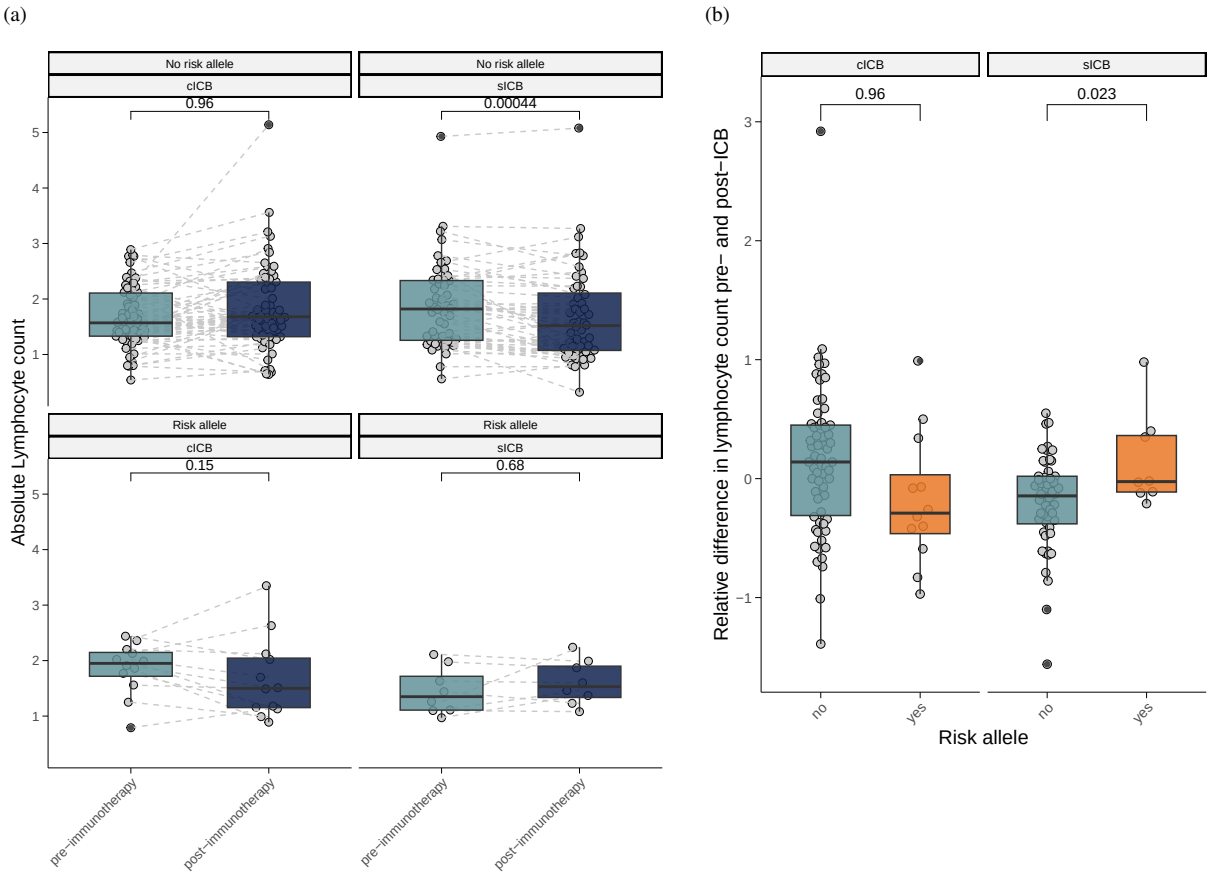


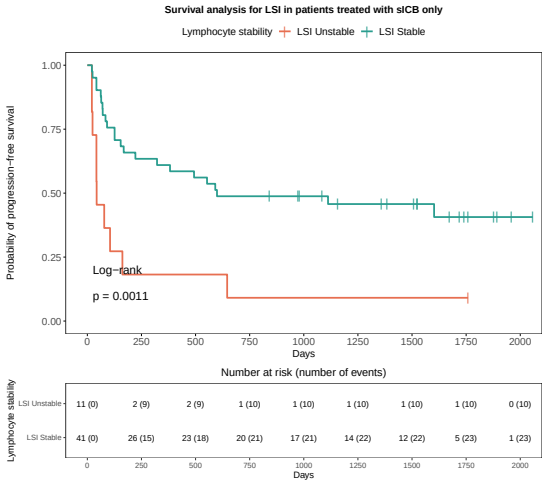
Figure 6.8. (a) Absolute lymphocyte count pre- and immediately post-ICB, faceted by genotype (presence/absence of risk allele) and treatment given. (b) Change in lymphocyte count from pre- and immediately post-ICB, coloured by genotype and faceted by treatment. Statistics with Wilcoxon signed rank test (a) or Wilcoxon rank sum test (b).

6.4.4 Lymphocyte stability predicts clinical outcome in discovery melanoma cohort

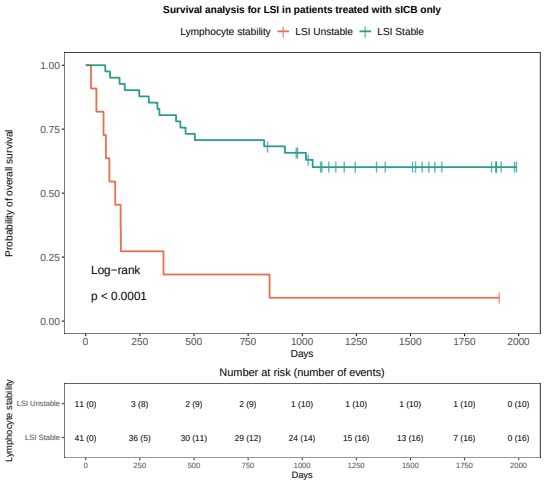
I wished to further explore lymphocyte stability, focussing on the lymphocyte stability index (LSI) - simply a ratio of first post-treatment lymphocyte count over the pre-treatment count. In order to determine a cut-off for classifying LSI as high or low, I performed a receiver operating characteristic (ROC) curve analysis using the *R* package *cutpointr*. This suggested an optimal cut-point of 0.80. Whilst this did not give a very impressive AUC (0.56), with a low sum of sensitivity+specificity, the sensitivity at this cut-point was 0.91. Additionally, in individuals whose LSI was <1, the median LSI was 0.80. As such, this was set as the cut-off.

I took individuals with MM who had not previously been treated with ipilimumab (n=111) and classified as either high or low LSI on the basis of this cut-off - i.e. if post-treatment lymphocyte count/pre-treatment lymphocyte count >0.8, that is 'stable LSI'. This resulted in a highly significant OS and PFS benefit (Figure 6.9) which was apparent for both sICB and cICB.

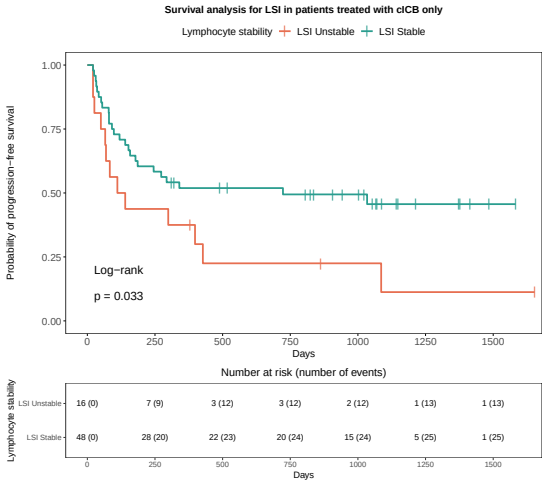
(a)



(b)



(c)



(d)

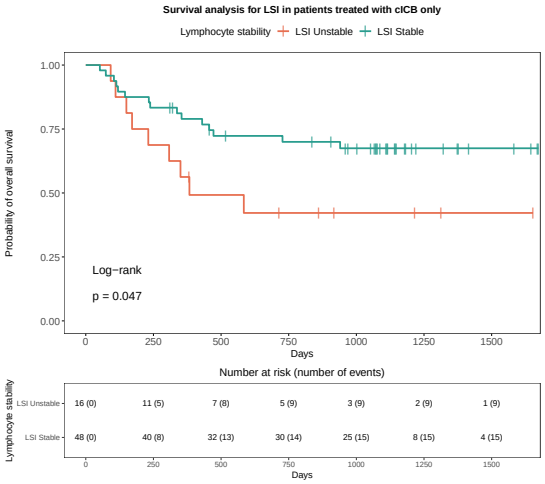


Figure 6.9. (a) Kaplan-Meier curve (KM) for progression-free survival (PFS) in patients with MM treated with sICB. (b) as per (a) but for overall survival (OS). (c) and (d) as per (a) and (b) but for patients treated with cICB. Statistics with Log-rank test.

6.4.5 Lymphocyte stability predicts clinical outcome in melanoma replication cohort and across multiple tumour types

In order to further investigate and validate this metric, I sought a larger data set and thus applied for HRA approval to obtain retrospectively-collected outcome data for all patients that received ICB for any indication at OUHFT since 2014 (see methods section 2.1.3, page 66). Following data cleaning and merging, there were 706 individual cases across a range of tumours (Table 6.3). Due to the nature of the data collection, I focussed solely on overall survival.

Tumour Type	Number of patients
colorectal	13
connective tissue	1
gynae	6
haematological	2
head&neck	14
melanoma	311
mesothelioma	15
NSCLC	184
renal	91
skin squamous	18
uGI	12
urothelial	39

Table 6.3. Patient numbers and tumour type for all individuals treated with ICB in OUHFT from 2014-2022 following data QC.

For melanoma, excluding the 111 patients from the discovery cohort, there were 200 patients, 62 treated with cICB, 85 with sICB and 53 treated with single-agent ipilimumab. There was a OS benefit based on LSI (defined with the 0.80 cut-off) across the whole validation cohort (Figure 6.10a). This was not significant for sICB alone, although the trend was maintained (Figure 6.10b) but was for cICB (Figure 6.10c). Pooling the melanoma discovery and validation cohorts together led to highly significant outcomes across all treatment types (Figures 6.10d-6.10f).

I next investigated the association with of LSI with NSCLC and mRCC. For NSCLC patients (all

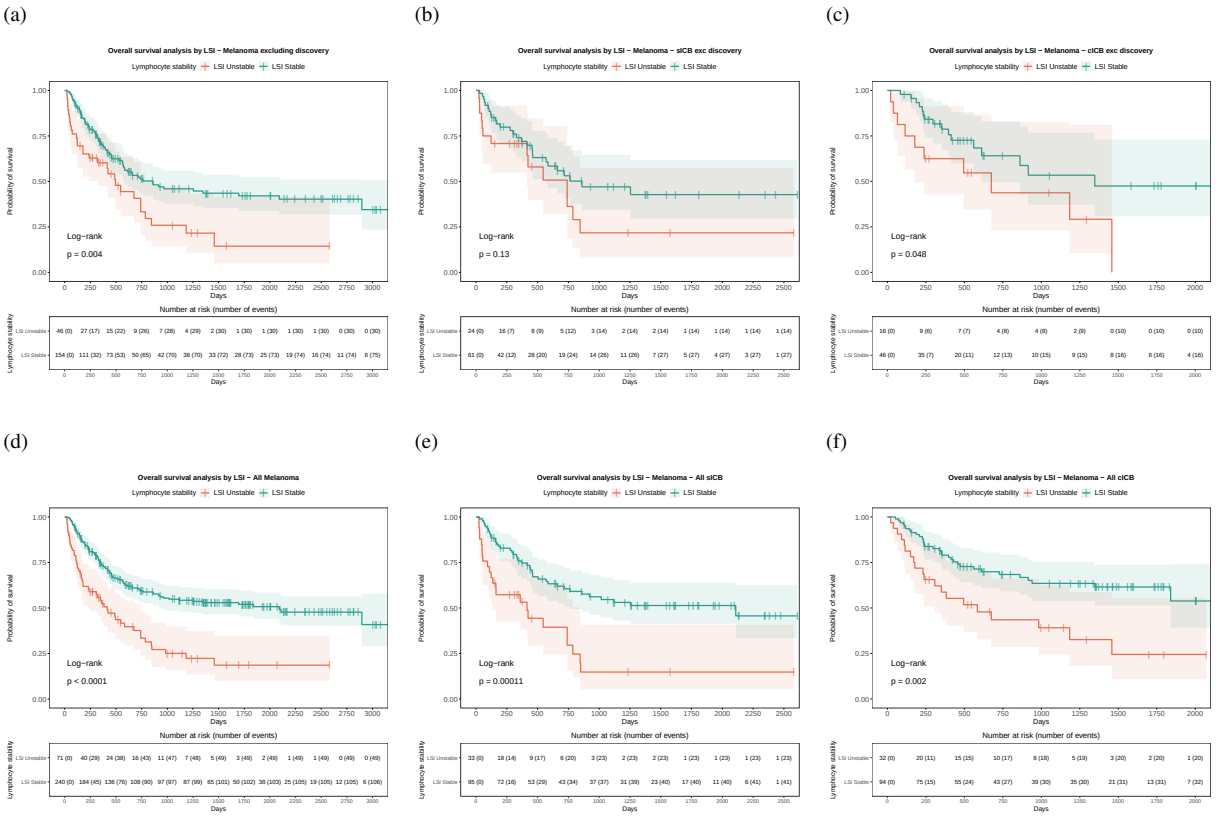


Figure 6.10. (a) KM survival curve for OS, dichotomsed on stable/unstable LSI (on cut-point of 0.80) in melanoma replication cohort (all treatments). (b) as per (a) but for sICB only. (c) as per (a) but for cICB only. (d-f) as per (a-c) but for pooled discovery and replication cohorts. Statistics with log-rank.

treated with sICB), there was a significant OS benefit of stable LSI using the cut-off of 0.80 (log-rank p=0.024, plot not shown). However, given that NSCLC is a separate tumour type, I re-ran the ROC analysis. This gave an optimal cut-point of 0.95 (AUC 0.64). Using this cut-off resulted in an increase in effect, with greater statistical significance (log-rank p<0.001 for all treatments, Figure 6.11a). The majority (100/184) of patients with NSCLC received immunotherapy second line, following progression on first-line chemotherapy. This has the potential to affect lymphocyte counts, and so I analysed each of these subgroups separately. Notably, LSI was only associated with OS in those with NSCLC who had not received pre-treatment (Figure 6.11b), although the trend was still present in those with pre-treatment (Figure 6.11c). This same pattern was seen with the 0.80 LSI cut-off, albeit with reduced significance (log-rank for those with no pre-treatment,

p=0.025, plot not shown).

For mRCC, whilst there was no association with LSI and OS in all-comers, or those who had not received pre-treatment, LSI (cut-off 0.80) was associated with outcome in those who had received pre-treatment (Figure 6.11d-6.11f). Nonetheless, with the small sample size, large confidence intervals and modest p value (Figure 6.11f), I interpret this result with some caution. Further, re-doing the ROC analysis to generate an mRCC-specific cut-point gives a cut-off of 0.98 for LSI. Using this value, there is no statistically significant association between LSI and outcome for all patients with mRCC, those who received pre-treatment and those without pre-treatment (log-rank p values 0.097, 0.27 and 0.23 respectively, plots not shown). Nonetheless, there is a biological plausibility for the difference in those who have and have not received pre-treatment. In mRCC only those with IMDC intermediate or poor risk disease are given ICB first-line, whilst those with 'good' risk disease are eligible for other treatments - as such those with pre-treatment are more likely to have IMDC good prognosis disease.

There was no association between LSI and outcome for urothelial cancer and all other tumours combined (log-rank p=0.57 and p=0.4, respectively; plots not shown).

To control for confounding variables within the survival analysis, I performed a Cox proportional hazards analysis, controlling for key confounding variables. Primarily these were age, sex, other cancer diagnoses, whether pre-treatment was given or whether the patient previously received adjuvant treatment. Full details of the models used are given in Supplementary Table A.2 (page 272). For multiple tumours and subgroups a stable LSI carries a substantial and significantly reduced risk of hazard - e.g. for all melanoma patients, the HR is 0.38 (95% CI: 0.26-0.56, p<0.0001), (Figure 6.12, Supplementary Table A.2). Adjusting for confounding variables, there is a significant association between LSI and OS for NSCLC, regardless of pre-treatment. Similarly, LSI in mRCC with pre-treatment remains significantly associated with OS (Figure 6.12).

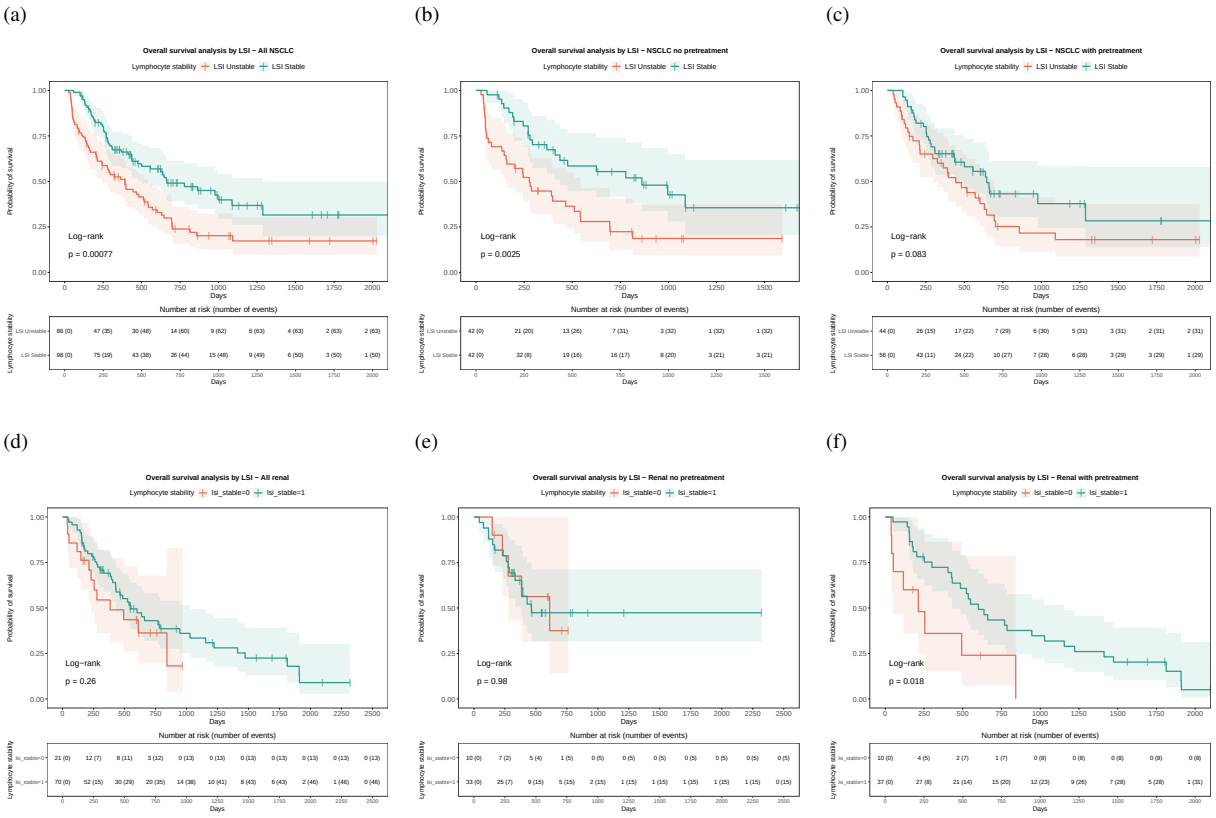


Figure 6.11. (a) KM survival curve for OS, dichotomsed on stable/unstable LSI (on cut-point of 0.95) in patients with NSCLC. (b) as per (a) but for patients who had not been pre-treated with chemotherapy. (c) as per (a) but for patients who had received pre-treatment with chemotherapy. (d-f) as per (a-c) but for mRCC. Statistics with log-rank.

6.4.6 LSI and outcome in a third cohort (Liverpool)

To further validate these findings, we collaborated with colleagues (Dr Anna Olssen-Brown) at Clatterbridge Cancer Centre, Liverpool, to collect a third set of data in NSCLC and MM. However, whilst the trends towards an association between LSI and OS persisted in this dataset, there were no significant differences between groups (Figure 6.13). No significant differences were seen for subgroups of NSCLC based on prior treatment or subgroups of MM based on ICB type received (plots not shown).

To understand the reasons for this lack of replication, I explored the data, finding no difference between the Oxford and Liverpool cohorts for LSI (Figure 6.14a). However, the time to death

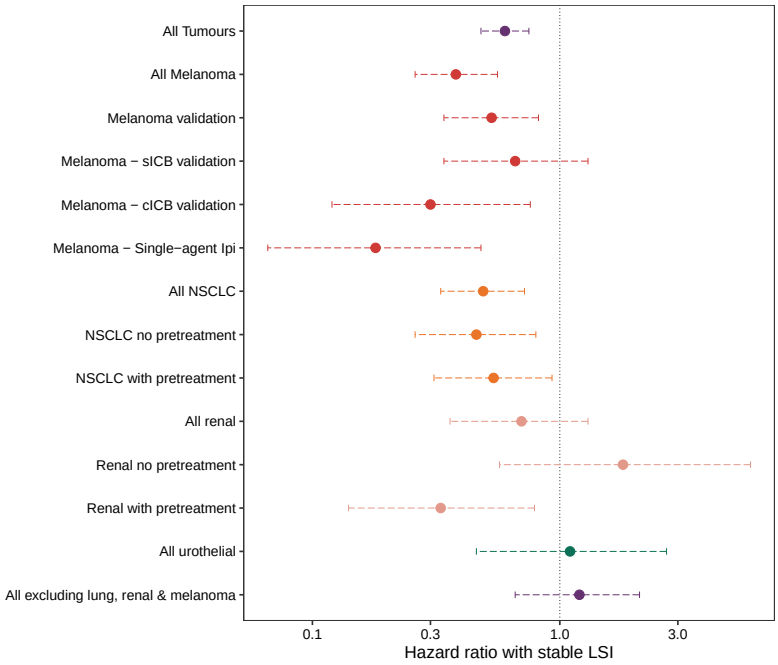


Figure 6.12. Hazard ratios for death for each tumour subgroup based on LSI. HRs generated via Cox proportional hazards, model as given in Supplementary Table A.2 (page 272). Whiskers represent 95% CI. For NSCLC the LSI cut-off is 0.95. For all other tumours, it is 0.80.

was slightly longer for patients with NSCLC in the Oxford cohort (Figure 6.14b) and follow-up time was significantly longer for both cancers in the Oxford cohort (Figure 6.14c). Given that the outcome is OS this could be an explanation for lack of detected effect significance. Further, the metastatic melanoma dataset from Liverpool comprised only 50 patients, and could therefore be underpowered. I thus decided to pool all Oxford and Liverpool data together - finding a highly significant association between LSI and OS across both MM and NSCLC for all-comers across both centres (Figure 6.15).

6.4.7 LSI may enable improved patient stratification

Finally, I wished to understand if LSI could aid in patient stratification following just one cycle of ICB. I therefore categorised all MM patients into four groups - LSI stable or unstable and cICB or sICB (Figure 6.16a). Whilst those with unstable LSI and sICB had the poorest outcomes,

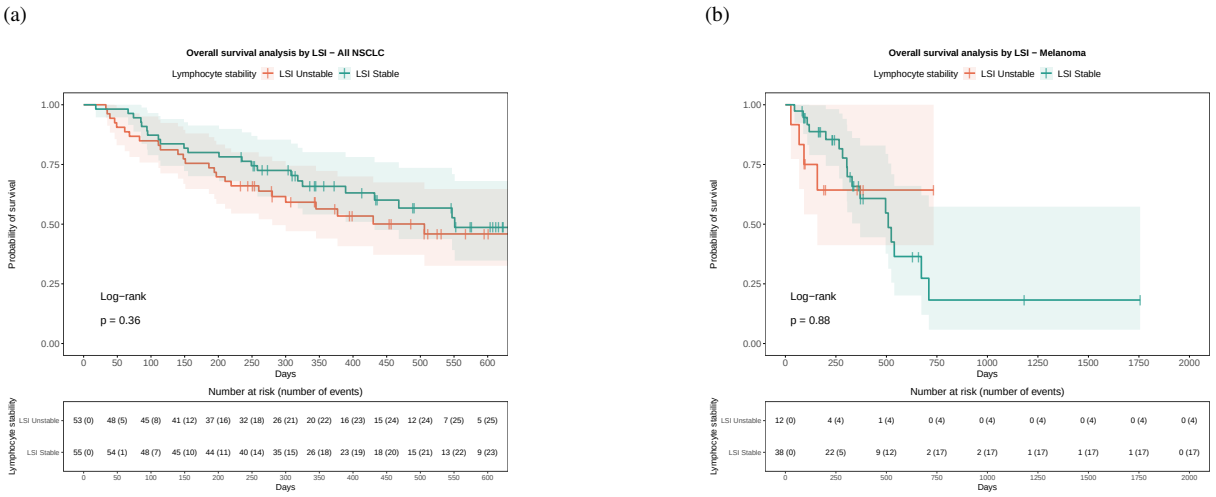


Figure 6.13. (a) Kaplan-Meier curve (KM) for overall survival (OS) in patients with NSCLC treated with sICB in Liverpool replication cohort, dichotomised by LSI (cut-off 0.95). (b) as per (a) but for patients with MM treated with sICB, cICB and single-agent ipilimumab; LSI cut-off 0.80. Statistics with log-rank test.

there was no difference between those with a stable LSI treated with sICB and those treated with cICB - the hazard ratio for those who received sICB and had a stable LSI compared to those who got cICB, with stable LSI is 1.02 (95% CI 0.61-1.55, p=0.91, Table 6.16b). Conversely, those who had unstable LSI - even if they were treated with cICB - had much higher hazard of death compared to those who had sICB with a stable LSI (HR 0.49, 95% CI 1.16-3.54, p<0.001, Table 6.16b).

6.4.8 Section summary

Working with colleagues in the Fairfax lab, I was able to replicate findings that the minor allele at rs16906115 led to increased odds of irAEs following ICB in melanoma. Further, I was able to describe the effect that carriage of the minor, risk, allele had on T cell subsets following ICB - namely a gain in T_{effs} and reduction in naive cells, primarily in CD8⁺ T cells. Further, carriers of the minor allele had repertoire skewing with a greater number of large clones and fewer smaller clones. There was also a genetic effect on lymphocyte stability - with carriers of the SNP having a stable lymphocyte count from pre- to post-ICB. Following up on this observation, I investigated

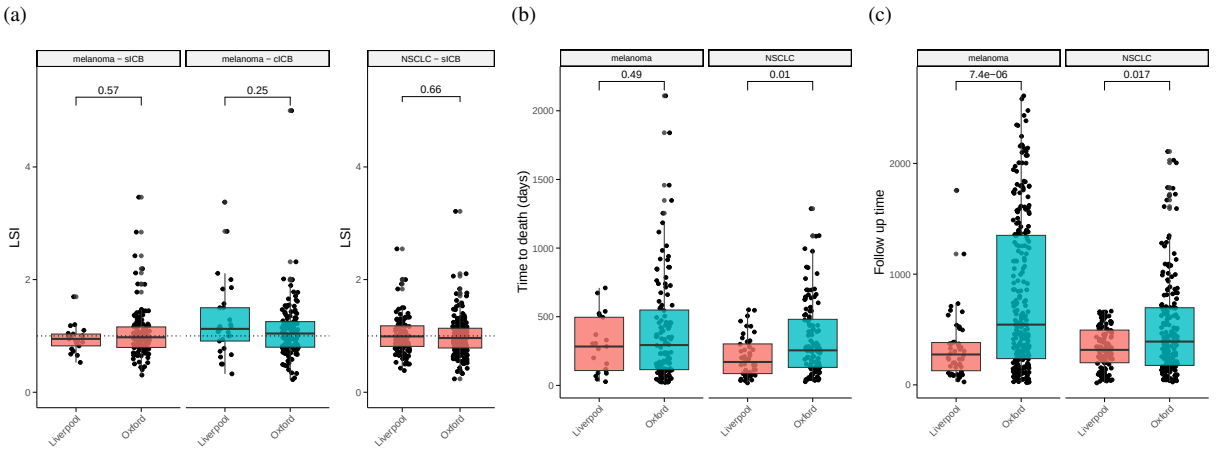


Figure 6.14. (a) LSI for Liverpool and Oxford cohorts, faceted by tumour type and treatment. (b) Time to death for Liverpool and Oxford cohorts, faceted by tumour type. (c) Follow-up time for Liverpool and Oxford cohorts, faceted by tumour type. Statistics with Wilcoxon rank sum test.

the clinical implications of the lymphocyte stability index (LSI), showing that in patients with MM, a stable LSI was associated with significantly improved progression-free survival (PFS) and overall survival (OS). This finding validated in a separate cohort of patients with MM and replicated across patients with NSCLC and those with mRCC who received ICB second-line. Whilst this did not replicate in a smaller, immature, cohort from Liverpool, the highly significant association remained when all data was pooled. Importantly, those who received sICB with a stable LSI had an OS equivalent to those receiving cICB with stable LSI and significantly superior to those with unstable LSI, regardless of treatment.

6.5 Discussion

In this chapter, I have examined T cell repertoire features and genetic mechanisms of irAEs, taking these molecular findings and applying them to develop a potential dynamic biomarker. This chapter consists of two distinct work streams, based around the core aim of gaining further insight into the mechanisms of irAEs and applying these findings clinically. In the first part

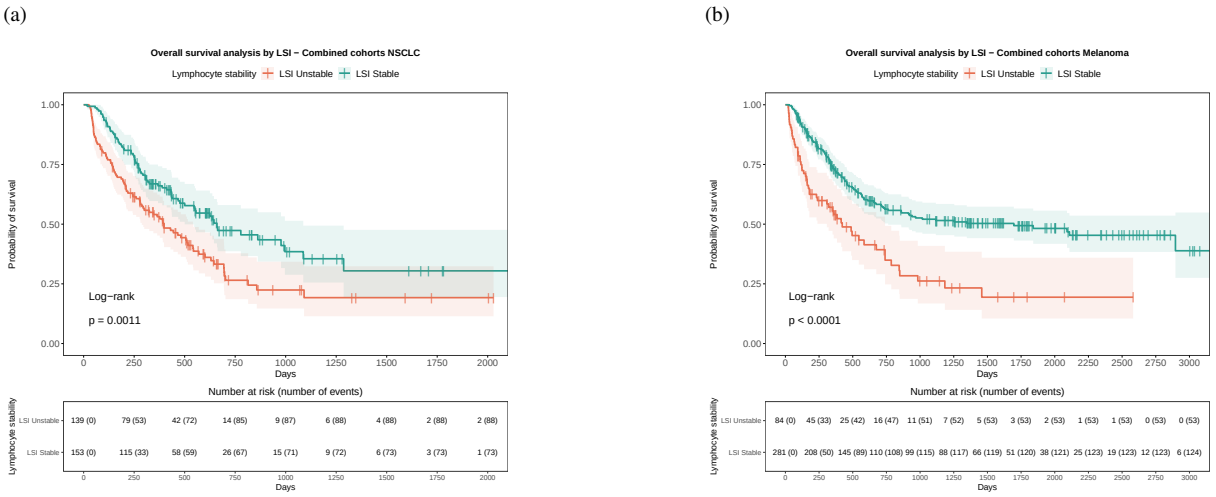
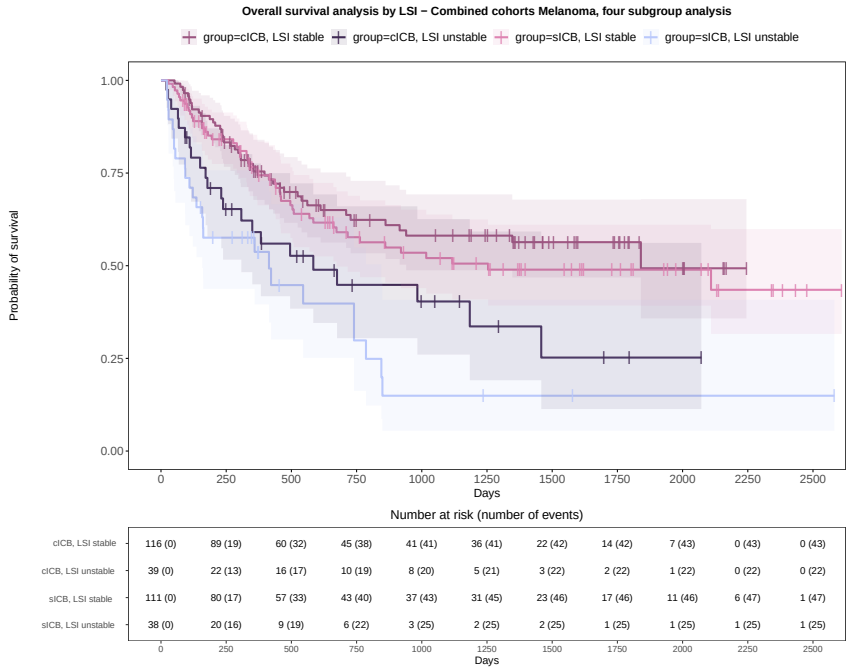


Figure 6.15. (a) Kaplan-Meier curve (KM) for overall survival (OS) in patients with NSCLC treated with sICB across the combined Liverpool and Oxford cohorts, dichotomised by LSI (cut-off 0.95). (b) as per (a) but for patients with MM treated with sICB, cICB and single-agent ipilimumab; LSI cut-off 0.80. Statistics with log-rank test.

of this chapter, I explored three cases of extreme myositis with myocarditis, observed in the context of the Covid-19 booster campaign. These caught our attention because whilst myocarditis following ICB therapy is well-described[42,266,267], so is an association with mRNA Covid-19 vaccines[257–260]. Cardiomyocytes express high levels of PD-L1 which is upregulated in the context of myocardial injury, serving to abrogate severe myocarditis[268–272]. Expression of mRNA vaccine-derived antigen in muscle triggers local inflammation, which may elicit a degree of muscle autoimmunity. In the context of subsequent early anti-PD-1 treatment, the physiological feedback through PD-L1:PD-1 ligation and peripheral tolerance mechanisms preventing development of systemic autoimmunity may be overcome.

I investigated these cases due to a hypothesis that they represented the consequence of *de novo* anti-PD-1 infusion post-boost vaccination - a suspicion based on the above background, and an observed increase in incidence of myocarditis post-ICB that has been reported by others since the beginning of the Covid-19 pandemic[273]. I report a striking degree of overlap between tissue sites of the three affected patients, which is significantly greater than the overlap observed between unrelated control tissue samples. Further, when adjusting for counts of each clone, there appeared

(a)



(b)

Comparators: sICB stable vs:	HR	95% CIs	p value
cICB stable	0.97	0.61-1.55	0.91
cICB unstable	2.03	1.16-3.54	<0.001
sICB unstable	2.47	1.52-4.04	0.013

Figure 6.16. (a) Kaplan-Meier curve (KM) for overall survival (OS) in patients with MM treated with sICB and cICB across both Liverpool and Oxford cohorts, grouped by both treatment and LSI. The pink colours represent stable LSI and the blues unstable LSI, with darker colours cICB and lighter colours sICB. (b) HRs and 95% CIs for comparisons of groups using cox proportional hazards. The index is sICB, stable LSI, with HRs representing the hazard associated with having the status in the comparator column (e.g. sICB, unstable LSI has 2.5 times hazard of death when compared to the index sICB, stable LSI). The model used is Surv(follow-up time, death status) ∼ treatment and LSI groups + age + sex + presence of multiple cancer diagnoses + number of lines of treatment given.

to be enrichment for spike-specific clones in the skeletal muscle, compared to the peripheral blood, of one patient on whom we had paired samples. Whilst this work is lacking the *in vitro* experiments proving that key expanded clones identified within tissues are cross-reactive to, or stimulated by exposure to the spike protein, the striking repertoire similarities lend credence to this postulation.

In the second half of the chapter, I outline my contributions to work describing the molecular mechanisms underpinning the observed association between a polymorphism at rs16906115 and increased risk of irAEs. The finding that this is due to increased expression of *IL7* by B cells, with pleiotropic effects not just on B cells but also on both CD4⁺ T cells and CD8⁺ T

cells, has fundamental implications for tumour immunology. Firstly, it shines a spotlight on IL-7 - previously mooted as a potential therapeutic target[274,275]- as a key player in the immune response following ICB and justifies further work understanding the pathways associated with its expression. Secondly, it highlights the important role of B cells in the tumour-specific immune response. Thirdly, given the role of B cells, and their effect on T cells, it supports work suggesting the importance of tertiary lymphoid structures (TLS)[103,104]. Finally, it validates a number of approaches undertaken in this thesis - demonstrating the power of genetic, transcriptomic and TCR analysis of peripheral blood to derive meaningful insights into cancer immunology.

This final point is further vindicated by the observation that LSI significantly correlates with outcome across multiple tumour types - leading to the description of a novel, on-treatment, peripheral biomarker for response to ICB. The fact that patients who received sICB (with a toxicity rate approximately one third that of cICB) and had stable LSI did just as well as those who received cICB with stable LSI and had significantly better outcomes than those with unstable LSI, regardless of treatment, provides a unique opportunity for patient stratification and rationalisation of treatments. Given the markedly safer toxicity profile of sICB - and the ability to schedule pembrolizumab six-weekly - it would be the treatment of choice, were its response rate equivalent to cICB. By incorporating LSI it may be possible to tell - 21 days post-ICB - which patients can expect an equivalent response and thereby maintain them on the less-toxic sICB. This approach would need to be robustly tested in a prospective randomised study but, if proven, would have the potential to change the treatment paradigm of ICB in MM and radically reduce toxicities from this treatment.

6.5.1 Conclusion

In conclusion, by studying irAEs at both a patient-specific and broader cohort level, I have been able to derive meaningful findings which have the potential to inform both basic immunological understanding and clinical practice.

7 | Discussion

7.1 Summary of key findings

I set out to examine transcriptional and repertoire changes in peripheral $CD8^+$ T cells over time in order to investigate molecular and clonal responses to immune checkpoint blockade (ICB) and describe clinically-applicable biomarkers for outcome and immune-related adverse events (irAEs).

In Chapter 3, the first results chapter, I focussed on early changes in peripheral $CD8^+$ T cells following ICB at a single-cell level. By analysing data from eight patients with metastatic melanoma (MM) at baseline and 21 days after receiving ICB, I showed that gene expression changes following ICB diverge as a result of $CD8^+$ T cell clone size, with clones occupying >0.5% of the peripheral repertoire (large clones) modulating markedly more genes with treatment than small clones (those occupying $\leq$0.5%). Further, large clones were more cytotoxic and more likely to persist long term in the peripheral blood. Comparing to similar scRNAseq data from a cohort of individuals with metastatic renal cell carcinoma (mRCC), I replicated these findings across tumour types, with clone size shown to affect gene expression following ICB in mRCC and larger clones having a more cytotoxic gene expression profile. There were limited differences in gene expression of effector T cells (T_{effs}) pre-treatment between MM and mRCC. Applying the cytotoxicity score to a large cohort of patients with bulk RNAseq demonstrated that the baseline, *a priori*, cytotoxicity of $CD8^+$ T cells was significantly correlated with PFS in MM.

In Chapter 4, the second results chapter, I turned my attention to early and late repertoire changes following ICB. Primarily, I wished to follow up on two observations. Firstly, from my single cell analysis in Chapter 3, that clones that are stable/expanding from baseline to day 21 are more

cytotoxic than those that involute, whilst those that are 'novel' at 21 days are equally cytotoxic as all other clones. Secondly, the fact that the number of large clones at day 21, but not baseline, correlates with clinical response[93]. The combination of these findings suggested that following ICB there may be selective expansion of key clones responsible for mediating the anti-cancer effect. I hypothesised that a subset of these might be shared between individuals, and that I could detect these in the peripheral blood.

To investigate this, I performed bulk TCRseq on 364 samples, primarily peripheral $CD8^+$ T cells but also $CD4^+$ T cells and resected tumour, from 139 individuals (43 healthy donors and 96 patients with MM). Firstly, I explored repertoire metrics and demonstrated that the Gini coefficient, of both the entire repertoire and just large clones, following ICB associated with clinical outcome. The Gini of TCRα and TCRβ chains significantly correlated and there is concordance between the repertoires of $CD4^+$ memory T cells and $CD8^+$ T cells, but not $CD4^+$ naive cells. Focussing on $CD8^+$ T cell TCRβ chains, I used the *GLIPH2* algorithm[188] to cluster TCR into 'specificity groups' of putative shared antigen specificity. Filtering for groups containing expanded TCR from at least three individuals, I then identified those that significantly increased in size primarily in responders to treatment - calling these Emergent Responder Specificity Groups (ERSGs) and their member clones Emergent Responder (ER) clones. These ER clones significantly associated with outcome in the discovery cohort - not just post-treatment, following expansion - but at baseline. ER clones are large, cytotoxic and of memory phenotype, as well as demonstrating HLA specificity. Filtering for HLA-restricted ER clones maintained the association with response whilst reducing the list of key clones to just several dozen. Further, ER clones were found to be enriched and expanded within resected tumours pre-treatment and persist long term in the peripheral blood. Finally, these findings validated in two replication cohorts - a peripheral blood dataset from our group and a public TIL dataset.

Intrigued by the phenomenon of long-term clonal persistence - including of putative key clones such as ER clones, as identified in my TCRseq work, I wished to further understand long-term clonal changes at a molecular level. In Chapter 5, I presented the results of scRNAseq of both transcriptomes and TCR receptors across a cohort of 18 patients with MM and two HDs. 10 patients with MM had an ongoing CR following single-agent PD-1 blockade (sICB) and blood was sampled many years after cessation of ICB. Using this dataset, I first examined changes in abundance over time. Using *Milo*[228] to perform DA tests at a cell neighbourhood (sub-cluster) level, I found a long-term increase in abundance of a group of cells with a highly cytotoxic, 'killer-like' phenotype. Examining patterns of expression of the genes differentially upregulated by this neighbourhood of cells across multiple samples demonstrated that in those with a CR to treatment, there is a modest but significant increase in expression of this killer phenotype over time, which is not seen in patients with PD or in HDs. Further, increases in expression of so-called killer genes over time were evident across a much larger cohort of bulk RNAseq data. Examining clonal dynamics over long term demonstrated remarkable clonal stability, with baseline highly-expanded clones remaining stable and of similar size for many years. Surprisingly, clones which expand from pre- to post-ICB, are large (occupying >0.5% of the repertoire) at the post-treatment time point and persist long term (which I term large expanding persistent (LEP) clones) are primarily made up of cytotoxic effector cells and have a gene expression profile consistent with a recently-described subset called long-lived effector cells (LLECs)[248]. They markedly upregulate gene sets shown by others to be associated with tumour specificity and cytotoxicity, and this transcriptional change remains elevated above baseline for years post-cessation of ICB.

Finally, in Chapter 6, the fourth results chapter, I investigated molecular and clonal changes in the context of irAEs. In the first section of this chapter, I performed TCRseq on peripheral blood and tissue samples taken from three individuals with severe myocarditis and myositis. These cases were unusual in their extreme severity and clustering around the time of introduction of the

Covid-19 booster vaccine. They demonstrated high levels of repertoire overlap, significantly in excess of that seen between control samples. Further, when adjusting for number of chains, there was a marked increase in TCR described to recognise the Spike protein of SARS-CoV-2 virus in public datasets.

The second half of Chapter 6 focussed on the T cell effects of carriage of an SNP at rs16906115 - intronic to *IL7*. I firstly replicated an observed association between this allele and the development of irAEs following ICB, before showing that carriers of this polymorphism had changes to their $CD8^+$ T cell subsets and clonal repertoires. Further, those with the minor allele had stable lymphocyte counts from pre-treatment to post-treatment, a finding I subsequently followed up in a larger dataset, describing the lymphocyte stability index (LSI) and showing that a stable LSI strongly associates with both improved PFS and OS across multiple tumour types.

7.2 Importance of results in the context of existing literature

Understanding the key $CD8^+$ T cell states in response to cancer is a key question which the field continues to try to unpick, alongside the fine molecular detail as to the effects of ICB on the $CD8^+$ T cell compartment. There are conflicting theories of the primary site of action ICB: many maintain the dogma that it mostly acts on the TI cohort[63,77], whilst a contrasting notion, emphasising the role of mobilisation of extra-tumoural $CD8^+$ T cells, is increasingly gaining popularity[74]. Importantly, these two models are not mutually exclusive. In a widely-cited 2020 review overseen by Ton Schumacher on this topic[67], the authors write *"it remains to be established whether ICB primarily reinvigorates a tumour-resident T cell population or also acts through mobilization of T cells from outside the tumour"*. In their article, the authors go on to define a 'dysfunctional' state which most closely resembles tumour-reactive $CD8^+$ T cells[67] (see Figure 1.3; gene list is given in Table A.1). In my single cell data (Chapter 5) I note that in patients with a

CR, there is an increase in the proportion of $CD8^+$ T cells with the tumour-reactive/'dysfunctional' gene expression - suggesting post-treatment expansion, potentially following mobilisation, of this 'dysfunctional' cohort, suspected of being TI cells that recognise tumour. As such, these findings therefore support the more 'traditional' site of action of ICB - i.e. on the tumour-resident population. Other results in this thesis are similarly aligned with this theory. My novel finding that the transcriptional response is dependent on $CD8^+$ T cell clone size (Chapter 3), with large expanded clones highly susceptible to the effects of ICB, is consistent with the notion that the key cellular targets of ICB have been in contact with tumour antigen (i.e. have been in the TME) in order to both have become enlarged and primed for re-invigoration. Further, my discovery that key expanding clones post-ICB can be found in the tumour an average of six months prior to treatment (Chapter 4) suggests that TILs are being affected by treatment.

Nonetheless, the vast majority of my samples are peripheral blood - i.e. tumour-extrinsic - and therefore many of my findings are entirely consistent with a model whereby following ICB there is increased activation and mobilisation of tumour-extrinsic clones[74]. In Chapters 3 and 5, I demonstrate transcriptional changes and increases in cytotoxicity being observed in peripheral $CD8^+$ T cells, suggesting significant effects of ICB on circulating clones. Additionally, my results in Chapter 4, illustrating the significant and highly-relevant expansion of key response clones in the peripheral blood, support the notion of peripheral expansion of critical tumour-extrinsic $CD8^+$ T cells. Whilst I cannot definitively say whether these peripheral clones traffic to tumours, they are frequently shown to upregulate tissue-homing markers and the fact that I am able to find such significant changes in the periphery suggests a degree of recirculation of key clones.

I therefore propose a hybrid model, postulating that following ICB not only do tumour-extrinsic clones become activated and *ingress* into tumours, pre-existing TIL similarly are invigorated and *egress*, mobilise and circulate - potentially via supportive TLS - before likely returning

to the tumour. I hypothesise that we are able to sample key cells from both 'sides' - i.e. those tumour-extrinsic on their way towards the cancer, and those tumour-intrinsic on their way out - as they pass through the peripheral blood. The fact that I find increases in TIL gene signatures in peripheral large clones post ICB (Chapter 5) supports this hypothesis, as do my findings of repertoire changes, flux and upregulation of tissue trafficking markers post-ICB. Further, I find increases in a 'dual-expanded' gene signature in peripheral clones[92] - consistent with the theory that these are enlarged in both the periphery and the TME, and very possibly recirculating between the two compartments. What is particularly remarkable, and is an entirely novel finding, is that many of the initial transcriptomic changes, including substantial increases in cytotoxicity score and tumour reactivity score, endure for the very long term following treatment - indeed for several years after the removal of the drug. It is possible that - in the case of a complete response - the ongoing recirculation and mobilisation of key clones only needs to be set in motion by ICB in order for the loop to continue autonomously.

Others have previously observed and reported long term persistence and maintenance of clone size following ICB in MM and NSCLC[70,164]. However, the transcriptional profiles of these cells were hitherto not described and had relied previously on clone-matching to TILs. Very recent work has suggested that a good response to PD-1 blockade in MM is the result of polyclonal expansion and T cell targeting - by clones present in both the tumour and peripheral blood - of a restricted set of antigens recurrently over time[252]. This lends credence to the theory that observed maintenance of large expanded clones is due to ongoing tumour ligation. However, to my surprise, I found that long term persistent clones had a highly cytotoxic phenotype - rather than a memory or exhausted one - over many years. This profile was very similar to that of LLECs which have only recently been described[248]. However, not only are long-term persistent clones particularly cytotoxic, but further, over time in patients with a good response to ICB, there is a chronic increase in an extremely cytotoxic, killer-like, subset of cells. The fact that

this so-called 'killer-like' sub-cluster actually becomes more abundant in the long term is most curious and suggests either a cell-intrinsic or exogenous factor, or factors, that are maintaining and growing this subtype of cell. Further, transcriptomic signatures derived from this cluster were seen to increase in the long term in those with a CR but not in those with PD, suggesting that this expression profile might play a role in preventing recurrence.

However, these reflections pose some additional questions. What are the benefits to $CD8^+$ T cells of emigrating from tumours and recirculating, and what type of factors might be maintaining cytotoxicity in the long term? Whilst these should surely be the subject of further experiments (as discussed below - section 7.4), our work characterising the effects by which the minor allele at rs16906115 confers increased odds of developing irAEs uncovered the vital role played by B cell *IL7*. Increased *IL7* expression led to skewed T cell subsets and repertoires, contrasting gene expression, increased toxicity and improved outcomes in early melanoma (using public data). The finding that B cell expression of this cytokine is so important may provide the glue to stick a number of these disparate questions together. Could ICB-mediated mobilisation of both tumour-extrinsic and tumour-instrinsic $CD8^+$ T cell clones be resulting in increased movement to lymph structures - both nodes and TLS? Could this result in more B-T cell interactions and increased T cell exposure to B cell-derived IL-7 and other cytokines further re-invigorating ICB-exposed $CD8^+$ T cells? Perhaps this results in improved $CD8^+$ T cell survival and longevity - thus explaining the maintenance of large persistent clones in the relative absence of increased mitosis? Might prolonged exposure to cytokines such as IL-7, already known to play a key role in T lymphocyte maintenance and homeostasis[263–265], continue to drive a highly-cytotoxic killer-like phenotype, even in the face of recurrent antigen exposure? Does this, in individuals who have genetically-patterned high levels of B cell IL-7, lead to toxicity but also, when maintained, keep the malignancy in check long-term? Whilst primarily conjecture, this hypothesis (Figure 7.1) unifies a number of findings from all four results chapters of this thesis, is consistent with current

literature, and provides a possible molecular theory for how ICB kick-starts sustained, long term $CD8^+$ T cell responses.

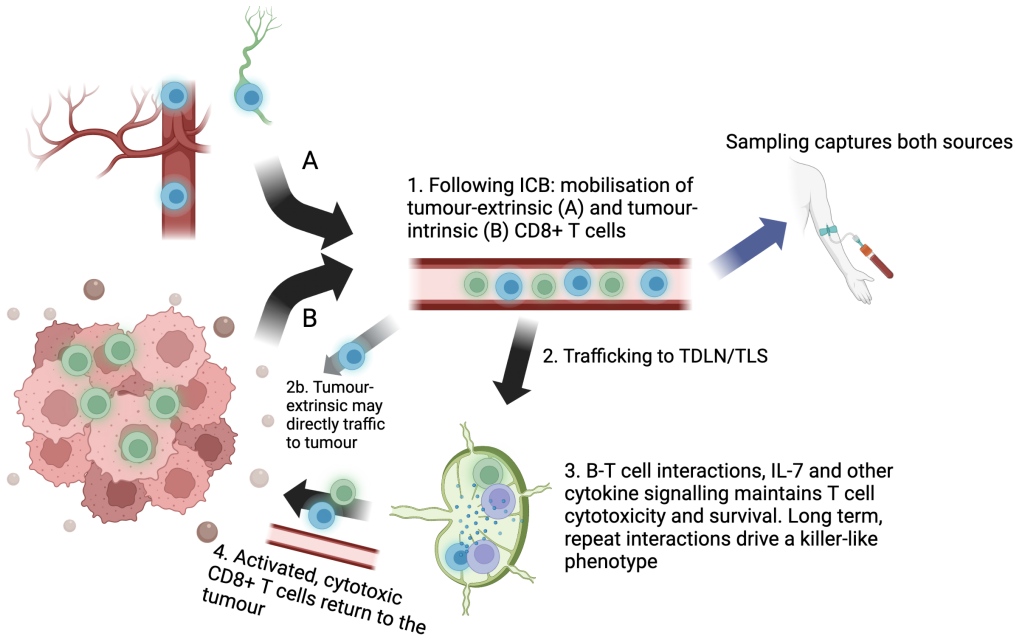


Figure 7.1. Cartoon of proposed model for T cell activation and persistence in the peripheral blood following ICB based on existing literature and novel findings in this thesis. In the case of a complete response, whilst the tumour recesses, the T cells can still be sampled as they recirculate between nodal tissues. Enlarged clones continue to be maintained in a large and highly cytotoxic state by as-yet unidentified factors. Created in *BioRender.com*.

Finally, my thesis has taken a relatively novel approach to antigen identification in cancer. Finding key, public, tumour-specific antigens and TCR is the aim of multiple investigators, who can take a variety of approaches including screening TCR with known peptide libraries[194,195]. However, I have taken the reverse approach, and by adapting methods previously used by others[188], started with individuals with a good response to treatment and aimed to identify key, expanding, TCR (Chapter 4). Whilst this tackles the question from an orthogonal direction, it is agnostic to *a priori* hypotheses about the relative importance of particular antigens. By focussing on TCR that are highly-public, these findings are of broader relevance, and this widespread applicability is demonstrated by the replication of these results in two separate cohorts. Using TCRseq I further explored the relationship between episodes of severe myositis with myocarditis and the Covid-19

vaccination. Whilst I was unable to definitively prove a link, there was an exceptionally high level of overlap between the repertoires of the three cases, potentially suggesting cross-reactivity between muscle antigens, melanoma and SARS-CoV-2, consistent with previous reports of ICB-associated myositis[42,266] as well as the observed association between Covid-19 disease and vaccination and myocarditis[258–260].

7.3 Strengths and weaknesses

There are a number of strengths of this work. Firstly, by using RNA sequencing, I have gained substantially more insight into both repertoire features and gene expression than would have been possible under previous technologies. For example, historically, immune receptors would be profiled simply using antibodies to the V(D)J genes, and/or traditional tetramer sorting approaches[276]. Further, gene expression profiling using real-time quantitative reverse transcription PCR (qRT-PCR) could only give limited insight into the expression of a small number of *a priori*-defined genes. By using NGS approaches, I have been able to agnostically profile thousands of genes per cell, as well as probe the immune repertoires in depth using the highly-variable CDR3 region to gain extremely granular clonal information. Further, I have used a combination of both single-cell and bulk approaches to provide a mix of cell-level detail, coupled with statistical power across a much wider cohort. When comparisons have been made between single-cell and bulk data, there is good concordance, suggesting that this approach is robust and valid. The sample size of the bulk RNAseq datasets mean that truly meaningful outcome analyses are possible.

Secondly, I have validated findings across further modalities - such as with flow cytometry and public datasets - to give confidence in the results. Thirdly, all experiments are conducted on human tissue samples in the target conditions, thus increasing external validity of the results. Together, the use of cutting-edge technologies, multiple orthogonal approaches and large cohort

mean that I have been able to generate a number of entirely novel and highly relevant insights into the effect of ICB, many of which have direct translational potential.

Nonetheless, it is important to recognise the limitations of this work. As acknowledged in the chapter-specific discussion sections, the descriptive and observational nature of the study design does not allow for causation to be assigned. Whilst HD controls have been used as a comparison in the TCRseq work (Chapter 4), due to the nature of the resource required for single-cell sequencing experiments, the control cohort of HDs for the scRNAseq work is limited to just two individuals, making it a challenge to draw meaningful comparisons between groups. Further, this thesis has focussed mostly on peripheral blood - this was an active decision based on the fact that not only is the TI compartment extremely well-studied whilst peripheral blood is relatively under-investigated, but also because findings from the peripheral blood are - practically speaking - more likely to have clinical utility. Nonetheless, the relative lack of intra-tumoural information, particularly at a single-cell level, is a limitation. Thirdly, there are some assumptions made - for example, that RNA expression correlates with protein expression and that the number of TCR RNA molecules correlates with number of T cells. However, these are normal experimental assumptions for this field and I have mitigated the risk of these being incorrect by validating across modalities - e.g. correlating clone size in bulk and single cell data (both in this thesis and in previously-published work - ref [93], extended data Figure 10) and demonstrating subset changes identified by sequencing on flow cytometry samples. Finally, whilst I have multiplexed samples to maximise power in the single-cell experiments, the total number of individuals remains low, particularly, for example, at some time points in the mRCC single-cell cohort. This increases the risk of inter-individual variation confounding results. However, again, I have tried to mitigate this impact by validating findings in a larger bulk dataset where possible.

7.4 Future directions

There are a number of ways to take these findings forward. Firstly, a clear next step is identification of the cognate antigens of ER clones. I have postulated that these clones are key mediators of the anti-melanoma immune response, and have presented an array of evidence to support this - however currently it is circumstantial. Proving that these TCR recognise melanoma-associated antigens would bring two major benefits. Firstly, it would validate my approach and demonstrate that this is an effective method to find cancer antigens and the TCR that recognise them. Secondly, it would potentially allow for the identification of high-value melanoma antigens which are successfully being ligated by human $CD8^+$ T cells in the context of a response to ICB. Such epitopes could form the basis of future vaccines or targeted immunotherapies - e.g. bispecific T cell engagers (BiTEs) - or the relevant TCR could be used in adoptive cell therapies. Alternatively, should key antigens be identified, high affinity peptide-tetramers could be used as an on- or pre-treatment biomarker to screen a patient's blood for the presence of key TCR. Aware of these possibilities, we are collaborating with colleagues in Oxford (Ricardo Fernandes and Julia McCarthy) who are adept at using yeast-based screening approaches to identify antigens (see introduction section 1.5.5, page 59).

Secondly, the identification of an LLEC-like highly cytotoxic phenotype in long term persistent clones and that increases over time in patients with a CR to ICB warrants further investigation. The mechanisms that drive, and potentially fix, this transcriptional programme over the very long term are not yet defined. Is there a master transcription factor driving this profile? What - if any - are the associated epigenetic features? Do these cells reside in a tissue (e.g. lymph) compartment and do they need help (e.g. from B cells, $CD4^+$ T cells or APCs) to survive in this state? How accurate is my postulated model, above (Figure 7.1)? These are key questions - the

answers to which are fundamentally important for anti-cancer immunology as well as potentially more generally. The fact that cells of this phenotype persist long term in HD blood samples may be a response to chronic viral infection (where this LLEC phenotype was first described[248]) and, as such, understanding their role in health and disease could have widespread applications.

Specifically for immuno-oncology, a key aim of adoptive cell transfer therapies, such as TIL therapy, is to furnish the host with T cells that will mediate tumour rejection. In TIL therapy, T cells are expanded and cultured *ex vivo* before being re-implanted - with response rates of up to 50% in melanoma[277–279]. Whilst traditionally TIL cultures were conducted for long duration (up to 36 days), and required screening for activation (i.e. IFNγ secretion following co-culture with HLA-matched melanoma cells), newer protocols using 'Young-TILs' have been developed to simplify the process. Here, TILs are simply co-cultured with IL-2 for 10-22 days to massively expand the population, before being re-infused[277,280]. Whilst the simplicity of the approach is an advantage, Young-TIL therapies - with non-specific expansion and no selection - represent a relatively blunt approach and whilst response rates are around 50%, there is clearly room for refinement of this nascent field. My current work, which describes a key transcriptional profile of long term clones in complete response, has direct relevance to this area. If an increased understanding can be gained of the cytokines and processes that pattern and fix this cell type, there would be an opportunity to translate this to TIL therapy and, during the expansion phase, pattern the TILs with the most effective phenotype and, ideally, one that would last long term. As such, understanding the properties of highly-cytotoxic long term persistent peripheral clones is of great pertinence and opens up a range of exciting future directions.

Thirdly, the identification of an association between carriage of the minor allele at rs16906115 and the development of irAEs, the fact that this polymorphism also appears to impact the natural history of melanoma and the discovery that the underlying mechanisms are mediated by the

expression of *IL7* in B cells lead to multiple avenues for further work. These findings have shone a spotlight on IL-7 as an important molecule in the anti-tumour immune response, a previously-considered drug candidate[274,275]. However, from our work, the main effects of IL-7 appear to be coming from the B cell expression, potentially occurring in lymph tissue such as TLS. Whilst simply giving IL-7 to patients may result in significant toxicity and would be a fairly crude approach, boosting overall *IL7* expression by B cells, particularly in those with a poor initial response to ICB might be a viable therapeutic strategy. As such, further work to understand the pathways determining IL-7 production and signalling in B and T cells is a logical next step.

Finally, I have described the LSI which appears to predict outcome following ICB in multiple cancer types. This metric was based on observations of differences in lymphocyte count pre- and post-ICB in individuals with and without the risk allele (rs16906115) and as such has a sound molecular and genetic basis. Given its simplicity, the fact that it derived from routine, NHS, blood tests and can be conducted rapidly and early in treatment, it has many characteristics of an 'ideal' biomarker[281]. It could potentially be used to stratify patients and identify those who - after just one cycle of ICB - are likely to derive benefit from sICB and those in whom cICB, and the increased risk of toxicity, is justified. As such, it has the potential to change the treatment paradigm in MM from the current, whereby cICB is the choice standard-of-care unless there is a relative contra-indication, to a model whereby standard-of-care is sICB with escalation in the context of unstable LSI. However, in order for such an approach to be acceptable, it would need validation in a robust, prospective, randomised controlled trial.

7.5 Concluding remarks

Whilst ICB has brought significant benefits to the field of immuno-oncology, there remain a range of unmet clinical needs including improved patient stratification, prediction and mitigation

of irAEs risk and a better understanding of - and therefore ability to manipulate - the molecular immunological mechanisms of these drugs. My DPhil, and this thesis, has sought to further advance this field and has shed new light on previously undescribed transcriptomic and clonal effects of ICB across a wide range of patients and multiple tumour types.

If I were to summarise three key conclusions from this work, they would be as follows:

1. *The baseline immune repertoire is key in determining future outcomes*. I have provided multiple pieces of evidence to support the conclusion that the *a priori* immune landscape is a crucial factor in determining future responses. I have shown that large clones are more susceptible to ICB, that key expanding clones are present at greater size pre-treatment in those with a good response and that highly-cytotoxic, long term persistent clones are present in the expanded state pre-treatment. This conclusion has important implications, as it suggests that future therapeutic approaches would be best served by focussing on antigen recognition, rather than additional strategies aimed at T cell activation. Further, if we can refine the definition of a "good pre-existing response", this could result in an ideal biomarker to ICB.

2. *Clones that persist long-term following a CR to ICB have a cytotoxic LLEC phenotype*. Contrary to the perceived wisdom that chronically-expanded clones have a memory or exhausted phenotype, I have shown that in the context of a CR to ICB, these clones actually have a highly cytotoxic, ‘killer-like’ gene expression profile, with a number of important implications as discussed above.

3. *The peripheral blood provides a fertile ground for investigation of responses to ICB with key response clones identifiable*. Throughout my DPhil, I have worked primarily on peripheral blood specimens and have been able to draw key insights into the response to ICB, including the identification of putatively key clones which are mediating tumour rejection. The study

of this tissue allows high-throughput approaches across large cohorts, allowing insights to be applied to large sample sizes.

Many of the findings from my DPhil are impactful in their own right, but they also ask new questions, the investigation of which is likely to yield even greater insight into the tumour-specific T cell response and provide answers as to how we can improve this. Whilst there is still progress to make, by using systematic molecular biology techniques and leveraging the power of large cohorts with carefully-annotated follow-up data, it is possible to meaningfully advance towards novel biomarkers and therapeutic approaches - and with that, improved quality and length of life for those with cancer.

References

1. *Nobel Prize in Physiology or Medicine 2018* Nature. https://www.nature.com/collections/gqznlfngkz (2022).
2. Larkin, J., Chiarion-Sileni, V., Gonzalez, R., *et al.* Five-Year Survival with Combined Nivolumab and Ipilimumab in Advanced Melanoma. *New England Journal of Medicine* **381,** 1535–1546 (17, 2019).
3. Ribas, A. & Wolchok, J. D. Cancer immunotherapy using checkpoint blockade. *Science* **359,** 1350–1355 (23, 2018).
4. Pardoll, D. M. The blockade of immune checkpoints in cancer immunotherapy. *Nature Reviews Cancer* **12,** 252–264 (2012).
5. Seidel, J. A., Otsuka, A. & Kabashima, K. Anti-PD-1 and Anti-CTLA-4 Therapies in Cancer: Mechanisms of Action, Efficacy, and Limitations. *Frontiers in Oncology* **8** (2018).
6. Chambers, C. A., Kuhns, M. S., Egen, J. G. & Allison, J. P. CTLA-4-mediated inhibition in regulation of T cell responses: mechanisms and manipulation in tumor immunotherapy. *Annual Review of Immunology* **19,** 565–594 (2001).
7. Qureshi, O. S., Zheng, Y., Nakamura, K., *et al.* Trans-Endocytosis of CD80 and CD86: A Molecular Basis for the Cell-Extrinsic Function of CTLA-4. *Science* **332,** 600–603 (29, 2011).
8. Wing, K., Onishi, Y., Prieto-Martin, P., *et al.* CTLA-4 Control over Foxp3+ Regulatory T Cell Function. *Science* **322,** 271–275 (10, 2008).
9. Tivol, E. A., Borriello, F., Schweitzer, A. N., *et al.* Loss of CTLA-4 leads to massive lymphoproliferation and fatal multiorgan tissue destruction, revealing a critical negative regulatory role of CTLA-4. *Immunity* **3,** 541–547 (1995).

10. Kuehn, H. S., Ouyang, W., Lo, B., *et al.* Immune dysregulation in human subjects with heterozygous germline mutations in CTLA4. *Science (New York, N.Y.)* **345,** 1623–1627 (26, 2014).

11. Selby, M. J., Engelhardt, J. J., Quigley, M., *et al.* Anti-CTLA-4 antibodies of IgG2a isotype enhance antitumor activity through reduction of intratumoral regulatory T cells. *Cancer Immunology Research* **1,** 32–42 (2013).

12. Bulliard, Y., Jolicoeur, R., Windman, M., *et al.* Activating Fc ɣ receptors contribute to the antitumor activities of immunoregulatory receptor-targeting antibodies. *The Journal of Experimental Medicine* **210,** 1685–1693 (26, 2013).

13. Simpson, T. R., Li, F., Montalvo-Ortiz, W., *et al.* Fc-dependent depletion of tumor-infiltrating regulatory T cells co-defines the efficacy of anti-CTLA-4 therapy against melanoma. *The Journal of Experimental Medicine* **210,** 1695–1710 (26, 2013).

14. Sharma, A., Subudhi, S. K., Blando, J., *et al.* Anti-CTLA-4 Immunotherapy Does Not Deplete FOXP3+ Regulatory T Cells (Tregs) in Human Cancers. *Clinical Cancer Research* **25,** 1233–1238 (15, 2019).

15. Quezada, S. A. & Peggs, K. S. Lost in Translation: Deciphering the Mechanism of Action of Anti-human CTLA-4. *Clinical Cancer Research* **25,** 1130–1132 (15, 2019).

16. Peggs, K. S., Quezada, S. A., Chambers, C. A., Korman, A. J. & Allison, J. P. Blockade of CTLA-4 on both effector and regulatory T cell compartments contributes to the antitumor activity of anti-CTLA-4 antibodies. *The Journal of Experimental Medicine* **206,** 1717–1725 (3, 2009).

17. Keir, M. E., Butte, M. J., Freeman, G. J. & Sharpe, A. H. PD-1 and its ligands in tolerance and immunity. *Annual Review of Immunology* **26,** 677–704 (2008).

18. Freeman, G. J., Long, A. J., Iwai, Y., *et al.* Engagement of the PD-1 immunoinhibitory receptor by a novel B7 family member leads to negative regulation of lymphocyte activation. *The Journal of Experimental Medicine* **192,** 1027–1034 (2, 2000).

19. Kinter, A. L., Godbout, E. J., McNally, J. P., *et al.* The common gamma-chain cytokines IL-2, IL-7, IL-15, and IL-21 induce the expression of programmed death-1 and its ligands. *Journal of Immunology (Baltimore, Md.: 1950)* **181,** 6738–6746 (15, 2008).

20. Kulpa, D. A., Lawani, M., Cooper, A., *et al.* PD-1 coinhibitory signals: the link between pathogenesis and protection. *Seminars in Immunology* **25,** 219–227 (31, 2013).

21. Fife, B. T., Pauken, K. E., Eagar, T. N., *et al.* Interactions between PD-1 and PD-L1 promote tolerance by blocking the TCR–induced stop signal. *Nature Immunology* **10,** 1185–1192 (2009).

22. Keir, M. E., Liang, S. C., Guleria, I., *et al.* Tissue expression of PD-L1 mediates peripheral T cell tolerance. *The Journal of Experimental Medicine* **203,** 883–895 (17, 2006).

23. Nishimura, H., Nose, M., Hiai, H., Minato, N. & Honjo, T. Development of lupus-like autoimmune diseases by disruption of the PD-1 gene encoding an ITIM motif-carrying immunoreceptor. *Immunity* **11,** 141–151 (1999).

24. Garcia-Diaz, A., Shin, D. S., Moreno, B. H., *et al.* Interferon Receptor Signaling Pathways Regulating PD-L1 and PD-L2 Expression. *Cell Reports* **19,** 1189–1201 (9, 2017).

25. Sen, D. R., Kaminski, J., Barnitz, R. A., *et al.* The epigenetic landscape of T cell exhaustion. *Science (New York, N.Y.)* **354,** 1165–1169 (2, 2016).

26. Francisco, L. M., Salinas, V. H., Brown, K. E., *et al.* PD-L1 regulates the development, maintenance, and function of induced regulatory T cells. *The Journal of Experimental Medicine* **206,** 3015–3029 (21, 2009).

27. Topalian, S. L., Taube, J. M., Anders, R. A. & Pardoll, D. M. Mechanism-driven biomarkers to guide immune checkpoint blockade in cancer therapy. *Nature Reviews Cancer* **16,** 275–287 (2016).

28. Dong, H., Strome, S. E., Salomao, D. R., *et al.* Tumor-associated B7-H1 promotes T-cell apoptosis: a potential mechanism of immune evasion. *Nature Medicine* **8,** 793–800 (2002).

29. Parsa, A. T., Waldron, J. S., Panner, A., *et al.* Loss of tumor suppressor PTEN function increases B7-H1 expression and immunoresistance in glioma. *Nature Medicine* **13,** 84–88 (2007).

30. Taube, J. M., Anders, R. A., Young, G. D., *et al.* Colocalization of inflammatory response with B7-h1 expression in human melanocytic lesions supports an adaptive resistance mechanism of immune escape. *Science Translational Medicine* **4,** 127ra37 (28, 2012).

31. Atkins, M. B., Lee, S. J., Chmielowski, B., *et al.* Combination Dabrafenib and Trametinib Versus Combination Nivolumab and Ipilimumab for Patients With Advanced BRAF-Mutant Melanoma: The DREAMseq Trial-ECOG-ACRIN EA6134. *Journal of Clinical Oncology: Official Journal of the American Society of Clinical Oncology* **41,** 186–197 (10, 2023).

32. Powles, T., Albiges, L., Bex, A., *et al.* ESMO Clinical Practice Guideline update on the use of immunotherapy in early stage and advanced renal cell carcinoma. *Annals of Oncology* **32,** 1511–1519 (1, 2021).

33. Albiges, L., Tannir, N. M., Burotto, M., *et al.* Nivolumab plus ipilimumab versus sunitinib for first-line treatment of advanced renal cell carcinoma: extended 4-year follow-up of the phase III CheckMate 214 trial. *ESMO open* **5,** e001079 (2020).

34. *Common Terminology Criteria for Adverse Events (CTCAE) | Protocol Development | CTEP* https://ctep.cancer.gov/protocolDevelopment/electronic_applications/ctc.htm (2022).

35. Yoest, J. M. Clinical features, predictive correlates, and pathophysiology of immune-related adverse events in immune checkpoint inhibitor treatments in cancer: a short review. *ImmunoTargets and Therapy* **6,** 73–82 (2017).

36. Ramos-Casals, M., Brahmer, J. R., Callahan, M. K., *et al.* Immune-related adverse events of checkpoint inhibitors. *Nature Reviews Disease Primers* **6,** 1–21 (7, 2020).

37. Xu, C., Chen, Y.-P., Du, X.-J., *et al.* Comparative safety of immune checkpoint inhibitors in cancer: systematic review and network meta-analysis. *BMJ (Clinical research ed.)* **363,** k4226 (8, 2018).

38. Haanen, J. B. a. G., Carbonnel, F., Robert, C., *et al.* Management of toxicities from immunotherapy: ESMO Clinical Practice Guidelines for diagnosis, treatment and follow-up. *Annals of Oncology: Official Journal of the European Society for Medical Oncology* **28,** iv119–iv142 (suppl_4 1, 2017).

39. Hommes, J. W., Verheijden, R. J., Suijkerbuijk, K. P. M. & Hamann, D. Biomarkers of Checkpoint Inhibitor Induced Immune-Related Adverse Events—A Comprehensive Review. *Frontiers in Oncology* **10** (2021).

40. Byrne, E. H. & Fisher, D. E. Immune and molecular correlates in melanoma treated with immune checkpoint blockade. *Cancer* **123,** 2143–2153 (S11 1, 2017).

41. Sandigursky, S. & Mor, A. Immune-Related Adverse Events in Cancer Patients Treated With Immune Checkpoint Inhibitors. *Current Rheumatology Reports* **20,** 65 (6, 2018).

42. Johnson, D. B., Balko, J. M., Compton, M. L., *et al.* Fulminant Myocarditis with Combination Immune Checkpoint Blockade. *New England Journal of Medicine* **375,** 1749–1755 (2016).

43. Ye, W., Olsson-Brown, A., Watson, R. A., *et al.* Checkpoint-blocker-induced autoimmunity is associated with favourable outcome in metastatic melanoma and distinct T-cell expression profiles. *British Journal of Cancer* **124,** 1661–1669 (2021).

44. Foster, C. C., Couey, M. A., Kochanny, S. E., *et al.* Immune-related adverse events are associated with improved response, progression-free survival, and overall survival for patients with head and neck cancer receiving immune checkpoint inhibitors. *Cancer* **127,** 4565–4573 (15, 2021).

45. Ikeda, T., Ishihara, H., Nemoto, Y., *et al.* Prognostic impact of immune-related adverse events in metastatic renal cell carcinoma treated with nivolumab plus ipilimumab. *Urologic Oncology: Seminars and Original Investigations* **39,** 735.e9–735.e16 (1, 2021).

46. Iwama, S., De Remigis, A., Callahan, M. K., *et al.* Pituitary expression of CTLA-4 mediates hypophysitis secondary to administration of CTLA-4 blocking antibody. *Science Translational Medicine* **6,** 230ra45 (2, 2014).

47. Damuzzo, V., Solito, S., Pinton, L., *et al.* Clinical implication of tumor-associated and immunological parameters in melanoma patients treated with ipilimumab. *OncoImmunology* **5,** e1249559 (1, 2016).

48. Subudhi, S. K., Aparicio, A., Gao, J., *et al.* Clonal expansion of CD8 T cells in the systemic circulation precedes development of ipilimumab-induced toxicities. *Proceedings of the National Academy of Sciences of the United States of America* **113,** 11919–11924 (18, 2016).

49. Oh, D. Y., Cham, J., Zhang, L., *et al.* Immune Toxicities Elicted by CTLA-4 Blockade in Cancer Patients Are Associated with Early Diversification of the T-cell Repertoire. *Cancer Research* **77,** 1322–1330 (15, 2017).

50. Valpione, S., Pasquali, S., Campana, L. G., *et al.* Sex and interleukin-6 are prognostic factors for autoimmune toxicity following treatment with anti-CTLA4 blockade. *Journal of Translational Medicine* **16,** 94 (11, 2018).

51. Patel, S. A. A. & Gooderham, N. J. IL6 Mediates Immune and Colorectal Cancer Cell Cross-talk via miR-21 and miR-29b. *Molecular cancer research: MCR* **13,** 1502–1508 (2015).

52. Tarhini, A. A., Zahoor, H., Lin, Y., *et al.* Baseline circulating IL-17 predicts toxicity while TGF-β1 and IL-10 are prognostic of relapse in ipilimumab neoadjuvant therapy of melanoma. *Journal for ImmunoTherapy of Cancer* **3,** 39 (15, 2015).

53. Refae, S., Gal, J., Ebran, N., *et al.* Germinal Immunogenetics predict treatment outcome for PD-1/PD-L1 checkpoint inhibitors. *Investigational New Drugs* **38,** 160–171 (2020).

54. Bins, S., Basak, E. A., El Bouazzaoui, S., *et al.* Association between single-nucleotide polymorphisms and adverse events in nivolumab-treated non-small cell lung cancer patients. *British Journal of Cancer* **118,** 1296–1301 (2018).

55. Khan, Z., Di Nucci, F., Kwan, A., *et al.* Polygenic risk for skin autoimmunity impacts immune checkpoint blockade in bladder cancer. *Proceedings of the National Academy of Sciences of the United States of America* **117,** 12288–12294 (2, 2020).

56. Groha, S., Alaiwi, S. A., Xu, W., *et al.* Germline variants associated with toxicity to immune checkpoint blockade. *Nature Medicine* **28,** 2584–2591 (2022).

57. Schneider, B. J., Naidoo, J., Santomasso, B. D., *et al.* Management of Immune-Related Adverse Events in Patients Treated With Immune Checkpoint Inhibitor Therapy: ASCO Guideline Update. *Journal of clinical oncology : official journal of the American Society of Clinical Oncology* **39,** 4073–4126 (2021).

58. Bai, X., Hu, J., Betof Warner, A., *et al.* Early Use of High-Dose Glucocorticoid for the Management of irAE Is Associated with Poorer Survival in Patients with Advanced Melanoma Treated with Anti–PD-1 Monotherapy. *Clinical Cancer Research* **27,** 5993–6000 (1, 2021).

59. Van Not, O. J., Verheijden, R. J., van den Eertwegh, A. J. M., *et al.* Association of Immune-Related Adverse Event Management With Survival in Patients With Advanced Melanoma. *JAMA Oncology* (27, 2022).

60. Raskov, H., Orhan, A., Christensen, J. P. & Gögenur, I. Cytotoxic CD8+ T cells in cancer and cancer immunotherapy. *British Journal of Cancer* **124,** 359–367 (2021).

61. Basu, R., Whitlock, B. M., Husson, J., *et al.* Cytotoxic T Cells Use Mechanical Force to Potentiate Target Cell Killing. *Cell* **165,** 100–110 (24, 2016).

62. Fu, Q., Fu, T.-M., Cruz, A. C., *et al.* Structural Basis and Functional Role of Intramembrane Trimerization of the Fas/CD95 Death Receptor. *Molecular Cell* **61,** 602–613 (18, 2016).

63. Fridman, W. H., Pagès, F., Sautès-Fridman, C. & Galon, J. The immune contexture in human tumours: impact on clinical outcome. *Nature Reviews Cancer* **12,** 298–306 (2012).

64. Tumeh, P. C., Harview, C. L., Yearley, J. H., *et al.* PD-1 blockade induces responses by inhibiting adaptive immune resistance. *Nature* **515,** 568–71 (2014).

65. Chen, D. S. & Mellman, I. Elements of cancer immunity and the cancer-immune set point. *Nature* **541,** 321–330 (18, 2017).

66. Simoni, Y., Becht, E., Fehlings, M., *et al.* Bystander CD8+ T cells are abundant and phenotypically distinct in human tumour infiltrates. *Nature* **557,** 575–579 (2018).

67. Van der Leun, A. M., Thommen, D. S. & Schumacher, T. N. CD8+ T cell states in human cancer: insights from single-cell analysis. *Nature Reviews Cancer* **20,** 218–232 (2020).

68. Tirosh, I., Izar, B., Prakadan, S. M., *et al.* Dissecting the multicellular ecosystem of metastatic melanoma by single-cell RNA-seq. *Science (New York, N.Y.)* **352,** 189–196 (8, 2016).

69. Li, H., van der Leun, A. M., Yofe, I., *et al.* Dysfunctional CD8 T Cells Form a Proliferative, Dynamically Regulated Compartment within Human Melanoma. *Cell* **176,** 775–789.e18 (2019).

70. Oliveira, G., Stromhaug, K., Klaeger, S., *et al.* Phenotype, specificity and avidity of antitumour CD8+ T cells in melanoma. *Nature* **596,** 119–125 (2021).

71. Osorio, J. C., Arbour, K. C., Le, D. T., *et al.* Lesion-Level Response Dynamics to Programmed Cell Death Protein (PD-1) Blockade. *Journal of Clinical Oncology: Official Journal of the American Society of Clinical Oncology* **37,** 3546–3555 (20, 2019).

72. Spitzer, M. H., Carmi, Y., Reticker-Flynn, N. E., *et al.* Systemic Immunity Is Required for Effective Cancer Immunotherapy. *Cell* **168,** 487–502.e15 (26, 2017).

73. Dammeijer, F., van Gulijk, M., Mulder, E. E., *et al.* The PD-1/PD-L1-Checkpoint Restrains T cell Immunity in Tumor-Draining Lymph Nodes. *Cancer Cell* **38,** 685–700.e8 (9, 2020).

74. Yost, K. E., Chang, H. Y. & Satpathy, A. T. Recruiting T cells in cancer immunotherapy. *Science* **372,** 130–131 (9, 2021).

75. McLane, L. M., Abdel-Hakeem, M. S. & Wherry, E. J. CD8 T Cell Exhaustion During Chronic Viral Infection and Cancer. *Annual Review of Immunology* **37,** 457–495 (26, 2019).

76. Kallies, A., Zehn, D. & Utzschneider, D. T. Precursor exhausted T cells: key to successful immunotherapy? *Nature Reviews Immunology* **20,** 128–136 (2020).

77. Huang, A. C., Postow, M. A., Orlowski, R. J., *et al.* T-cell invigoration to tumour burden ratio associated with anti-PD-1 response. *Nature* **545,** 60–65 (2017).

78. Watson, R. A., Tong, O., Cooper, R., *et al.* Immune checkpoint blockade sensitivity and progression-free survival associates with baseline CD8+ T cell clone size and cytotoxicity. *Science Immunology* **6** (2021).

79. Khan, O., Giles, J. R., McDonald, S., *et al.* TOX transcriptionally and epigenetically programs CD8+ T cell exhaustion. *Nature* **571,** 211–218 (2019).

80. Scott, A. C., Dündar, F., Zumbo, P., *et al.* TOX is a critical regulator of tumour-specific T cell differentiation. *Nature* **571,** 270–274 (2019).

81. Arce, L., Yokoyama, N. N. & Waterman, M. L. Diversity of LEF/TCF action in development and disease. *Oncogene* **25,** 7492–7504 (4, 2006).

82. Zhao, X., Shan, Q. & Xue, H.-H. TCF1 in T cell immunity: a broadened frontier. *Nature Reviews Immunology* **22,** 147–157 (2022).

83. Sade-Feldman, M., Yizhak, K., Bjorgaard, S. L., *et al.* Defining T Cell States Associated with Response to Checkpoint Immunotherapy in Melanoma. *Cell* **175,** 998–1013.e20 (1, 2018).

84. Miller, B. C., Sen, D. R., Al Abosy, R., *et al.* Subsets of exhausted CD8+ T cells differentially mediate tumor control and respond to checkpoint blockade. *Nature Immunology* **20,** 326–336 (2019).

85. Kurtulus, S., Madi, A., Escobar, G., *et al.* Checkpoint Blockade Immunotherapy Induces Dynamic Changes in PD-1-CD8+ Tumor-Infiltrating T Cells. *Immunity* **50,** 181–194.e6 (15, 2019).

86. Brummelman, J., Mazza, E. M. C., Alvisi, G., *et al.* High-dimensional single cell analysis identifies stem-like cytotoxic CD8+ T cells infiltrating human tumors. *The Journal of Experimental Medicine* **215,** 2520–2535 (1, 2018).

87. Siddiqui, I., Schaeuble, K., Chennupati, V., *et al.* Intratumoral Tcf1+PD-1+CD8+ T Cells with Stem-like Properties Promote Tumor Control in Response to Vaccination and Checkpoint Blockade Immunotherapy. *Immunity* **50,** 195–211.e10 (15, 2019).

88. Connolly, K. A., Kuchroo, M., Venkat, A., *et al.* A reservoir of stem-like CD8+ T cells in the tumor-draining lymph node preserves the ongoing antitumor immune response. *Science Immunology* **6,** eabg7836 (2021).

89. Gearty, S. V., Dündar, F., Zumbo, P., *et al.* An autoimmune stem-like CD8 T cell population drives type 1 diabetes. *Nature* **602,** 156–161 (2022).

90. Pai, J. A., Chow, A., Sauter, J. L., *et al. Regional and clonal T cell dynamics at single cell resolution in immune checkpoint blockade* 27, 2021.

91. Yost, K. E., Satpathy, A. T., Wells, D. K., *et al.* Clonal replacement of tumor-specific T cells following PD-1 blockade. *Nature Medicine* **25,** 1251–1259 (2019).

92. Wu, T. D., Madireddi, S., de Almeida, P. E., *et al.* Peripheral T cell expansion predicts tumour infiltration and clinical response. *Nature* **579,** 274–278 (2020).

93. Fairfax, B. P., Taylor, C. A., Watson, R. A., *et al. Peripheral CD8+ T cell characteristics associated with durable responses to immune checkpoint blockade in patients with metastatic melanoma* 2020.

94. Riaz, N., Havel, J. J., Makarov, V., *et al.* Tumor and Microenvironment Evolution during Immunotherapy with Nivolumab. *Cell* **171,** 934–949.e15 (2017).

95. Valpione, S., Galvani, E., Tweedy, J., *et al.* Immune awakening revealed by peripheral T cell dynamics after one cycle of immunotherapy. *Nature Cancer* **1,** 210–221 (2020).

96. Forde, P. M., Chaft, J. E., Smith, K. N., *et al.* Neoadjuvant PD-1 Blockade in Resectable Lung Cancer. *New England Journal of Medicine* **378,** 1976–1986 (2018).

97. Joshi, K., Robert de Massy, M., Ismail, M., *et al.* Spatial heterogeneity of the T cell receptor repertoire reflects the mutational landscape in lung cancer. *Nature Medicine* **25,** 1549–1559 (2019).

98. Lucca, L. E., Axisa, P. P., Lu, B., *et al.* Circulating clonally expanded T cells reflect functions of tumor-infiltrating T cells. *Journal of Experimental Medicine* **218** (2021).

99. Cha, E., Klinger, M., Hou, Y., *et al.* Improved Survival with T Cell Clonotype Stability After Anti-CTLA-4 Treatment in Cancer Patients. *Science Translational Medicine* **6,** 238ra70–238ra70 (2014).

100. Han, J., Zhao, Y., Shirai, K., *et al.* Resident and circulating memory T cells persist for years in melanoma patients with durable responses to immunotherapy. *Nature Cancer* **2,** 300–311 (2021).

101. Taylor, C. A., Watson, R. A., Tong, O., *et al.* IL7 genetic variation and toxicity to immune checkpoint blockade in patients with melanoma. *Nature Medicine* **28,** 2592–2600 (2022).

102. Colbeck, E. J., Ager, A., Gallimore, A. & Jones, G. W. Tertiary Lymphoid Structures in Cancer: Drivers of Antitumor Immunity, Immunosuppression, or Bystander Sentinels in Disease? *Frontiers in Immunology* **8,** 1830 (2017).

103. Cabrita, R., Lauss, M., Sanna, A., *et al.* Tertiary lymphoid structures improve immunotherapy and survival in melanoma. *Nature* **577,** 561–565 (2020).

104. Helmink, B. A., Reddy, S. M., Gao, J., *et al.* B cells and tertiary lymphoid structures promote immunotherapy response. *Nature* **577,** 549–555 (2020).

105. Havel, J. J., Chowell, D. & Chan, T. A. The evolving landscape of biomarkers for checkpoint inhibitor immunotherapy. *Nature Reviews. Cancer* **19,** 133–150 (2019).

106. Sankar, K., Ye, J. C., Li, Z., *et al.* The role of biomarkers in personalized immunotherapy. *Biomarker Research* **10,** 32 (18, 2022).

107. Coulie, P. G., Van den Eynde, B. J., van der Bruggen, P. & Boon, T. Tumour antigens recognized by T lymphocytes: at the core of cancer immunotherapy. *Nature Reviews. Cancer* **14,** 135–146 (2014).

108. Gjerstorff, M. F., Andersen, M. H. & Ditzel, H. J. Oncogenic cancer/testis antigens: prime candidates for immunotherapy. *Oncotarget* **6,** 15772–15787 (30, 2015).

109. Shukla, S. A., Bachireddy, P., Schilling, B., *et al.* Cancer-Germline Antigen Expression Discriminates Clinical Outcome to CTLA-4 Blockade. *Cell* **173,** 624–633.e8 (19, 2018).

110. Snyder, A., Makarov, V., Merghoub, T., *et al.* Genetic basis for clinical response to CTLA-4 blockade in melanoma. *The New England Journal of Medicine* **371,** 2189–2199 (4, 2014).

111. Van Allen, E. M., Miao, D., Schilling, B., *et al.* Genomic correlates of response to CTLA-4 blockade in metastatic melanoma. *Science (New York, N.Y.)* **350,** 207–211 (9, 2015).

112. Rizvi, N. A., Hellmann, M. D., Snyder, A., *et al.* Cancer immunology. Mutational landscape determines sensitivity to PD-1 blockade in non-small cell lung cancer. *Science (New York, N.Y.)* **348,** 124–128 (3, 2015).

113. Alexandrov, L. B., Nik-Zainal, S., Wedge, D. C., *et al.* Signatures of mutational processes in human cancer. *Nature* **500,** 415–421 (22, 2013).

114. McGranahan, N., Furness, A. J. S., Rosenthal, R., *et al.* Clonal neoantigens elicit T cell immunoreactivity and sensitivity to immune checkpoint blockade. *Science (New York, N.Y.)* **351,** 1463–1469 (25, 2016).

115. Biswas, D., Birkbak, N. J., Rosenthal, R., *et al.* A clonal expression biomarker associates with lung cancer mortality. *Nature Medicine* **25,** 1540–1548 (2019).

116. Le, D. T., Uram, J. N., Wang, H., *et al.* PD-1 Blockade in Tumors with Mismatch-Repair Deficiency. *The New England Journal of Medicine* **372,** 2509–2520 (25, 2015).

117. Le, D. T., Durham, J. N., Smith, K. N., *et al.* Mismatch repair deficiency predicts response of solid tumors to PD-1 blockade. *Science (New York, N.Y.)* **357,** 409–413 (28, 2017).

118. Sayaman, R. W., Saad, M., Thorsson, V., *et al.* Germline genetic contribution to the immune landscape of cancer. *Immunity* **54,** 367–386.e8 (9, 2021).

119. Shahamatdar, S., He, M. X., Reyna, M. A., *et al.* Germline Features Associated with Immune Infiltration in Solid Tumors. *Cell Reports* **30,** 2900–2908.e4 (3, 2020).

120. Chowell, D., Morris, L. G. T., Grigg, C. M., *et al.* Patient HLA class I genotype influences cancer response to checkpoint blockade immunotherapy. *Science (New York, N.Y.)* **359,** 582–587 (2, 2018).

121. Montesion, M., Murugesan, K., Jin, D. X., *et al.* Somatic HLA Class I Loss Is a Widespread Mechanism of Immune Evasion Which Refines the Use of Tumor Mutational Burden as a Biomarker of Checkpoint Inhibitor Response. *Cancer Discovery* **11,** 282–292 (2, 2021).

122. Chhibber, A., Huang, L., Zhang, H., *et al.* Germline HLA landscape does not predict efficacy of pembrolizumab monotherapy across solid tumor types. *Immunity* **55,** 56–64.e4 (11, 2022).

123. Negrao, M. V., Lam, V. K., Reuben, A., *et al.* PD-L1 Expression, Tumor Mutational Burden, and Cancer Gene Mutations Are Stronger Predictors of Benefit from Immune Checkpoint Blockade than HLA Class I Genotype in Non–Small Cell Lung Cancer. *Journal of Thoracic Oncology* **14,** 1021–1031 (1, 2019).

124. Anagnostou, V., Niknafs, N., Marrone, K., *et al.* Multimodal genomic features predict outcome of immune checkpoint blockade in non-small-cell lung cancer. *Nature Cancer* **1,** 99–111 (2020).

125. Gibney, G. T., Weiner, L. M. & Atkins, M. B. Predictive biomarkers for checkpoint inhibitor-based immunotherapy. *The Lancet. Oncology* **17,** e542–e551 (2016).

126. Tsao, M. S., Kerr, K. M., Kockx, M., *et al.* PD-L1 Immunohistochemistry Comparability Study in Real-Life Clinical Samples: Results of Blueprint Phase 2 Project. *Journal of Thoracic Oncology: Official Publication of the International Association for the Study of Lung Cancer* **13,** 1302–1311 (2018).

127. Davis, A. A. & Patel, V. G. The role of PD-L1 expression as a predictive biomarker: an analysis of all US Food and Drug Administration (FDA) approvals of immune checkpoint inhibitors. *Journal for Immunotherapy of Cancer* **7,** 278 (26, 2019).

128. Noy, R. & Pollard, J. W. Tumor-associated macrophages: from mechanisms to therapy. *Immunity* **41,** 49–61 (17, 2014).

129. Neubert, N. J., Schmittnaegel, M., Bordry, N., *et al.* T cell-induced CSF1 promotes melanoma resistance to PD1 blockade. *Science Translational Medicine* **10,** eaan3311 (11, 2018).

130. Arlauckas, S. P., Garris, C. S., Kohler, R. H., *et al.* In vivo imaging reveals a tumor-associated macrophage-mediated resistance pathway in anti-PD-1 therapy. *Science Translational Medicine* **9,** eaal3604 (10, 2017).

131. Bruni, D., Angell, H. K. & Galon, J. The immune contexture and Immunoscore in cancer prognosis and therapeutic efficacy. *Nature Reviews Cancer* **20,** 662–680 (2020).

132. Pagès, F., Mlecnik, B., Marliot, F., *et al.* International validation of the consensus Immunoscore for the classification of colon cancer: a prognostic and accuracy study. *Lancet (London, England)* **391,** 2128–2139 (26, 2018).

133. Galon, J., Costes, A., Sanchez-Cabo, F., *et al.* Type, density, and location of immune cells within human colorectal tumors predict clinical outcome. *Science (New York, N.Y.)* **313,** 1960–1964 (29, 2006).

134. Galon, J. & Lanzi, A. Immunoscore and its introduction in clinical practice. *The quarterly journal of nuclear medicine and molecular imaging: official publication of the Italian Association of Nuclear Medicine (AIMN) [and] the International Association of Radiopharmacology (IAR), [and] Section of the Society of...* **64,** 152–161 (2020).

135. *Expert comments | Immunoscore for predicting risk of colon cancer relapse | Advice | NICE* https://www.nice.org.uk/advice/mib269/chapter/Expert-comments (2022).

136. Jiang, T., Qiao, M., Zhao, C., *et al.* Pretreatment neutrophil-to-lymphocyte ratio is associated with outcome of advanced-stage cancer patients treated with immunotherapy: a meta-analysis. *Cancer immunology, immunotherapy: CII* **67,** 713–727 (2018).

137. Taipale, K., Liikanen, I., Koski, A., *et al.* Predictive and Prognostic Clinical Variables in Cancer Patients Treated With Adenoviral Oncolytic Immunotherapy. *Molecular Therapy: The Journal of the American Society of Gene Therapy* **24,** 1323–1332 (2016).

138. Kuzman, J. A., Stenehjem, D. D., Merriman, J., *et al.* Neutrophil-lymphocyte ratio as a predictive biomarker for response to high dose interleukin-2 in patients with renal cell carcinoma. *BMC urology* **17,** 1 (5, 2017).

139. Manjarrez-Orduño, N., Menard, L. C., Kansal, S., *et al.* Circulating T Cell Subpopulations Correlate With Immune Responses at the Tumor Site and Clinical Response to PD1 Inhibition in Non-Small Cell Lung Cancer. *Frontiers in Immunology* **9,** 1613 (2018).

140. Kitano, S., Postow, M. A., Ziegler, C. G. K., *et al.* Computational algorithm-driven evaluation of monocytic myeloid-derived suppressor cell frequency for prediction of clinical outcomes. *Cancer Immunology Research* **2,** 812–821 (2014).

141. Hj, A., Hj, C. & C, K. Peripheral Blood-Based Biomarkers for Immune Checkpoint Inhibitors. *International journal of molecular sciences* **22** (30, 2021).

142. Keegan, A., Ricciuti, B., Garden, P., *et al.* Plasma IL-6 changes correlate to PD-1 inhibitor responses in NSCLC. *Journal for ImmunoTherapy of Cancer* **8,** e000678 (1, 2020).

143. Hoejberg, L., Bastholt, L., Johansen, J. S., *et al.* Serum interleukin-6 as a prognostic biomarker in patients with metastatic melanoma. *Melanoma Research* **22,** 287–293 (2012).

144. Guo, Y., Xu, F., Lu, T., Duan, Z. & Zhang, Z. Interleukin-6 signaling pathway in targeted therapy for cancer. *Cancer Treatment Reviews* **38,** 904–910 (2012).

145. Sanmamed, M. F., Perez-Gracia, J. L., Schalper, K. A., *et al.* Changes in serum interleukin-8 (IL-8) levels reflect and predict response to anti-PD-1 treatment in melanoma and non-small-cell lung cancer patients. *Annals of Oncology* **28,** 1988–1995 (1, 2017).

146. Yuen, K. C., Liu, L.-F., Gupta, V., *et al.* High systemic and tumor-associated IL-8 correlates with reduced clinical benefit of PD-L1 blockade. *Nature Medicine* **26,** 693–698 (2020).

147. Buder-Bakhaya, K. & Hassel, J. C. Biomarkers for Clinical Benefit of Immune Checkpoint Inhibitor Treatment-A Review From the Melanoma Perspective and Beyond. *Frontiers in Immunology* **9,** 1474 (2018).

148. Pistillo, M. P., Fontana, V., Morabito, A., *et al.* Soluble CTLA-4 as a favorable predictive biomarker in metastatic melanoma patients treated with ipilimumab: an Italian melanoma intergroup study. *Cancer Immunology, Immunotherapy* **68,** 97–107 (1, 2019).

149. Ugurel, S., Schadendorf, D., Horny, K., *et al.* Elevated baseline serum PD-1 or PD-L1 predicts poor outcome of PD-1 inhibition therapy in metastatic melanoma. *Annals of Oncology* **31,** 144–152 (1, 2020).

150. Bratman, S. V., Yang, S. Y. C., Iafolla, M. A. J., *et al.* Personalized circulating tumor DNA analysis as a predictive biomarker in solid tumor patients treated with pembrolizumab. *Nature Cancer* **1,** 873–881 (2020).

151. Goldberg, S. B., Narayan, A., Kole, A. J., *et al.* Early Assessment of Lung Cancer Immunotherapy Response via Circulating Tumor DNA. *Clinical Cancer Research: An Official Journal of the American Association for Cancer Research* **24,** 1872–1880 (15, 2018).

152. Tamminga, M., Wit, S. d., Hiltermann, T. J. N., *et al.* Circulating tumor cells in advanced non-small cell lung cancer patients are associated with worse tumor response to checkpoint inhibitors. *Journal for ImmunoTherapy of Cancer* **7,** 173 (1, 2019).

153. Matson, V., Fessler, J., Bao, R., *et al.* The commensal microbiome is associated with anti-PD-1 efficacy in metastatic melanoma patients. *Science (New York, N.Y.)* **359,** 104–108 (5, 2018).

154. Chaput, N., Lepage, P., Coutzac, C., *et al.* Baseline gut microbiota predicts clinical response and colitis in metastatic melanoma patients treated with ipilimumab. *Annals of Oncology: Official Journal of the European Society for Medical Oncology* **28,** 1368–1379 (1, 2017).

155. Sivan, A., Corrales, L., Hubert, N., *et al.* Commensal Bifidobacterium promotes antitumor immunity and facilitates anti-PD-L1 efficacy. *Science (New York, N.Y.)* **350,** 1084–1089 (27, 2015).

156. Charles A Janeway, J., Travers, P., Walport, M. & Shlomchik, M. J. The generation of diversity in immunoglobulins. *Immunobiology: The Immune System in Health and Disease. 5th edition* (2001).

157. Davis, M. M. & Bjorkman, P. J. T-cell antigen receptor genes and T-cell recognition. *Nature* **334,** 395–402 (1988).

158. Goldrath, A. W. & Bevan, M. J. Selecting and maintaining a diverse T-cell repertoire. *Nature* **402,** 6–13 (1999).

159. Thakkar, N. & Bailey-Kellogg, C. Balancing sensitivity and specificity in distinguishing TCR groups by CDR sequence similarity. *BMC Bioinformatics* **20,** 241 (15, 2019).

160. Nikolich-Zugich, J., Slifka, M. K. & Messaoudi, I. The many important facets of T-cell repertoire diversity. *Nature Reviews. Immunology* **4,** 123–132 (2004).

161. Shah, K., Al-Haidari, A., Sun, J. & Kazi, J. U. T cell receptor (TCR) signaling in health and disease. *Signal Transduction and Targeted Therapy* **6,** 1–26 (13, 2021).

162. Brady, B. L., Steinel, N. C. & Bassing, C. H. Antigen Receptor Allelic Exclusion: An Update and Reappraisal. *Journal of immunology (Baltimore, Md. : 1950)* **185,** 3801–3808 (1, 2010).

163. Chiffelle, J., Genolet, R., Perez, M. A., *et al. T-cell repertoire analysis and metrics of diversity and clonality* 2020.

164. Pai, J. A. & Satpathy, A. T. High-throughput and single-cell T cell receptor sequencing technologies. *Nature Methods* **18,** 881–892 (2021).

165. Rapid amplification of 5' complementary DNA ends (5' RACE). *Nature Methods* **2,** 629–630 (2005).

166. Barennes, P., Quiniou, V., Shugay, M., *et al.* Benchmarking of T cell receptor repertoire profiling methods reveals large systematic biases. *Nature Biotechnology* **39,** 236–245 (2021).

167. Shugay, M., Britanova, O. V., Merzlyak, E. M., *et al.* Towards error-free profiling of immune repertoires. *Nature Methods* **11,** 653–655 (2014).

168. Rosati, E., Dowds, C. M., Liaskou, E., *et al.* Overview of methodologies for T-cell receptor repertoire analysis. *BMC Biotechnology* **17,** 61 (10, 2017).

169. *What is the difference between Single Cell 3' and 5' Gene Expression libraries?* 10X Genomics. https://kb.10xgenomics.com/hc/en-us/articles/360000939852-What-is-the-difference-between-Single-Cell-3-and-5-Gene-Expression-libraries- (2022).

170. De Simone, M., Rossetti, G. & Pagani, M. Single Cell T Cell Receptor Sequencing: Techniques and Future Challenges. *Frontiers in Immunology* **9** (2018).

171. *Single Cell Immune Profiling* 10x Genomics. https://www.10xgenomics.com/products/single-cell-immune-profiling (2022).

172. Kim, B.-R., Shin, J., Guevarra, R., *et al.* Deciphering Diversity Indices for a Better Understanding of Microbial Communities. *Journal of Microbiology and Biotechnology* **27,** 2089–2093 (28, 2017).

173. Rousseau, R., Van Hecke, P., NIjssen, D. & Bogaert, J. The relationship between diversity profiles, evenness and species richness based on partial ordering. *Environmental and Ecological Statistics* **6,** 211–223 (1, 1999).

174. Wolda, H. Similarity indices, sample size and diversity. *Oecologia* **50,** 296–302 (1981).

175. M, M. Measuring of interspecific association and similarity between communities. *Mem. Fac. Sci. Kyushu Univ. Ser. E (Biol.)* **3,** 65–80 (1959).

176. Roh, W., Chen, P.-L., Reuben, A., *et al.* Integrated molecular analysis of tumor biopsies on sequential CTLA-4 and PD-1 blockade reveals markers of response and resistance. *Science Translational Medicine* **9,** eaah3560 (2017).

177. Pruessmann, W., Rytlewski, J., Wilmott, J., *et al.* Molecular analysis of primary melanoma T cells identifies patients at risk for metastatic recurrence. *Nature Cancer* **1,** 197–209 (2020).

178. Inoue, H., Park, J.-H., Kiyotani, K., *et al.* Intratumoral expression levels of PD-L1, GZMA, and HLA-A along with oligoclonal T cell expansion associate with response to nivolumab in metastatic melanoma. *Oncoimmunology* **5,** e1204507 (2016).

179. Reuben, A., Spencer, C. N., Prieto, P. A., *et al.* Genomic and immune heterogeneity are associated with differential responses to therapy in melanoma. *NPJ genomic medicine* **2,** 10 (2017).

180. Robert, L., Tsoi, J., Wang, X., *et al.* CTLA4 blockade broadens the peripheral T-cell receptor repertoire. *Clinical Cancer Research: An Official Journal of the American Association for Cancer Research* **20,** 2424–2432 (1, 2014).

181. Kvistborg, P., Philips, D., Kelderman, S., *et al.* Anti-CTLA-4 therapy broadens the melanoma-reactive CD8+ T cell response. *Science Translational Medicine* **6,** 254ra128 (17, 2014).

182. Kato, T., Kiyotani, K., Tomiyama, E., *et al.* Peripheral T cell receptor repertoire features predict durable responses to anti-PD-1 inhibitor monotherapy in advanced renal cell carcinoma. *Oncoimmunology* **10,** 1862948 (19, 2021).

183. Naidus, E., Bouquet, J., Oh, D. Y., *et al.* Early changes in the circulating T cells are associated with clinical outcomes after PD-L1 blockade by durvalumab in advanced NSCLC patients. *Cancer immunology, immunotherapy: CII* **70,** 2095–2102 (2021).

184. Dong, N., Moreno-Manuel, A., Calabuig-Fariñas, S., *et al.* Characterization of Circulating T Cell Receptor Repertoire Provides Information about Clinical Outcome after PD-1 Blockade in Advanced Non-Small Cell Lung Cancer Patients. *Cancers* **13,** 2950 (12, 2021).

185. Han, J., Duan, J., Bai, H., *et al.* TCR Repertoire Diversity of Peripheral PD-1+CD8+ T Cells Predicts Clinical Outcomes after Immunotherapy in Patients with Non–Small Cell Lung Cancer. *Cancer Immunology Research* **8,** 146–154 (2, 2020).

186. Katayama, Y., Yokota, R., Akiyama, T. & Kobayashi, T. J. Machine Learning Approaches to TCR Repertoire Analysis. *Frontiers in Immunology* **13** (2022).

187. Glanville, J., Huang, H., Nau, A., *et al.* Identifying specificity groups in the T cell receptor repertoire. *Nature* **547,** 94–98 (2017).

188. Huang, H., Wang, C., Rubelt, F., Scriba, T. J. & Davis, M. M. Analyzing the Mycobacterium tuberculosis immune response by T-cell receptor clustering with GLIPH2 and genome-wide antigen screening. *Nature Biotechnology 2020 38:10* **38,** 1194–1202 (2020).

189. *IMGT Scientific chart* https://www.imgt.org/IMGTScientificChart/Numbering/IMGTIGVLsuperfamily.html (2022).

190. Chiou, S. H., Tseng, D., Reuben, A., *et al.* Global analysis of shared T cell specificities in human non-small cell lung cancer enables HLA inference and antigen discovery. *Immunity* **54,** 586 (2021).

191. Dash, P., Fiore-Gartland, A. J., Hertz, T., *et al.* Quantifiable predictive features define epitope-specific T cell receptor repertoires. *Nature* **547,** 89–93 (2017).

192. Sidhom, J.-W., Larman, H. B., Pardoll, D. M. & Baras, A. S. DeepTCR is a deep learning framework for revealing sequence concepts within T-cell repertoires. *Nature Communications* **12,** 1605 (11, 2021).

193. Sidhom, J.-W., Oliveira, G., Ross-MacDonald, P., *et al.* Deep learning reveals predictive sequence concepts within immune repertoires to immunotherapy. *Science Advances* **8,** eabq5089 (16, 2022).

194. Altman, J. D., Moss, P. A., Goulder, P. J., *et al.* Phenotypic analysis of antigen-specific T lymphocytes. *Science (New York, N.Y.)* **274,** 94–96 (4, 1996).

195. Davis, M. M., Altman, J. D. & Newell, E. W. Interrogating the repertoire: broadening the scope of peptide-MHC multimer analysis. *Nature Reviews. Immunology* **11,** 551–558 (15, 2011).

196. Goncharov, M., Bagaev, D., Shcherbinin, D., *et al.* VDJdb in the pandemic era: a compendium of T cell receptors specific for SARS-CoV-2. *Nature Methods,* 1–3 (15, 2022).

197. Vita, R., Mahajan, S., Overton, J. A., *et al.* The Immune Epitope Database (IEDB): 2018 update. *Nucleic Acids Research* **47,** D339–D343 (D1 8, 2019).

198. Tickotsky, N., Sagiv, T., Prilusky, J., Shifrut, E. & Friedman, N. McPAS-TCR: a manually curated catalogue of pathology-associated T cell receptor sequences. *Bioinformatics* **33,** 2924–2929 (15, 2017).

199. Chen, S.-Y., Yue, T., Lei, Q. & Guo, A.-Y. TCRdb: a comprehensive database for T-cell receptor sequences with powerful search function. *Nucleic Acids Research* **49,** D468–D474 (D1 8, 2021).

200. Fischer, D. S., Wu, Y., Schubert, B. & Theis, F. J. Predicting antigen specificity of single T cells based on TCR CDR3 regions. *Molecular Systems Biology* **16,** e9416 (2020).

201. De Neuter, N., Bittremieux, W., Beirnaert, C., *et al.* On the feasibility of mining CD8+ T cell receptor patterns underlying immunogenic peptide recognition. *Immunogenetics* **70,** 159–168 (2018).

202. Hudson, D., Fernandes, R. A., Basham, M., Ogg, G. & Koohy, H. Can we predict T cell specificity with digital biology and machine learning? *Nature Reviews Immunology,* 1–11 (8, 2023).

203. Gee, M. H., Han, A., Lofgren, S. M., *et al.* Antigen Identification for Orphan T Cell Receptors Expressed on Tumor-Infiltrating Lymphocytes. *Cell* **172,** 549–563.e16 (25, 2018).

204. Birnbaum, M. E., Mendoza, J. L., Sethi, D. K., *et al.* Deconstructing the Peptide-MHC Specificity of T Cell Recognition. *Cell* **157,** 1073–1087 (22, 2014).

205. Gilchrist, J. J., Makino, S., Naranbhai, V., *et al.* Natural Killer cells demonstrate distinct eQTL and transcriptome-wide disease associations, highlighting their role in autoimmunity. *Nature Communications* **13,** 4073 (14, 2022).

206. Mazet, J. M., Mahale, J. N., Tong, O., *et al.* IFNγ signaling in cytotoxic T cells restricts anti-tumor responses by inhibiting the maintenance and diversity of intra-tumoral stem-like T cells. *Nature Communications* **14,** 321 (19, 2023).

207. Tsakok, M. T., Watson, R. A., Saujani, S. J., *et al.* Chest CT and Hospital Outcomes in Patients with Omicron Compared with Delta Variant SARS-CoV-2 Infection. *Radiology,* 220533 (21, 2022).

208. Peng, Y., Felce, S. L., Dong, D., *et al.* An immunodominant NP105–113-B*07:02 cytotoxic T cell response controls viral replication and is associated with less severe COVID-19 disease. *Nature Immunology* **23,** 50–61 (2022).

209. Ahern, D. J., Ai, Z., Ainsworth, M., *et al.* A blood atlas of COVID-19 defines hallmarks of disease severity and specificity. *Cell* **185,** 916–938.e58 (3, 2022).

210. *Chromium Family* 10x Genomics. https://www.10xgenomics.com/instruments/chromium-family (2023).

211. McCarthy, D. J., Campbell, K. R., Lun, A. T. & Wills, Q. F. Scater: Pre-processing, quality control, normalization and visualization of single-cell RNA-seq data in R. *Bioinformatics* **33,** 1179–1186 (2017).

212. Butler, A., Hoffman, P., Smibert, P., Papalexi, E. & Satija, R. Integrating single-cell transcriptomic data across different conditions, technologies, and species. *Nature Biotechnology* **36,** 411–420 (2018).

213. Lun, A. T., Riesenfeld, S., Andrews, T., *et al.* EmptyDrops: Distinguishing cells from empty droplets in droplet-based single-cell RNA sequencing data. *Genome Biology* **20** (2019).

214. Huang, Y., McCarthy, D. J. & Stegle, O. Vireo: Bayesian demultiplexing of pooled single-cell RNA-seq data without genotype reference. *Genome Biology* **20,** 273 (13, 2019).

215. Wolock, S. *Scrublet* 10, 2023.

216. Zappia, L. & Oshlack, A. Clustering trees: a visualization for evaluating clusterings at multiple resolutions. *GigaScience* **7** (2018).

217. Guo, X., Zhang, Y., Zheng, L., *et al.* Global characterization of T cells in non-small-cell lung cancer by single-cell sequencing. *Nature Medicine* **24,** 978–985 (2018).

218. Savas, P., Virassamy, B., Ye, C., *et al.* Single-cell profiling of breast cancer T cells reveals a tissue-resident memory subset associated with improved prognosis. *Nature Medicine* **24,** 986–993 (2018).

219. Zhang, L., Yu, X., Zheng, L., *et al.* Lineage tracking reveals dynamic relationships of T cells in colorectal cancer. *Nature* **564,** 268–272 (2018).

220. Aran, D., Looney, A. P., Liu, L., *et al.* Reference-based analysis of lung single-cell sequencing reveals a transitional profibrotic macrophage. *Nature Immunology* **20,** 163–172 (2019).

221. Wolf, F. A., Angerer, P. & Theis, F. J. SCANPY: large-scale single-cell gene expression data analysis. *Genome Biology* **19,** 15 (2018).

222. *scvi-tools* https://scvi-tools.org/ (2023).

223. Lopez, R., Regier, J., Cole, M. B., Jordan, M. I. & Yosef, N. Deep generative modeling for single-cell transcriptomics. *Nature Methods* **15,** 1053–1058 (2018).

224. Lotfollahi, M., Naghipourfar, M., Luecken, M. D., *et al. Query to reference single-cell integration with transfer learning* 16, 2020.

225. Domínguez Conde, C., Xu, C., Jarvis, L. B., *et al.* Cross-tissue immune cell analysis reveals tissue-specific features in humans. *Science (New York, N.Y.)* **376,** eabl5197 (13, 2022).

226. *Chapter 6 Changes in cluster abundance | Multi-Sample Single-Cell Analyses with Bioconductor* https://bioconductor.org/books/3.13/OSCA.multisample/differential-abundance.html (2023).

227. Lun, A. T. L., Richard, A. C. & Marioni, J. C. Testing for differential abundance in mass cytometry data. *Nature Methods* **14,** 707–709 (2017).

228. Dann, E., Henderson, N. C., Teichmann, S. A., Morgan, M. D. & Marioni, J. C. Differential abundance testing on single-cell data using k-nearest neighbor graphs. *Nature Biotechnology* **40,** 245–253 (2022).

229. Andreatta, M. & Carmona, S. J. UCell: Robust and scalable single-cell gene signature scoring. *Computational and Structural Biotechnology Journal* **19,** 3796–3798 (1, 2021).

230. Satija, R., Farrell, J. A., Gennert, D., Schier, A. F. & Regev, A. Spatial reconstruction of single-cell gene expression data. *Nature Biotechnology* **33,** 495–502 (2015).

231. Love, M. I., Huber, W. & Anders, S. Moderated estimation of fold change and dispersion for RNA-seq data with DESeq2. *Genome Biology* **15,** 550 (5, 2014).

232. Fang, H., Knezevic, B., Burnham, K. L. & Knight, J. C. XGR software for enhanced interpretation of genomic summary data, illustrated by application to immunological traits. *Genome Medicine* **8,** 129 (2016).

233. Bagaev, D. V., Vroomans, R. M., Samir, J., *et al.* VDJdb in 2019: Database extension, new analysis infrastructure and a T-cell receptor motif compendium. *Nucleic Acids Research* **48,** D1057–D1062 (D1 2020).

234. Kim, D., Langmead, B. & Salzberg, S. L. HISAT: a fast spliced aligner with low memory requirements. *Nature Methods* **12,** 357–360 (2015).

235. Anders, S., Pyl, P. T. & Huber, W. HTSeq—a Python framework to work with high-throughput sequencing data. *Bioinformatics* **31,** 166–169 (15, 2015).

236. Li, H., Handsaker, B., Wysoker, A., *et al.* The Sequence Alignment/Map format and SAMtools. *Bioinformatics (Oxford, England)* **25,** 2078–2079 (15, 2009).

237. Bolotin, D. A., Poslavsky, S., Mitrophanov, I., *et al.* MiXCR: software for comprehensive adaptive immunity profiling. *Nature methods* **12,** 380–1 (2015).

238. *Bioinformatics Analysis of T-Cell and B-Cell Immune Repertoires* https://immunarch.com/ (2023).

239. Yusko, E., Vignali, M., Wilson, R. K., *et al.* Association of Tumor Microenvironment T-cell Repertoire and Mutational Load with Clinical Outcome after Sequential Checkpoint Blockade in Melanoma. *Cancer immunology research* **7,** 458–465 (2019).

240. Squair, J. W., Gautier, M., Kathe, C., *et al.* Confronting false discoveries in single-cell differential expression. *Nature Communications* **12,** 5692 (28, 2021).

241. Valpione, S., Galvani, E., Tweedy, J., *et al.* Immune-awakening revealed by peripheral T cell dynamics after one cycle of immunotherapy. *Nature Cancer* **1,** 210–221 (2020).

242. Farouni, R., Djambazian, H., Ferri, L. E., Ragoussis, J. & Najafabadi, H. S. Model-based analysis of sample index hopping reveals its widespread artifacts in multiplexed single-cell RNA-sequencing. *Nature Communications* **11,** 2704 (1, 2020).

243. Klenerman, P. & Oxenius, A. T cell responses to cytomegalovirus. *Nature Reviews Immunology* **16,** 367–377 (2016).

244. Qi, Q., Liu, Y., Cheng, Y., *et al.* Diversity and clonal selection in the human T-cell repertoire. *Proceedings of the National Academy of Sciences* **111,** 13139–13144 (9, 2014).

245. Scheper, W., Kelderman, S., Fanchi, L. F., *et al.* Low and variable tumor reactivity of the intratumoral TCR repertoire in human cancers. *Nature Medicine* **25,** 89–94 (2019).

246. Pearlman, A. H., Hwang, M. S., Konig, M. F., *et al.* Targeting public neoantigens for cancer immunotherapy. *Nature Cancer* **2,** 487–497 (2021).

247. Charles A Janeway, J., Travers, P., Walport, M. & Shlomchik, M. J. The course of the adaptive response to infection. *Immunobiology: The Immune System in Health and Disease. 5th edition* (2001).

248. Renkema, K. R., Huggins, M. A., Borges da Silva, H., *et al.* KLRG1+ Memory CD8 T Cells Combine Properties of Short-Lived Effectors and Long-Lived Memory. *Journal of Immunology (Baltimore, Md.: 1950)* **205,** 1059–1069 (15, 2020).

249. Bourens, M. & Barrientos, A. A CMC1-knockout reveals translation-independent control of human mitochondrial complex IV biogenesis. *EMBO Reports* **18,** 477–494 (2017).

250. *Differential abundance testing with Milo - Mouse gastrulation example* https://rawcdn.githack.com/MarioniLab/miloR/7c7f906b94a73e62e36e095ddb3e3567b414144e/vignettes/milo_gastrulation.html#37_Testing (2023).

251. Ng, S. S., De Labastida Rivera, F., Yan, J., *et al.* The NK cell granule protein NKG7 regulates cytotoxic granule exocytosis and inflammation. *Nature Immunology* **21,** 1205–1218 (2020).

252. Puig-Saus, C., Sennino, B., Peng, S., *et al.* Neoantigen-targeted CD8+ T cell responses with PD-1 blockade therapy. *Nature,* 1–8 (8, 2023).

253. Melenhorst, J. J., Chen, G. M., Wang, M., *et al.* Decade-long leukaemia remissions with persistence of CD4+ CAR T cells. *Nature* **602,** 503–509 (2022).

254. Aldrich, J., Pundole, X., Tummala, S., *et al.* Incidence and outcomes of immune checkpoint inhibitor-related myositis. *Journal of Clinical Oncology* **38,** e15128–e15128 (2020).

255. Mahmood, S. S., Fradley, M. G., Cohen, J. V., *et al.* Myocarditis in Patients Treated With Immune Checkpoint Inhibitors. *Journal of the American College of Cardiology* **71,** 1755–1764 (24, 2018).

256. Megremis, S., Walker, T. D., He, X., *et al. Antibodies against immunogenic epitopes with high sequence identity to SARS-CoV-2 in patients with autoimmune dermatomyositis* 2020.

257. Husby, A., Hansen, J. V., Fosbøl, E., *et al.* SARS-CoV-2 vaccination and myocarditis or myopericarditis: population based cohort study. *BMJ (Clinical research ed.)* **375,** e068665 (2021).

258. Mevorach, D., Anis, E., Cedar, N., *et al.* Myocarditis after BNT162b2 mRNA Vaccine against Covid-19 in Israel. *New England Journal of Medicine* **385,** 2140–2149 (2021).

259. Pillay, J., Gaudet, L., Wingert, A., *et al.* Incidence, risk factors, natural history, and hypothesised mechanisms of myocarditis and pericarditis following covid-19 vaccination: living evidence syntheses and review. *BMJ* **378,** e069445 (13, 2022).

260. Wong, H.-L., Hu, M., Zhou, C. K., *et al.* Risk of myocarditis and pericarditis after the COVID-19 mRNA vaccination in the USA: a cohort study in claims databases. *The Lancet* **399,** 2191–2199 (11, 2022).

261. Montagne, J. M., Zheng, X. A., Pinal-Fernandez, I., *et al.* Ultra-efficient sequencing of T Cell receptor repertoires reveals shared responses in muscle from patients with Myositis. *EBioMedicine* **59,** 102972 (2020).

262. Rempała, G. A. & Seweryn, M. Methods for diversity and overlap analysis in T-cell receptor populations. *Journal of mathematical biology* **67,** 10.1007/s00285–012–0589–7 (2013).

263. Fry, T. J. & Mackall, C. L. The Many Faces of IL-7: From Lymphopoiesis to Peripheral T Cell Maintenance. *The Journal of Immunology* **174,** 6571–6576 (2005).

264. Clark, M. R., Mandal, M., Ochiai, K. & Singh, H. *Orchestrating B cell lymphopoiesis through interplay of IL-7 receptor and pre-B cell receptor signalling* 2014.

265. Widmer, M. B., Morrissey, P. J., Goodwin, R. G., *et al.* Lymphopoiesis and IL-7. *The International Journal of Cell Cloning* **8,** 168–172 (1990).

266. Zhu, H., Galdos, F. X., Lee, D., *et al.* Identification of Pathogenic Immune Cell Subsets Associated With Checkpoint Inhibitor–Induced Myocarditis. *Circulation* **146,** 316–335 (26, 2022).

267. Ji, C., Roy, M. D., Golas, J., *et al.* Myocarditis in cynomolgus monkeys following treatment with immune checkpoint inhibitors. *Clinical Cancer Research* **25,** 4735–4748 (2019).

268. Grabie, N., Gotsman, I., DaCosta, R., *et al.* Endothelial programmed death-1 ligand 1 (PD-L1) regulates CD8+ T-cell-mediated injury in the heart. *Circulation* **116,** 2062–2071 (2007).

269. Okazaki, T., Tanaka, Y., Nishio, R., *et al.* Autoantibodies against cardiac troponin I are responsible for dilated cardiomyopathy in PD-1-deficient mice. *Nature Medicine* **9,** 1477–1483 (2003).

270. Tarrio, M. L., Grabie, N., Bu, D.-x., Sharpe, A. H. & Lichtman, A. H. PD-1 Protects against Inflammation and Myocyte Damage in T Cell-Mediated Myocarditis. *The Journal of Immunology* **188,** 4876–4884 (2012).

271. Nishimura, H., Okazaki, T., Tanaka, Y., *et al.* Autoimmune dilated cardiomyopathy in PD-1 receptor-deficient mice. *Science (New York, N.Y.)* **291,** 319–322 (12, 2001).

272. Baban, B., Liu, J. Y., Qin, X., Weintraub, N. L. & Mozaffari, M. S. Upregulation of Programmed Death-1 and Its Ligand in Cardiac Injury Models: Interaction with GADD153. *PloS One* **10,** e0124059 (2015).

273. Gradone, A., Ma, V. T., Fecher, L. A., *et al.* Increased incidence of immune-mediated myocarditis in advanced skin malignancies treated with immune checkpoint inhibitors in the COVID-19 era. *Journal of Clinical Oncology* **40,** 2664–2664 (2022).

274. Lynch, D. H. & Miller, R. E. Interleukin 7 promotes long-term in vitro growth of antitumor cytotoxic T lymphocytes with immunotherapeutic efficacy in vivo. *Journal of Experimental Medicine* **179,** 31–42 (1994).

275. Pellegrini, M., Calzascia, T., Elford, A. R., *et al.* Adjuvant IL-7 antagonizes multiple cellular and molecular inhibitory networks to enhance immunotherapies. *Nature Medicine* **15,** 528–536 (2009).

276. Liu, X. & Wu, J. History, applications, and challenges of immune repertoire research. *Cell Biology and Toxicology* **34,** 441–457 (1, 2018).

277. Itzhaki, O., Hovav, E., Ziporen, Y., *et al.* Establishment and large-scale expansion of minimally cultured "young" tumor infiltrating lymphocytes for adoptive transfer therapy. *Journal of Immunotherapy (Hagerstown, Md.: 1997)* **34,** 212–220 (2011).

278. Berg, J. H. v. d., Heemskerk, B., Rooij, N. v., *et al.* Tumor infiltrating lymphocytes (TIL) therapy in metastatic melanoma: boosting of neoantigen-specific T cell reactivity and long-term follow-up. *Journal for ImmunoTherapy of Cancer* **8,** e000848 (1, 2020).

279. Dudley, M. E., Wunderlich, J. R., Yang, J. C., *et al.* Adoptive cell transfer therapy following non-myeloablative but lymphodepleting chemotherapy for the treatment of patients with refractory metastatic melanoma. *Journal of Clinical Oncology: Official Journal of the American Society of Clinical Oncology* **23,** 2346–2357 (1, 2005).

280. Besser, M. J., Shapira-Frommer, R., Treves, A. J., *et al.* Clinical responses in a phase II study using adoptive transfer of short-term cultured tumor infiltration lymphocytes in metastatic melanoma patients. *Clinical Cancer Research: An Official Journal of the American Association for Cancer Research* **16,** 2646–2655 (1, 2010).

281. Lesterhuis, W. J., Bosco, A., Millward, M. J., *et al.* Dynamic versus static biomarkers in cancer immune checkpoint blockade: unravelling complexity. *Nature Reviews Drug Discovery* **16,** 264–272 (2017).

282. Michielin, O., Akkooi, A. C. J. v., Ascierto, P. A., Dummer, R. & Keilholz, U. Cutaneous melanoma: ESMO Clinical Practice Guidelines for diagnosis, treatment and follow-up †. *Annals of Oncology* **30,** 1884–1901 (1, 2019).

283. Eggermont, A. M., Blank, C. U., Mandala, M., *et al.* Adjuvant Pembrolizumab versus Placebo in Resected Stage III Melanoma. *New England Journal of Medicine* **378,** 1789–1801 (10, 2018).

284. Eggermont, A. M. M., Blank, C. U., Mandalà, M., *et al.* Adjuvant pembrolizumab versus placebo in resected stage III melanoma (EORTC 1325-MG/KEYNOTE-054): distant metastasis-free survival results from a double-blind, randomised, controlled, phase 3 trial. *The Lancet Oncology* **22,** 643–654 (1, 2021).

285. Weber, J., Mandala, M., Del Vecchio, M., *et al.* Adjuvant Nivolumab versus Ipilimumab in Resected Stage III or IV Melanoma. *New England Journal of Medicine* **377,** 1824–1835 (2017).

286. Luke, J. J., Rutkowski, P., Queirolo, P., *et al.* Pembrolizumab versus placebo as adjuvant therapy in completely resected stage IIB or IIC melanoma (KEYNOTE-716): a randomised, double-blind, phase 3 trial. *The Lancet* **399,** 1718–1729 (30, 2022).

287. Wilson, M., Geskin, L. J., Carvajal, R. D., *et al.* Adjuvant nivolumab in high-risk stage IIb/IIc melanoma patients: Results from investigator initiated clinical trial. *Journal of Clinical Oncology* **39,** 9583–9583 (20, 2021).

288. Shelly, S., Triplett, J. D., Pinto, M. V., *et al.* Immune checkpoint inhibitor-associated myopathy: a clinicoseropathologically distinct myopathy. *Brain Communications* **2,** fcaa181 (1, 2020).

A | Supplementary Tables

Proliferating peripheral CD8+	Tumor Specific		Dual Expanded	Cytotoxic		Cytotoxic	Exhausted	Tumour Reactive
Huang, Wherry, *Nature* 2017	Oliviera, Wu, *Nature* 2021		Wu, Grogan, *Nature* 2020	Watson, Tong, *Science Immunology* 2021		Lucca, *JEM* 2021	Lucca, *JEM* 2021	van der Leun, Schumacher, *Nat Rev Cancer* 2020
MKI67	KRT86	GALNT2	CCL5	IFNG	GZMA	CX3CR1	HAVCR2	ENTPD1
CTLA4	RDH10	FXYD2	NKG7	NKG7	CX3CR1	PRF1	IFNG	ITGAE
HLA-DQB1	TYMS	PLPP1	CD8A	ARPC2	HLA-DQA1	GZMA	ITGAE	PDCD1
CENPF	HMOX1	LMCD1	GZMH	S100A4	CLIC3	GZMH	PDCD1	TNFRSF9
RRM2	GNG4	MYL6B	CD8B	PRF1	FCGR3A	GNLY	CXCL13	TNFRSF4
KIR3DX1	CXCL13	LAG3	HCST	PLEK	PRSS23	FGFBP2	LAYN	CXCL13
KIF19	AFAP1L2	HLA-DRA	CST7	C12orf75	ACTB	KLRG1	LAG3	MKI67
ARHGAP11A	ACP5	IGFLR1	KLRD1	GZMB	APOBEC3G	GZMM	TIGIT	HAVCR2
IFI6	MYO1E	CCDC50	GZMA	CCL4	HLA-DPA1	LYAR	CTLA4	LAG3
SYNGR1	LAYN	CD27	CTSW	SH3BGRL3	LGALS1	TXNIP	ENTPD1	
HLA-DRB1	TNS3	KIAA1324	PRF1	TMSB4X	GZMH	FCRL6		
EPB41L4A	TNFSF4	CDKN2A	GZMB	ADGRG1	FLNA	NKG7		
FADS2	AKAP5	CD70	HOPX	CCL5	HLA-DRA	KLRD1		
CDCA7	HAVCR2	ABHD6	GZMM	CST7	HLA-DRB5			
HAVCR2	ENTPD1	CTLA4	KLRK1	PFN1	CLIC1			
LDLR	SLC2A8	PDCD1	HLA-C	FGR	SPON2			
FBXO5	AC243829.4	GEM	GSTP1	IDH2	TGFBR3			
ITGAD	ZBED2	NUSAP1	CLEC2B	GNLY	ANXA2			
ALDOC	MCM5	TOX	CD63	KLRD1	HLA-DRB1			
GAMT	CAV1	CXCR6	CD99	PPP1CA	FGFBP2			
CD38	GOLIM4	NMB	KLRC4	IL32	HLA-DPB1			
RFC2	TRAV21	HOPX	AOAH	MYL6	ZEB2			
ORMDL3	VCAM1	CLIC3	GNLY	CD99	TTC38			
COL5A3	PON2	INPP5F	CCL4	CD74	YWHAQ			
TPD3l11	MTSS1	SNAP47	MATK	KLRG1	GBP5			
HLA-K	CD38	TSHZ2	C12orf75					
LMNB1	TRBV11-2	HLA-DMA	CCL4L1					
PRKAR1B	MS4A6A	SIT1	ZNF683					
CLSPN	TOX2	HLA-DRB1	ABI3					
UBE2L6	CSF1	TUBB	KLRC2					
	HIPK2	PYCARD						
	CHST12	ADGRG1						
	LSP1	HLA-DQA1						
	FAM3C	PRF1						
	SLC1A4	HLA-DPA1						
	NUDT1	PTMS						
	DNPH1	CKS1B						

Table A.1. List of genes which make up a range of expression scores applied in Chapter 3 and 5. References - Huang [77]; Oliveira [70]; Wu [92]; Watson, Tong [78]; Lucca [98]; van der Leun [67].

Tumour group	HR	lowerCI	upperCI	pval	model
All NSCLC	0.49	0.33	0.72	0.00027	Surv(fu_time_death, death_status) ~ lsi_stable + age + sex + multiple_cancers + n_lines_rx + pre_treatment
NSCLC no pretreatment	0.46	0.26	0.8	0.0066	Surv(fu_time_death, death_status) ~ lsi_stable + age + sex + multiple_cancers + n_lines_rx
NSCLC with pretreatment	0.54	0.31	0.93	0.026	Surv(fu_time_death, death_status) ~ lsi_stable + age + sex + multiple_cancers + n_lines_rx
All Melanoma	0.38	0.26	0.56	1.30E-06	Surv(fu_time_death, death_status) ~ lsi_stable + age + sex + multiple_cancers + n_lines_rx + pre_treatment + pre_adj_icb
Melanoma - Single-agent Ipi	0.18	0.066	0.48	7.00E-04	Surv(fu_time_death, death_status) ~ lsi_stable + age + sex + multiple_cancers + n_lines_rx + pre_treatment + pre_adj_icb
Melanoma - cICB validation	0.3	0.12	0.76	0.012	Surv(fu_time_death, death_status) ~ lsi_stable + age + sex + multiple_cancers + n_lines_rx + pre_treatment + pre_adj_icb
Melanoma - sICB validation	0.66	0.34	1.3	0.22	Surv(fu_time_death, death_status) ~ lsi_stable + age + sex + multiple_cancers + n_lines_rx + pre_treatment
Melanoma validation	0.53	0.34	0.82	0.0041	Surv(fu_time_death, death_status) ~ lsi_stable + age + sex + multiple_cancers + n_lines_rx + pre_treatment + pre_adj_icb
All excluding lung, renal & melanoma	1.2	0.66	2.1	0.59	Surv(fu_time_death, death_status) ~ lsi_stable + age + sex + multiple_cancers + n_lines_rx + pre_treatment + diagnosis + first_mICB_type
All Tumours	0.6	0.48	0.75	4.60E-06	Surv(fu_time_death, death_status) ~ lsi_stable + age + sex + diagnosis + multiple_cancers + n_lines_rx + pre_treatment
All renal	0.7	0.36	1.3	0.28	Surv(fu_time_death, death_status) ~ lsi_stable + age + sex + multiple_cancers + n_lines_rx + pre_treatment
Renal no pretreatment	1.8	0.57	5.9	0.31	Surv(fu_time_death, death_status) ~ lsi_stable + age + sex + multiple_cancers + n_lines_rx
Renal with pretreatment	0.33	0.14	0.79	0.013	Surv(fu_time_death, death_status) ~ lsi_stable + age + sex + multiple_cancers + n_lines_rx
All urothelial	1.1	0.46	2.7	0.8	Surv(fu_time_death, death_status) ~ lsi_stable + age + sex + multiple_cancers + n_lines_rx + pre_treatment

Table A.2. Table of Cox PH models used in assessing association between LSI and OS across multiple tumour types. Accompanies Figure 6.12. The model is given in the format of the *survival* package in *R*. lsi_stable is a binary variable indicating whether LSI is stable. The cut-off used was 0.95 for NSCLC and 0.80 for all other tumours. fu_time_death is a numeric variable giving the time to death or censor in days. death_status is a binary variable indicating whether or not the patient has died before the follow-up date. multiple_cancers is a binary variable indicating whether the patient has been diagnosed with 2 or more cancers. n_lines_rx is an ordinal variable indicating how many lines of SACT in total the patient received. pre_treatment is a binary variable indicating whether the patient received treatment prior to ICB. pre_adj_icb is a binary variable indicated whether the patient received adjuvant ICB prior to metastatic treatment. first_mICB_type is a categorical variable naming the ICB given.

B | Treatment of melanoma based on stage

The clinical management of melanoma, based on the stage of disease, can be broadly summarised as follows (this is based on European Society for Medical Oncology (ESMO)[282] and NICE guidance NG14, July 2022 Update):

- Locoregional disease: i.e. stage 0-II, with no evidence of metastases clinically or on imaging:
  - Management is primarily surgical and the lesion should be excised with a wide margin of 1-2cm from stage I and 2cm for stage II.
  - A sentinel lymph node biopsy should be performed for pT1b melanoma or higher (a tumour thickness of >0.8mm or <0.8mm with ulceration).
  - Routine complete lymph node dissection is no longer recommended due to the limited benefits and high morbidity associated.
  - For stage IIB and C disease, adjuvant treatment is a possibility (see section 1.1.2.2 below).
- Stage III disease:
  - Should have a primary resection, sentinel lymph node biopsy and therapeutic lymph node dissection (removal) for palpable nodes, or those visible on imaging.
  - For stage III disease (i.e. with lymph node metastases) that has been completely resected, adjuvant treatment should be offered (see section 1.1.2.2 below).
  - For stage III disease that is un-resectable, systemic therapy can be offered, as can local-regional therapy such as talimogene laherparepvec (T-VEC).

- Stage IV metastatic disease:
  - Should be treated with systemic anti-cancer therapy. For the purposes of this thesis, this would be ICB. However, if there is a BRAF mutation present in the melanoma, treatment can also be given with a BRAF inhibitor, in combination with a MEK inhibitor.
  - Surgical removal should be considered for some stage IV patients if there is a locoregional recurrent or single distant metastasis.

C | Clinical trial data to support the use of ICB in the adjuvant setting

There are a number of seminal trials demonstrating the benefit of using ICB in the adjuvant setting for melanoma - i.e. following complete resection. KEYNOTE-054[283] compared adjuvant pembrolizumab with placebo in 1019 adults with complete resection of stage III melanoma. At 15 months follow up, pembrolizumab gave a HR of 0.57 for recurrence or death. Of note, this was significant only for stage IIIB and C with the 95% CIs for HR being 0.11-1.31 for stage IIIA. This benefit continued with a longer follow-up time of 42.3 months[284] (HR 0.60, p<0.0001), although overall survival was not assessed at this time point. Despite this, NICE believes that there will also be an overall survival benefit from this approach and hence agreed to licence it.

Similar benefit was seen in the CheckMate 238 study[285] which looked at the benefit of nivolumab versus ipilimumab (not placebo as in KEYNOTE-054) and found a HR of 0.65 (p<0.0001) - although this study excluded patients with stage IIIA disease and included those with resected stage IV. At 4 years follow up, this study showed an ongoing benefit for recurrence (HR 0.71, 95% CI 0.60-0.86) but no overall survival benefit (HR 0.87, 95% CI 0.66-1.14).

In 2022 KEYNOTE-716 reported, demonstrating benefit of adjuvant pembrolizumab for resected stage IIB or IIC melanoma (HR 0.61, 95% CI 0.45-0.82 at 20.9 months of follow up)[286]. Similar trials for nivolumab are ongoing[287] and these treatments were licensed for adjuvant treatment in this context in late 2022.

D | Myositis and myocarditis - full clinical cases

These are the full clinical case histories of the three patients with severe myocarditis with myositis, samples from whom form the basis of results presented in Chapter 6 (*$CD8^+$ T cell features associated with immune-related adverse events*), section 6.3.

Patient 1

A 72 year-old man with pre-treatment ECOG performance status (PS) 0 presented with dizziness and dyspnoea 28 days post-initiation of pembrolizumab (six week infusion, 400 mg) for adjuvant treatment of resected Stage IIIC melanoma. Medical history consisted of atrial fibrillation and type 2 diabetes. He attended a nearby hospital five days prior for non-specific chest pain, treated with analgesia. On arrival, he reported lethargy, weakness and inability to support his head, with associated bulbar symptoms. He had no chest pain or ischaemic ECG changes, but serum CK and troponin were markedly elevated, (CK: 2,236 U/L, range 30-200 U/L; Troponin: 267 ng/l, range 0-34 ng/l; Figure 6.1 and Table 6.2) as were liver enzymes (alanine aminotransferase, ALT, 394 U/L, range 10-45 U/L; alkaline phosphatase, ALP, 1,044 U/L, range 30-130 U/L) and bilirubin (68 umol/L, range 0-21 umol/L). His condition acutely worsened, developing type II respiratory failure with reduced consciousness, precipitating transfer to critical care with vasopressor support and ventilation. Initial management was with intravenous methylprednisolone (2mg/kg) for five days but upon further deterioration, intravenous immunoglobulin (IVIg) was given for a further five days. An electromyogram demonstrated a necrotic myopathic process involving proximal limbs with background neuropathy. Autoantibody screening revealed positivity for anti-acetylcholine receptor antibodies (AChR). A muscle biopsy showed multifocal clusters of necrotic fibres, consistent with an ICB-associated myositis[288] (Figure 6.1). The final diagnosis was pembrolizumab-associated myositis, myocarditis and myasthaenia gravis. Pyridostigmine

was commenced, with little initial benefit, followed by plasma exchange (commenced 3 weeks following IVIg). A slow but sustained clinical improvement ensued and he was discharged to a rehabilitation unit. He received a booster vaccination (BNT162b2) 28 days prior to pembrolizumab.

Patient 2

An 82 year-old woman with pre-treatment PS 0 and no relevant medical history was admitted 39 days post-initiation of pembrolizumab (400mg) for stage IV melanoma. She developed diarrhoea and severe myalgia 11 days after treatment, attending a local hospital where oral prednisolone (60mg) was commenced. Subsequently, the diarrhoea resolved whereas the myalgia worsened and on day 23 she was re-admitted having collapsed with loss of consciousness. She was in complete heart block but without ECG features of acute ischaemia, however serum troponin was elevated (1,124 ng/L). Coronary angiography demonstrated a possible ruptured left anterior descending artery plaque and she was managed with percutaneous stent placement and a permanent pacemaker. Despite this, blood tests six days post-discharge showed further elevation of serum troponin (2,101 ng/L) and elevated CK (1,186 U/L) (Figure 6.1 and Table 6.2) which precipitated admission to our centre (day 39 post-treatment). ALT was also mildly elevated (216 U/L), ALP was normal. A clinical diagnosis of immunotherapy-associated myositis and myocarditis was made and intravenous methylprednisolone was given for three days, followed by oral prednisolone with slow clinical and biochemical improvement. However, ten weeks post-discharge she was readmitted with increasing fatigue, weakness, dysarthria, diplopia and ptosis. AChR antibodies were negative. A clinical diagnosis of pembrolizumab-associated ocular myopathy and myositis was made; management was with oral corticosteroids, a course of IVIg and physiotherapy rehabilitation. She received a booster vaccination (BNT162b2) 74 days prior to pembrolizumab.

Patient 3

An 81 year-old woman with pre-treatment PS 0 was admitted with five days of reduced mobility, fatigue and myalgia (on movement but not palpation) 23 days post-initiation of pembrolizumab (400mg) for stage IV melanoma. CK was markedly elevated (11,301 U/L) (Figure 6.1, Table 6.2), as were liver enzymes (ALT 705 U/L, ALP 155 U/L). Troponin, measured on day 4 post-admission was 2,931 ng/L (Figure 6.1, Table 6.2). Management was with intravenous methylprednisolone, switched to oral prednisolone after four days. Supplemental oxygen was started but weaned due to symptomatic improvement and decline in CK (Figure 6.1) over four days, although bulbar symptoms and dysphagia then developed. An echocardiogram performed five days post-admission demonstrated normal bi-ventricular systolic function. Six days post-admission, she acutely deteriorated with type II respiratory failure and subsequent cardiac arrest. A post-mortem (PM) examination demonstrated multiple foci of inflammation and myocyte necrosis throughout the myocardium. Replacement fibrosis was absent, indicating a two-week timeframe, and there was minimal atheroma and no myocardial infarction. Skeletal muscle examination demonstrated multiple foci of inflammation and necrosis, similar to the sampled myocardium. Of note, a metastatic tumour deposit from the serosal surface of the small bowel displayed brisk lymphocyte infiltration (Figure 6.1). She had received a booster vaccination (BNT162b2) 74 days prior to pembrolizumab.

All three patients were negative for SARS-CoV2 anti-nucleocapsid IgG and positive for anti-spike IgG.

E | Science Immunology Paper

Not included in online version - please find paper at this webpage.

F | Nature Medicine Paper (2022)

Not included in online version - please find paper at this webpage.